



## Durham E-Theses

---

### *Structural properties of polyaniline films*

Milton, A.J.

#### How to cite:

---

Milton, A.J. (1993) *Structural properties of polyaniline films*, Durham theses, Durham University.  
Available at Durham E-Theses Online: <http://etheses.dur.ac.uk/5548/>

#### Use policy

---

The full-text may be used and/or reproduced, and given to third parties in any format or medium, without prior permission or charge, for personal research or study, educational, or not-for-profit purposes provided that:

- a full bibliographic reference is made to the original source
- a [link](#) is made to the metadata record in Durham E-Theses
- the full-text is not changed in any way

The full-text must not be sold in any format or medium without the formal permission of the copyright holders.

Please consult the [full Durham E-Theses policy](#) for further details.

The copyright of this thesis rests with the author.  
No quotation from it should be published without  
his prior written consent and information derived  
from it should be acknowledged.

## STRUCTURAL PROPERTIES OF POLYANILINE FILMS

by

**A. J. MILTON**

A thesis submitted in partial fulfilment  
of the requirements for the degree of PhD.

Department of Physics  
University of Durham  
October 1993



28 MAR 1994

## DECLARATION

The material contained in this thesis has not been submitted for examination for any other degree or part thereof, at the University of Durham, or any other institution. The material contained in this thesis is the work of the author except where formally acknowledged by reference.

The copyright of this thesis rests with the author. No quotation from it should be published without his prior consent and information derived from it should be acknowledged.

# DEDICATION

To HBW

## Acknowledgements

First of all I would like to thank my supervisor Dr Andy Monkman for his skill, advice and enthusiasm in guiding me through my project and especially the writing of this thesis. Also I would like to thank Dr P. Adams for sharing his in-depth knowledge of polyaniline and providing much help during the initial stages of this project. Many thanks too to all the members of our research group, especially Mr Steve Pomfret and Mr Paul Laughlin and all my other friends in the department. Without your help and friendship this thesis would have been impossible.

Outside the department, I am extremely grateful to SERC for funding and BICC Cables Ltd for the provision of a CASE award. Much of this work has relied on BICC and I am especially indebted to many people, in particular my industrial supervisor Dr Simon Rowland, at the Helsby Technology Centre, for his professionalism, encouragement and willingness to help no matter what the problem or request! Other people I would like to thank at Helsby are Dr Tony Blythe, Mr Andy Platt and Ms Lynn Addison for their invaluable assistance. On all my trips to Helsby everyone went out of their way to be friendly and helpful. Thanks also to Dr John McCormack at BICC Head Office for his continued support of this project and Dr Jo Jutson at the Wrexham Technology Centre for tirelessly running my samples on the Siemens Diffractometer and much assistance in explaining the X-ray diffraction technique. Thank you one and all.

Special thanks are also extended to Dr Nick Bernhoeft for his knowledge and expertise during the neutron diffraction experiments and Dr Alex Hannon, instrument scientist on LAD. Also I am indebted to all the members of the departmental workshop, but especially Harry, for building the stretch rig and making numerous other items, even when my design brief was just a blank piece of paper! Also I would like to thank the technical staff, Mr Norman Thompson, Mr Chris Pearson and Mr Davy Pattinson for so often helping me out with my project work. Champion mon!

Finally I would like to thank my parents for helping me through what must seemed to have been endless years of education and Margaret for her unwavering encouragement, understanding and support - without you I could never have written this thesis. Thank you everyone.

## Abstract

This thesis describes the experimental investigations of the structural properties of the conductive polymer, polyaniline. These studies have been performed on free-standing film samples, solution cast using the solvent N-methyl-2-pyrrolidinone (NMP). Such specimens have enabled a wealth of detailed information about polyaniline to be derived.

The polymer itself was synthesised in the emeraldine base form using a chemical route optimised at Durham. The product was then assessed for its chemical structure and molecular weight using  $^{13}\text{C}$  NMR, elemental analysis and gel permeation chromatography. The process of fabricating the polymer into free-standing films is discussed and assessed. It has been shown that such films may be oriented by the application of uniaxial stress at elevated temperatures and this procedure has been described and analysed in detail. This stretching process aligns the polymer chains on a molecular level and hence produces changes in the physical properties of films. In particular, upon doping to the conducting emeraldine salt form by protonation in aqueous HCl, stretch oriented films display a remarkable increase in conductivity (parallel to the stretch direction) over their unstretched, doped counterparts.

Various thermal analysis techniques, including dynamic mechanical thermal analysis, dielectric thermal analysis, thermomechanical analysis and infrared spectroscopy have been used to probe the physical properties of polyaniline films. Using these techniques a number of important thermal transitions have been observed and furthermore the stretch alignment process has been rationalised.

Infrared orientational analysis has revealed detailed information about the molecular orientation produced during macroscopic stretching of a film. The type and degree of chain orientation has been analysed as well as the geometrical structure of a single chain. X-ray diffraction has probed the crystalline fraction of polyaniline films. Various aspects concerning the crystalline fraction of film samples has been derived along with an orientational analysis which has been contrasted with the infrared results. An even greater amount of structural information has been revealed by neutron diffraction and this technique has enabled a detailed examination of the structure of the crystalline phases of polyaniline to be made.

## CONTENTS

CHAPTER 1	INTRODUCTION	1
CHAPTER 2	A REVIEW OF POLYANILINE	3
2.1	Introduction	3
2.1.1	Polyaniline as a Conducting Polymer	4
2.1.2	Historical Survey	6
2.2	Synthesis of Polyaniline	7
2.2.1	Chemical Synthesis	7
2.2.2	Electrochemical Synthesis and Other Methods	8
2.2.3	Polymerisation Mechanism	9
2.3	The Structure of Polyaniline	11
2.3.1	Chemical Structure	11
2.3.2	Geometric Structure	13
2.4	Processing Techniques	18
2.4.1	NMP Cast Films	19
2.4.2	Other Methods	21
2.5	Conductivity	24
2.5.1	Film Doping and Conductivity	24
2.5.2	Mechanisms of Conduction	25
2.6	Electronic Properties	31
2.6.1	Theoretical Studies	31
2.6.2	Optical and Photoinduced Absorption Studies	35
2.7	Applications	41
	References	42



CHAPTER 3	SYNTHESIS AND PROCESSING PROCEDURES	47
3.1	Introduction	47
3.2	Chemical Synthesis of Polyaniline	47
3.3	Analysis of Chemical Composition	48
3.3.1	Chemical Structure	49
3.3.2	Molecular Weight Distribution	56
3.3.3	Optimisation of Synthesis	58
3.4	Polyaniline Films	60
3.4.1	Film Formation	60
3.4.2	Film Quality and Composition	63
3.5	Orientation of Polyaniline	67
3.5.1	The Orientation Process	68
3.5.2	Stretching Apparatus	72
3.5.3	Results and Behaviour	75
3.6	Conducting Samples	80
3.7	Summary	84
	References	87
CHAPTER 4	THERMAL PROPERTIES OF POLYANILINE FILMS	90
4.1	Introduction	90
4.2	Dynamic Mechanical Thermal Analysis	90
4.2.1	Theory	92
4.2.2	Behaviour of Polymer Systems	95
4.3	Dielectric Thermal Analysis	101
4.4	Infrared Spectroscopy	104
4.5	Thermomechanical Analysis	104
4.6	Experimental Section	105
4.7	Results and Discussion	110
4.7.1	Mechanical Analysis	110
4.7.2	Dielectric Analysis	118

4.7.3	Infrared Spectroscopy	121
4.7.4	Further Discussion	126
4.8	Summary	127
	References	129
<b>CHAPTER 5</b>	<b>INFRARED ORIENTATION STUDIES</b>	<b>131</b>
5.1	Introduction	131
5.2	Orientation and Infrared Dichroism	131
5.3	Theoretical Analysis	134
5.3.1	Partial Axial Orientation	134
5.3.2	The Dichroic Formula	137
5.4	Experimental Details	139
5.5	Results and Discussion	142
5.5.1	Assignment of Vibrational Bands	142
5.5.2	Orientation Measurements	150
5.6	Summary	158
	References	159
<b>CHAPTER 6</b>	<b>X-RAY DIFFRACTION STUDIES</b>	<b>161</b>
6.1	Introduction to X-ray Diffraction	161
6.2	Diffraction by Polymers	164
6.2.1	The 'Fringed Micelle' Model	164
6.2.2	Structural Analysis	166
6.3	Polyaniline Diffraction Data	169
6.4	Experimental Details	171
6.4.1	The Diffractometer	171
6.4.2	Data Processing and Analysis	173
6.4.3	Flat-Film Photographs	174
6.5	Experimental Results	176
6.6	Discussion of Results	185
6.7	Summary	191
	References	192

CHAPTER 7	NEUTRON DIFFRACTION STUDIES	194
7.1	Introduction	194
7.2	Aspects of Neutron Diffraction	194
7.3	Experimental Section	198
7.3.1	The LAD Diffractometer	198
7.3.2	Samples	200
7.4	Results and Analysis	202
7.5	Summary	214
	References	215
CHAPTER 8	CONCLUSIONS	217
8.1	Overall Summary	217
8.2	Suggestions for Further Work	223
APPENDIX	PUBLICATIONS	225

## Chapter 1

### Introduction

Over the last few decades synthetic polymers have had a phenomenal impact on our day-to-day living. Properties such as strength, elasticity, plasticity and toughness combined with remarkable lightness and very low cost have given these materials a whole multitude of uses, from simple disposable coffee cups to space age applications. However, now a new and potentially very important class of polymer has been discovered based on an extraordinary intrinsic property - conductivity. At the moment perhaps one material more than any other is at the forefront of conductive polymer research - polyaniline - and it is this polymer which is the subject of this thesis.

Polyaniline is a complex but highly challenging conductive polymer with many potentially very important technological applications. This latter point is undoubtedly one of the reasons why it has been the subject of so much interest. However, another relates to the polymer itself and in particular the way in which it can be processed. Often early studies of other such conductive polymers were severely hampered by the inherent lack of processibility of the material so causing extreme difficulties with sample analysis and characterisation. With polyaniline, a major breakthrough occurred when it was discovered that the polymer could be processed into air-stable, free-standing films. A remarkable property of these films is that they can be further processed by stretch alignment so as to dramatically increase the bulk conductivity of the polymer. Such film specimens afford the chance to study and characterise polyaniline in great detail.

This thesis has set out to investigate some of the many structural aspects of polyaniline films, particularly those on a microscopic scale which are associated with the dramatic increase in conductivity observed upon stretch alignment. The work presented has been carried out in conjunction with BICC Cables Ltd, through the provision of a CASE award. As such the results are aimed to be not only of pure research interest, but also

endeavour to give an insight into the polymer so that possible applications in cable technology may be assessed. For instance, despite not yet being conductive enough to replace the central aluminium/copper core of a cable product, polyaniline does have the potential to act as the conductive element in R.F. screening coatings around a cable.

The layout of this thesis as follows: in chapter 2 a review of the current understanding of polyaniline is presented and in particular that pertaining to free-standing films. Chapter 3 then goes on to discuss the synthesis and processing procedures used in this work and reports on some very important findings concerned with sample preparation. Chapter 4 describes the use of various thermal analysis techniques to investigate the thermal properties of film samples, the results of which also provide a detailed insight into sample orientation. Chapter 5 reports on infrared orientation studies which have been used to assess the degree of alignment and other structural aspects of the polymer chains in stretch aligned specimens. Chapter 6 looks at the results of X-ray diffraction studies on films and links the results to those previously obtained by infrared analysis. Chapter 7 reports on neutron diffraction studies of polyaniline, the first time the polymer has been investigated by this technique. Analysis has allowed the structures of the crystalline fractions of various polyaniline films to be derived. Finally, chapter 8 concludes all the results and gives suggestions for further work.

## Chapter 2

### A Review of Polyaniline

#### 2.1 Introduction

Conducting polymers have been of special interest ever since the first reports of p and n type doping of polyacetylene to a metallic state<sup>1-3</sup>. As a function of the doping level it was found that the room temperature conductivity of this polymer could be varied<sup>4-6</sup> from  $10^{-13}$  to  $10^5$  S cm<sup>-1</sup>. This conductive behaviour was realised to be connected with the conjugated nature of the  $\pi$ -electron system along the polyacetylene backbone. The charges added, through doping, cause strong lattice relaxations so forming self-localised charge carriers or defects, with electronic levels in the band gap. Much interest then centred on the new physics associated with these defects.

Subsequently, many other possible conducting polymers, based on similar conjugated chain structures, were also studied. However, the inherent lack of solubility (due to the chain rigidity imparted by the  $\pi$ -electron network) and stability of most of these materials provided many problems with detailed characterisation. In particular this was the case for polyaniline, which despite being regarded as a complex, challenging and technologically very important conducting polymer, could only be prepared in a undesirable powder form. However, recently a major breakthrough in the processing of polyaniline has been made, whereby the polymer can be dissolved in a highly polar solvent. This has led to an explosion of interest in the material with many hundreds of reports concerning polyaniline appearing in the literature. Therefore, it is the aim of this chapter to explain some of the background concepts behind polyaniline (but by no means all since the literature is so vast) and especially those in relation to the work being carried out in this thesis.

### 2.1.1 Polyaniline as a Conducting Polymer

Polyaniline is the generic term for a family of polymers, the base form of which has a generalised formula as in Figure 2.1. The representation consists of  $y$  reduced and  $(1-y)$  oxidised units and the polymer is known to exist in three main oxidation states. The fully reduced ( $y = 1$ ) and fully oxidised ( $y = 0$ ) forms, termed leucoemeraldine base (LEB) and pernigraniline base (PNB) respectively, are both insulators. Intermediate between these two is the emeraldine oxidation state, where  $y = 1/2$ , the base form of which is also insulating. However, this latter emeraldine base (EB) polyaniline can be protonated i.e. doped by aqueous acids to give an emeraldine salt (ES) form. This doping procedure increases the conductivity of the polymer by almost 10 orders of magnitude. For example a pressed pellet of emeraldine hydrochloride (dopant 1 M HCl) typically displays a conductivity of  $5 \text{ S cm}^{-1}$ . It is primarily due to this conducting nature that much of the research on polyaniline has been undertaken.

A recent advancement in the polyaniline field is the ability to solution process the polymer into air-stable, free-standing films. Such processing yields samples in the EB state which, when doped (1 M HCl), have a conductivity in the region  $60\text{-}70 \text{ S cm}^{-1}$ . Alternatively, base films can be mechanically stretch aligned and then subsequently doped. These doped ES specimens exhibit a marked increase in conductivity parallel to the stretch direction compared to an unstretched film, typically  $350 \text{ S cm}^{-1}$  for a 300% stretched film. This enhancement of conductivity is a very exciting and highly important feature of polyaniline, particularly with regards to potential applications, but one which, as yet, is not fully understood, particularly on a molecular level. Therefore, it has been a main aim of this thesis to investigate the microscopic structure of polyaniline and the molecular changes which allow such a large increase in the bulk conductivity.

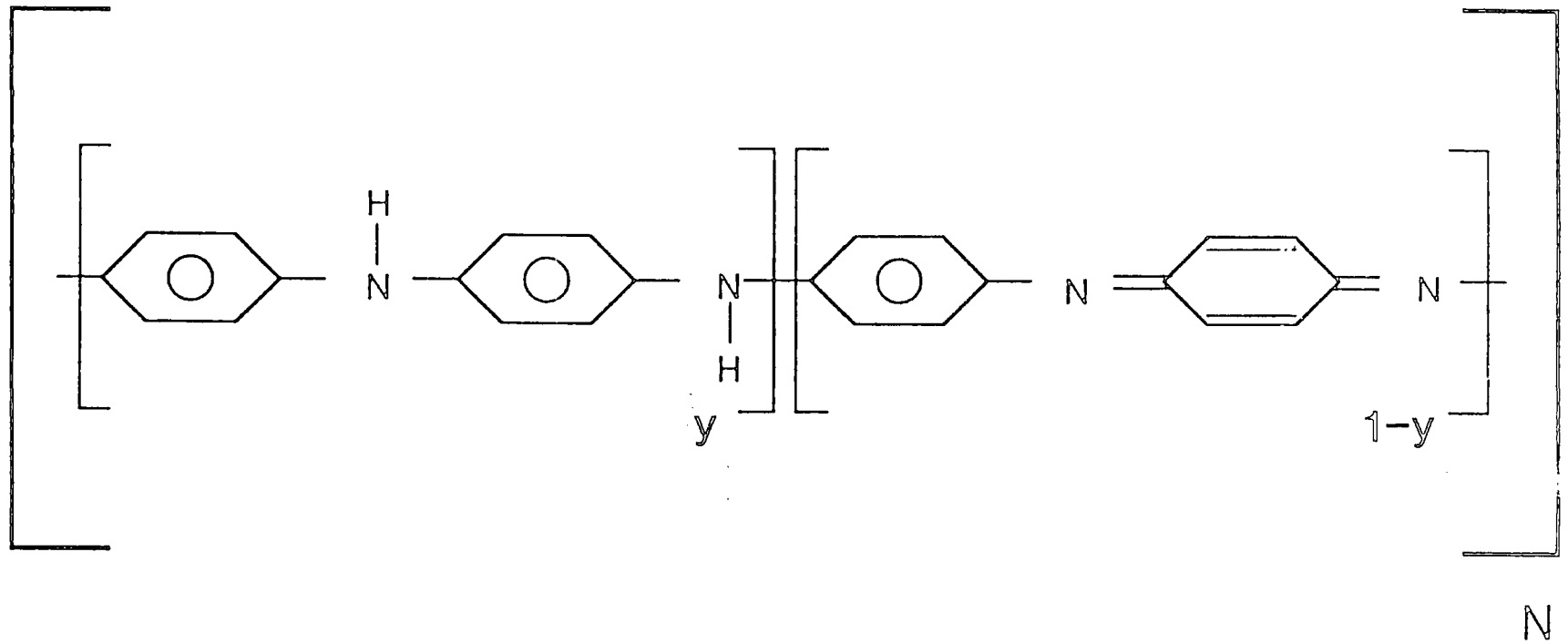


Figure 2.1 Generalised formula for the base forms of polyaniline.



### 2.1.2 Historical Survey

Polyaniline is the oldest known synthetic organic polymer, having first been discovered by Letherby<sup>7</sup> as a result of the anodic oxidation of aniline. The product formed was a dark green precipitate and was known as aniline black. Subsequently, other workers also reported their findings concerning this new material<sup>8-11</sup>. In 1910-1912 Green and Woodhead proposed<sup>12,13</sup> that the polymer existed in four different oxidation states, each of which was an octamer. Further scattered papers appeared in following years, but these early studies were severely hampered by much controversy due to the uncertain composition of the polymer. However, the work of Josefowicz *et al* in the mid 1960s and early 70s<sup>14-16</sup> lead to a more detailed understanding of polyaniline. In particular, the conducting nature of the protonated emeraldine oxidation state was discovered (although the structure of this conducting form was still unknown) and the possible use in aqueous electrolyte rechargeable batteries reported. A brief lull then ensued until the early 1980s when Diaz and Logan<sup>17</sup> discovered polyaniline to be electrochromic. Following this and with the advent of sophisticated analysis techniques there then proceeded an explosion of interest in polyaniline. In particular the group of MacDiarmid undertook some detailed investigations and 'rediscovered' much of the previous work on polyaniline<sup>18,19</sup>. The driving forces for all this research were the complex and challenging nature of the polymer coupled with many potential applications, in particular concerning the conducting state - a highly important feature of this salt form is that, unlike the conducting form of previous materials such as polyacetylene, it is air-stable.

Many academic researchers and indeed major industrial companies are now highly involved with research into polyaniline. This huge interest can be seen from the fact that over the last five years, from the end of 1992, 575 papers have been published in the literature and this is based on the use of the word polyaniline in the title alone! Further findings and novel applications are being reported all the time and it seems the interest in polyaniline is still very much on the increase.

## 2.2 Synthesis of Polyaniline

Polyaniline is generally prepared by the direct oxidation of aniline using an appropriate chemical oxidant or by electrochemical oxidation utilising various electrode materials. However, it is generally understood that the characteristics of the polymer differ according to the method of synthesis. In early studies electrochemical synthesis was almost exclusively used, but more recently chemical synthesis has been the major preparative route. This is because the chemically synthesised material is more suitable for the fabrication of free-standing films, due to its longer chain length and also because the polyaniline can be produced in much larger amounts.

### 2.2.1 Chemical Synthesis

The chemical synthesis of polyaniline requires the use of a reagent to oxidise the aniline monomer. For this purpose various oxidising agent can be used, but by far the most common is ammonium peroxodisulphate (persulphate)<sup>18-21</sup>. The reaction stoichiometry indicates an ideal oxidant/aniline ratio of 1.25, but it has been reported<sup>22</sup> that the product is essentially independent of the ratio below this value, so that normally a 1:1 mixture can be used. Above an oxidant/aniline ratio of 1.25, however, the polyaniline becomes over-oxidised with a resulting decrease in conductivity<sup>22</sup>.

The reaction is carried out in aqueous acid media, 1-2 M HCl being the most common<sup>18-20</sup>. When oxidant and aniline are added an exothermic reaction ensues, the mixture darkens in colour and a dark blue/green precipitate is formed, emeraldine salt. The precipitate is then isolated by filtration and washed with an appropriate solvent, water or aqueous acid, to remove any impurities. This conducting material may then be deprotonated in a basic media, such as ammonia, to give the EB state, which is needed for solution processing. The reaction yield is high, typically 80%, but there are a number of reaction variables which control the quality of the final product. These are of the utmost importance (and are described in detail in the next

chapter) since a poorly synthesised product can lead to erroneous results concerning the further characterisation of the polymer.

### 2.2.2 Electrochemical Synthesis and Other Methods

In the early stages of research into polyaniline, electrochemical synthesis of polyaniline using an inert metal electrode was a widely used technique<sup>23-25</sup> and is still sometimes used nowadays. For this method electrodes such as platinum or conducting indium tin oxide glass are normally used. The polymer is formed as thin depositions, in the protonated state, on these working electrodes through the anodic oxidation of aniline contained in a suitable electrolyte such as aqueous HCl. Polymerisation can be achieved by holding the working electrode at a constant potential with respect to a standard calomel reference electrode (SCE); the oxidation potential of aniline in 2M HCl is ca. 0.70-0.75 volts with respect to a SCE<sup>23</sup>. This is known as potentiostatic growth. Alternatively, the voltage may be cycled between -0.20 and 0.70 volts (cyclic growth) or films may be grown galvanostatically, where a constant current is passed through the electrolyte. The samples produced have a fibrillar morphology<sup>23</sup> and if grown thick enough can be removed from the electrode to give a free-standing film. However, such films are mechanically very poor (due to the low molecular weight of the polymer) and are not really suitable for further characterisation. One advantage of this method though is that *insitu* experiments may be carried out during the synthesis itself, allowing the polymerisation reaction to be studied in detail.

Polyaniline may also be synthesised by a step-wise condensation process, where the oxidised and reduced repeat units must alternate<sup>26,27</sup>. This material is reported to have very similar infrared and electronic spectra to both electrochemically made polyaniline and also the phenyl capped octamer of aniline as well. As such, EB synthesised from aniline is proposed to consist principally of alternating oxidised and reduced repeat units. Other synthesis methods also reported include a gas-phase plasma route<sup>28</sup> and vapour phase deposition<sup>29</sup>.

### 2.2.3 Polymerisation Mechanism

The wide variety of methods used to synthesise polyaniline have led to a number of polymerisation mechanisms being proposed by various authors. In general though the mechanism is agreed to be an oxidative coupling polymerisation<sup>24,30</sup>. The scheme proposed by Genies *et al*<sup>30</sup> is shown in Figure 2.2 and results from studies of the electrochemical synthesis of the polymer in a HF/NH<sub>3</sub> eutectic. The first step and also that of other plausible mechanisms, is the formation of an aniline radical cation. This intermediate is resonance stabilised by several canonical forms, allowing two radicals to join to form a dimer. Subsequent coupling of the oxidised dimers leads to formation of the polymer chain.

With regards to chemical synthesis, Manohar *et al*<sup>31</sup> report that the fully oxidised form of the polymer, pernigraniline, is formed during the initial stages of the polymerisation. This oxidised polyaniline is then able to oxidise remaining monomer units while it is itself reduced, so that the emeraldine oxidation state is the final product. Furthermore, the authors also report that it is feasible that pernigraniline may be isolated during the reaction, allowing a relatively simple preparative method for the fully oxidised polymer, albeit with short chain lengths.

The polymerisation has been shown to involve predominantly para i.e. head-to-tail coupling<sup>25,27</sup>, although since the mechanism is a chain growth involving a radical cation, it is also possible to have ortho coupling as well as chain branching, crosslinking e.t.c. Such side reactions usually lead to low yields, involving other products and also low molecular weights through the inclusion of 'defects' on the polymer chains. Defects, as discussed more in the next chapter, greatly alter the physical properties of polyaniline, effectively masking the true features of the polymer. The differing properties of electrochemically and chemically synthesised polyaniline are probably reflected in differing amounts of these defects.

As regards to these defects, Bacon and Adams<sup>25</sup> have reported that benzidine may be formed during the anodic oxidation of aniline, as a result of a tail-to-tail linked dimer. Benzidine is a highly carcinogenic substance

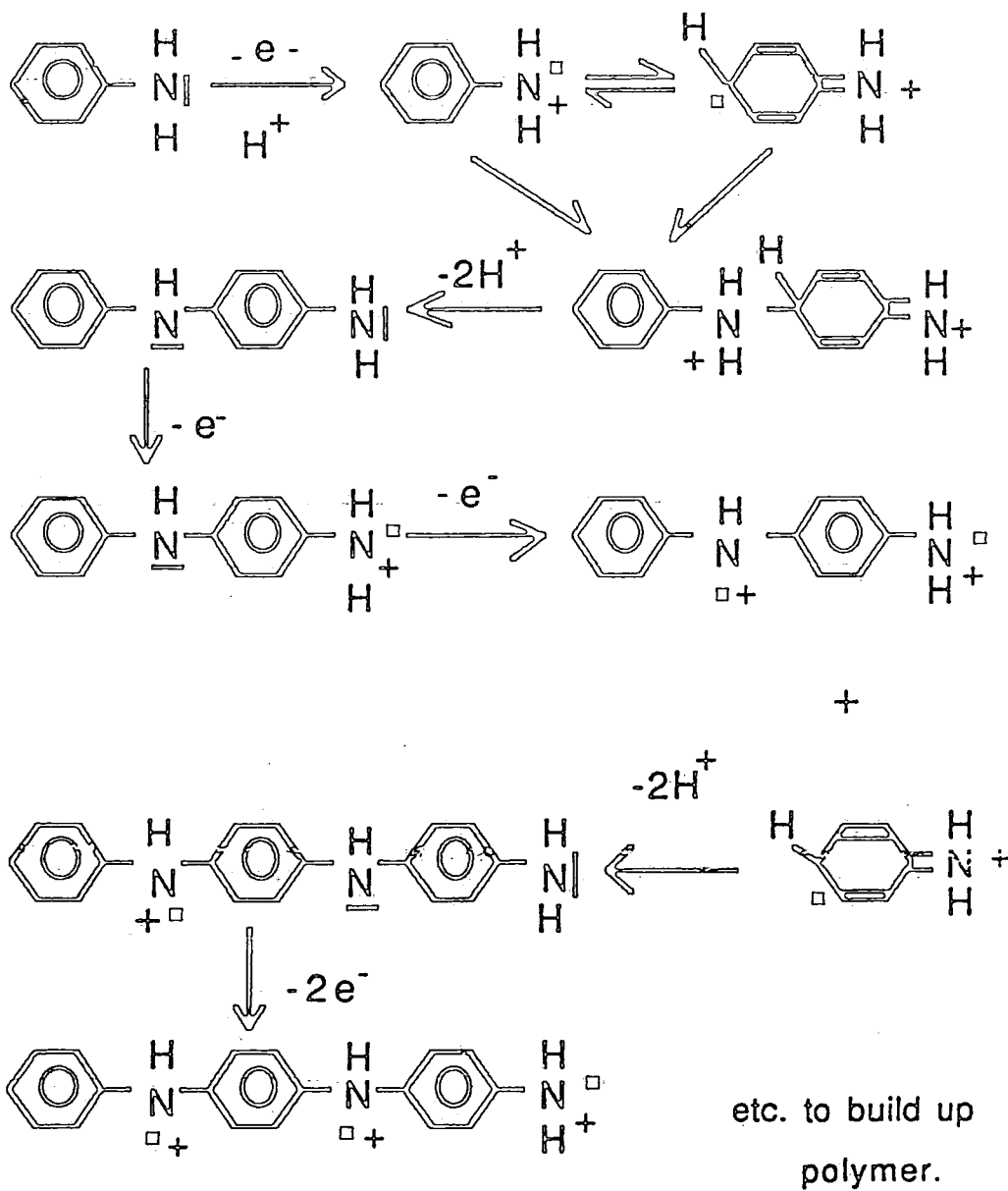


Figure 2.2 The polymerisation mechanism for polyaniline as proposed by Genies *et al*<sup>21</sup>.

and this has fuelled much speculation as to the health and safety aspect of polyaniline. However, this by-product may only occur when using a highly acidic polymerising solution below a pH of -2; indeed such a medium is not used to polymerise aniline as the resulting material is of very poor quality<sup>22</sup>. Also, in a recent study of electrochemically prepared material<sup>23</sup>, no benzidine was found at levels above 1ppb in any of the waste products. Furthermore, there is no evidence to suggest that this carcinogen is formed during the chemical synthesis of the polymer and even if it were it would likely be locked into the chain structure and, as such, far less hazardous.

## 2.3 The Structure of Polyaniline

### 2.3.1 Chemical Structure

As mentioned previously much of the early work on polyaniline was fraught with difficulty due to the ill-defined nature of the material. At the beginning of the current phase of research the chemical structure of the polymer had not been defined, but nowadays the ideal base forms of the polymer are normally represented by the general formula of Figure 2.1. This structural deduction has been achieved through comparisons to model compounds<sup>32,33</sup>, elemental analysis<sup>34</sup>, direct chemical synthesis methods<sup>26,27</sup> and infrared spectroscopy<sup>35,36</sup>. It is very important to realise though that these techniques and methods do not unequivocally establish such chain structures; the general formula is the best fit to the available data. However, as reported in section 3.3.1, a highly accurate analysis method has been utilised in this work which has shown the EB structure to be in virtual agreement with the general formula structure. One important limitation is also highlighted though; the formula of Figure 2.1 gives idealised chain structures, i.e. any 'structural' defects are neglected.

The three primary oxidation states are depicted in Figure 2.3, the fully reduced leucoemeraldine base, a white solid, the fully oxidised pernigraniline base, a blue/black solid and the semi-oxidised, blue/purple emeraldine base. It is evident that these forms only differ by relatively few

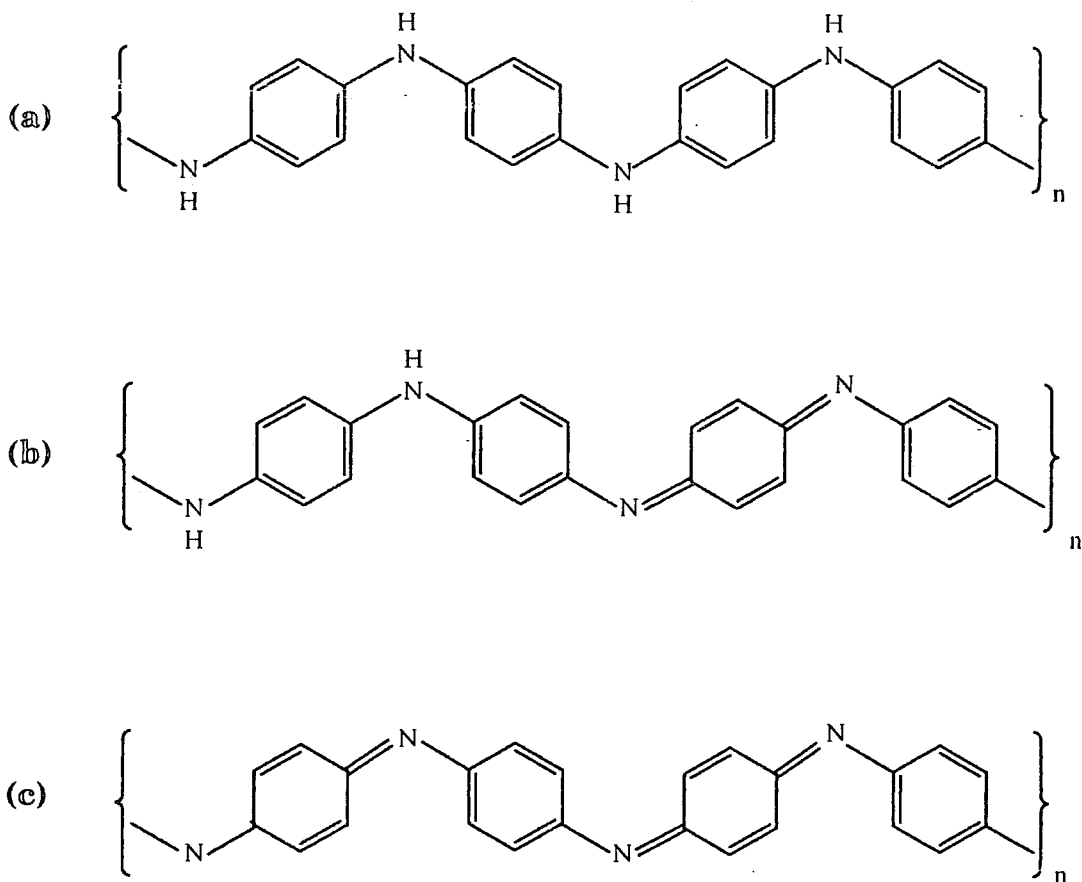


**Figure 2.3** The three primary oxidation states of the base forms of polyaniline: (a) the fully reduced leucoemeraldine base (LEB); (b) the semi-oxidised emeraldine base (EB); (c) the fully oxidised pernigraniline base (PNB). Note these are idealised chain structures in which possible structural defects are neglected.

hydrogens, so a technique such as elemental analysis is not always sufficiently accurate to determine the oxidation state of the product. However, Ray *et al*<sup>37</sup> have described a  $\text{TiCl}_3$  volumetric analysis technique which has allowed the number of oxidised and reduced repeat units for polyaniline synthesised under different conditions to be assessed. Such a method is still not highly accurate, but the results are interesting nevertheless. When synthesis is carried out under an inert atmosphere the resulting EB is slightly reduced ( $y = 0.6$ ) whereas in air the product is somewhat over-oxidised ( $y = 0.4$ ). They conclude that the true emeraldine oxidation state where  $y = 0.5$ , may not really exist and that the term emeraldine actually refers to a composition where  $y$  is only approximately equal to 0.5.

As also mentioned previously, EB polyaniline can be protonated to a conducting ES form by doping in aqueous acids. This doping process is unique among conducting polymers in that the number of electrons associated with the chain backbone remains unchanged<sup>20</sup>. The process involves the protonation of imine,  $-\text{N}=\text{}$ , sites associated with oxidised units and is believed to occur<sup>38,39</sup> as shown in Figure 2.4. Upon protonation of the imine units, two bipolarons (doubly charged, spinless defects) are formed, Figure 2.4(b). However, these are energetically unstable and undergo a two-step transformation involving an internal redox reaction. Eventually a polaron or polysemiquinone radical cation structure is formed, Figure 2.4(d). This latter polaron structure is normally used as a representation of the conducting form of the polymer. However, there is still much debate as to whether the bipolaron structure will actually be so unstable as to disproportionate into two polarons. This controversy is particularly prevalent with regards to charge transport and optical studies, discussed later on, where there are various arguments for and against both structures.

### 2.3.2 Geometric Structure

The generalised chemical formula infact gives rather a naive representation of the true polyaniline chain. The backbone of the polymer is



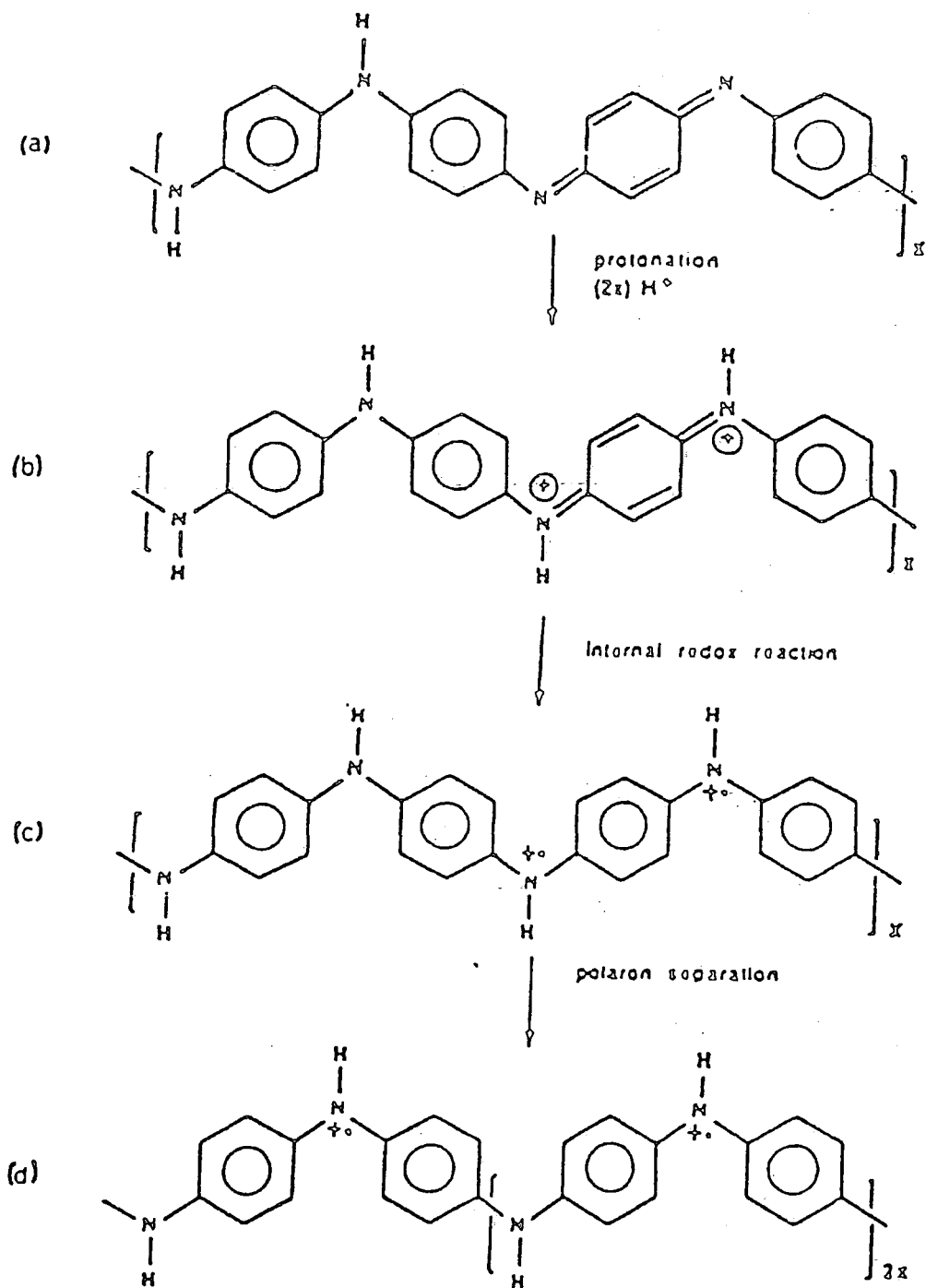


**Figure 2.4** The protonation scheme for emeraldine base: (a) before protonation; (b) formation of bipolarons upon protonation of imine sites; (c) dissociation of bipolarons into two polarons; (d) polarons separate to form polaron lattice.

not linear but consists of a nitrogen-nitrogen (N-N) zigzag arrangement, rather like a herring bone. Only the fully oxidised PNB is actually conjugated, although EB may be described as being semi-conjugated. Note though that polyaniline is an A-B type polymer with the nitrogen heteroatoms contributing to the chain structure. These atoms are able to donate  $p_z$  orbitals, containing 2 electrons per N atom, to the  $\pi$ -electron system. However, the most important aspect of the polymer's geometric structure arises from the fact that the  $C_6$  rings along the chain are twisted. This ring twisting effectively reduces the amount of  $p_\pi$  orbital overlap and hence the extent of  $\pi$ -electron delocalisation along the polymer chain for all three oxidation states. A major effect of these ring distortions is the localisation of charge defects, as will be discussed later on.

Bredas<sup>40</sup> has examined theoretically the structures of a four ring oligomer of LEB and a three ring structure of PNB as a basis for electronic transitions in polyaniline. Quantum-mechanical calculations show that for the fully reduced oligomer, the optimum geometry occurs when the benzenoid rings are twisted by a torsional angle (relative to the N-N plane) of the order of  $30^\circ$  as shown in Figure 2.5. Furthermore, this torsional angle alternates along the chain so that neighbouring rings are oppositely oriented. Similar theoretical results have also been reported by MacDiarmid *et al*<sup>41</sup>.

Considering the three ring, fully oxidised oligomer, the most stable configuration occurs for a dimerised structure, Figure 2.6, where there is a marked alteration between the quinoid and benzenoid character of the rings. This is contrasted with the less stable undimerised configuration where all the carbon-nitrogen bonds are equal in length and all the rings have the same semi-quinoid like geometry i.e. here the quinoid structure is not localised. For the dimerised structure the rings with quinoid character are twisted by an insignificant amount ( only  $1.1^\circ$ ) relative to the N-N plane whereas the benzenoid ring has a torsional angle of approximately  $61^\circ$ . The angle between adjacent rings is thus around  $60^\circ$ , of the same order of that found in the reduced oligomer. Both these optimised oligomer geometries can be used as a basis to assess EB. This semi-oxidised form of

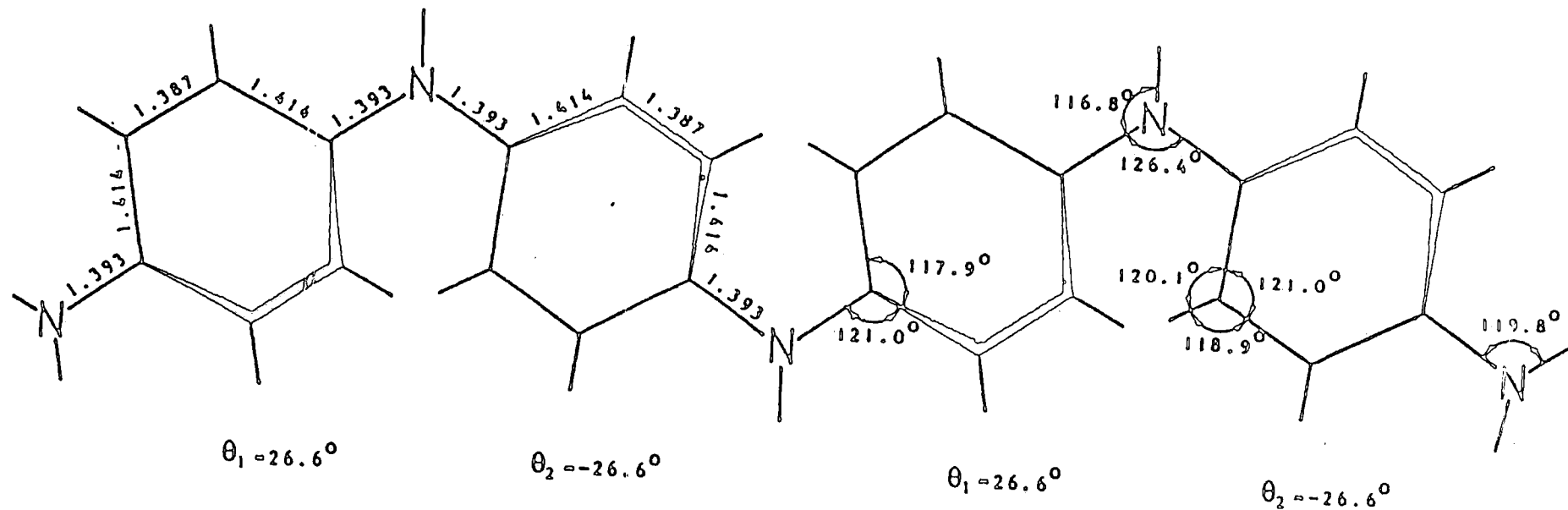


Figure 2.5 Optimised geometry for a four-ring oligomer of leucoemeraldine base, according to Bredas<sup>42</sup>. Bond lengths are in Å and angles in degrees. The  $\theta$  values represent the torsional angles of each phenylene ring with respect to the nitrogen-nitrogen plane.

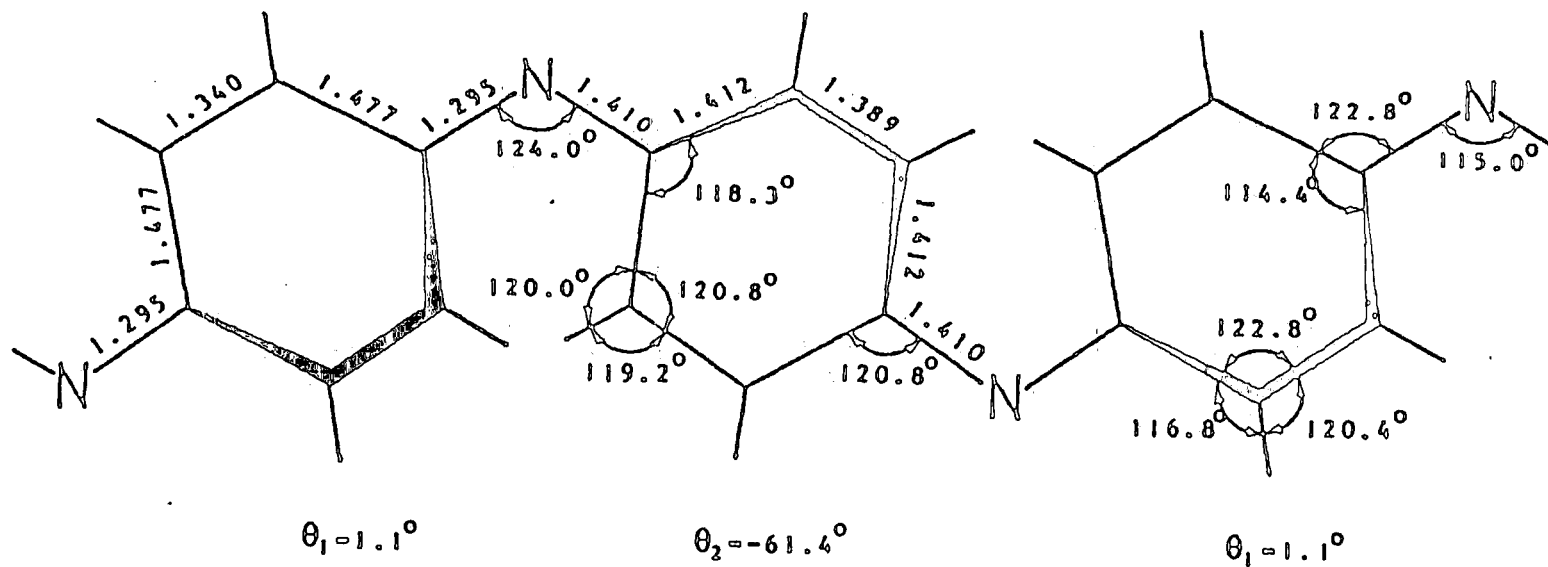


Figure 2.6 Optimised geometry for a three-ring oligomer of pernigraniline base in a dimerised configuration, according to Bredas<sup>42</sup>. The same notation as in Figure 2.5 applies.

polyaniline is itself difficult to model explicitly not only due to the more complicated repeat unit, but also due to the lack of stable, non-protonated, semi-oxidised oligomers.

The work of Baughmann *et al*<sup>32,33</sup> concerning X-ray diffraction studies of perchlorate and tetrafluoroborate polyaniline oligomers has allowed information to be derived about conducting, ES polymer chains. In these reports, quinoid rings of the salt oligomers were found not to be highly localised as in the base trimer previously discussed, but strongly distorted along the chain. The corresponding partial multiple bond character of the nitrogen-ring bonds, as deduced from bond length calculations, drives all the rings to within a torsional angle of about  $+15^\circ$  and  $-15^\circ$  alternatively with respect to the N-N plane. The derived structure of the salt form of a phenyl capped tetramer of polyaniline is shown in Figure 2.7. For the parent ES polymer this delocalisation of the quinoid ring unit likely extends over the repeat unit of the polymer i.e. four C<sub>6</sub> rings. This decrease in ring torsional angle, as compared to the base form, increases the extent of the  $\pi$ -conjugation along the chain due to increasing the extent of p $_{\pi}$  orbital overlap. The charge of  $+2e$  associated with the two radical cations (polarons) of the ES repeat unit (see Figure 2.4(d)) can then extend over the four C<sub>6</sub> ring units. It is this delocalised nature of the salt structure which is thought to be responsible for extended conduction along the polymer chain.

## 2.4 Processing Techniques

Perhaps the main reason behind much of the controversy concerning early studies of polyaniline was the lack of processibility of the polymer. The material was reported to be insoluble in common organic and aqueous solvents. This lack of processibility, in turn, caused many difficulties with sample purification and also characterisation. There has, however, been a major breakthrough in the polyaniline field which has changed this situation dramatically, as outlined below.

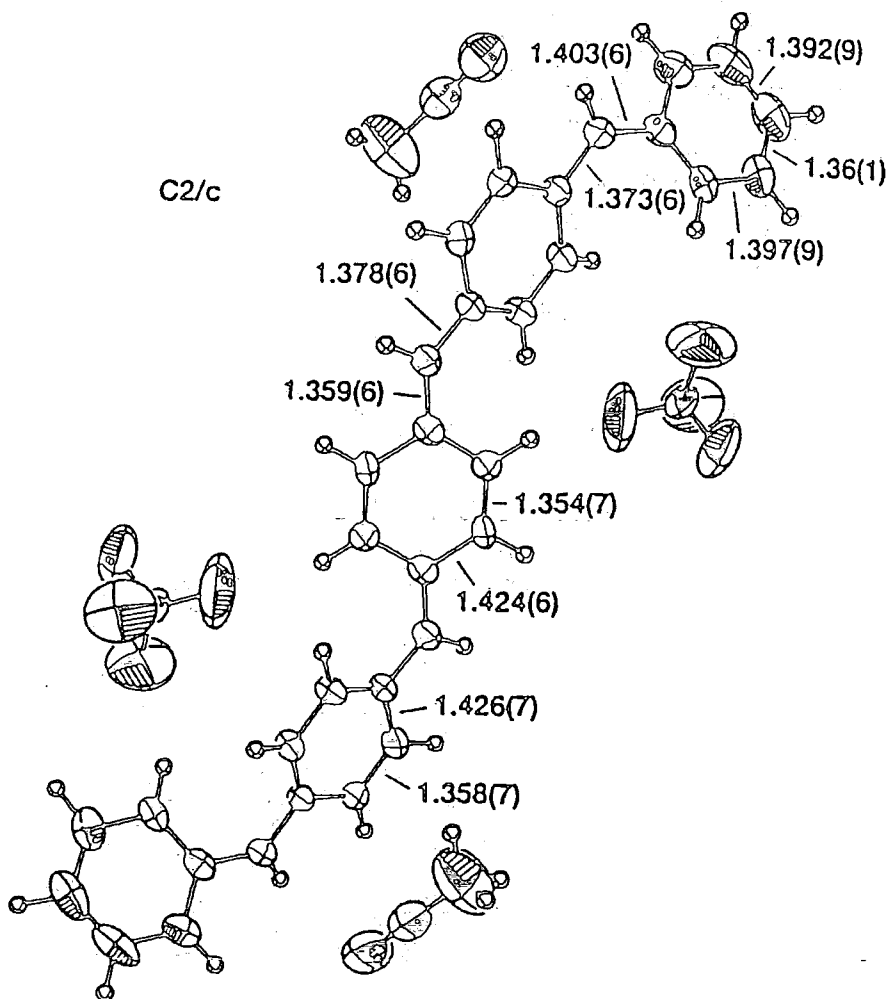


Figure 2.7 The crystal structure of the salt form of a phenyl end capped tetramer of polyaniline, derived by Baughmann *et al*<sup>34,35</sup>. Bond lengths are in Å with the calculated standard deviation in the least significant figure in parentheses.

#### 2.4.1 NMP Cast Films

Recently, Angelopoulos *et al*<sup>42,43</sup> have discovered that polyaniline, in the EB form, is soluble in the solvent N-methyl-2-pyrrolidinone (NMP), shown in Figure 2.8. NMP is a highly polar solvent commonly used to process azo dyes. The polymer is readily solution-processible in this solvent, although

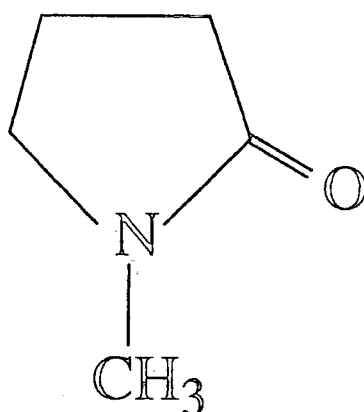


Figure 2.8 N-methyl-2-pyrrolidone.

the extent to which it is truly soluble is rather uncertain<sup>42</sup>. Copper-coloured, flexible, free-standing films can be cast by coating a suitable substrate with an EB/NMP solution. Typically some 10 wt% polyaniline in NMP is used<sup>44</sup>. Excess solvent is removed by drying in a vacuum oven. The film may then be carefully peeled from the substrate. To facilitate this latter step Angelopoulos *et al* have found it necessary to immerse the whole sample in water. However, by carefully adjusting the drying times films can be peeled from the substrate without soaking in water, as described in the next chapter. Samples prepared by solution casting from NMP typically have thicknesses of the order of 10-100 $\mu$ m. Unfortunately such films are too thick for transmission optical absorption studies. Films of sub-micron thicknesses needed for such analysis can be fabricated through spin coating<sup>45</sup>, but these are too thin to be removed from the substrate.

An added feature of these free-standing films is that they may be further processed, through the application of uniaxial stress. Such stretching was first demonstrated by Cromack *et al*<sup>46</sup> and has been a very significant development in the continued characterisation of polyaniline. Using this technique it has been demonstrated that samples may be readily elongated by several hundred percent<sup>47,48</sup>, with individual specimens having been stretched to beyond 600%<sup>47</sup>. The details of the stretching technique are

discussed in the next chapter, but it has been found in this work that these solvent cast films can be elongated up to 300% on a fairly reproducible scale. Higher extensions were found to have a much lower degree of reproducibility. However, very recently the stretching technique has been further optimised so that extensions up to some 700-800% are readily achievable<sup>49</sup>.

It is necessary to process and stretch these polyaniline films in the EB i.e. insulating form. Samples can be subsequently fully converted to conducting ES (emeraldine hydrochloride) by doping (immersion) in aqueous 1-2 M HCl<sup>47,48</sup>. For unstretched samples doping in 1M HCl yields conductivities<sup>47</sup> in the region of 60-70 S cm<sup>-1</sup>. However, for oriented films, conductivities can be increased up to 350 S cm<sup>-1</sup>, parallel to the stretch direction, with conductivity anisotropy as high as 24:1. This behaviour is described in detail in section 2.5.1.

#### 2.4.2 Other Methods

As early as 1910 Green and Woodhead reported<sup>12,13</sup> that octamers of aniline were soluble in 80% acetic acid, 60% formic acid, pyridine and concentrated sulfuric acid (H<sub>2</sub>SO<sub>4</sub>). In recent years the EB form of polyaniline has also been reported to be soluble in conc. H<sub>2</sub>SO<sub>4</sub><sup>50</sup>. Accordingly, films and fibres have been fabricated, which due to the nature of the solvent are in the conducting emeraldine sulfate form. These films and fibres, in a unstretched format, display comparable conductivities to those of HCl doped films. However, the samples were also found to be mechanically very weak and unsuitable for stretch alignment. Aqueous acetic acid has also been reported as a film casting solvent<sup>51</sup>. However, such samples have conductivities of only 0.5-2 S cm<sup>-1</sup> and again, due to their conducting nature, cannot be oriented to enhance the conductivity.

Further reports<sup>43,52</sup> have claimed solvents such as tetrahydrofuran, dimethylformamide, benzene and chloroform can be used to process polyaniline. The polymer has previously been stated to be insoluble in such common organic solvents, but it has been found that very low molecular



weight material is in fact partially soluble. Film casting is simply not possible using such solutions though, since the extent of solubility and the fraction of low molecular material in a batch of polyaniline is only very small. Furthermore, low molecular weight polymers are not conducive to high conductivities.

Another method utilised to induce solubility in polyaniline has been to synthesise derivatives<sup>53,54</sup> of the parent EB, as illustrated in Figure 2.9. One such derivative which is particularly interesting is the sulfonic acid substituted polyaniline ( $R = SO_3^-H^+$ ), known as SPAN<sup>55</sup>. This polymer is 'self-doped' since the proton from the substituent sulfonate group is able to protonate the imine nitrogens. However the conductivity is only moderate (ca.  $1-2 \text{ S cm}^{-1}$  in pressed powder pellet form). Typically such substituted polyanilines are synthesised in the same manner as the parent polymer, but using the corresponding aniline monomer (although SPAN is produced by treating EB with fuming  $H_2SO_4$ ). These materials offer enhanced processibility, but unfortunately, when in conducting form display significantly reduced conductivities compared to the unmodified homopolymer. This is thought to be due to the increased steric hindrance of the substituent groups which increase the amount of  $C_6$  ring twisting and hence reduce the amount of  $\pi$ -conjugation.

A recent paper<sup>56</sup> has discussed the use of functionalised protonic acid doping to induce solubility of conducting polyaniline in common non-polar or weakly polar organic solvents. Such functionalised protonic acids are denoted by  $H^+(M^-R)$  where the counterion anionic species ( $M^-$ ) contains the R functional group which is chosen to be compatible with organic solvents. An example is dodecylbenzenesulfonic acid where  $M^- = SO_3^-$  and  $R = -C_6H_4-C_{12}H_{25}$ , with reported solubility in solvents such as toluene, m-cresol and chloroform. However, most of these high molecular weight acids appear to give only modest conductivities. A notable exception is camphor sulfonic acid (CSA) for which films solution cast from m-cresol display conductivities in the range  $200-400 \text{ S cm}^{-1}$ , although such films cannot be stretch aligned. A result of this increased solubility though is that a functionalised polyaniline sample may be soluble in a solvent in which other polymers are also soluble and thus complexes formed. As an

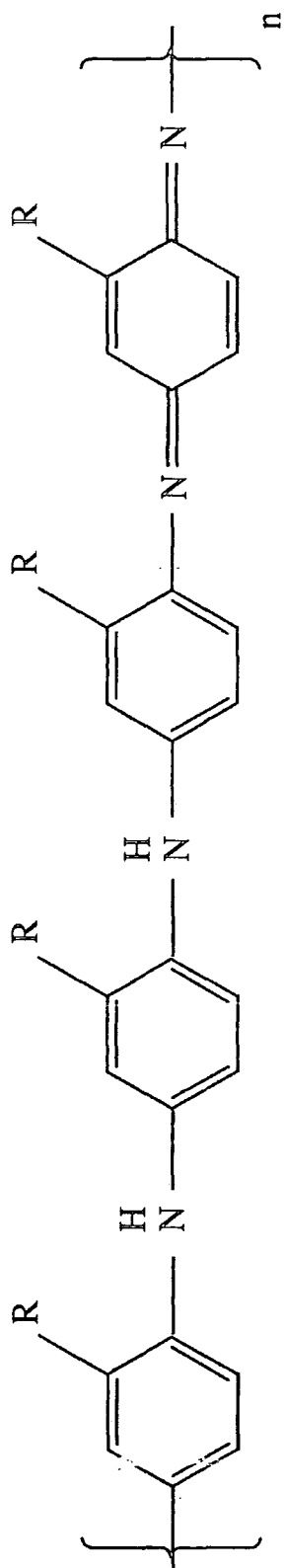


Figure 2.9 General formula for polyaniline derivatives where, for example,  $R = \text{CH}_3, \text{CH}_3\text{O}, \text{C}_2\text{H}_5\text{O}$  or  $\text{SO}_3^-\text{H}^+$ .

example, polyaniline complexed with CSA will dissolve in m-cresol, which is also an excellent solvent for poly(methyl methacrylate) (PMMA). The PMMA/ CSA-polyaniline complex displays remarkable properties in that conductivities of around  $1 \text{ S cm}^{-1}$  are possible using only some 2% of the conducting polyaniline component. Such complexes are hoped to further enhance the potential applications of polyaniline and are starting to become a rather active area of research.

## 2.5 Conductivity

### 2.5.1 Film Doping and Conductivity

The nature of conductivity in polyaniline is different to that in other conducting polymers in that it depends on both the extent of oxidation and also the extent of protonation of the polymer. For the emeraldine oxidation state full doping is achieved when 50% of all of the nitrogens i.e. the imine units become protonated. A variety of protonic acids may be used for this purpose but the most common is aqueous HCl. Chiang and MacDiarmid<sup>19</sup> have investigated the effect of this doping level, as a function of  $[\text{Cl}] / [\text{N}_{\text{total}}]$ , for emeraldine powder samples as a function of conductivity and pH of acid dopant (aqueous HCl). The graph of conductivity versus percentage doping exhibits a percolative behaviour, with the conductivity reaching a saturation point when some 20% of nitrogens are protonated. Similar results have been found for the aqueous HCl doping of NMP cast films<sup>48</sup>. Figure 2.10 shows the derived graph of conductivity versus acid concentration for this latter paper, indicating that for full protonation HCl of about 1M or greater should be used.

The variation of doping level has also induced some interesting results in magnetic studies of polyaniline<sup>57</sup>. Powder and film samples are seen to behave somewhat differently as shown in Figure 2.11. The paramagnetic behaviour of powder samples increases linearly from 0% doping, so indicating defects with spin i.e. polarons are being formed. However, for films no Pauli susceptibility is measured until a doping level of around 20% is reached. This behaviour below 20% doping implies the presence of

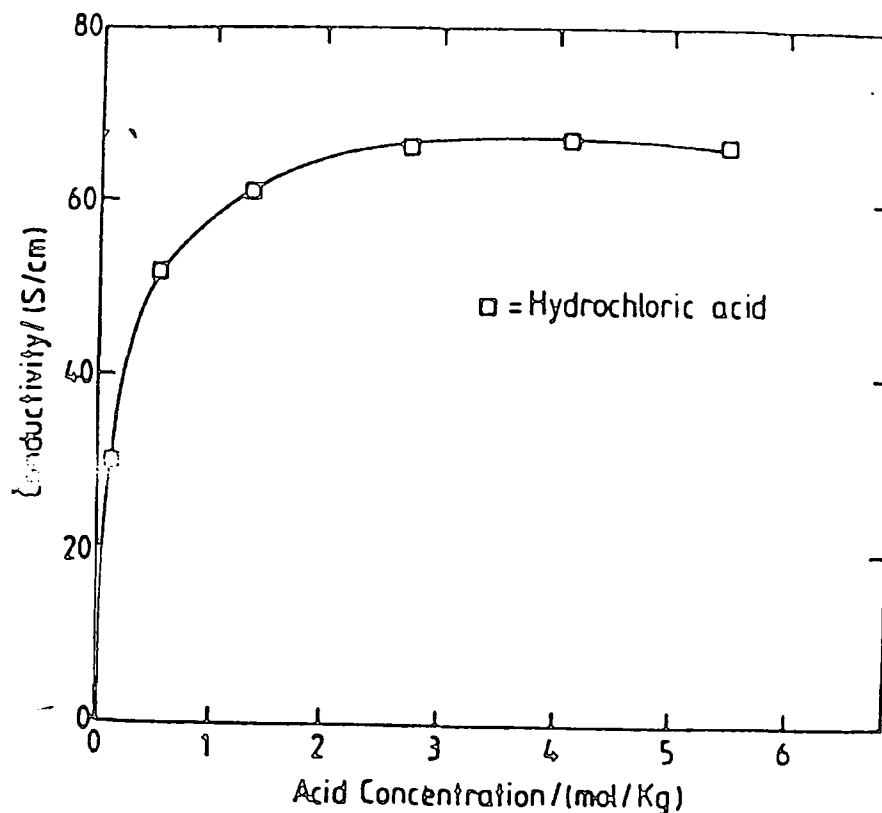


Figure 2.10 Effect of HCl dopant concentration on film conductivity (from Monkman and Adams<sup>47</sup>).

spinless defect states i.e. bipolarons and is proposed to be connected with the sample morphology; unordered regions are protonated first, forming bipolarons and only on completion of this stage are polarons created in the more ordered film regions.

The conductivity behaviour of oriented polyaniline films, when fully protonated in aqueous HCl, has been studied at Durham<sup>47</sup> and is depicted in Figure 2.12. The graph shows conductivity parallel ( $\sigma_{//}$ ) and perpendicular ( $\sigma_{\perp}$ ) to the stretch direction versus elongation measured using the four point probe method. The parallel conductivity increases rapidly above 150% elongation, while that in the perpendicular direction appears to follow a more linear behaviour and only decreases slightly. For a

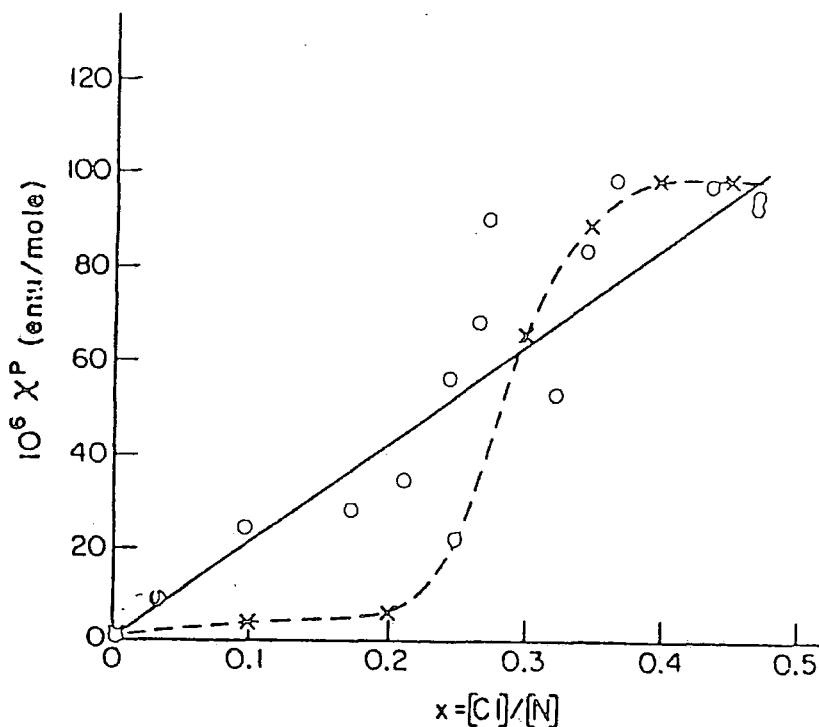


Figure 2.11 The paramagnetic behaviour with doping level for emeraldine powder (o) and film (x) samples (from Jozefowicz *et al*<sup>58</sup>).

film elongated by some 300% the parallel conductivity is about  $350 \text{ S cm}^{-1}$ . The conductivity anisotropy ratio ( $\sigma_{//} / \sigma_{\perp}$ ) as a function of elongation was also measured, see Figure 2.13. Again the anisotropy of these doped, stretched samples is seen to increase rapidly above ca. 150%. This behaviour is similar to that reported for other conducting polymers<sup>58</sup>.

## 2.5.2 Mechanisms of Conduction

The mechanism of charge conduction in polyaniline, in the emeraldine salt form, has been the subject of intensive study. The presence of localised electronic states of energies less than the band gap, including polarons and bipolarons (as discussed in section 2.7) have lead to various conduction

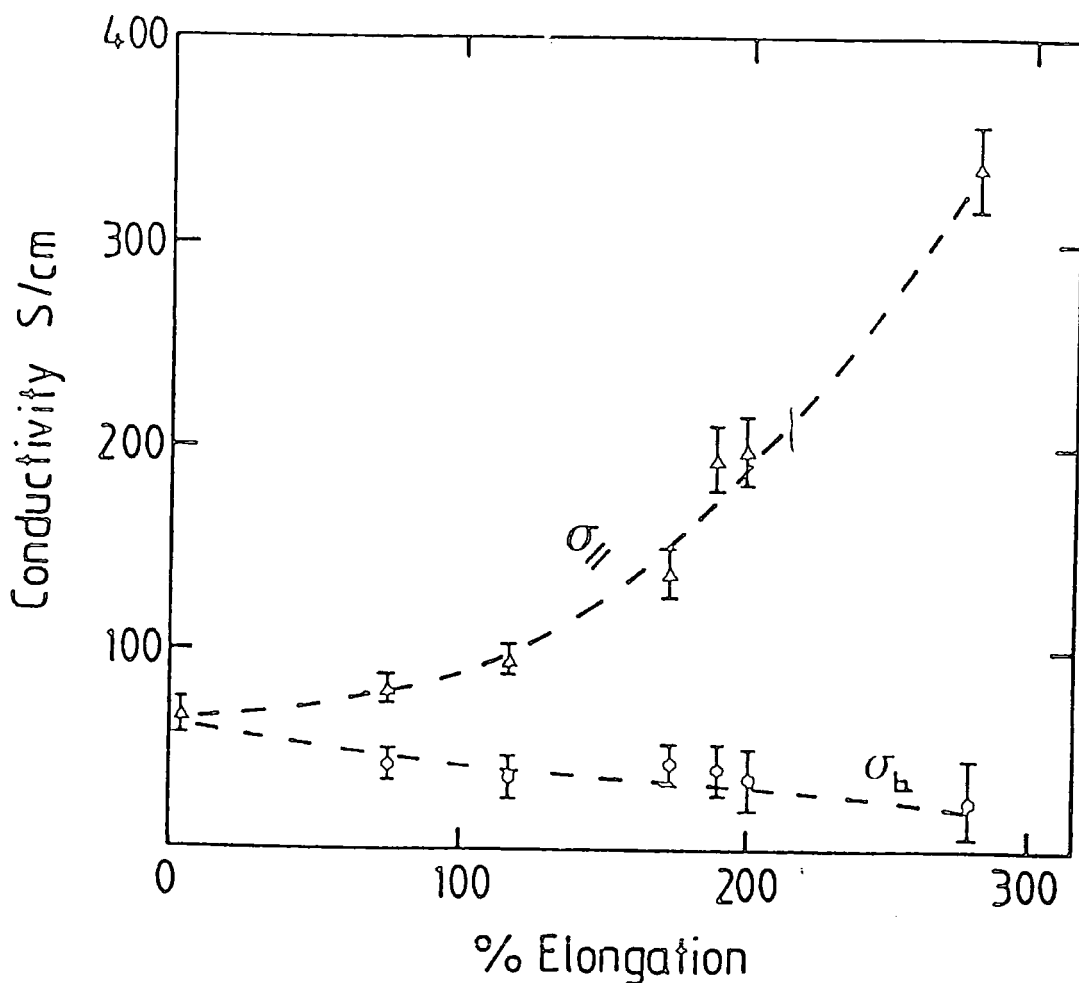
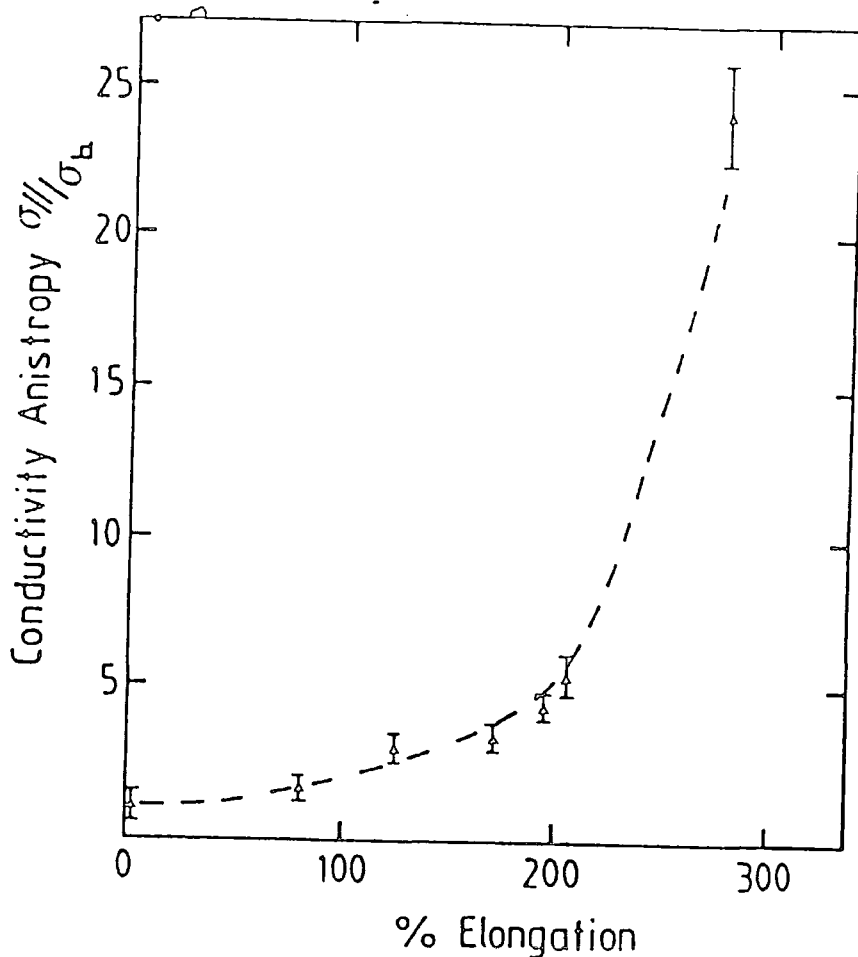


Figure 2.12 Conductivity parallel and perpendicular to the stretch direction as a function of elongation for ES films (from Monkman and Adams<sup>47</sup>).

mechanisms, initially proposed for similar polymer systems such as polyacetylene, being considered and examined. These include variable range hopping<sup>59</sup>, fluctuation induced tunnelling<sup>60</sup>, charge limited tunnelling (CLT)<sup>61</sup> and metallic conductivity. Experimental data has been provided by a variety of physical studies including electric field dependent conductivity<sup>62</sup>, audiofrequency<sup>63</sup> and microwave frequency<sup>64</sup> conductivity, dielectric constant<sup>65</sup> and thermoelectric power studies<sup>62</sup>. Most of these



**Figure 2.13** Dependence of conductivity anisotropy on film elongation (from Monkman and Adams<sup>47</sup>).

investigations were made using electrochemically synthesised powder samples though.

The mechanism most generally seen to fit the experimental data is one involving a granular metal island model invoking CLT<sup>64,66</sup>. Such a model can be inferred from the linear increase of Pauli susceptibility during protonation of emeraldine base powder, as described in the last section. This behaviour may be assigned to a non-homogeneous doping phenomenon

involving the formation of small, completely doped 3-D islands in a matrix of the non-doped polymer. Increasing the doping level, increases the size of the islands and also nucleates new ones. It can be concluded that the intrinsic conductivity within these metal islands, based on a polaronic metal lattice, is substantially higher than the macroscopic bulk conductivity. However, even at maximum levels of doping, the islands are thought to be surrounded by insulating 'beaches' through which CLT occurs, so allowing conduction from one island to another. Theoretical studies were also in agreement with this model<sup>41,67</sup> although it was by no means universally accepted<sup>68</sup>.

More recently though, using free-standing polyaniline films, the interconnection of charge conduction with microscopic structural properties such as crystal structure, coherence, order and chain separation has been realised, particularly with respect to producing highly conducting samples. The temperature dependence of the d.c. conductivity of a stretched emeraldine hydrochloride film from a report by Scherr *et al*<sup>69</sup> is shown in Figure 2.14. Together with other transport data and an initial structural analysis these authors report cigar shaped metallic regions for stretched samples in which electronic states are extended over bundles of chains in crystalline regions. Signs of quasi-1-D variable range hopping are also present though, which are thought to result from hopping in the amorphous regions. These hopping and localisation effects in disordered regions effectively dominate the d.c. conductivity. It is concluded that improved orientation and crystallinity should dramatically increase the conductivity. These results clearly indicate the importance link between the microscopic structure of polyaniline and conductivity. This is a reason why a large part of this project has been to further probe and understand the nature of polyaniline structure on a molecular level, the results of which will no doubt lead to even higher conductivity and also help to elucidate the true charge conduction in the polymer as well.



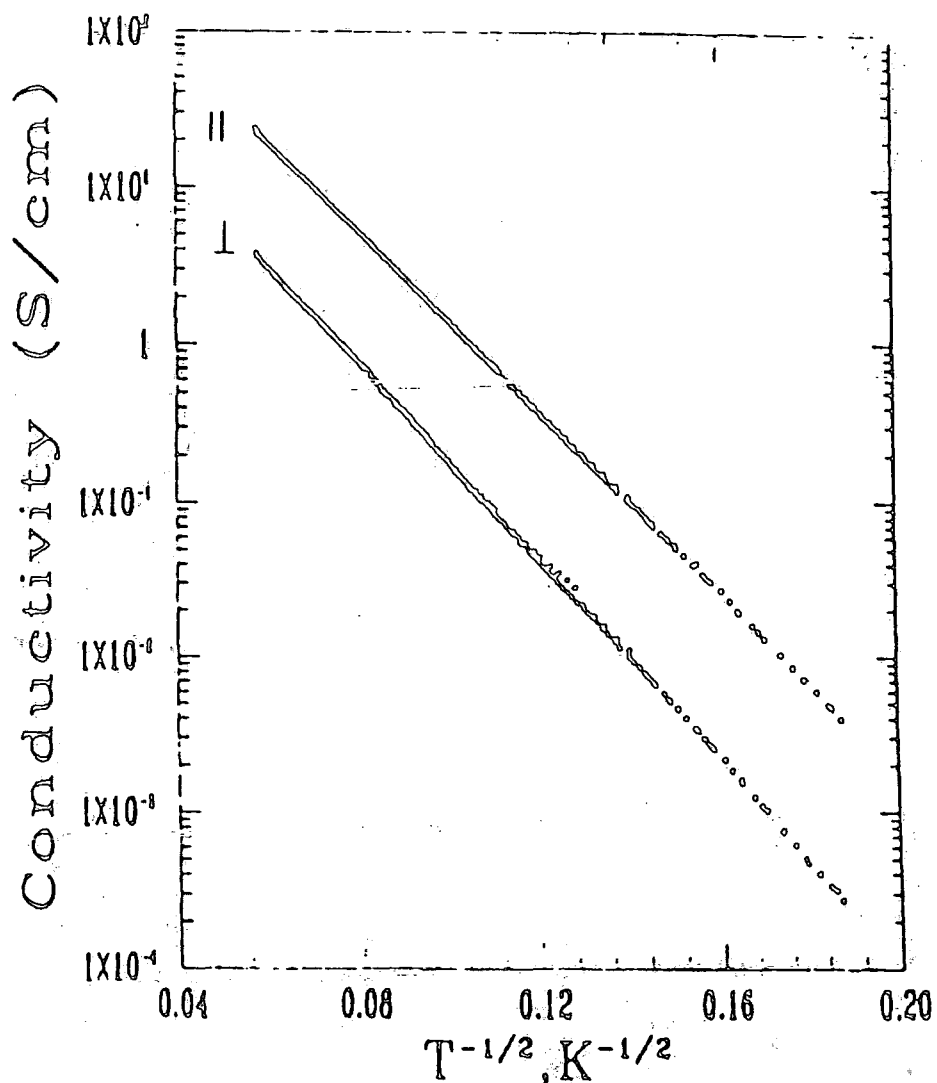


Figure 2.14

Temperature dependence of the d.c. conductivity of a four-fold elongated ES (emeraldine hydrochloride) film (from Scherr *et al* 69).

## 2.6 Electronic Properties

The main experimental tool for investigating the electronic properties of polymers is (transmission) optical spectroscopy. Although, as mentioned previously, free-standing specimens are not suited to this technique and as such optical studies do not form part of this thesis, the electronic states and the nature of charge carriers in polyaniline are of great importance and have been the subject of extensive reports in the literature. Optical spectra have been obtained using ultra-thin film or KBr disc samples and compared with the findings of theoretical studies. The results though are by no means consistent or conclusive, so that there is still much speculation as to the electronic structure of polyaniline. However, these investigations do illustrate the strong interconnection between chemical, geometric and electronic structures for this family of polymers. In particular the role of ring twists and their effect on charge carrier localisation is highlighted.

### 2.6.1 Theoretical Studies

Many reports in the literature have probed the electronic structure of polyaniline, using a variety of quantum-mechanical approaches<sup>42,70-72</sup>. It is important to realise though that the calculations are based on the structures of small oligomers or finite, ordered (i.e. idealised) polyaniline chains. In a recent publication by Bredas<sup>42</sup> a detailed study of the electronic structure of the base forms of polyaniline is presented, based on the optimised oligomeric geometries previously described in section 2.4.2. Figure 2.15 shows the Valence Effective Hamiltonian (VEH) band structures for leucoemeraldine, emeraldine and pernigraniline base, derived by Bredas. The fully reduced LEB is calculated to have a large band gap of 3.8 eV of 'external' (molecular and chemical structure) origin. In the band structure, the upper occupied valence band consists of two branches a and b. The fully oxidised PNB is calculated to have an energy gap of some 1.4 eV which is 'internal' in origin due to a Peierls-type interaction (bond length and ring torsional angle dimerisation). Branch a is the highest occupied and branch b the lowest unoccupied band in the VEH structure.

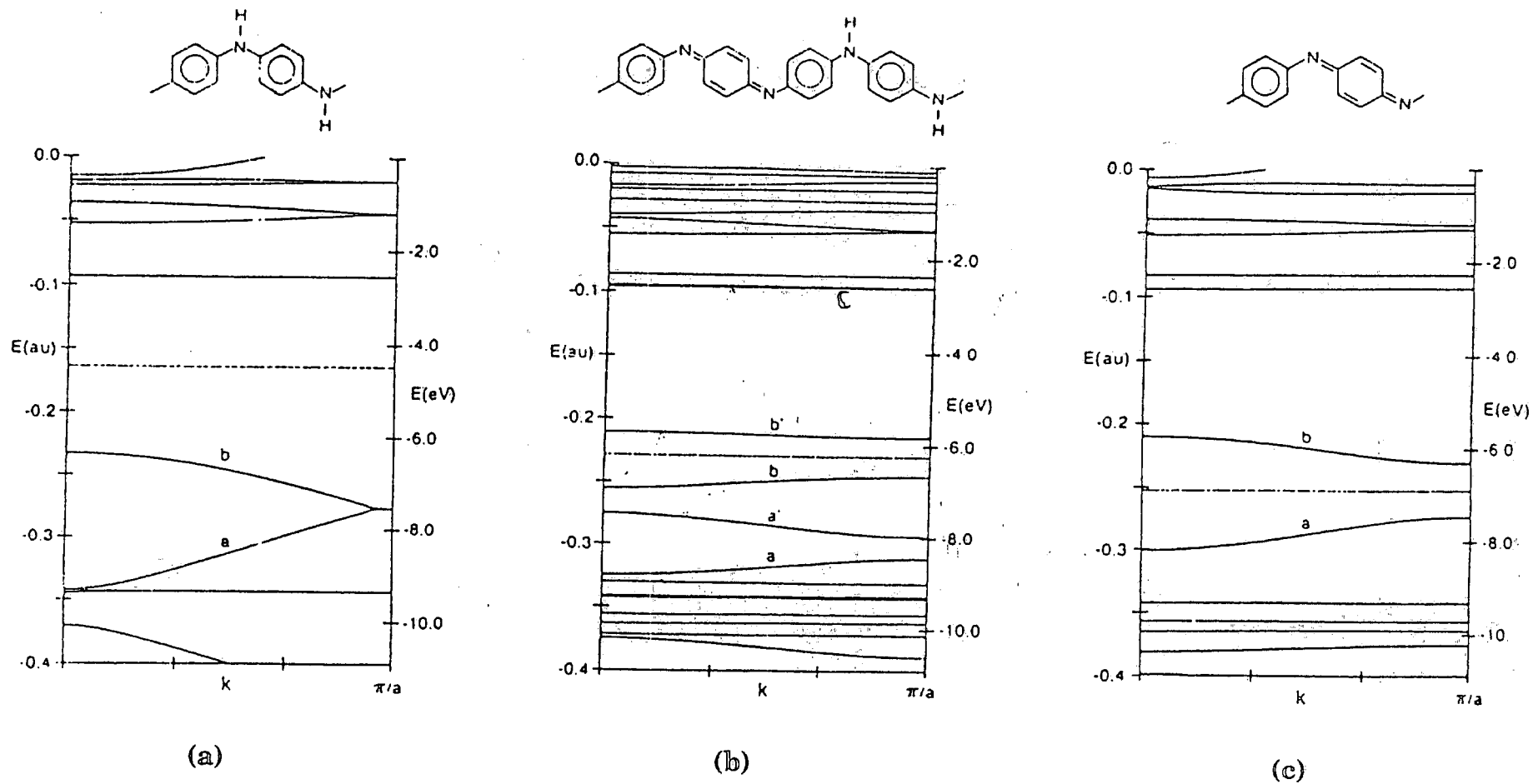
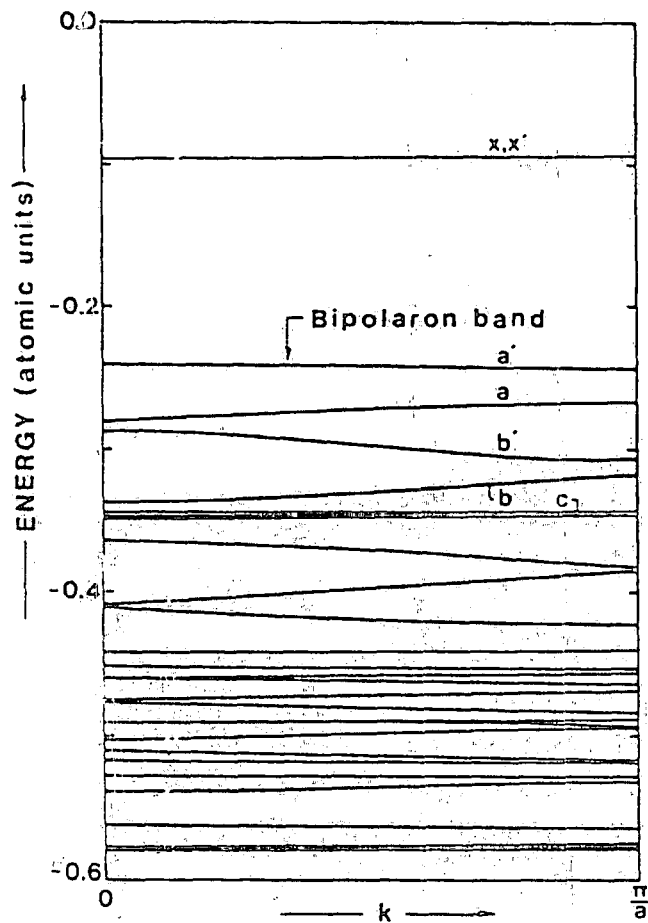


Figure 2.15 VEH band structures for: (a) LEB; (b) EB; (c) PNB (from Bredas<sup>42</sup>).

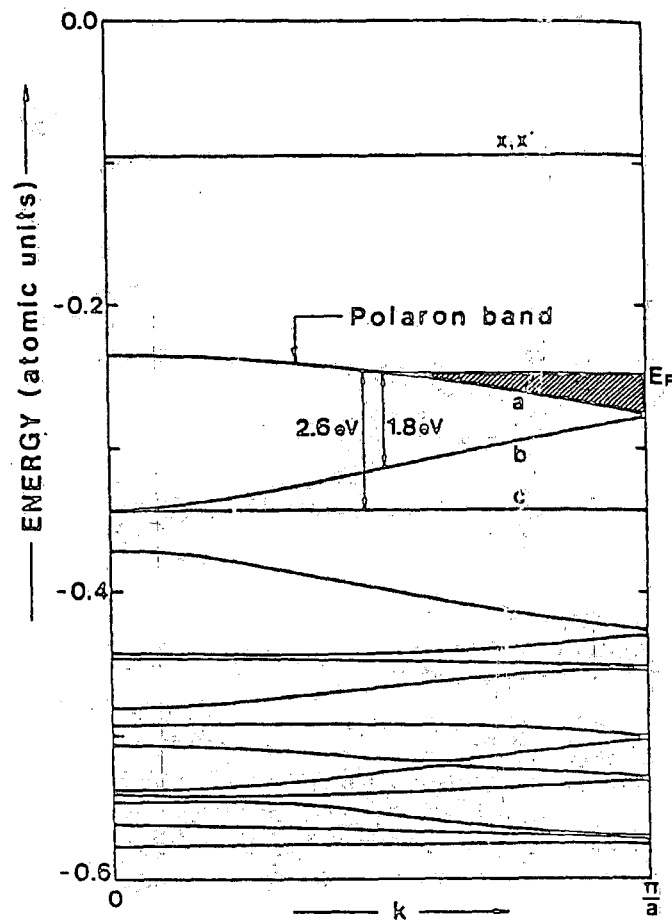
The basic unit cell of EB is twice as large as those of the fully reduced or oxidised forms (four ring units as opposed to two) so that twice as many bands appear in the band structure. The upper occupied band of LEB (branches a and b) split in two for this semi-oxidised state (branches a, a', b and b') with b' being the lowest unoccupied band. A band gap of ca. 1.4 eV (of both 'internal' and 'external' origin) is suggested although other calculations (and indeed experimental results) indicate a larger gap of 3.6 eV, similar to LEB<sup>77</sup>. A feature of this band structure is that while branches a, a' and b are derived from atomic orbitals in the three benzenoid units, branch b', the lowest unoccupied band, is derived from the quinoid ring orbitals. As such there is a difference in localisation between these two sets of bands.

This difference in localisation was first recognised by Duke *et al*<sup>73,74</sup>. These authors describe electronic transitions between the EB bands in terms of molecular conformations, using a simple localised orbital approach based on the  $2p_{\pi}$  atomic orbitals. For instance, in oligomers of aniline a transition of a  $\pi$ -electron between the highest occupied molecular orbital (HOMO) and the lowest unoccupied molecular orbital (LUMO) is observed at ca. 4.3 eV, the  $\pi$ - $\pi^*$  transition. This feature is invariant of chain length and thus may be applied to the parent polymer. Further, the authors have described the transition between bands b and b' (calculated to be ca. 2.2 eV) in terms of a molecular exciton, associated with a quinoid moiety. They predict that excitation of this system causes the quinoid ring to twist  $90^{\circ}$  out-of-plane with respect to the adjacent phenyl rings, thereby causing the localised exciton to be 'self-trapped'.

The electronic structure of 50% protonated emeraldine (ES) has been investigated by Stafstrom *et al*<sup>72</sup> for both bipolaron and polaron lattices. Figure 2.16 shows the calculated VEH band structures, based on optimised geometries of protonated aniline oligomers (ring torsional angles set to  $30^{\circ}$ ). The unit cell of the bipolaron lattice is twice as big as that of the polaron lattice (see Figure 2.4) leading to twice as many bands in the first Brillouin zone. For the former structure a is the highest occupied band and band x the conduction band. The first unoccupied band though is band a', the bipolaron band. For the polaron lattice the half-occupied band a constitutes



(a)



(b)

Figure 2.16

VEH band structures for 50% doped emeraldine in the case of (a) a bipolaron lattice and (b) a polaron lattice (from Stafstrom *et al*<sup>72</sup>).

the polaron band. In both cases, these are the only defect bands in the gap, since the upper defect bands, denoted  $x'$ , are almost degenerate with the conduction band,  $x$ .

All these band structure calculations are based upon optimised geometries, where ring torsional angles have absolute values. However, in reality modifications in these torsional angles may occur due to temperature fluctuations, resulting in modified electronic structures<sup>43</sup>. For emeraldine base though, another important aspect of electronic structure is highlighted by the large extent of conformational complexity along the polymer chain. Such a result may be deduced from <sup>13</sup>C NMR analysis presented later on in this thesis. The many conformations, based on various possible ring geometries along the chain (see Figure 3.4), may alter the proposed band structure presented above quite drastically. Indeed, Galvao *et al*<sup>75</sup>, in a theoretical treatment of polyaniline electronic structure, have realised the importance of disorder along the chain. Furthermore, an undoubted consequence of ring torsional angle disorder will be to increase defect localisation. This latter effect is apparent in photoinduced absorption studies which together with optical spectroscopy are now discussed below.

### 2.6.2 Optical and Photoinduced Absorption Studies

Monkman and Adams<sup>47,76</sup> have presented optical absorption spectra of emeraldine, both in the base and salt forms (fully protonated), using thin films spun onto quartz. The resulting spectra, shown in Figure 2.17, are also typical of other optical studies<sup>72</sup>. The base spectrum shows characteristic absorptions at 360 nm (3.5 eV) and 620 nm (2.0 eV) which are ascribed to a  $\pi$ - $\pi^*$  transition (of the benzenoid rings) and formation of self-trapped excitons on quinoid moieties respectively. The absorption spectrum of the salt form exhibits a metallic behaviour with only a small molecular type of absorption at around 390 nm (3.2 eV) and no sign of the exciton transition. This 390 nm feature has been suggested to arise from protonated benzenoid rings<sup>77</sup>. Also, from around 700 nm (1.8 eV) there is a broad absorption band which is nearly constant in energy down to 2600 nm. Stafstrom *et al*<sup>72</sup> have indicated that their polaron lattice band structure

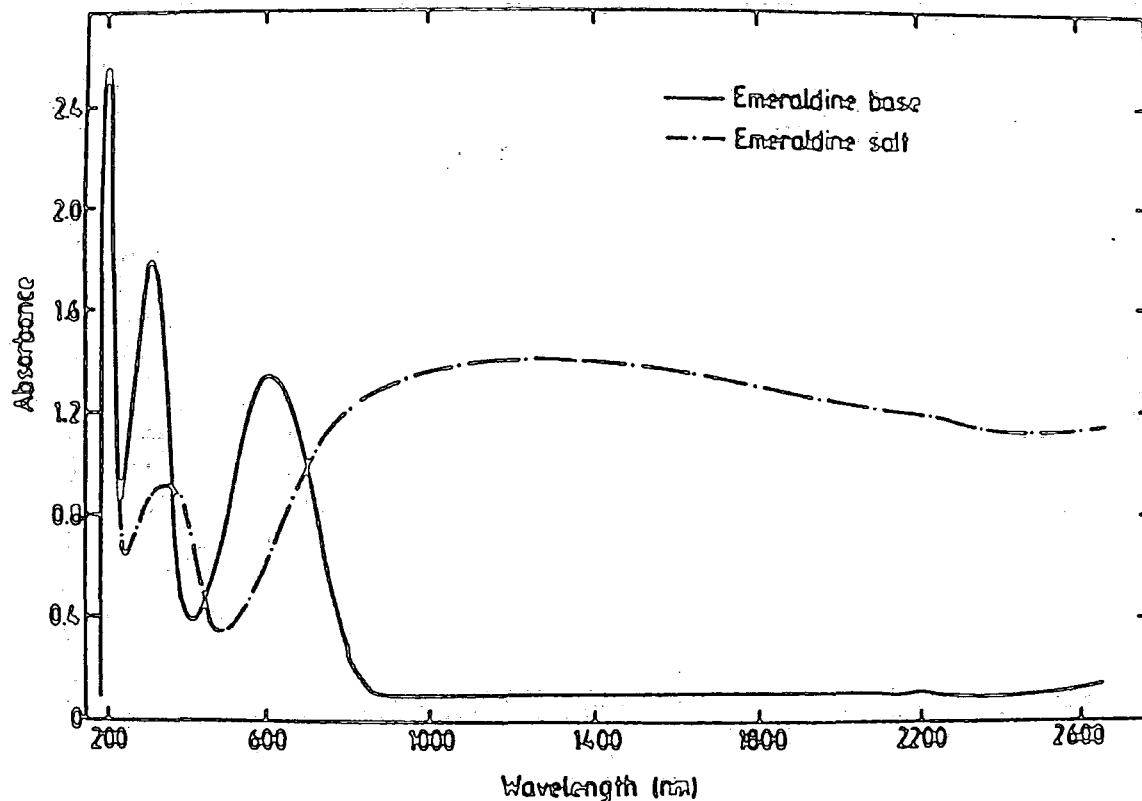


Figure 2.17 Optical absorption spectra of EB and ES spun films on quartz substrates (from Monkman and Adams<sup>76</sup>).

previously described can account for many of the features in an ES optical absorption spectrum, whereas the bipolaron structure cannot. These authors therefore propose that a polaron lattice most readily described the nature of the conducting state of emeraldine.

Despite the fact that free-standing, NMP cast films are unsuitable for transmission optical absorption studies (as they are too thick), Monkman and Adams<sup>47,70</sup> have been able to examine such samples in the optical wavelength regime using a reflection technique. For the base form, reflectance peaks associated with the previously discussed optical transitions are observed. In the salt spectrum metal-like reflectivity is

observed very similar to that of metallic polyacetylene<sup>78</sup>. The onset of high NIR reflectivity occurs at ca. 700 nm with a corresponding plateau region at 2000-2600 nm (maximum reflectivity 30% relative to Al reference). Also observed is a small reflectivity peak at 400 nm, again in accordance with the optical absorption spectrum.

Added to this the authors have also investigated the optical anisotropy in stretch aligned specimens. Figure 2.18 shows the results for a 250% elongated film in base and salt forms. In both cases the optical anisotropy is not as large as the measured electrical anisotropy. However, some interesting features are seen, in particular the difference in reflectivity minima for orthogonal polarisations. This effect is assumed to be due to the preferential alignment of short polyaniline chains.

Recent reports<sup>41,79</sup> have used photoinduced absorption (PA) to probe the electronic structure and defect states in polyaniline. The near-steady-state PA spectrum of EB is discussed for pumping into the  $\pi$ - $\pi^*$  transition at 3.8 eV and into the exciton band near 2.5 eV. The results are very similar, indicating that the same type of defect state is generated in both cases. Figure 2.19 shows the long-lived PA spectrum of the same sample at the two pump energies. In both experiments several photoinduced infrared active vibrational (IRAV) modes are induced as well as a much stronger, broad PA feature at ca. 1.4 eV (ca. 11200  $\text{cm}^{-1}$ ). These IRAV modes are associated with  $\text{C}_6$  ring vibrations and reflect the connection between ring rotations and electronic states in polyaniline. As such the conclusion from this data is that polarons are formed upon photoexcitation, which are strongly localised due to concomitant ring rotations. These charge defect states are also very long-lived since the new chain conformations formed due to ring twisting effectively inhibit recombination or relaxation to the ground state (where the rings are in the most stable conformation). Furthermore, the photoinduced signals are virtually unchanged after many minutes when the sample is held at 80K, see Figure 2.20. This further indicates the importance of ring rotation in charge defect states, in that the rotations are not active at low temperatures and as such recombination is not possible.



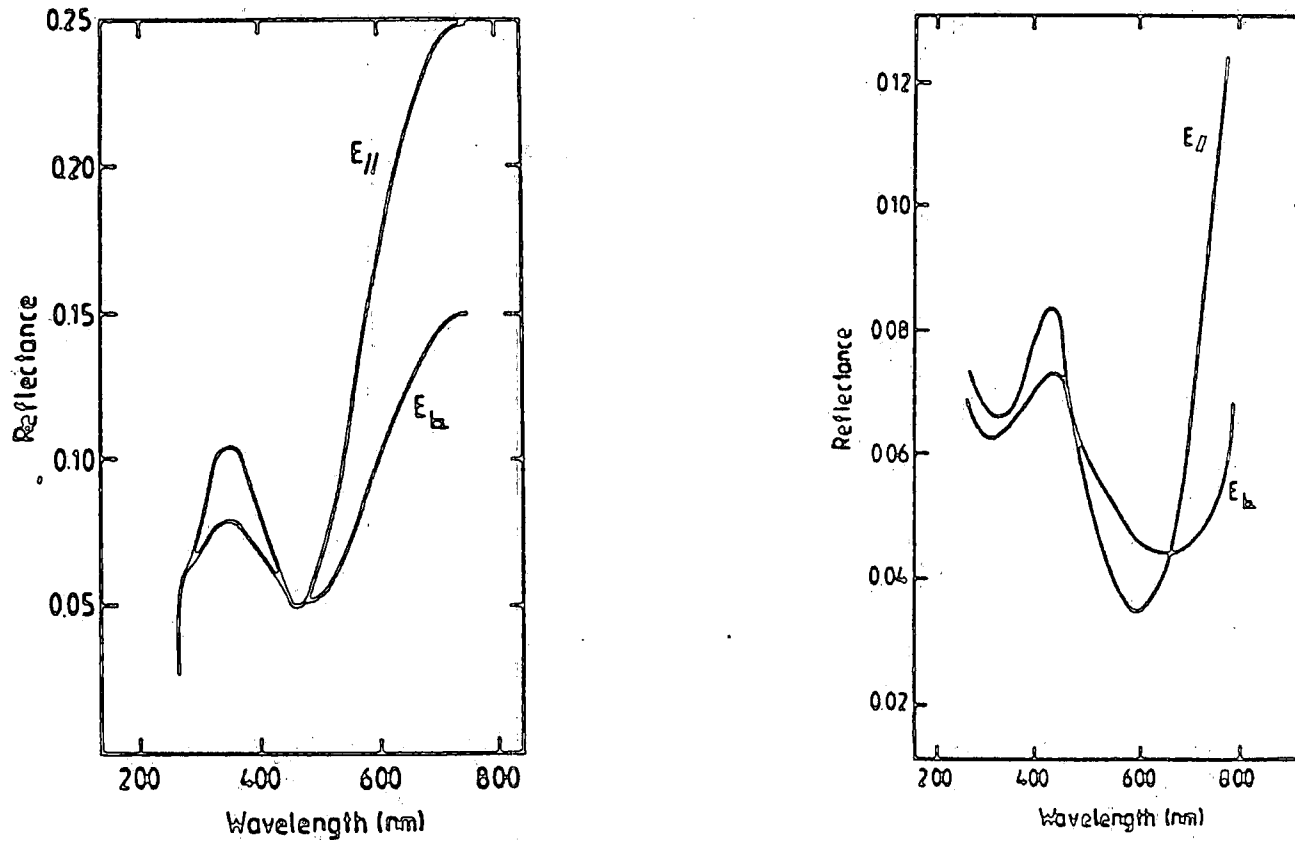


Figure 2.18

Polarised reflectance spectra of an EB (left) and an ES (right) film extended by 250% (from Monkman and Adams<sup>48</sup>).

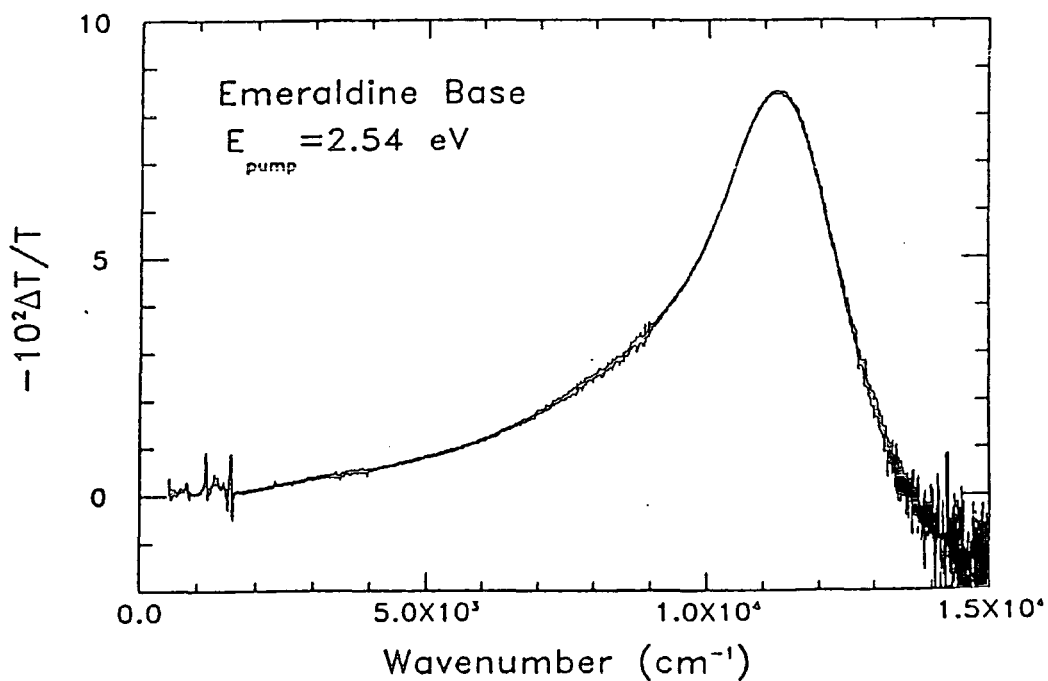
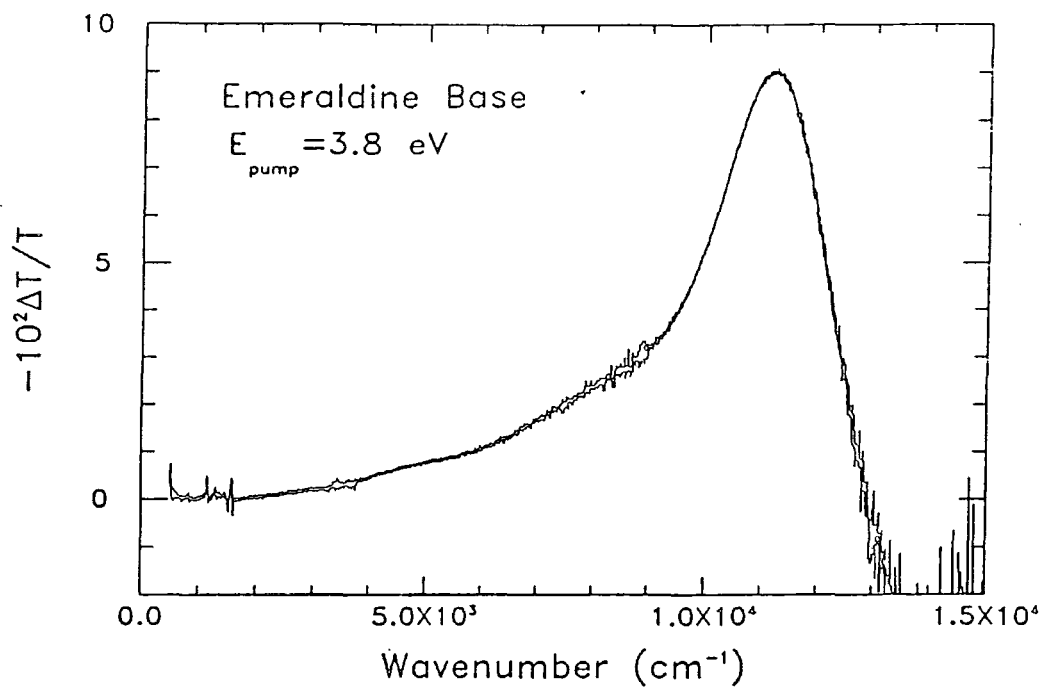
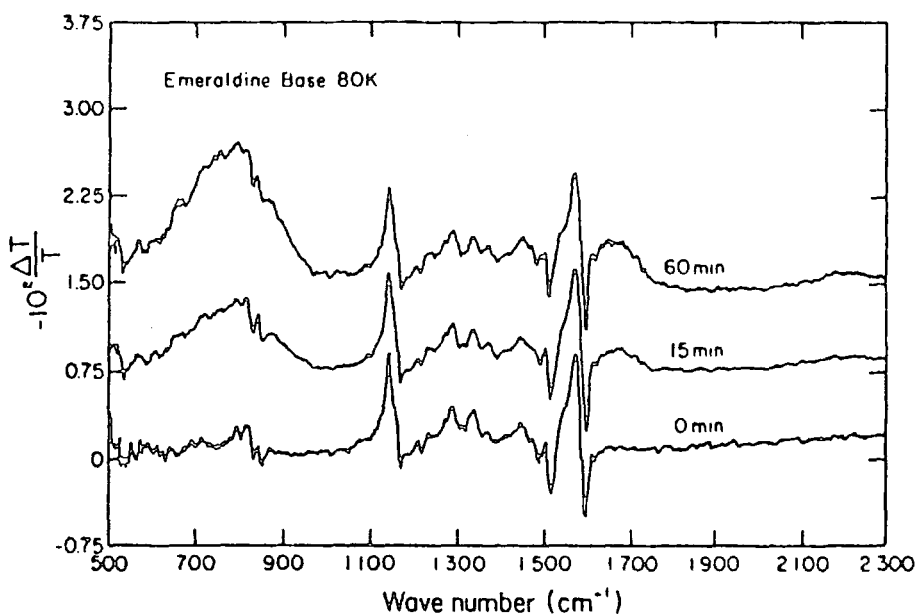
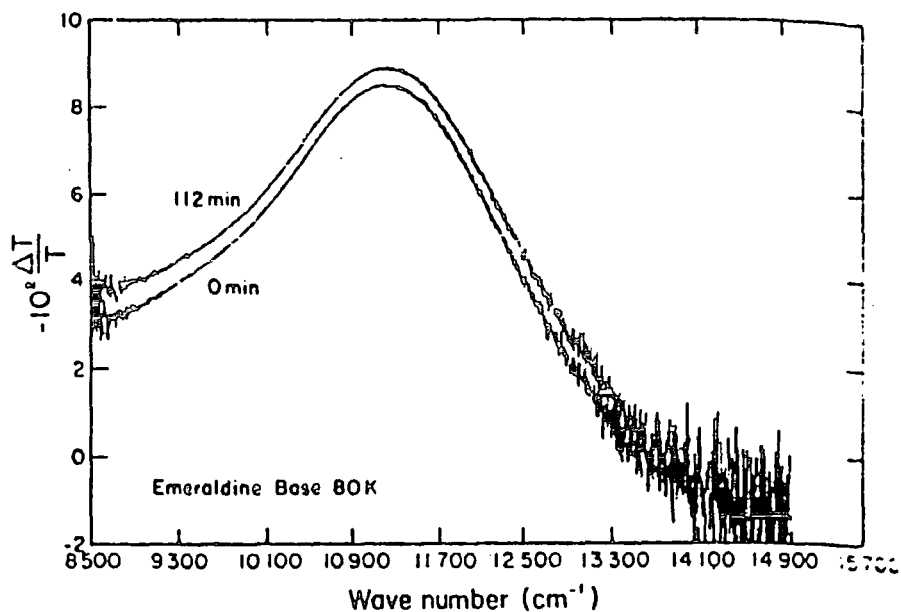


Figure 2.19 Photoinduced absorption spectra (at 80 K) of EB at two different pump energies, as discussed in the text (from McCall *et al*<sup>79</sup>).



(a)



(b)

**Figure 2.20** Photoinduced mid-ir (a) and near-ir (b) absorption spectra of EB at stated times after laser excitation. The larger timescale spectra are offset along the y-axis (from McCall *et al*<sup>79</sup>).

## 2.7 Applications

Undoubtedly the best known potential use for polyaniline is that of an electrode material for rechargeable batteries, first reported by Jozefowicz *et al*<sup>14-16</sup>. Indeed, such a device has been fabricated commercially<sup>80</sup>. Several similar applications have also been suggested based on the electrochemical properties of the material- see, for example, Genies *et al*<sup>81</sup>. In particular the electrochromism exhibited by polyaniline, first reported by Diaz and Logan<sup>17</sup>, raised a great deal of interest in applications as the active element in display devices and optical switches.

A more novel application recently proposed is that of optical data storage, based upon the long-lived photogenerated defect states at low temperatures. The polymer has also recently been patented as the active element in gas sensing devices<sup>82</sup>. Also the conducting state of polyaniline may be utilised in R.F. shielding. For instance, in cable technology such screening is provided by screening layers comprised of a carbon black loaded polyethylene matrix. Since ES is intrinsically a much better conductor than carbon black, the use of polyaniline as the conductive component would allow much financial gain since a much smaller amount would be needed for the same overall conductivity. Indeed the percolative behaviour of various doped polyaniline species has recently become of great interest<sup>56</sup>. With regards to the high conductivity displayed by oriented, doped films the possibility of grinding such samples to provide highly conducting particles which can be dispersed in a host matrix has also been proposed<sup>83</sup>.

The above represent some of the potential applications which have been uncovered to date. However, with the continued keen interest in this challenging polymer many more uses are likely to be reported.

## References

- 1 C.K. Chiang, C.R. Fulcher, Y.W. Park, A.J. Heeger, H. Shirakawa, E.J. Louis, S.C. Gani and A.G. MacDiarmid, *Phys. Rev. Lett.*, **39**, (1977), 1305.
- 2 *Handbook of Conducting Polymers*, Volumes 1 and 2, ed. T. Skotheim, Dekker, New York, 1986.
- 3 *Proceedings of the International Conference on Synthetic Metals*, Kyoto, Japan, *Synth. Met.*, 17-19, (1987).
- 4 A.J. Epstein in *Handbook of Conducting Polymers*, ed. T. Skotheim, Dekker, New York, 1986, Volume 2, p1041.
- 5 H. Naarmann and N. Theophilou, *Synth. Met.*, **22**, (1987), 1.
- 6 N. Theophilou, D.B. Swanson, A.G. MacDiarmid, A. Chakraborty, H.H.S. Javadi, R.P. McCall, F. Zuo, A.P. Treat and A.J. Epstein, *Synth. Met.*, **28**, (1989), 35.
- 7 H. Letherby, *J. Chem. Soc.*, **15**, (1862), 161.
- 8 Lightfoot, *Br. Patent*, **151**, (1863).
- 9 T. Yasin, *Bull. Chem. Soc. Jpn.*, **10**, (1935), 306.
- 10 J.J. Coquillon, *Compt. Rend.*, **81**, (1875), 408; **82**, (1876), 228.
- 11 R. Willstatter and S. Dorogi, *Ber.*, **42**, (1909), 4118.
- 12 A.G. Green and A.E. Woodhead, *J. Chem. Soc. Trans.*, **97**, (1910), 2388.
- 13 A.G. Green and A.E. Woodhead, *J. Chem. Soc. Trans.*, **101**, (1910), 1117.
- 14 P. Constantini, G. Belorgey, M. Jozefowicz and R. Buvet, *Comm. Symp. Int. Chim. Macromol. IUPAC*, Prague 1965, A. 481
- 15 M. Doriomedoff, F.H. Cristofini, R. De Surville, M. Jozefowicz, L.T. Yu, and R. Buvet, *J. Chim. Phys.*, **68**, (1971), 1055.
- 16 M. Jozefowicz, L.T. Yu, G Belorgey, and R. Buvet, *J. Polym. Sci. C*, **16**, (1967), 2931.
- 17 A.F. Diaz and J.A. Logan, *J. Electroanal. Chem.*, **11**, (1980), 11.
- 18 A.G. MacDiarmid, J-C, Chaing, M. Halpern, W.S. Huang, S.L. Mu, N.L.D. Somasisi, W.Wu and S.I. Yaniger, *Mol. Cryst. Liq. Cryst.*, **121**, (1985), 173.
- 19 A.G. MacDiarmid, N.L.D. Somasisi, W.R. Salaneck, I. Lundstrom, B. Liedberg, M.A. Hasan, R. Erlandsson and P. Konrasson, *Springer*

- Series in Solid State Sciences*, Volume 63, Springer, Berlin, 1985, p.218.
- 20 J-C. Chiang and A.G. MacDiarmid, *Synth. Met.*, **13**, (1986), 193.
- 21 L.T. Yu, M.S. Borredon, M. Jozefowicz, G. Belorgey and R. Buvet, *J. Polym. Sci.*, **10**, (1987), 2931.
- 22 S.P. Armes and J.F. Miller, *Synth. Met.*, **20**, (1987), 365.
- 23 A.P. Monkman, *thesis*, University of London, 1989.
- 24 D.M. Mohilner, R.N. Adams and W.J. Argersinger, *J. Am. Chem. Soc.*, **84**, (1962), 3618.
- 25 J. Bacon and R.N. Adams, *J. Am. Chem. Soc.*, **90**, (1968), 6596.
- 26 F. Wudl, R.O. Angus Jr., F.L. Lu, P.M. Allemand, D.J. Vachon, M. Nowak, Z.X. Liu and A.J. Heeger, *J. Am. Chem. Soc.*, **109**, (1987), 3677.
- 27 D. Vachon, R.O. Angus Jr., F.L. Lu, M. Nowak, H. Schaffer, F. Wudl and A.J. Heeger, *Synth. Met.*, **18**, (1987), 297.
- 28 M. Millard, *Synthesis of Organic Films in Plasmas* in J.R. Hollohan and T Bell (eds.), *Techniques and Applications of Plasma Chemistry*, Wiley, New York, Ch. 5, 1974.
- 29 K. Uvdal, M. Loglund, P. Danneton, L. Bertilsson, S. Strafstrom, W.R. Salaneck, A.G. MacDiarmid, A. Ray, E.M. Scherr, T. Hjertberg and A.J. Epstein, *Synth. Met.*, **29**, (1989), E451.
- 30 E.M. Genies, C. Tsintavis and A.A. Syed, *Mol. Cryst. Liq. Cryst.*, **121**, (1985), 181.
- 31 S.K. Manohar, A.G. MacDiarmid and A.J. Epstein, *Synth. Met.*, **41-43**, (1991), 711.
- 32 L.W. Schaklette, J.F. Wolf, S. Gould and R.H. Baughman, *J. Chem. Phys.*, **88**, (1988), 3955.
- 33 R.H. Baughman, J.F. Wolf, H. Eckhardt and L.W. Schaklette, *Synth. Met.*, **25**, (1988), 121.
- 34 A.G. MacDiarmid, J-C. Chiang, A.F. Richter, N.L.D. Somasiri and A.J. Epstein, *Conducting Polymers*, p.105 ed. L Acaer, D. Reidel Pub. Co. (1987).
- 35 Y. Furakawa, F. Ueda, Y. Hyodo, I. Harada, T. Nakajima and T. Kawayoe, *Macromolecules*, **21**, (1989), 1297.
- 36 T. Ohsaka, Y. Ohnuki, N. Oyama, G. Katagiri and K. Kamisaka, *J. Electroanal. Chem.*, **161**, (1984), 399.

- 37 A. Ray, G.E. Asturias, D.L. Kerschner, A.F. Richter, A.G. MacDiarmid and A.J. Epstein, *Synth. Met.*, **29**, (1989), E243.
- 38 J.M. Ginder, A.F. Richter, A.G. MacDiarmid and A.J. Epstein, *Solid State Commun.*, **63**, (1987), 67.
- 39 G. Wnek, *Synth. Met.*, **16**, (1986), 213.
- 40 J. L. Bredas in *Proceedings of the Nobel Symposium on Conjugated Polymers and Related Materials*, ed. W. R. Salaneck, Oxford University Press, 1992.
- 41 A. J. Epstein, R. P. McCall, J. M. Ginder and A. G. MacDiarmid, in *Spectroscopy of Advanced Materials*, Volume 19, eds. R. J. H. Clark and R. E. Hester, John Wiley and Sons Ltd, 1991, pp 355-392.
- 42 M. Angelopoulos, G.E. Asturias, S.P. Ermar, A. Ray, E.M. Scherr, A.G. MacDiarmid, M. Akhtar, Z. Kiss and A.J. Epstein, *Mol. Cryst. Liq. Cryst*, **160**, (1988), 151.
- 43 M. Angelopoulos, A. Ray, A.G. MacDiarmid and A.J. Epstein, *Synth. Met.*, **21**, (1987), 21.
- 44 A.P. Monkman and P. Adams, *Synth. Met.*, **40**, (1991), 87.
- 45 M. Scully, M.Sc thesis, University of Durham, 1993.
- 46 K.R. Cromack, M.E. Jozefowicz, J.M. Ginder, R.P. McCall, A.J. Epstein, E.M. Scherr and A.G. MacDiarmid, *Bull. Am. Chem. Soc.*, **24**, (1989), 583.
- 47 A.P. Monkman and P. Adams, *Synth. Met.*, **41-43**, (1991), 627.
- 48 K. R. Kromack, M. E. Jozefowicz, J. M. Ginder, A. J. Epstein, R. P. McCall, G. Du, J. M. Leng, K. Kim, C. Li, Z. H. Wang, M. A. Druy, P. J. Glatkowski, E. M. Scherr and A. G. MacDiarmid, *Macromolecules*, **24**, (1991), 4157.
- 49 P. Laughlin, University of Durham, unpublished observations.
- 50 A. Andreatta, Y. Cao, J-C Chiang, A.J. Heeger and P. Smith, *Synth. Met.*, **26**, (1988), 383.
- 51 M. Angelopoulos, A. Ray, A.G. MacDiarmid and A.J. Epstein, *Synth. Met.*, **21**, (1987), 21 .
- 52 S. Wang, F. Wang, and X. Ge, *Synth. Met.*, **16**, (1986), 69.
- 53 Y. Wei, W.W. Focke, G.E. Wnek, A.Ray and A.G. MacDiarmid, *J. Chem. Phys.*, **93**, (1989), 495.
- 54 S.K. Manohar, A.G. MacDiarmid and A.J. Epstein, *Bull. Am. Phys. Soc.*, **34**, (1989), 583.

- 55 J. Yue and A.J. Epstein, *J. Am. Chem. Soc.*, **109**, (1990), 2800.
- 56 Y. Cao, P. Smith and A. J. Heeger, *Synth. Met.*, **48**, (1992), 91.
- 57 M.E. Jozefowicz, R. Laversanne, H.H.S. Javadi, A.J. Epstein, J.P. Pouget, X. Tang and A.G. MacDiarmid, *Phys. Rev. B*, **39**, (1989), 12958.
- 58 A.J. Heeger, *Synth. Met.*, **41-43**, (1991), 1027.
- 59 N.F. Mott and E.A. Davies, *Electronic Properties of Non-Crystalline Materials*, Clarendon Press, Oxford, 1979.
- 60 P. Sheng, *Phys. Rev. B*, **21**, (1980), 2180.
- 61 B. Ables, P. Sheng, M.D. Coutts and Y. Arie, *Adv. in Phys.*, **24**, (1975), 407.
- 62 F. Zuo, M. Angelopoulos, A.G. MacDiarmid and A.J. Epstein, *Phys. Rev. B*, **36**, (1987), 3475.
- 63 F. Zuo, M. Angelopoulos, A.G. MacDiarmid and A.J. Epstein, *Phys. Rev. B*, **39**, (1989), 3570.
- 64 H.H.S. Javadi, K.R. Cromack, A.G. MacDiarmid and A.J. Epstein, *Phys. Rev. B*, **39**, (1989), 3579.
- 65 R.P. McCall, M.G. Roe, J.M. Ginder, T. Kusumoto, A.J. Epstein, G.E. Austrias, E.M. Scherr and A.G. MacDiarmid, *Synth. Met.*, **29**, (1989), E433.
- 66 A.J. Epstein and A. G. MacDiarmid, in *Electronic Properties of Conjugated Polymers*, eds. H. Kuzmany, M. Mehring and S. Roth, Springer-Verlag, Berlin, 1989.
- 67 P. Phillips and H-L. Wu, *Science*, **252**, (1991), 1805.
- 68 A. Litzelmann, B. Scherrer, J. Fink, K. Meerholz, J. Heinze, N.S. Saricitci and H. Kuzmany, *Synth. Met.*, **29**, (1989), E313.
- 69 E. M. Scherr, A. G. MacDiarmid, S. K. Manohar, J. G. Masters, Y. Sun, X. Tang, M. A. Druy, P. J. Glatkowski, V. B. Cajipe, J. E. Fischer, K. R. Kromack, M. E. Jozefowicz, J. M. Ginder, R. P. McCall and A. J. Epstein, *Synth. Met.*, **41-43**, (1991), 735.
- 70 S. Stafstrom and J.L. Bredas, *Synth. Met.*, **14**, (1986), 297.
- 71 D.S. Boudreaux, R.R. Chance, J.F. Wolf, L.W. Schaklette, J.L. Bredas, B. Themans, J.M. Andre and R. Silberg, *J. Chem. Phys.*, **85**, (1986), 4584.
- 72 S. Stafstrom, J.L. Bredas, A.J. Epstein, H.S. Woo, D.B. Tanner, W.S. Huang and A.G. MacDiarmid, *Phys. Rev. Lett.*, **59**, (1987), 1464.



- 73 C.B. Duke, E.M. Conwell and A. Paton, *Chem. Phys. Lett.*, 131, (1988), 42.
- 74 C.B. Duke, A. Paton, E.M. Conwell, W.R. Salaneck and I. Lundstrom, *J. Chem. Phys.*, 88, (1987), 3414.
- 75 D.S. Galvao, P.A. dos Santos, B. Laks, C.P. de Melo and M.J. Caldas, *Phys. Rev. Lett.*, 63, (1989), 786.
- 76 A.P. Monkman and P. Adams, *Solid State Comm.*, 78, (1991), 29.
- 77 A.P. Monkman in *Conjugated Polymeric Materials*, eds. J.L. Bredas and R.R. Chance, NATO ASI Series E: Applied Physics Volume 182, Kluwer Academic Press, 1990, p273.
- 78 G. Leisling, *Synth. Met.*, 28, (1989), D215.
- 79 R.P. McCall, J.M. Ginder, M.G. Roe, G.E. Asturias, E.M. Scherr, A.G. MacDiarmid and A.J. Epstein, *Phys. Rev. B*, 39, (1989), 10174.
- 80 T. Nakajima and T. Kawagoe, *Synth. Met.*, 28, (1989), C629
- 81 E.M. Genies, A. Boyle, M. Lapkowski and C. Tsintavis, *Synth. Met.*, 36, (1990), 139.
- 82 N.E Agbor, M.C. Petty, M. Scully and A.P. Monkman, UK Patent No. 9300560.1, 1993.
- 83 S.R. Rowland, BICC Cables Ltd, personal communication.

## Chapter 3

### Synthesis and Processing Procedures

#### 3.1 Introduction

This chapter describes the preparation and production of various polyaniline samples used for the experimental analyses described in the remaining chapters of this thesis. First of all, the synthesis of emeraldine base polyaniline is discussed and then a number of important techniques are reported which have analysed the product of this synthesis route. The latter sections then deal with the fabrication of free-standing films and in particular with the uniaxial stretch alignment procedure used to orient such samples. Finally, some aspects of the conducting nature of polyaniline films are considered.

#### 3.2 Chemical Synthesis of Polyaniline

In this work polyaniline was chemically synthesised as follows:

12.96g (0.1mol) of aniline hydrochloride (Aldrich Chemical Co.) was dissolved, with stirring in a beaker, in 100ml of doubly deionised, Millipore water. In a separate beaker, 22.82g (0.1 mol) of ammonium persulfate (Aldrich Chemical Co.) was dissolved in 60 ml of the Millipore water. The persulfate oxidant was then added to the acidic aniline solution, at room temperature with constant stirring, using a multistep addition method, 6ml aliquots every 30 mins. Upon oxidant addition the mixture turns a dark blue/green colour and is observed to be slightly exothermic for a few minutes. Having completed the addition after  $4\frac{1}{2}$  hrs, the reaction mixture was then left to stir for an additional 20 hrs. After this stage, the mixture was filtered using a Buchner funnel (Whatman No. 3 filter paper) and washed with 2 quantities of 100ml of water, so as to remove any impurities. The filter cake was then added to 100ml of 35% ammonia solution and allowed to stir for no less than 4 hrs before being refiltered. The product was

then repeatedly washed with water and finally isopropanol, typically 2 x 100mls. At this point the filtrate was colourless. Finally the filter cake was dried under vacuum at 70°C for 24 hrs to give a brown/purple product, emeraldine base, with a typical yield of 80-85%. The powder was then finely ground using a pestle and mortar and stored in an air-tight container ready for further use.

This synthesis route has been specifically developed by the group at Durham and is a modified version of that given by Angelopolous *et al*<sup>1</sup>. The main alteration is in the way the oxidant is added to the acidic aniline solution. Most methods incorporate a single step addition in which the oxidant is added instantaneously or, at best, in a dropwise process over about 30 mins. However, since the reaction is very exothermic we have observed large increases in temperature, even up to 80°C, during a single step addition. This is not a desirable effect as it increases the likelihood of detrimental parallel reactions. Indeed, we have found the product of a single step oxidant addition procedure to have far inferior properties, in terms of molecular weight and amount of defects, to that prepared by the method given above. By gradually adding the oxidant though, in small amounts every 30 mins, the temperature rise due to the exothermic nature of the reaction may be minimised (typically no more than 7°C for each addition). This has been found to produce a material with much improved properties, as discussed below.

### **3.3 Analysis of Chemical Composition**

The synthesis of a polymer such as polyaniline is normally quite a trivial procedure, simply involving following a documented experimental method. But what hard evidence is there to support the assumption that the product is what you think it is? The answer to this question, all too frequently, is very little if any at all. Rather unfortunately, a prime example of this lack of care towards sample preparation can be found in studies of polyaniline. Furthermore, the only outcome of such an approach can be a large disparity between interpretation and conclusions, due to the poor and often false assumptions as to the nature of the material. The varied and often

contradictory experimental results reported for polyaniline are wholly testament to this argument.

To avoid falling into this trap, a series of experiments have been performed so as to assess the composition of the emeraldine base powder used in these studies. These experiments have probed both chemical structure and molecular weight, the two facets of polymer composition which affect, either directly or indirectly, all aspects of a material's properties. They are, therefore, of fundamental importance and clearly must be analysed and understood before any meaningful interpretation can be derived from further experimental data.

### 3.3.1 Chemical Structure

One of the most simple and routine test of chemical composition is elemental analysis. For a batch of polyaniline, prepared as described in Section 3.2, a typical result is carbon, 75.97 wt%; nitrogen, 14.56%; hydrogen, 4.99 wt%. These values are in good agreement with the theoretical elemental composition (carbon, 79.56 wt%; nitrogen, 15.47 wt%; hydrogen, 4.97 wt%), calculated from the ideal EB repeat unit of Figure 2.4(b). However, small amounts of chlorine (0.50 wt%) and sulphur (0.38 wt%) can also be detected. The remaining 4.69 wt%, which cannot be accounted for, is ascribed to oxygen. These 'contaminants' are normally found in the products of such preparation and in this case remain largely unchanged by attempts to wash them out. This suggest that they may be associated with defects on the polymer backbone.

Another analysis technique which has been used to give more detailed structural information is solution-state  $^{13}\text{C}$  nuclear magnetic resonance (NMR). The results of this work have highlighted some very important aspects of polyaniline chain structure and have also been reported in a recent publication<sup>2</sup>. The technique utilises the solubility of polyaniline (EB) in the solvent NMP to give high quality spectra, with significantly greater resolution than that seen in solid-state  $^{13}\text{C}$  and  $^{15}\text{N}$  NMR studies<sup>3-5</sup>. This, in turn, allows a much greater insight into the possible structures present.

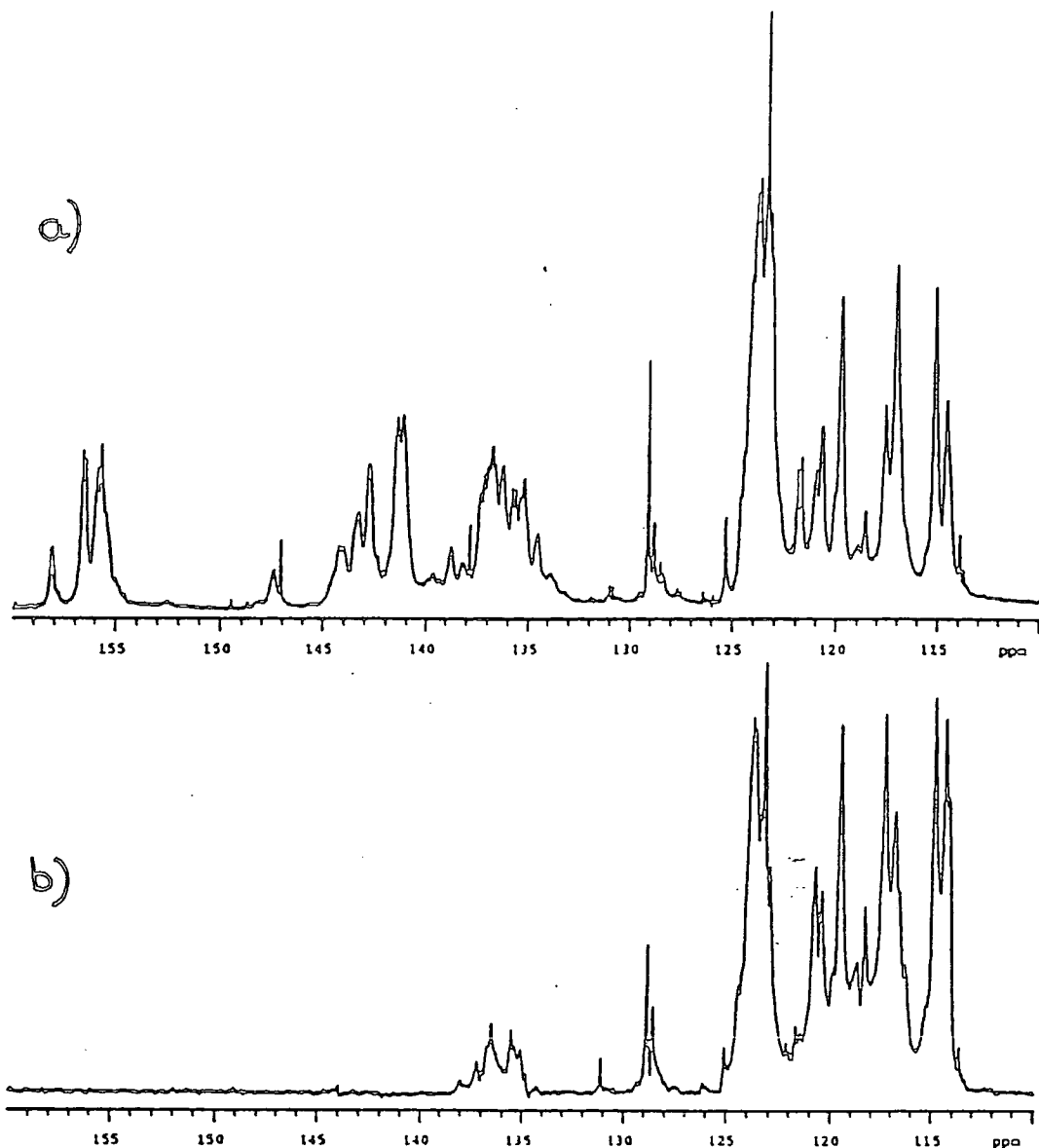


Figure 3.1 Proton-decoupled  $^{13}\text{C}$  (a) and d.e.p.t.-90 (b) NMR spectrum for an 'as-made' EB (10 wt% in NMP) sample.

A proton-decoupled  $^{13}\text{C}$  and a d.e.p.t.-90 (distortionless enhancement by polarisation transfer)<sup>6</sup> spectrum are shown in Figure 3.1 for an 'as-made' EB sample (10 wt% solution in NMP). The latter technique selects only those carbons having one directly bonded proton, thus aiding identification. Thus the quaternary carbons (i.e. those with no attached proton groups) can be readily identified. While peaks occur in all the spectral regions than would be expected from the postulated EB structure, it is also evident that the

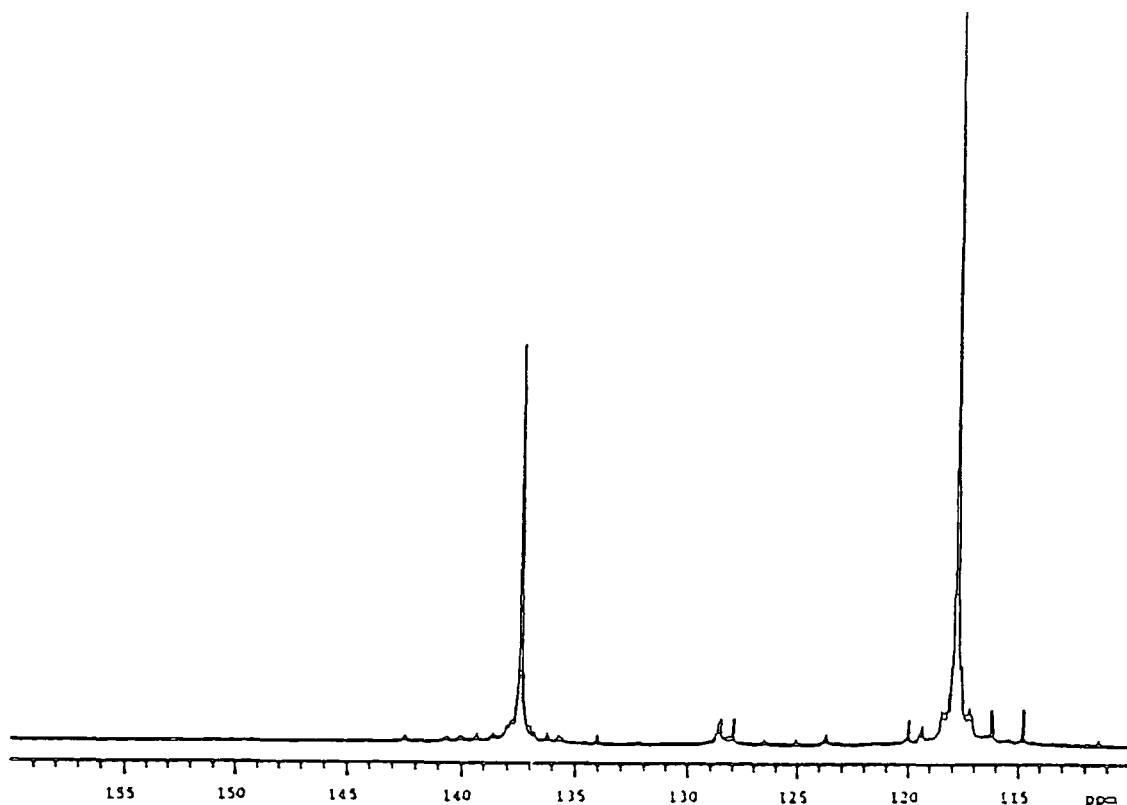


Figure 3.2 Proton-decoupled  $^{13}\text{C}$  NMR spectrum of LEB.

spectra are a great deal more complicated that might have been expected from consideration of the structure as illustrated in Figure 2.4(b).

The next step, therefore, was to examine a solution of the fully reduced LEB form of polyaniline, which has a much simpler repeat unit. This sample was prepared by reduction of EB (in NMP) with phenyl hydrazine followed by slow addition of toluene to precipitate the leucoemeraldine. The procedure was carried out in a nitrogen atmosphere glove-box so as to avoid sample oxidation. A  $^{13}\text{C}$  spectrum for this material is shown in Figure 3.2 and exhibits just two major features at 117.84 and 137.44 ppm (note that there are few minor peaks in the baseline, but these are likely associated with the ca. 5 wt% of 'contaminants' in the original EB material). Under quantitative conditions the intensity ratio of this two peaks is 2:1, and furthermore they account for greater than 95% of the total intensity.

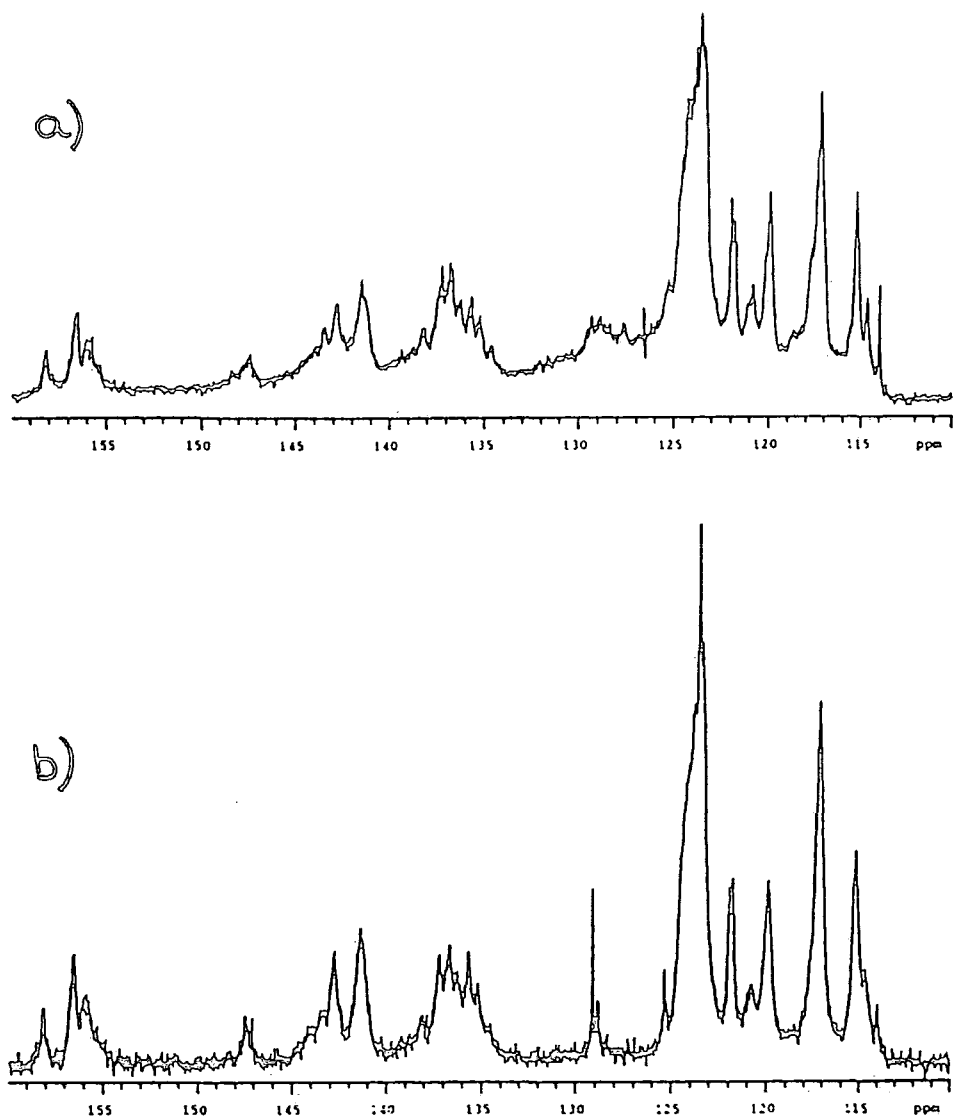


Figure 3.3 Comparison of EB proton-decoupled  $^{13}\text{C}$  spectra: (a) reoxidised from LEB; (b) 'as-made'.

account for greater than 95% of the total intensity. Using a d.e.p.t-90 sequence only the peak of lower chemical shift is seen. All this data is entirely consistent with the postulated LEB structure i.e. para-disubstituted phenylene rings linked by amine groups.

Following this the fully reduced sample was re-oxidised to the emeraldine state by treatment with  $\text{FeCl}_3$ <sup>7</sup>. The subsequent spectrum, as illustrated in Figure 3.3, was practically identical to that previously recorded for the 'as-made' EB. Added to this a g.p.c analysis (see next section) indicated that

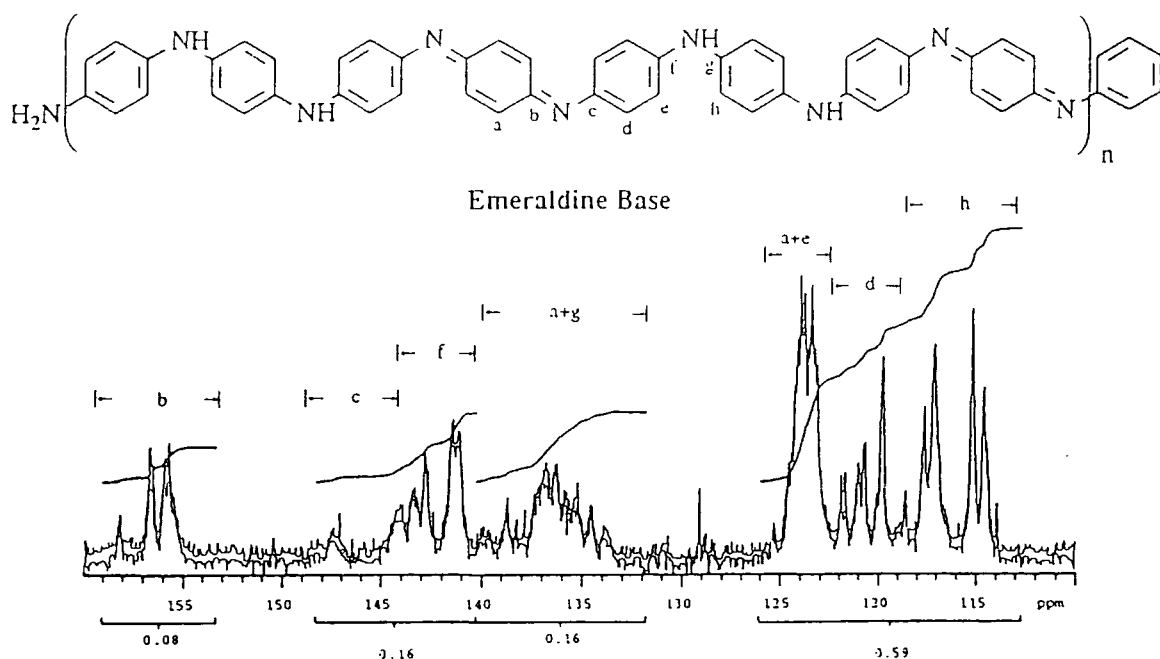


Figure 3.4 Regional assignments for the proton-decoupled  $^{13}\text{C}$  NMR spectrum of 'as-made' EB, recorded under quantitative conditions.

neither chain scission or crosslinking had occurred during interconversion of the two forms. It therefore follows that EB must have the same skeletal structure as LEB i.e. para-disubstituted rings linked through nitrogen atoms. This is entirely consistent with the postulated EB structure and is the first unequivocal confirmation of the structure. Regional assignments can then be made to the EB spectrum of Figure 3.1 on the basis of this information coupled with the d.e.p.t.-90 spectrum. Such an analysis is shown in Figure 3.4. Therefore, it can be stated with certainty that the product prepared in this work is indeed EB.

However, in such a spectrum there are many more peaks than assignable carbon atoms. Such an effect indicates the configurational and particularly conformational complexity of the polymer chain. It is known that for ring-atom-ring structures of this type there exists a torsional angle between



neighbouring rings<sup>8,9</sup> which could account for some band-splitting. However, it is also known<sup>10,11</sup> that ring-flipping motions ( $180^\circ$  jumps) occur for such systems, which would average any ring inequivalence. This is shown by the fact that the LEB sample has a very simple and uncomplicated spectrum. So the main reason for the complexity of the emeraldine data is the presence of quinoid-imine ring units in the structure. These rigid linkages significantly stiffen the polymer chain and thus reduce rates of conformational interchange to values greater than the NMR timescale (although clearly chain motion is still present). Furthermore, they also add a great deal of conformational complexity as illustrated by Figure 3.5. It should also be noted that it cannot be unequivocally established that the quinoid unit is entirely regularly distributed along the chain i.e. every fourth ring, although the majority seem to follow this pattern.

This stereochemical complexity is a very important result which, as will be seen later on in this work, has many, far-reaching repercussions. Another conclusion from these NMR studies concerns the contaminants present in polyaniline, as indicated by elemental analysis. Although some of these are due to residual sulphate and chloride anions which can be removed by further purification, a small percentage remains. Through analysing the minor NMR peaks it was found that some of the chemical shifts were consistent with defect structure associated with sulfonate and chloride ring substituents. Thus, it is clear that the postulated chemical structure is rather idealised. Despite the fact that these defects normally occur in levels of less than 5 wt%, they also have a considerable effect on the properties of the material, as discussed in Chapter 4.

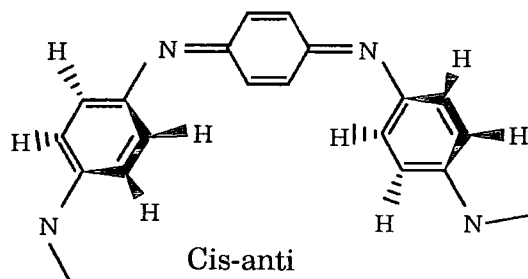
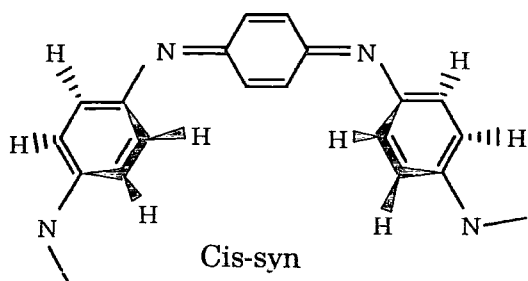
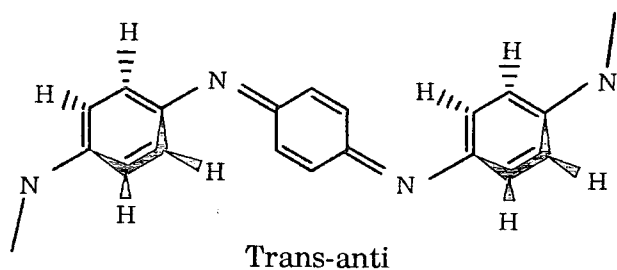
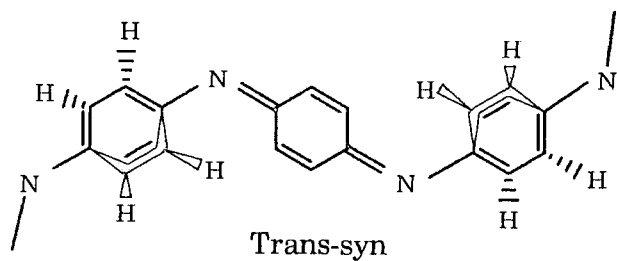


**Figure 3.5 Possible chain conformation about the quinoid-imine ring unit of an EB polyaniline chain. Cis/trans refers to the geometry of the phenylene rings in relation to the fixed quinoid-imine unit and syn/anti refers to the relative orientations of the phenylene ring hydrogens.**

### 3.3.2 Molecular Weight Distribution

The second polymer characteristic which defines physical behaviour is molecular weight or more accurately molecular weight distribution. Usually polymerisation reactions yield polymers having a very broad distribution of chain lengths, which may be characterised by some average molecular weight. The two most commonly used averages are the number average ( $\overline{M}_n$ ) and weight average ( $\overline{M}_w$ ) molecular weight obtained from osmotic pressure and light-scattering measurements respectively. These are:

$$\text{number average } \overline{M}_n = \frac{\sum N_i M_i}{\sum N_i}; \quad \text{weight average } \overline{M}_w = \frac{\sum (N_i M_i) M_i}{\sum N_i M_i}$$

where  $N_i$  is the number of molecules of molecular weight  $M_i$  and the summation is over all molecular weights,  $i$ .

However, gel permeation chromatography<sup>12,13</sup> (g.p.c), because of its ease of use and wide acceptability, has provided a routine method for assessing this molecular weight distribution for polyaniline. Unlike the light scattering technique, though, it is not an absolute method and therefore requires calibration against a standard. The choice of standard is a particularly important factor since not only must it be soluble in the same solvent as the polymer is dissolved in (in the case of polyaniline this is NMP), but it must also have a similar chain structure and flexibility in solution. These characteristics arises from the fact that g.p.c. is basically a size exclusion process. The molecular size of a dissolved polymer is directly related to the radius of gyration,  $R_g$ , which is, in turn, proportional to the molecular weight. But this proportionality varies according to different conformational arrangements (rods, spheres or random coils) of the chains. Thus it is clear

that the standard used for calibration must adopt a similar conformation, which is related to its structure and flexibility.

This is where the procedure used in this work differs to other g.p.c. analyses found in the literature<sup>14</sup>. In these latter reports a polystyrene standard is used, but it was noticed here that besides having a dissimilar structure to polyaniline this material also exhibits a very poor solubility in NMP. Thus any molecular weight values calibrated versus a polystyrene standard are likely to be highly erroneous. This problem was overcome by the use of poly (2-vinylpyridine) (PVP), a more suitable standard in both respects, particularly the latter. The calibration procedure used a range of molecular weight standards,  $\overline{M}_p = 1 \times 10^6, 2.4 \times 10^5, 1.1 \times 10^5, 7 \times 10^4, 2.8 \times 10^4, 1.05 \times 10^4, 7 \times 10^3, 2.9 \times 10^3$  and involved an analogous method to that outlined below for polyaniline samples.  $\overline{M}_p$  is a parameter used for calibration plots and derives from light scattering data  $\overline{M}_n$  and other absolute measurements in combination with g.p.c. measurements.

In a typical experiment, 0.5 wt% of polyaniline (EB) was dissolved in degassed HPLC grade NMP containing 0.5 wt% LiCl. This latter additive helps to uncoil tangled chains as indicated by the fact that the resulting chromatograph shows a single peak whereas, with no LiCl, a bimodal weight distribution is seen. This dilute EB /NMP/LiCl solution was then passed through a g.p.c. column to allow the molecular weight distribution to be assessed. The mechanism of this molecular separation and for g.p.c. in general is as follows. The g.p.c. column consists of a porous, crosslinked polystyrene gel, and the dilute polymer solution is passed through at a constant flow rate. The gel typically has a mean particle size of 35-75  $\mu\text{m}$  with pore sizes ranging from 30 $\text{\AA}$ -1mm in diameter. As the solution penetrates the gel the polymer molecules enter into those pores large enough to accept them. However, there is a distribution of pore sizes so that very large molecules have only a small number of pores available to them and pass through the column relatively quickly. Smaller molecules, on the other hand, are retained and held back, so effecting a separation of the polymer molecules.

In this case, the separated EB fractions that emerged from the g.p.c. column were measured by means of a UV detector (tuned to the benzenoid  $\pi$ - $\pi^*$  absorption of EB at 320 nm<sup>3</sup>). The residence time of each species in the column, the elution time, was then automatically plotted. From this data the peak value was determined and converted into an elution volume by multiplying by the flow rate (0.5 ml min<sup>-1</sup>). This value was then converted into an  $\overline{M}_p$  value by comparing to the PVP calibration curve of  $\log \overline{M}_p$  versus elution volume.

For a typical as prepared emeraldine base sample, a chromatograph such as Figure 3.6 was recorded. Using this data and calibration plots a value of  $\overline{M}_p = 3.2 \times 10^5$  was deduced. This corresponds to approximately 370 (C<sub>6</sub>H<sub>4.5</sub>N) repeat units. Thus the molecular weight of polyaniline is found to be moderately high. Furthermore, this  $\overline{M}_p$  value can be quoted with a high degree of certainty, unlike that for polystyrene calibrated data.

### 3.3.3 Optimisation of Synthesis

It is clearly desirable to utilise these two critical factors, chemical structure and molecular weight, and other parameters such as percentage yield to optimise the synthesis route. Although this is not within the scope of this project, the effects of reaction variables on polyaniline synthesis are currently being investigated at Durham by Dr P.N. Adams in conjunction with BICC Cables Ltd. However, it is very instructive to consider some of the preliminary results here in order to demonstrate just how crucial it is to have a highly precise synthesis procedure. Table 3.1 summarises the effects of certain reaction variables. Even seemingly trivial reaction variations may produce vast differences in the final state of the product. In turn, these will greatly alter the physical properties of polyaniline.

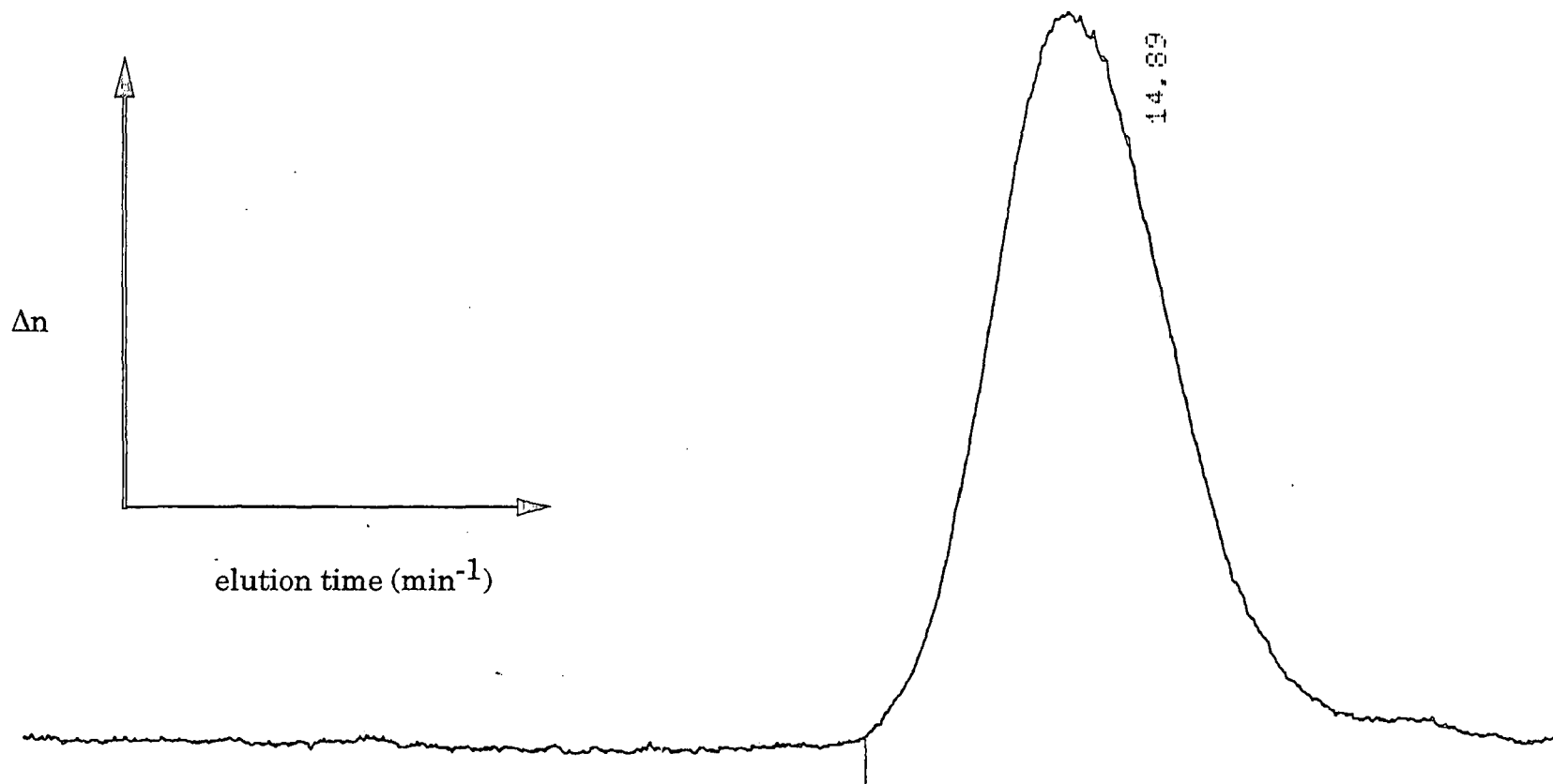


Figure 3.6 Typical g.p.c. chromatograph for an as-prepared EB sample (0.5 wt% in NMP containing 0.5 wt % LiCl). The annotation labels the elution time for the peak height of the chromatograph.

Reaction Variable	Effect
Temperature	$\overline{M}_p$ increases with decreasing temperature below 0°C
Time	$\overline{M}_p$ increases with increasing reaction time
Oxidant Addition	$\overline{M}_p$ increases with increasing time over which oxidant is added
pH	Reaction does not proceed above pH > 3. Low pH, < 0.5, gives low yield and $\overline{M}_p$ , and increases the degree of ring substitution

Table 3.1 The effect of various reaction variables on the synthesis of polyaniline.

### 3.4 Polyaniline Films

The ability to process polyaniline into free-standing, air-stable films using the solvent N-methyl-2-pyrrolidinone (NMP) has been the cause of much of the renewed interest in this material, as outlined in the previous chapter. The experimental aspects of this processing technique are now discussed below.

#### 3.4.1 Film Formation

The fabrication of polyaniline films is a relatively easy process, but one to which a degree of attention should be paid as films need to be of high quality if they are to be processed further. In a typical procedure a batch of approximately 10 films was produced as follows:

1.0g of finely ground EB powder was added to 12.5g of NMP in a boiling tube to give an 8 wt% polymer solution. The solution was then mixed in a Junke and Kenkel Ultra-Turrax homogeniser at 20000 rpm for 5 mins to break down any large lumps of polymeric material. Following this the mixture was transferred to a centrifuge (Eppendorf Hermle Z320) and spun at 4000 rpm for 10 mins. The mixture was then carefully decanted to give a homogeneous EB/NMP solution. This solution was then deposited onto 10 standard glass microscope slides, which had been cleaned in an isopropyl alcohol reflux overnight, to give a coating weight of approximately  $0.04 \text{ g cm}^{-2}$ . Other substrates such as polished silicon wafers, were also found to be suitable. The samples were then dried in a vacuum oven for about 1 hr at  $70^\circ\text{C}$  under vacuum (25mm Hg), ensuring that they were perfectly flat so that the solution did not run. At this stage just enough of the excess solvent has been removed so that the samples appear dry. Once cool, samples were then carefully peeled from the substrates to give free-standing polyaniline films which typical thicknesses of  $50\text{-}80\mu\text{m}$ , as measured by a digital micrometer. These samples are known as as-cast films, a term frequently used in this work, especially in the next chapter.

A few important remarks about this procedure are necessary. First of all, while polyaniline is undoubtedly processible in NMP there is still some debate as to whether the polymer is truly in solution. Some reports<sup>1,15</sup> argue that a concentrated EB solution (usually some 20 wt%) is a suspension of entangled polymer chains. Indeed in the previously discussed  $^{13}\text{C}$  NMR analysis it was found that the viscosity of an 8 wt% EB solution increased with time but also so did the number of resolvable features in the NMR spectrum. The conclusion reached was that polyaniline only dissolves slowly in NMP. This effect might explain the differences in opinion between the state of the mixture, but a solution containing as much as 20 wt% of polyaniline, though, would tend to display the attributes of a suspension not a solution.

While it is desirable to have a true solution it is not possible to allow the EB/NMP mixture to stand for too long ( $>$  a few hrs) as the increase in viscosity leads to the solution solidifying or turning into a 'gel'. Such gels are remarkable materials and are known to occur for many other



polymeric solutions often where the percentage of the polymer is extremely low, sometimes less than 5 wt%<sup>16</sup>. Although the origins of this gelation are not understood it is clear that the polymer chains must have in some way become highly connected or crosslinked. These gels are becoming a considerable source of interest for workers in the polyaniline field<sup>17,18</sup>. In this project there is considerable evidence to suggest that gel formation is linked to the presence of 'contaminants' in the polyaniline powder, which induce a chemical crosslinking process. These results are the subject of detailed discussion on chapter 4.

In order to overcome this problem of gelation, which renders the solution unusable for film casting, a rigorous mixing procedure, involving a homogeniser and centrifuge as described previously, is used. This action breaks down any 'lumps' and induces the polymer to dissolve more readily, so that the mixture is essentially a solution before the onset of gelation. Such a homogeneous solution then leads to good quality films. However, mechanical mixing methods often involve the dissipation of much heat in the mixture. In the case of polyaniline in NMP this greatly increases the rate of gelation. Indeed at first mixing was achieved by the use of an ultrasonic bath, but this method was found to produce so much heat that solutions solidified after only 10 mins. The homogeniser was found to be less severe in this respect, but still only the minimal time of 5 mins, needed for a lump-free solution, was used.

The as-cast polyaniline specimens produced by the above method are in the EB form. These unstretched samples may then be uniaxially aligned as discussed in the following section. Alternatively samples can be doped to the conducting ES form. This was achieved by immersing the films in 1M HCl for 1 hr. If left for longer periods samples tend to become very brittle. Following this, excess acid may be removed by blotting the film surface dry with filter paper. It is important to understand though that once films have been converted to the conducting form they cannot be processed further. The reason for this lack of processibility is revealed in the next chapter but as a consequence it is necessary to stretch films in the EB form and then, if conducting films are subsequently required, dope them in acid.

### 3.4.2 Film Quality and Composition

Until the fabrication of these solvent cast EB films, samples of polyaniline were usually produced in a free-standing format by carefully removing an electrochemically synthesised specimen from a conducting substrate<sup>19</sup> (deprotonation was also required since the specimens are in the ES form). Such films, however, possess an inhomogeneous fibrillar or powder morphology similar to Shirakawa route polyacetylene<sup>20</sup> and electrochemically prepared films of polythiophene<sup>21</sup> or polypyrrole<sup>22</sup>. These structural inhomogeneties make the interpretation of macroscopic conductivities very difficult. Furthermore, electrochemically prepared polyaniline films are very thin, extremely fragile and cannot be stretch oriented since they are formed in the conducting state.

Films cast from the solvent NMP, on the other hand, do not suffer from such powder morphologies. Dense, homogeneous samples are produced which, in the as cast EB state, are mechanically strong, flexible and can be readily elongated. The film formation procedure described previously gives high quality samples with smooth surfaces as shown by the photograph of Figure 3.7(a). The sample quality, however, is affected by variations in the casting procedure. If, for example, the excess solvent is removed too quickly large 'craters' form in the surface due to boiling-off of the solvent. A similar effect, though not so severe, happens for sulfonium precursor-route prepared poly(paraphenylenevinylene) films<sup>23</sup>. The rapid removal of solvent in this case results in a volume expansion to give a open-celled morphology analogous to a foam. The quality is also poor if the samples are prepared from an inadequately mixed solution; small lumps of undissolved material may appear on the film surface. Both 'craters' and 'lumps' are highly undesirable features since, during stretch alignment, they act as defect sites and often lead to premature film fracture. Figure 3.7(b) shows such a poor quality EB film.

Polyaniline films have also been examined using thermogravimetric analysis (TGA). This is a simple thermal analysis technique in which the weight of a sample is measured as a function of temperature<sup>24</sup>. For polymeric materials, the main use of this technique is in the assessment of

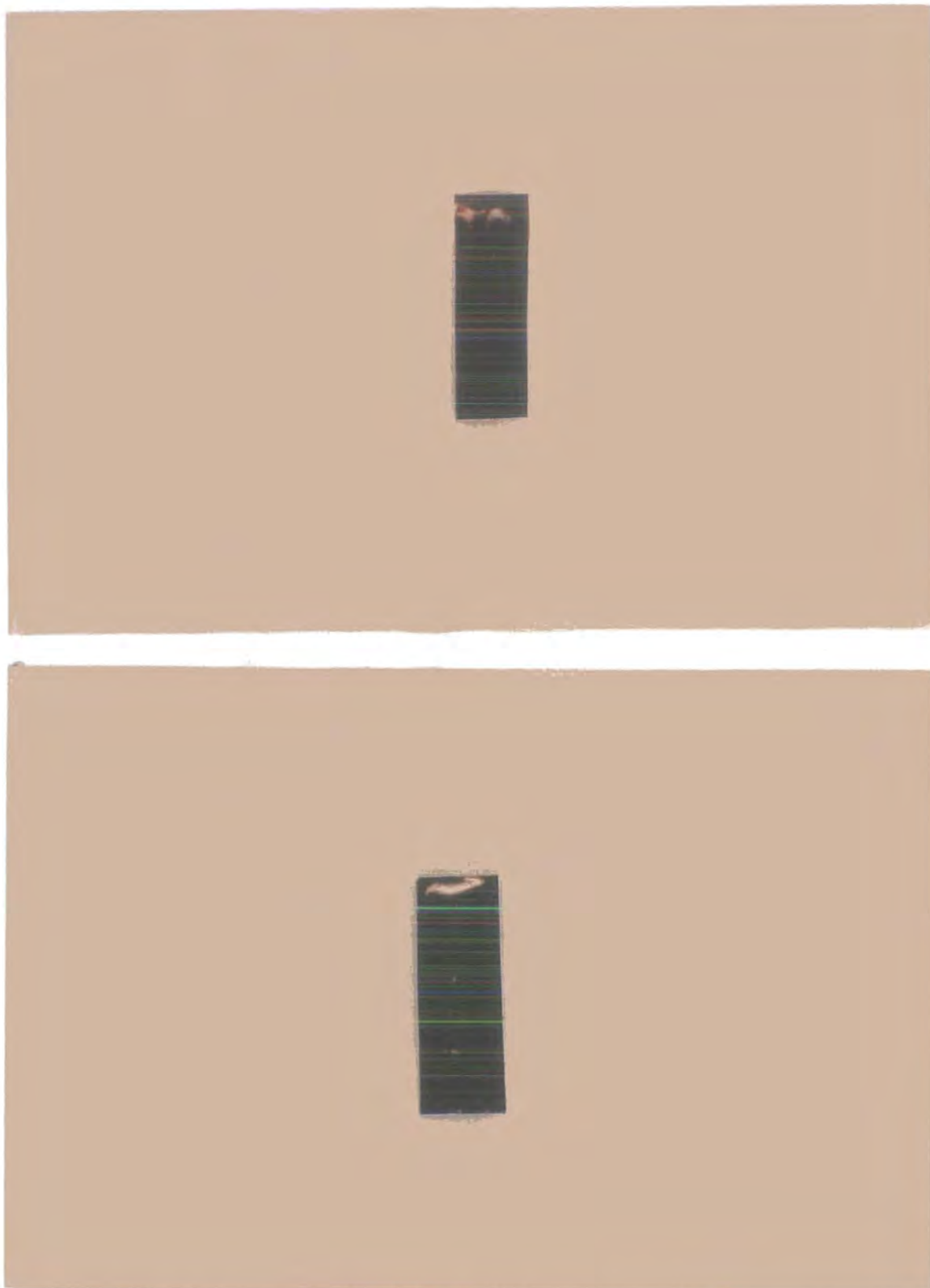


**Figure 3.7 (a) A photograph of a high quality EB film (top); (b) a poor quality specimen (bottom).**

thermal stability. However, the results may also be interpreted in terms of the composition of a specimen. This latter aspect in particular provides some very important information in the case of polyaniline since it is clear, from the experimental procedure, that as-cast films still contain a significant fraction of NMP solvent. In addition the percentage of Cl<sup>-</sup> ions in doped specimens can also be assessed. The instrument used in this analysis was a Stanton-Redcroft TG-770 belonging to BICC Cables Ltd, Helsby Technology Centre. This apparatus allowed polyaniline samples to be studied over the temperature range from room temperature up to 700°C. All the experiments were carried out under a nitrogen purge using a heating rate of 25°C min<sup>-1</sup>.

Figure 3.8(a) shows a typical TGA thermogram recorded for an as-cast EB film. For such samples there is a large weight loss recorded around 550°C which can be assigned to the break-down of polymer chains, in accordance with other analyses<sup>25,26</sup>. However, a more interesting feature occurs at lower temperature where some 25% weight loss is recorded by 250°C. Two pieces of information allow this 25% weight fraction to be assigned to residual NMP solvent. First of all, while thermally processing samples during orientation experiments, as discussed shortly, a colourless liquid was found to condense on the glass insulation jacket of the stretching apparatus above room temperature. This liquid had the odour of NMP and was further identifiable as the solvent without question by means of an infrared spectrum.

Secondly the results of infrared spectroscopic analysis on as-cast EB films, reported in chapters 4 and 5, also positively identify this weight loss as being due to NMP. These films exhibit a strong carbonyl absorption at 1675 cm<sup>-1</sup> due to the C=O group of the solvent. If, however, the spectrum is retaken after a sample has been annealed at 250°C, then the band is no longer observed, so indicating no NMP. Therefore, it can be stated that a typical as-cast EB film still contains some 25% NMP by weight. It is interesting to note that the boiling point of NMP as a pure liquid is some 202°C (760 mm Hg), so that the interactions between solvent molecules and the polymer chains is considerably less than those between the solvent molecules themselves.

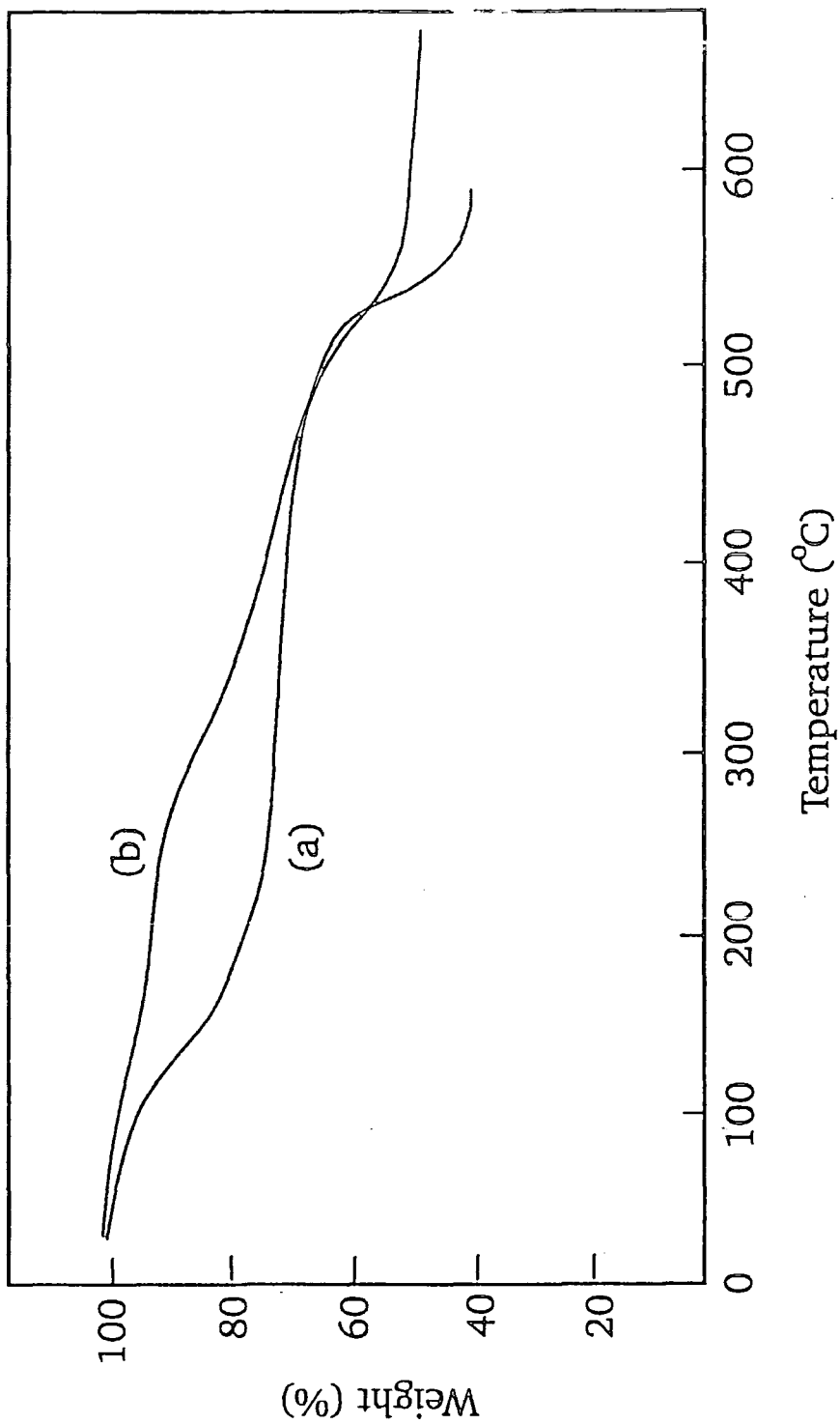


Figure 3.8 TGA thermograms for: (a) an as-cast EB film; (b) an ES film (doped in 1M HCl) .

It is clear, though, that this value of 25 wt% will be reduced if samples are over-dried i.e. for much longer than 1 hour. This is often the case with samples prepared by other workers where longer drying times mean less solvent retained in the samples. As a consequence these over-dried films can only be removed from the substrate by immersion in water. This process has the effect of removing even further amounts of NMP and also adding a third aqueous phase to the sample composition. This lack of solvent in such as-cast films turns out to be extremely detrimental to further processing i.e. orientation, since the results of the next chapter indicate that the ability to elongate a sample depends critically on there being a significant fraction of residual NMP.

An ES film, doped in 1M HCl, displays a markedly different thermogram to its as-cast, base counterpart, as illustrated in Figure 3.8(b). While the structural decomposition of the polymer is still observed at 550°C, the chains are also apparently rather less stable leading up to this temperature. Furthermore, the major weight loss due to removal of the volatile NMP is no longer seen. Instead, there is only a small, approximately 10% weight loss recorded by 200°C. This feature may be intuitively ascribed to the liberation of HCl and also a small fraction of associated water from the doped material. This assumption unfortunately cannot be readily assessed by infrared spectroscopy since the ES form of the material absorbs light in the infrared very strongly. However, it is confirmed by reference to extensive studies on ES powder reported in the literature<sup>26</sup> which concludes that HCl and H<sub>2</sub>O are eliminated up to 200°C. This clearly has very important repercussions with respect to any possible applications involving conducting polyaniline in a high temperature environment. Another important consequence is raised by the fact that NMP is no longer present in doped specimens, a factor which will be seen to explain the inability of such films to be stretch aligned.

### 3.5 Orientation of Polyaniline

The ability to orient an initially isotropic polyaniline specimen along one direction enables a degree of anisotropy to be produced in various

macroscopic physical properties of the material. Mechanical quantities such as tensile strength and yield strength are both increased in a direction parallel to that of stretching (the fibre axis)<sup>27</sup>. However, most notable for this investigation is the anisotropy in conductivity (when doped), with a large increase in the value parallel to the stretch direction over that observed for an unoriented film, as discussed in the previous chapter. This increase in conductivity essentially narrows the gap between polyaniline being just a pure research material and a whole host of commercial and industrial applications. Indeed, the continued narrowing of this gap through the further enhancement of conductivity is a prime concern for our group here at Durham. The main aim of this project, though, is to determine what is actually happening on a microscopic scale to allow such large increases in this macroscopic property. As such, the investigation of stretch oriented polyaniline films comprises the major part of the rest of this thesis, with experimental techniques such as polarised infrared spectroscopy, X-ray diffraction and neutron diffraction probing the amount and type of chain orientation.

### 3.5.1 The Orientation Process

The classical case of orientation is exhibited by thermoplastics such as low density polyethylene or nylon<sup>28,29</sup> and is normally described by a series of load-elongation or stress-strain curves, as shown in Figure 3.9. These materials and polymers in general are usually termed viscoelastic, since they may show all the features of a glassy, brittle solid or an elastic rubber or a viscous liquid depending on the temperature (and time scale) of measurement. At low temperatures the polymer is glass like (Young's modulus  $10^9$ - $10^{10}$  Pa) and breaks in a brittle manner at strains of greater than 5%, curve A. When the temperature is slightly higher, the presence of the glass-transition,  $T_g$ , is sensed and the material displays the behaviour of a ductile metal, curve B, showing a load maximum i.e. yield point before rupture occurs. At high temperatures the same polymer may be rubber-like, with a Young's modulus of  $10^6$ - $10^7$  Pa, and able to withstand large extensions without permanent deformation. At still higher temperatures

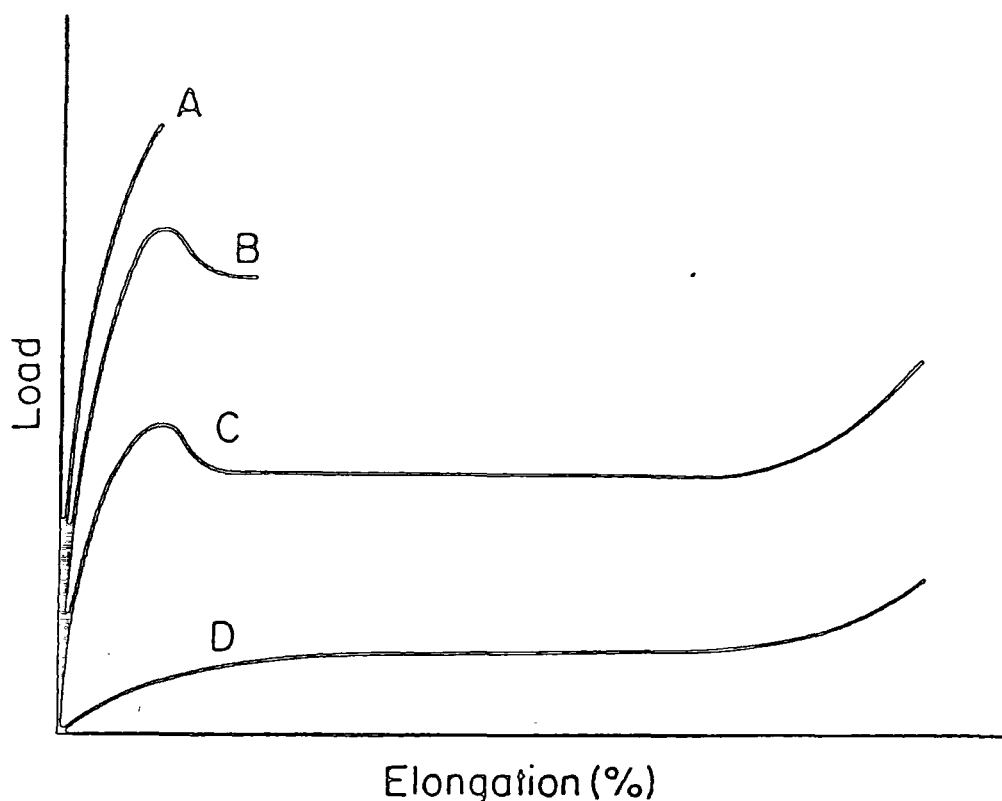


**Figure 3.9** Load-elongation curves for a polymer at different temperatures. Curve A: Brittle fracture. Curve B: Ductile fracture. Curve C: Cold-drawing. Curve D: Rubber-like behaviour.

the polymer behaves like a viscous liquid and may be deformed permanently under load, though without any chain alignment.

In the intermediate temperature range above curve B, but still below the glass transition temperature, the remarkable phenomenon of necking and cold-drawing is observed<sup>29</sup>, curve C. As for curve B, this type of behaviour also shows a yield point, where a neck is formed, and a subsequent decrease in true stress. However, with continuing strain, instead of thinning further until fracture occurs, the neck region actually propagates along the sample under a constant stress. This propagation is characterised by a non-uniform distribution of stress and strain along the specimen and may



result in very large deformation, even up to 1000%. Eventually the load begins to rise and fracture finally occurs. Not all thermoplastics exhibit this cold-drawing behaviour though. Certain requirements such as a minimum molecular weight need to be fulfilled, but the process is also dependent on a wide variety of other variables such as composition, morphology, stretch rate etc.

Conjugated polymers, more analogous to polyaniline, can also be stretch oriented. These include polyacetylene (PA)<sup>30,31</sup> and poly(phenylenevinylene) (PPV)<sup>31-33</sup>, materials which can similarly be doped to a conducting form. These two polymers, however, possess a distinct processing advantage over polyaniline; they can be made via a precursor synthesis route which facilitates an extremely useful method for producing highly oriented films. These routes involve a two stage preparative method where, in the intermediate stage, the polymer exists in a non-conjugated form. Subsequently, the fully conjugated polymer is obtained by a thermal elimination reaction. The preparations for PA and PPV, known as the Durham and sulfonium precursor routes respectively, are illustrated in Figure 3.10. The beauty of these precursor routes is that samples may be oriented during the transformation stage. This type of processing imparts a very high, uniform molecular orientation, with films sometimes being stretched to over ten times their initial length. In addition, because the procedure is carried out while the material is not in the fully conjugated form, the stresses required for elongation are relatively low. Polyaniline, on the other hand, must be oriented in the much more rigid, semi-conjugated EB form, since there is no known precursor synthesis route. Because of this, much higher loads must be used, greatly increasing the chance of sample fracture.

The orientation process for PA and PPV is somewhat different to the case for typical thermoplastics described previously. The evolution of volatile gases during the transformation step is believed to 'plasticise' the samples. This is not to say that thermoplastics cannot be plasticised, a process which effectively reduces the  $T_g$  of the material and hence lowers the processing temperature. For example, polyvinylchloride plasticised with various

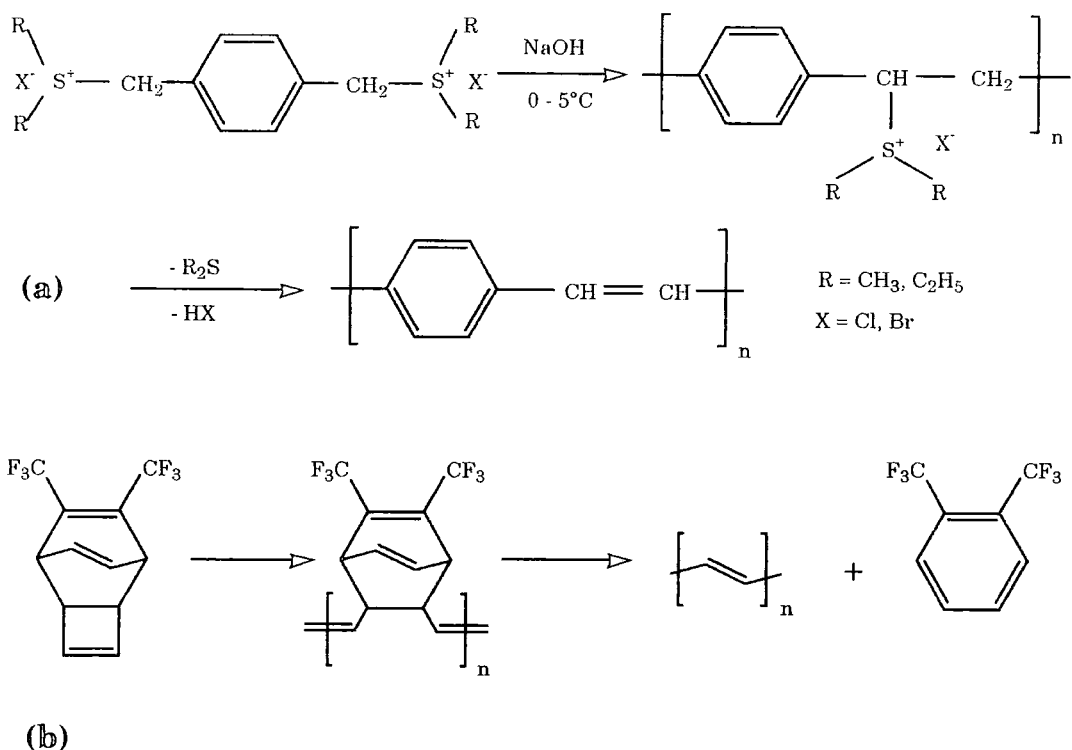


**Figure 3.10** (a) The sulfonium ion precursor route for PPV;  
 (b) The Durham precursor route for PA.

dialkylphthalate additives<sup>29</sup> has many industrial applications. However, for these conducting polymers the plasticisation effect results from the loss of these liberated gases, whereas for normal plasticisation the permanence of the additive is of fundamental importance. The orientation process for polyaniline is rather similar to the case of PA and PPV since samples contain a significant amount of NMP, which is lost as a vapour during thermal processing. Until now, the exact nature of this gaseous plasticisation effect has not been discussed in any great detail. However, this topic has been a main subject of extensive thermal analysis in this work. The results, which provide a clear picture of this process, are all reported in the next chapter.

Besides these macroscopic views of orientation, it is also useful to consider a polymeric material on a molecular level. In the case of polyaniline, this is the main aim of this thesis, but there are a few general principles which should be mentioned here. The preceding discussion, by referring to glass transition temperatures, implies that the material is in an amorphous state, described by a random tangle of polymer chains. If, however, the polymer is semi-crystalline then it may be envisaged as consisting of a crystalline and amorphous fraction. The former phase consists of highly ordered regions where chains are bound tightly together by van der Waals forces. Invoking the two phase model, as described in detail in chapter 6, these ordered regions will lie in a less well ordered matrix, the amorphous phase. Upon the application of a stress, each phase will then respond separately. The crystalline fraction might rotate and align in the direction of stretching, while the amorphous regions will also orient with the fibre direction, but to a much less extent.

Generally, for amorphous polymers the temperature required for orientation needs to be at or above the glass transition temperature. For crystalline materials the temperature must be above the crystal melting point, which occurs above  $T_g$ . Also the relaxation rate of the chains should be considered. If the material is kept too long at an elevated temperature, or re-heated above the stretching temperature, then the oriented chains may recoil to their unperturbed dimensions. Thus the sample will shrink and the orientation will be lost. Therefore, in any alignment process, the relaxation rate must be exceeded by the rates of deformation and cooling.

### 3.5.2 Stretching Apparatus

To orient EB films, an in-house uniaxial stretch rig was built, based on a design given by Townsend<sup>30</sup> for the alignment of polyacetylene samples. The apparatus is shown in the photographs of Figure 3.11(a) and (b). To stretch an as-cast film, the ends of the specimen are carefully wound around two metal rollers, ensuring that both ends are aligned. Each roller is then fixed by a locking pin, so that the film is securely held and then brought to tension by the means of a tensioning spring. This spring is

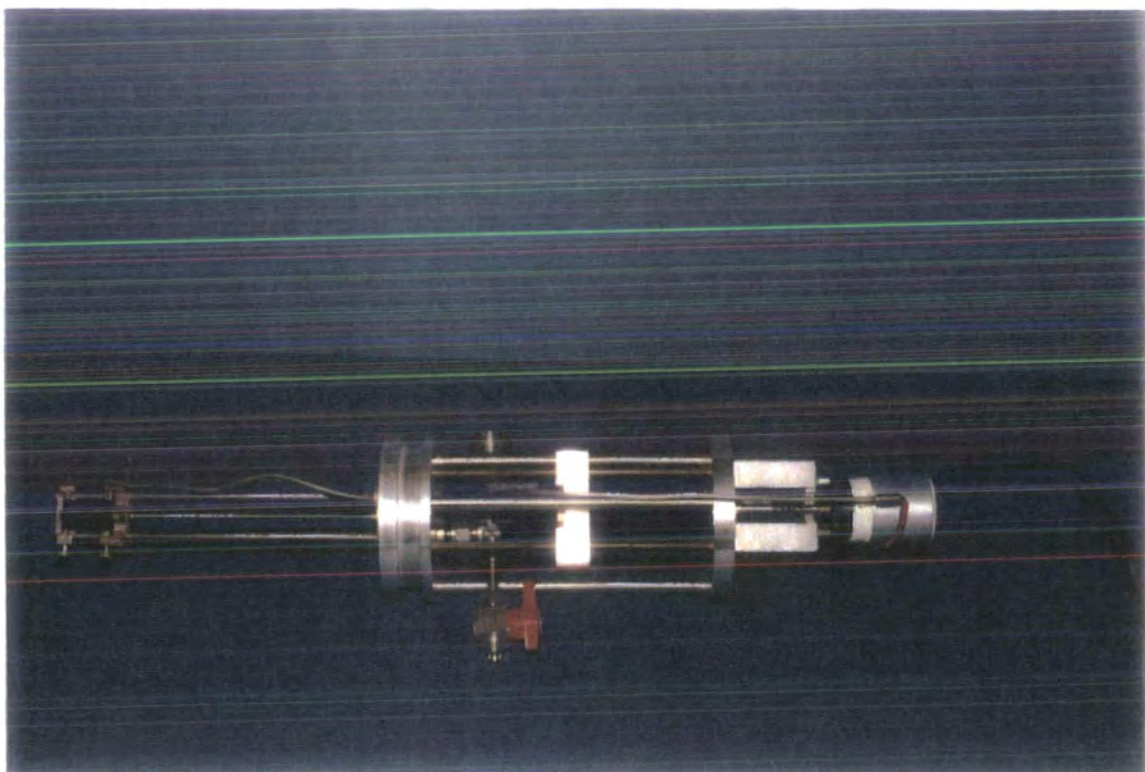
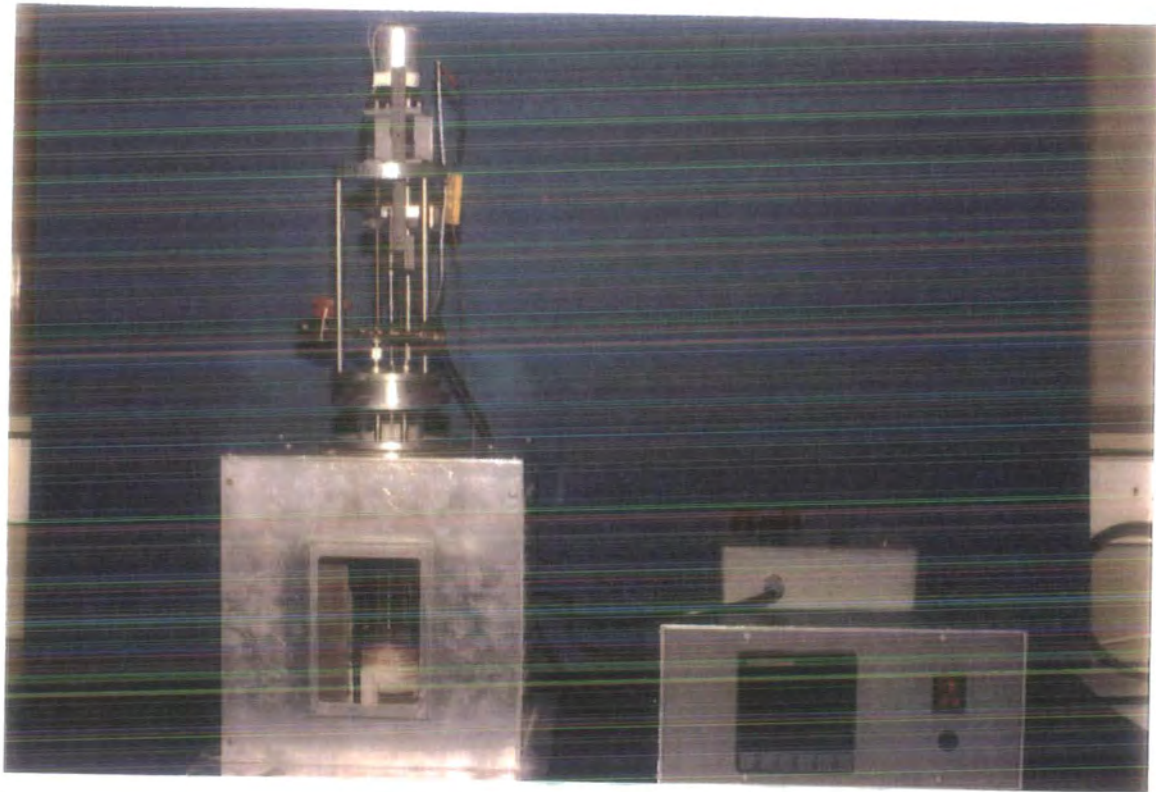


**Figure 3.11** The stretch rig: top photograph, whole apparatus;  
bottom photograph, sample clamping arrangement.

tensioned by a pulley system, driven by a high-torque d.c. motor and when elongated, exerts a force on the specimen, which pulls it taught. Once the slack has been taken up, two pen marks are made on the film and the distance between them measured, so that the final extension can be calculated. The whole sample arrangement is then mounted in a cylindrical glass vessel, around which a d.c. resistive heating coil is wound. The coil is kept in place by heat cement, but a narrow rectangle along the front face of the glass tube is left uncovered, to act as a viewing window. The glass jacket also has an air-tight o-ring seal at the top so that processing can be carried out under vacuum or inert gas atmospheres.

To begin stretching the film, the spring is extended beyond the tension applied to keep the sample taught. The spring itself has a known force constant (0.0944 kg per mm extension, linear up to 28 mm) so that when it is extended by an amount as measured on the steel rule, the precise load exerted is known. This value may be converted into the corresponding stress value by division of the initial cross-sectional area of the sample. At the same time as the force is exerted the specimen temperature is also raised. This is achieved by supplying a current to the heating coils by means of the Eurotherm Series 900 temperature controller. The sample temperature is measured by means of a thermocouple situated as close as possible to the film surface. For greater accuracy, the thermocouple was also coated in polyaniline.

The exact orientation procedures and parameters used are discussed in the next section in relation to the maximum achievable extensions. Once the film had been extended by the desired amount though, the sample arrangement was removed from the glass jacket and the final extension accurately measured. The extension value is quoted in this project is a percentage, so that if  $l_0$  is the initial length as measured between the two marker points and  $l$  the final length, then the extension is given by

$$\text{extension (\%)} = \frac{l - l_0}{l_0} \times 100$$

Often though, in other reports, the extension is quoted as the ratio  $l/l_0$ . It is important not to confuse this definition with the previous one since the  $l/l_0$  value may appear to be higher for a given extension e.g. an  $l/l_0$  of 4 correspond to a elongation of only 300%. Finally the film can then be carefully removed from the clamping arrangement. Usually it is quickest and most simple to cut the sample with a sharp scapel blade just by each roller, since the material wrapped around each roller, which has not been extended, often fuses together.

### 3.5.3 Results and Behaviour

The orientation of thermoplastics such as polyethylene is highly dependent on the conditions of testing e.g. rate of application of load, temperature. In the case of EB/NMP films, these stretching variables are further complicated by the effects of thermal processing. Unfortunately, all these effects combined to make stretch alignment a particularly difficult process to optimise with any great accuracy. However a large number of behavioural aspects of polyaniline have been studied through a highly extensive series of orientation experiments. The conclusions of this work are now discussed below.

For the orientation of EB films, a major requirement was found to be the variation of temperature during the alignment process. The reasons for this factor were not evident from these stretching experiments, but have been probed in the following chapter by a series of thermal analysis techniques. However, a number of points may be inferred here. First of all, the ability of films to be extended at elevated temperatures is clearly connected with the loss of NMP solvent (see TGA analysis). Furthermore, it was apparent that the amount by which a sample can be extended depends upon the rate at which these solvent molecules are removed. This is implied from the fact that if a sample is annealed at an elevated temperature of 100°C for several hours before stretching, only small extensions are possible. Such a procedure removes most of the NMP and clearly most of the potential for elongation as well. However, if a stress is exerted while the temperature is ramping up, much higher elongations are possible. It was

found though that a changing temperature further required that the applied load should also be varied. This is thought to be because the rate of NMP loss (and hence film elongation) is non-uniform so that at some point during the process a constant applied stress is highly likely to fracture the specimen. Therefore, in order to produce maximally stretched EB films the applied load and heating rate need to be synchronised and then optimised.

This interdependence of the heating rate and load makes the process, as a whole, rather difficult to control. For instance a slow heating rate of  $5^{\circ}\text{C min}^{-1}$  allowed the load to be accurately tuned. However, although following such a procedure a sample can be extended by several hundred percent, the polymer chains are able to recoil to their unperturbed dimensions because of the slow heating. This results in an amorphous stretched film as indicated by the X-ray diffraction pattern of a 200% elongated sample, Figure 3.12. Such unordered stretched polyaniline films have recently been reported by MacDiarmid *et al*<sup>34</sup> as a new phenomenon, but clearly it is the processing conditions which are responsible for such an effect. On the other hand, if the sample chamber is first preheated to a set temperature and a sample then inserted, the percentage of specimens fracturing is extremely high, even under a load sufficient for only a moderate extension (150%).

Added to this it was necessary to impose an upper temperature limit of about  $100^{\circ}\text{C}$ . Above this value film extensions decrease dramatically and require higher and higher loads to achieve them, so greatly increasing the chance of fracture. At excessively high temperatures ( $> 150^{\circ}\text{C}$ ) EB samples become extremely brittle and mechanically very weak. The use of inert gas, helium and nitrogen and also vacuum atmospheres was found to have little effect on this attribute or indeed any part of the stretching process. Another possible variable considered was the sample itself. The ideal shape to have the specimen in is a dumbbell<sup>35</sup>, since the centre portion of such a sample will be subject to a very uniform stress. However, dumbbell shaped samples were found to extend no further than rectangularly shaped ones. Also films with greater thicknesses (100-150  $\mu\text{m}$ ) than those of typical as-cast films (50-80 $\mu\text{m}$ ) were investigated, but to stretch such samples excessive heating times were needed.

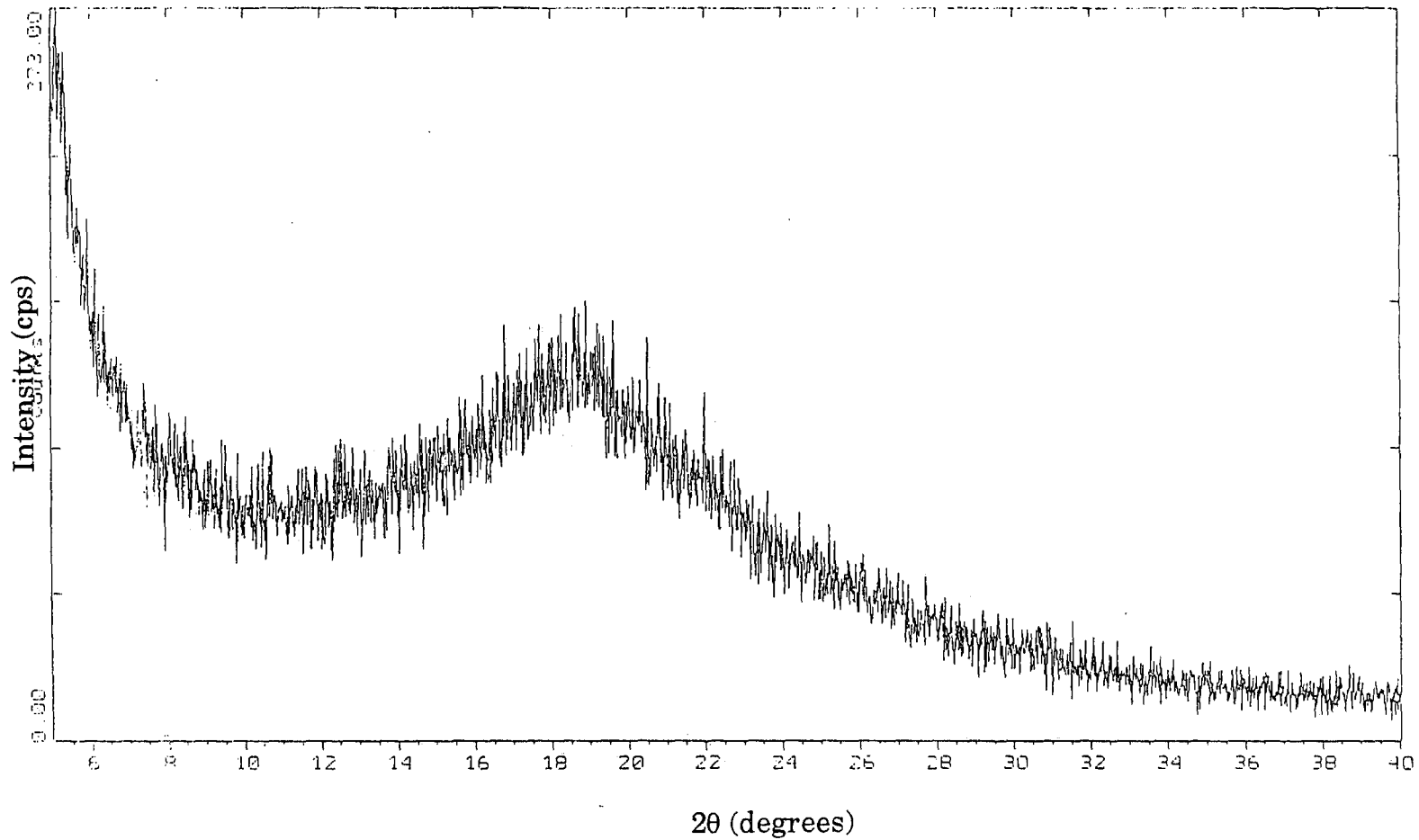


Figure 3.12

An X-ray diffraction pattern of a 200% elongated EB film. Only a broad amorphous curve can be seen with no signs of Bragg peaks and hence no crystalline order. Such an amorphous specimen results from a slow heating rate during stretch alignment, which allows the polymer chains to recoil to their unpreturbed i.e. unordered dimensions.



From these points it is clear just how many potential variables there are in the stretching process. However, a procedure was found which made possible elongations of up to 300% ( $l/l_0 = 4$ ), on a fairly reproducible scale. This result was deemed suitable for this work so that the method was subsequently adhered to. Significantly higher stretch values have been reported though<sup>36</sup>, but such highly extended samples were not frequently or readily achieved. However, this poor reproducibility aspect has been the subject of much further work here at Durham. A very recent outcome of these investigations, which will be reported soon, is the production of highly aligned specimens (~ 800%) on a very reproducible scale. These very new results will enable the scope of the work presented in this thesis to be extended.

A typical stretching procedure used here, though, was as follows. A rectangular as-cast EB film was employed, as peeled directly from the microscope slide substrate, but with the long edges trimmed with a sharp scapel blade. This removes any perforations which can act as possible fracture points. Next a tension corresponding to a 10 mm extension of the load spring was applied to the sample. This, in turn, corresponds to a initial load of 0.95 kg. Assuming a typical initial cross-sectional film area of  $1.3 \times 10^{-6} \text{ m}^2$  this is equivalent to a stress,  $\sigma$ , of  $7.3 \times 10^6 \text{ Nm}^{-2}$ . The sample was then placed in the glass heating jacket at room temperature and the temperature set to  $100^\circ\text{C}$ , without any control of the heating rate. Such a method gives a small ramping up time approximately equivalent to  $40^\circ\text{C min}^{-1}$ . As the temperature begins to rise the tension on the spring is slowly released as the sample extends so that by roughly  $35^\circ\text{C}$  the extension is about some 5mm. At this point the spring extension is increased back to 10 mm and carefully maintained at this value until the final temperature is reached. It should be noted that although the stress on the sample appears to be at a constant value equivalent to 10 mm extension of the spring i.e.  $7.3 \times 10^6 \text{ Nm}^{-2}$ , the true stress,  $\sigma_t$ , is actually increasing due to the reduction in the sample cross-sectional area. The true stress,  $\sigma_t$ , is given by the formula<sup>29</sup>;

$$\sigma_t \text{ (N m}^{-2}\text{)} = \frac{P \times l}{A_0 \times l_0}$$

where P is the load, l the length at any time of measurement,  $l_0$  the initial length and  $A_0$  the initial cross-sectional area.

Using a constant extension of 10 mm a film elongation of typically 200% is achieved. For even higher values the spring may be increased to 15 mm extension after the initial extension. Similarly for smaller elongations the spring needs to be kept at a value below 10 mm. As stated earlier, the maximum elongation achieved using this method is some 300%. However, the exact extension possible, under any spring tension, is critically dependent on the precise amount of residual NMP in a film. Since the NMP is volatile, even at ambient temperatures, this parameter is itself dependent on the exact drying time, sample age, environment e.t.c. and can thus vary from sample to sample. It is this NMP variability which appears to decrease the reproducibility of this stretching procedure, even under a rigorous quality control system.

Figure 3.13 shows a photograph of an as-cast EB sample which has been extended by some 200%. It can be seen that no 'necking' occurs during stretching, as for samples such as polyethylene. Rather the whole section of the sample under stress yields. Such stretched films are quite rigid due to elongation, but still possess a degree of flexibility. The thickness profile of a sample, as measured by a micrometer, reveals more about the nature of stretching for polyaniline films. Films are found to elongate more at the ends than in the middle. For a sample such as that shown in Figure 3.13, this means thicknesses of between 18-21 $\mu\text{m}$  at the end sections with the middle section around 25-30  $\mu\text{m}$ . Maximally i.e. 300% stretched samples have end thicknesses down to around 15 $\mu\text{m}$ , but if samples become even thinner sample fracture almost always occurs. Thus 15  $\mu\text{m}$  represents the minimum thickness value achieved for oriented polyaniline films. Such samples are quite suitable for many analysis techniques, such as polarised

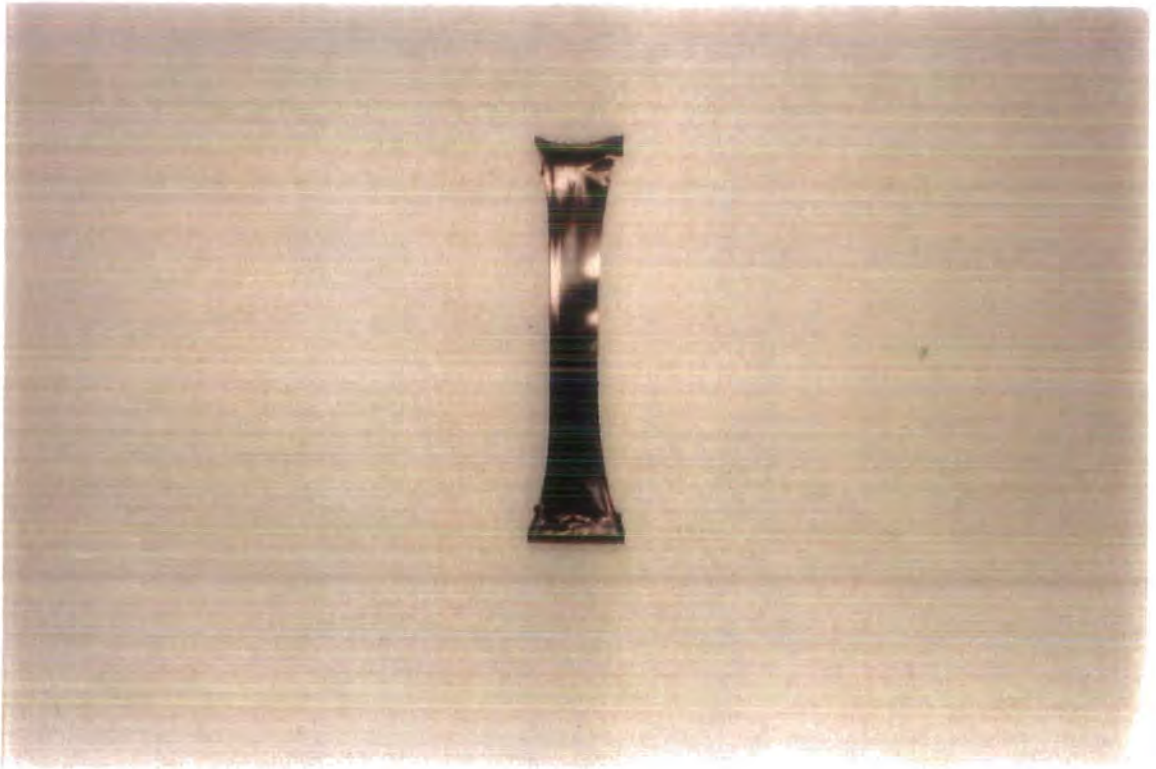


**Figure 3.13**      **A photograph of an EB film having been extended by ca. 200%.**

infrared spectroscopy and X-ray and neutron diffraction reported in later chapters, but unfortunately not for polarised optical spectroscopy. Film thicknesses need to be sub-micron, if possible, in order for there to be any radiation transmitted through the sample. Clearly stretched polyaniline films are rather a long way from this limit and it may be that a procedure such as stretching on a substrate e.g. polyethylene or polyimide may have to be adopted to produce suitable films.

### **3.6 Conducting Samples**

Once EB films have been stretch oriented they may then be doped to the conducting ES form by treatment with aqueous HCl. The procedure used was the same as for unstretched films, with immersion in 1 M HCl for



**Figure 3.14** A photograph of a 200% elongated, ES (doped in 1M HCl) film.

about 1 hr. This concentration is more than enough to fully protonate (i.e. 50% of nitrogen atoms) the polyaniline<sup>37</sup>, resulting in the highest possible conductivity. Samples were then blotted dry and the conductivity measured using the standard four point probe Montgomery method<sup>38</sup>, utilising a probe area of 0.5 cm<sup>2</sup>. Figure 3.14 shows a stretched (200%), doped ES film and demonstrates the lustrous blue sheen exhibited by such doped samples.

The behaviour of conductivity parallel and perpendicular to the stretch direction ( $\sigma_{//}$  and  $\sigma_{\perp}$  respectively) and anisotropy ( $\sigma_{//} / \sigma_{\perp}$ ) with elongation was practically the same as that shown in Figures 2.12 and 2.13 (experimental results from Durham group). Hence the reader is referred to these diagrams, but to recap, for maximally stretched specimens (300%), a parallel conductivity of 350 S cm<sup>-1</sup> was observed with an anisotropy of around 24. These values of conductivity are dependent on the thermal

history though, as inferred from the TGA studied loss of dopant at elevated temperature (see section 3.4.2). Thus if doped films are dried in an oven, the measured conductivity will be lower<sup>37</sup>. Furthermore, the highest values of conductivity are recorded for the thinnest areas of a stretched film i.e those at the end around 15-18  $\mu\text{m}$ . Thus it appears that for the thicker regions of a film full protonation may be inhibited and only 'surface' doping achieved. Possibly this effect is due to the ordered nature of the chains preventing chlorine counter-ions penetrating the sample, since it has been observed that very highly stretched samples cannot be doped effectively<sup>36</sup>.

Although HCl is the most common acid used to protonate EB, other aqueous acids can also be used. Methane sulfonic acid has been found to give even higher conductivity values than HCl<sup>39</sup>. For example, an unstretched film, when doped in an aqueous 10% solution of methane sulfonic acid had a measured conductivity of around 150  $\text{S cm}^{-1}$ , compared to the value of 60-70  $\text{S cm}^{-1}$  when doped in 1 M HCl. Furthermore, such a doped sample displayed rather good stability, with only a 50% decrease in conductivity over a period of 1 year when left in a benchtop environment.

Finally, as an aside, the ES samples prepared for this thesis were also used in a series of thermoelectric experiments<sup>40</sup>, which allow possible conduction mechanisms to be probed. These measurements have been reported in the literature<sup>41</sup> and may be briefly summarised as follows. Figure 3.15 shows the temperature dependence of the thermopower,  $S$ , of an unstretched polyaniline film, doped in 1M HCl ( $\sigma_{RT} = 80 \text{ S cm}^{-1}$ ). At room temperature  $S_{RT} = -18.3 \mu\text{V K}^{-1}$  and the temperature dependence shows a non-linear behaviour from 300 to 77K as similarly reported by Schaklette *et al*<sup>42</sup>. Two scenarios can be used to describe transport in polyaniline<sup>19</sup>; either a variable-range hopping (VRH) model<sup>43</sup> where

$$S = \frac{k^2}{2e} (T_0 T)^{1/2} \left( \frac{d \ln N(E)}{dE} \right)_{E = E_F}$$

or a metallic system where

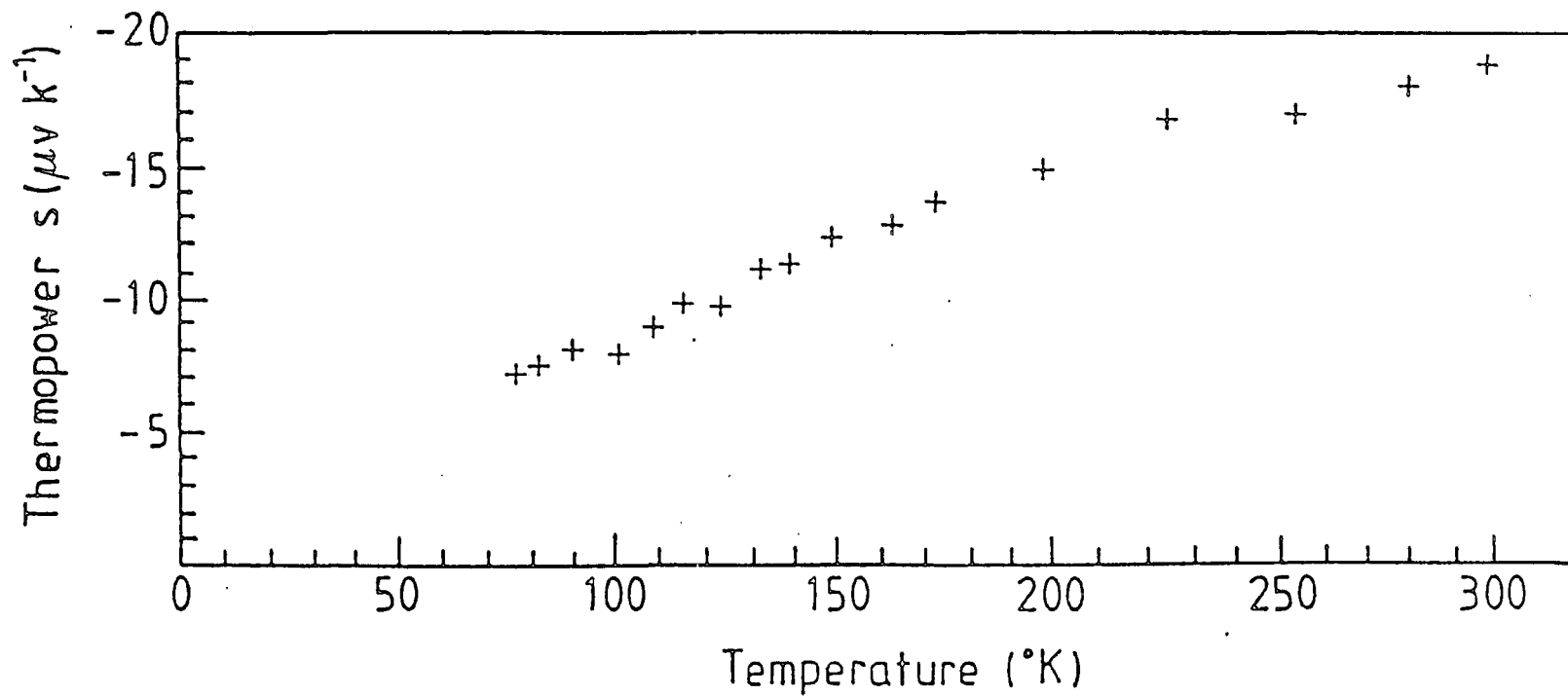


Figure 3.15

The temperature dependence of the thermopower,  $S$ , of an unstretched ES (doped in 1M HCl) film (from Monkman *et al*<sup>41</sup>).

$$S = \frac{\pi^2}{3} \frac{k^2 T}{e} \left( \frac{d \ln \sigma(E)}{dE} \right)_{E=E_F}$$

where  $\sigma(E) \propto (N(E))^2$ .

In both cases the negative sign of the thermopower has been taken to imply that the charge carriers have a negative sign i.e. they are electrons not holes (also this negative sign may imply that the quantity in brackets is negative i.e. the density of states at the Fermi level has curvature). However, in the VRH case,  $S \propto T^{1/2}$ , whereas for metallic conduction  $S \propto T$ . Figure 3.16 shows a plot of  $\log S$  versus  $\log T$  and indicates that the best fit to the experimental data occurs when  $S \propto T^{0.7}$ . The magnitude of  $S$  implies that the carriers giving rise to conduction come from states only a few  $kT$  from the Fermi level, so indicating a density of states at or near this Fermi level. Also since  $S$  is non-zero, these density of states must be non-stationary. This results points toward conduction in extended states i.e. metallic conductivity. However, the  $T$  dependence of  $S$  i.e.  $S \propto T^{0.7}$  is not entirely consistent with this picture. It can thus be concluded that either ES samples are not conducting enough or possess too many chain imperfections to allow true metallic behaviour. Certainly, with regards to the latter point, it has been shown in section 3.3 that there is a certain amount, albeit less than 5%, of defects present in the base powder. Therefore the conduction mechanism is still dominated by hopping and is likely to be so even for stretch aligned films.

### 3.7 Summary

This chapter has dealt with a number of important aspects of sample preparation, from the synthesis of polyaniline to the stretch alignment and subsequent doping of free-standing films cast from the solvent N-methyl-2-pyrrolidinone (NMP). Starting with the polymer synthesis, a procedure has been described and analysed. The emeraldine base powder (EB) produced

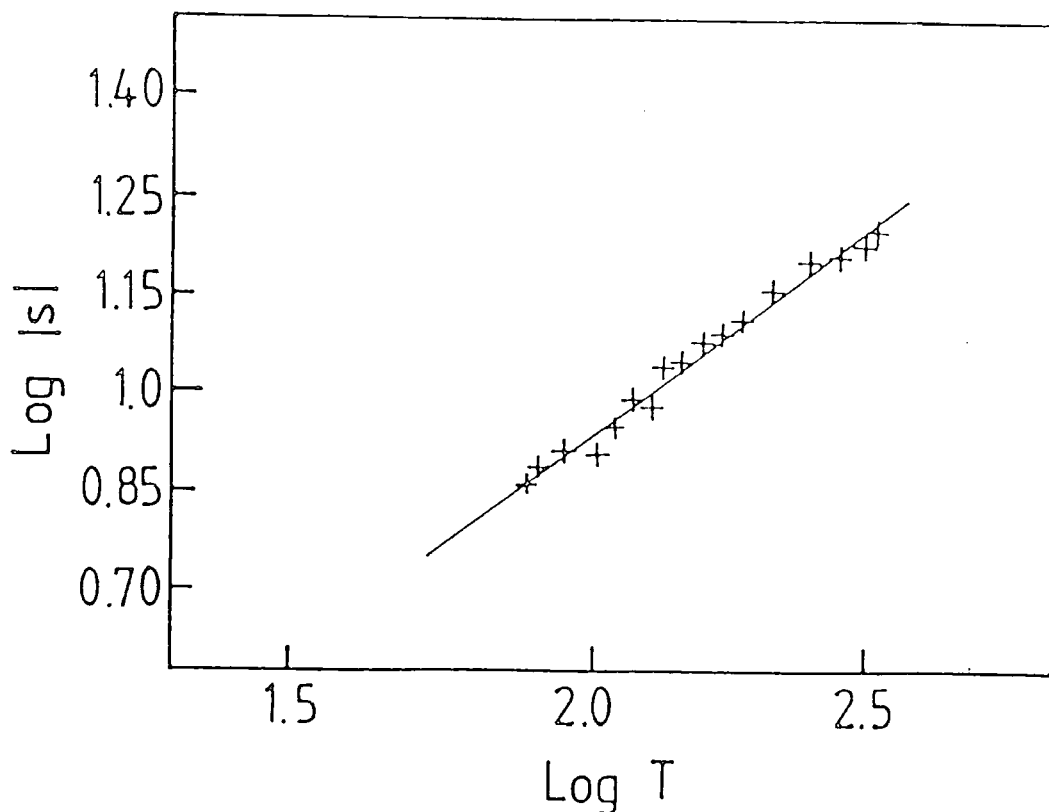


**Figure 3.16** Fit of thermopower data. Best straight line yields a  $T^{0.7}$  dependence (from Monkman *et al*<sup>41</sup>).

has been assessed for chemical composition using elemental analysis and  $^{13}\text{C}$  solution state NMR and for molecular weight using gel permeation chromatography (g.p.c.). The NMR results have unequivocally established that the product is indeed EB polyaniline. However, the polymer has also been shown to possess a high degree of stereochemical complexity. This complexity is likely responsible for many of the further problems encountered with detailed characterisation studies. Furthermore, the polymer was also found to contain a small fraction, ca. 5%, of contaminants, some of which may be associated with chain defects (as discussed later on). Through gel permeation chromatography, using poly (2-vinylpyridine) (PVP) as a calibration standard, the molecular weight of the polymer was determined to be typically  $\overline{M}_p = 3.2 \times 10^5$ . The choice of PVP as a standard has allowed the molecular weight to be estimated with a high degree of accuracy since, unlike previously used polystyrene standards, PVP displays



good solubility in NMP. Through these analysis techniques it has also been shown that only slight variation in synthesis procedure can greatly alter the chemical and in turn physical properties of the polymer. The importance of precise control of polyaniline synthesis is therefore strongly emphasised.

The fabrication of polyaniline films has been described using the solvent N-methyl-2-pyrrolidinone (NMP). These samples have been assessed for quality and also for composition using thermogravimetric analysis (TGA). This latter technique has indicated that as-cast EB films typically contain some 25% residual NMP. However, conducting specimens i.e. those protonated by aqueous HCl, contain no NMP and furthermore tend to lose dopant molecules at elevated temperatures. The orientation of polyaniline films has also been described in some detail, in particular in relation to the alignment of other conducting polymers and common thermoplastics such as polyethylene. Stretching can only be achieved for as-cast EB films and is crucially dependent on the residual NMP in the material. The stretching process itself depends on a wide number of variables and was found to be rather difficult to control. Nevertheless, a procedure was developed through which polyaniline samples with extensions of up to 300% could be produced on a quite reproducible scale.

After processing these base samples can be protonated to the emeraldine salt (ES) i.e. conducting form by doping films in 1M HCl. Unstretched, ES films have a conductivity of typically  $60\text{--}70\text{ S cm}^{-1}$ . However, extended samples display a remarkable increase in conductivity when measured parallel to the stretch direction. For maximally stretched films i.e. 300% this parallel conductivity reaches  $350\text{ S cm}^{-1}$ , with an anisotropy (parallel divided by perpendicular conductivity) of around 24. These conducting samples have also been studied using thermopower analysis, the results of which have enabled the mechanism of conduction to be assessed. The magnitude of the thermopower implies conduction in extended states i.e. metallic conductivity, but the temperature variation of this parameter indicates that variable range hopping dominates the conduction mechanism. A likely possible cause of this deviation from metallic behaviour is the presence of defect structures along the chain backbone.

Therefore the optimisation of the polyaniline itself (in terms of molecular weight and amount of defects) will undoubtedly move the values of conductivity ever closer to those needed for potential applications.

## References

- 1 M. Angelopoulos, C.E. Asturier, S.P. Ermer, E.M. Scherr, A.G. MacDiarmid, M.A. Akhtar, Z. Kiss and A. J. Epstein, *Mol. Cryst. Liq. Cryst.*, **160**, (1988), 151.
- 2 A.M. Kenwright, W.J. Feast, P. Adams, A.J. Milton, A.P. Monkman and B.J. Say, *Polymer*, **33**, (1992), 4292.
- 3 A.P. Monkman and P. Adams, *Synth. Met.*, **41-43**, (1991), 891.
- 4 S. Kaplan, E.M. Conwell, A.F. Richter and A.G. MacDiarmid, *J. Am. Chem. Soc.*, **110**, (1988), 7467.
- 5 A.F. Richter, A. Ray, K.V. Ramanathan, S.K. Manohar, G.T. Furst, S.J. Opella and A.G. MacDiarmid, *Synth. Met.*, **29**, (1988), E243.
- 6 M.R. Bendall and D.T. Pegg, *J. Mag. Res.*, **53**, (1983), 272.
- 7 G.V. Austerweil, *Chem. Abs.*, **46**, (1952), 10492.
- 8 L.W. Schaklette, J.F. Wolf, S. Gould and R.H. Baughman, *J. Chem. Phys.*, **88**, (1988), 3955.
- 9 A.J. Epstein, R.P. McCall, J.M. Ginder and A.G. MacDiarmid in *Spectroscopy of Advanced Materials*, Volume 19, eds. R.J.H. Clark and R.E. Hester, John Wiley & Sons Ltd, 1991.
- 10 H.W. Speiss, *Colloid Polym. Sci.*, **261**, (1983), 193.
- 11 S. Kaplan, E.M. Conwell, A.F. Richter, and A.G. MacDiarmid, *Macromolecules*, **22**, (1989), 1669.
- 12 J.M. Evans, *Poly. Mat. Sci. Eng.*, **13**, (1973), 401.
- 13 J.V. Dawkins and G. Yeadon, in *Developments in Polymer Characterisation -1*, ed. J.V. Dawkins, Applied Science Publishers, London, 1978.
- 14 E.M. Scherr, A.G. MacDiarmid, S.K. Manohar, J.G. Masters, Y. Sun, X. Tang, M.A. Drury, P.J. Glatkowski, V.J. Cajipe, J.E. Fischer, K.R. Kromack, M.E. Jozefowicz, J.M. Ginder, R.P. McCall and A.J. Epstein, *Synth. Met.*, **41-43**, (1991), 735.

- 15 A.G. MacDiarmid and A.J. Epstein, *Faraday Discuss. Chem. Soc.*, **88**, (1989), 317.
- 16 M.J. Miles in *Developments in Crystalline Polymers-2*, ed. D.C. Basset, Elsevier Applied Science, 1983.
- 17 K. Tzou and R.V. Gregory, *Synth. Met.*, Proceedings of ICSM 1992.
- 18 A.G. MacDiarmid, Y. Min, E.J. Oh, E.M. Scherr, X. Tang, J.G. Masters and A.J. Epstein, *Synth. Met.*, Proceedings of ICSM 1992.
- 19 A.P. Monkman, thesis, University of London, 1989.
- 20 Y.W. Park, M.A. Druy, C.K. Chaing, A.G. MacDiarmid, A.J. Heeger, H. Shirak and S. Ikeda, *J. Polym. Sci. (Lett.)*, **17**, (1979), 195.
- 21 G. Tourillon and F. Garnier, *J. Polym. Sci. (Phys.)*, **22**, (1984), 33.
- 22 M. Salmon, A.F. Diaz, A.J. Logan M. Krounbi, J. Bargon, *Mol. Cryst. Liq. Cryst.*, **83**, (1982), 265
- 23 D.D.C. Bradley, *J. Phys. D: Appl. Phys.*, **20**, (1987), 1389.
- 24 J.R. MacCallum in *Comprehensive Polymer Science- Volume 2* ed. G. Allen, Pergamon Press, 1989.
- 25 J. Yue, A.J. Epstein, Z. Zhong, P.K. Gallagher and A.G. MacDiarmid, *Synth. Met.*, **41-43**, (1991), 765.
- 26 Y. Wei and K.F. Hseuh, *J. Polym. Sci.: Part A*, **27**, (1989), 4351.
- 27 P.N. Adams, unpublished measurements.
- 28 I. Holliday and I.M. Ward in *Structure and Properties of Oriented Polymers*, ed. I.M. Ward, Applied Science Publishers, London, 1975.
- 29 *Mechanical Properties of Solid Polymers*, I.M. Ward, John Wiley & Son Ltd, 1971.
- 30 P.D. Townsend, C.M. Pereira, D.D.C. Bradley, M.E. Horton and R.H. Friend, *J. Phys. C*, **18**, (1985), L283.
- 31 D.D.C. Bradley, R.H. Friend, T. Hartmann. E.A. Marseglia, M.M. Sokolowski and P.D. Townsend, *Synth. Met.*, **17**, (1987), 473.
- 32 D.D.C. Bradley, R.H. Friend, H. Lindenberger and S. Roth, *Polymer*, **27**, (1986), 1709.
- 33 D.R. Gagnon, F.E. Karasz, E.L. Thomas and R.W. Lenz, *Synth. Met.*, **20**, (1987), 85.
- 34 A.G. MacDiarmid, *Synth Met.*, Proceedings of ICSM '92.
- 35 L.E. Alexander, *X-ray Diffraction Methods in Polymer Science*, Wiley-Interscience, 1969.
- 36 A.P. Monkman and P. Adams, *Synth. Met.*, **41-43**, (1991), 627.

- 37 J-C. Chiang and A.G. MacDiarmid, *Synth. Met.*, **13**, (1986), 193.
- 38 M.C. Montgomery, *J. Appl. Phys.*, **42**, (1971), 2971.
- 39 P.N. Adams, University of Durham, unpublished results.
- 40 R.D. Barnard, *Thermoelectricity in Metals and Alloys*, Taylor and Francis, London, 1972.
- 41 A.P. Monkman, F. Hampson and A.J. Milton in *Electronic Properties of Polymers*, eds. H. Kuzmany, M. Melring and S. Roth, Springer Verlag Series in Solid State Sciences, **107**, (1992), 255.
- 42 Y.W. Park, Y.S. Lee, C. Park, L.W. Schaklette and R.H. Baughmann, *Solid State Comm.*, **63**, (1987), 1063.
- 43 *Electronic processes in Non-Crystalline Materials*, N.F. Mott and E.A. Davies, 2nd edition, Clarendon Press, Oxford, 1979.

## Chapter 4

### Thermal Properties of Polyaniline Films

This chapter describes the use of a variety of thermal analysis techniques to probe the thermal properties of polyaniline and to analyse in more depth the processing behaviour of the film samples. Many of these results have also been published in a recent paper in the literature, see Appendix.

#### 4.1 Introduction

In the previous chapter the central role of thermal processing in the orientation of polyaniline films was described. Of particular interest was the apparent plasticisation effect induced by the residual NMP solvent in as-cast films, typically some 25%, which allows such samples to be stretch aligned at elevated temperatures. On the other hand, samples that contain no or very little NMP are ostensibly brittle and unprocessable. The thermal analysis techniques here have revealed the answers to this processing behaviour and have also identified a number of other important features. In particular a thermally induced hardening reaction has been observed, which greatly affects the properties of polyaniline films.

#### 4.2 Dynamic Mechanical Thermal Analysis

Dynamic Mechanical Thermal Analysis<sup>1,2</sup> (DMTA) is a form of relaxation spectroscopy which detects essentially all changes in molecular motion with changing temperature. It is thus a very powerful technique for studying molecular structure and has been used extensively in this work.

Measurements involve applying a small oscillating mechanical stress to a suitable sample and resolving the resulting strain into real and imaginary components. The type of data produced is shown schematically in Figure 4.1 for a typical semi-crystalline polymer. The labelling nomenclature follows

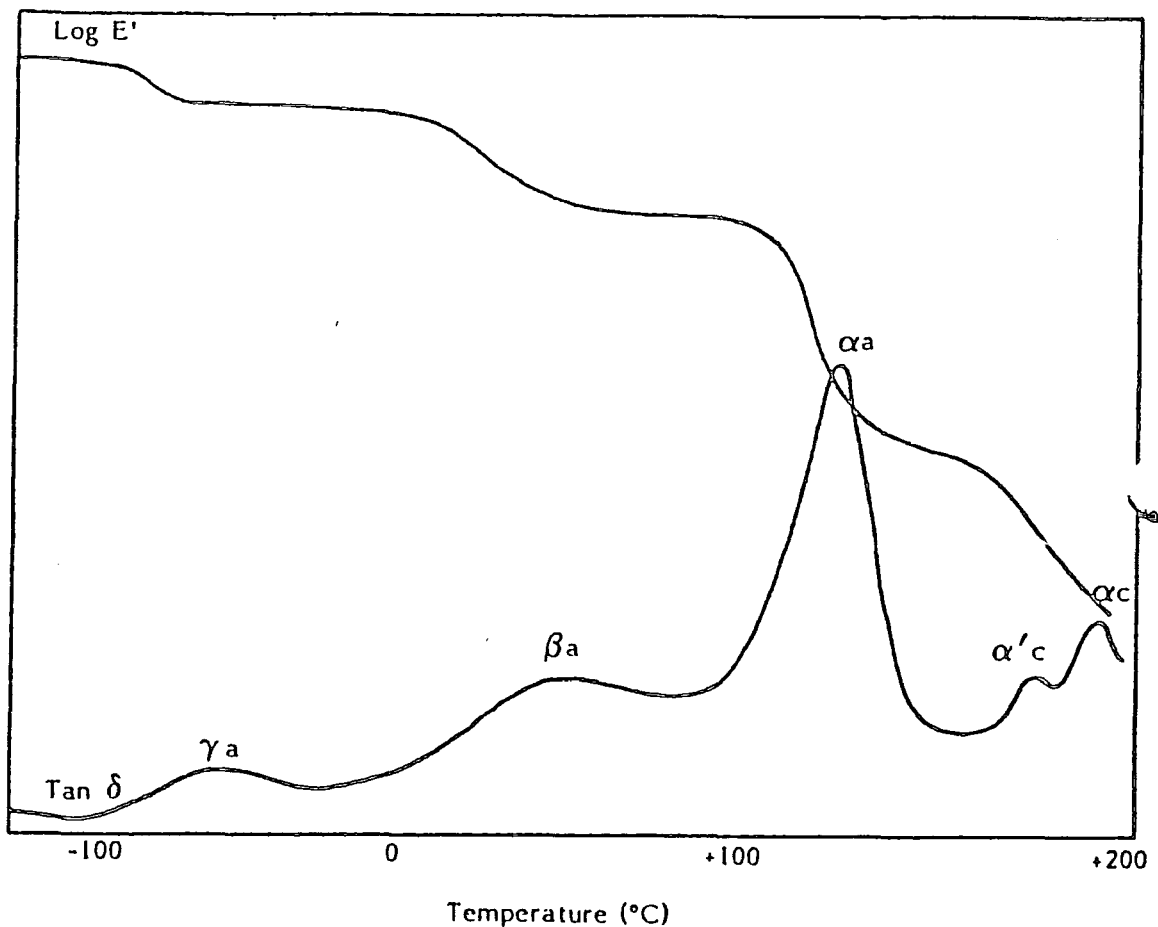


**Figure 4.1 DMTA data characteristic of a semi-crystalline polymer, as discussed in the text.**

the Greek alphabet running from high to low temperatures. The subscripts indicate motions ascribed to amorphous and crystalline components.

The DMTA spectrum characterises the motional changes occurring with temperature. The observation of a 'molecular transition' signifies the onset of some new mode of motion, at the measurement frequency. Those associated with the crystalline phase (e.g. melting) always occur at temperatures above the  $\alpha_a$  or glass transition ( $T_g$ ) process.  $T_g$  is measured with a very high degree of sensitivity, while secondary ( $\beta$ ,  $\gamma$ ,  $\delta$ ) transitions

(such as side group motions) are also observed and furthermore can be measured quantitatively.

#### 4.2.2 Theory

For a sinusoidal stress applied to a perfectly elastic solid the corresponding strain will be exactly in phase with the stress. In extension or bending experiments a dynamic Young's modulus,  $E^*$ , can then be defined<sup>3</sup> as

$$E^* = \text{stress amplitude/strain amplitude} \quad (1)$$

In shear deformation the dynamic rigidity modulus,  $G^*$  is obtained. However, if the frequency of the stress coincides with that of some internal molecular motion the material becomes viscoelastic in response. This results in the strain lagging behind the stress. In this situation it is appropriate to define a completely elastic component,  $E'$ , and a completely viscous component,  $E''$ , of the dynamic modulus,

$$E^* = E' + iE'' \quad (2)$$

$E'$  is the storage modulus and defined by the ratio of the in-phase amplitude components of stress and strain;  $E''$  is the loss modulus, the ratio of the out-of-phase components. The relationships are conveniently represented in an Argand diagram, Figure 4.2. From this diagram the mechanical loss tangent,  $\tan \delta$  can be derived,

$$\tan \delta = E''/E' \quad (3)$$

$\tan \delta$  is a dimensionless term quantified as the ratio of energy lost (dissipated as heat) to energy stored and so recovered per cycle.

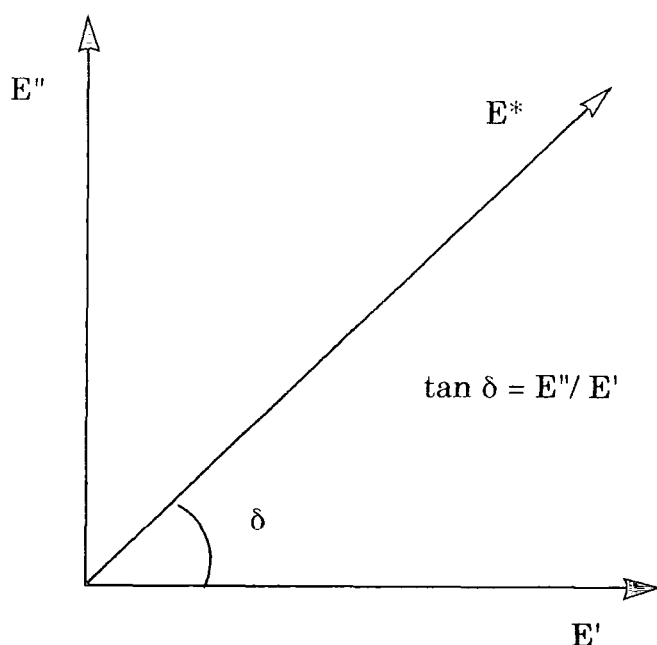


**Figure 4.2 Argand diagram showing the dynamic mechanical vector relationship between the storage ( $E'$ ) and loss ( $E''$ ) moduli.**

From this description one can see that excitation frequency is also a variable as well as temperature. Indeed theoretical models and interpretations<sup>1</sup> are primarily concerned with frequency plane data (i.e. scanning frequency at constant temperature). However, the range of frequencies experimentally available is limited and cannot completely measure even a single relaxation process. Thus, in general, scans are recorded at constant frequency, 1Hz being standard, while varying temperature. A discrete frequency range is of use though as loss peak positions change with frequency. Such data can be used in the calculation of an activation energy for a relaxation process.

In the frequency plane at any two temperature points, say  $T_1$  and  $T_2$ , a characteristic relaxation time,  $\tau$ , can be defined according to,



$$\begin{aligned}
&\text{at temperature } T_1 \text{ relaxation time } \tau_1 = 1/2\pi f_1 \\
&\text{at temperature } T_2 \text{ relaxation time } \tau_2 = 1/2\pi f_2
\end{aligned}
\tag{4}$$

Using transition state theory<sup>1</sup> the relaxation can be regarded as an energy barrier where,

$$\tau = \tau_0 \exp (\Delta H^*/ RT) \tag{5}$$

where  $\Delta H^*$  is the activation energy,  $T$  the absolute temperature and  $R$  the molar gas constant. From the loss peak position at frequencies  $f_1$  and  $f_2$  it can be shown that,

$$\Delta H^* = R \ln (f_1/ f_2)/ (1/ T_1 - 1/ T_2) \tag{6}$$

Using temperature plane data  $T_1$  and  $T_2$  are the positions of the loss peak maximum at frequencies  $f_1$  and  $f_2$ . A more accurate method is to obtain data covering, if possible, a three decade frequency range and plot  $\log f$  versus  $1/T_{\max}$ .

In principle the above interpretation requires peak position from loss modulus,  $E''$ , data. It is more convenient and reliable, though, to use  $\tan \delta$  curves. Although the two quantities do not peak at the same point the loss tangent is the same parameter whether derived from moduli or compliances and also responds in a systematic way to the volume fraction of any relaxing component. Neither is true for  $E''$ , introducing the possibility of ambiguity between results. Thus  $\tan \delta$  results are presented in this work, rather than loss moduli.

### 4.2.3 Behaviour of Polymer Systems

For amorphous polymers the primary relaxation occurs at or around  $T_g$  and is known as the glass-rubber transition. It is by far the most prominent mechanical relaxation and is accompanied by a drop in modulus from around  $10^{11}$  Pa to  $10^7$  Pa. From a molecular viewpoint it has been widely accepted for some time that this  $T_g$  process results from large-scale conformational rearrangements of the polymer chain backbone. The mechanism for such rearrangements is one of hindered rotation about the main chain bonds. This motion may be visualised as illustrated in Figure 4.3 and is sometimes known as reptation<sup>4</sup>, due to its resemblance to the motion of a snake.

Several theories have been developed to explain this molecular motion. The Gaussian Submolecular Model<sup>5</sup> describes a random gaussian chain which is arbitrarily subdivided into a number of segments, or 'submolecules'. The motion of this chain can then be approximated as a superposition of the normal modes of each segment. This treatment, however, neglects short-range motions, thus simplifying the mathematics. Other more detailed models have also been proposed<sup>6</sup>. A further case is the so-called 'free-volume' theory<sup>7</sup>, which despite having no rigorous definition, is a very useful semiquantitative concept. The basic idea is that the molecular mobility at any temperature is dependent on the available free-volume at that temperature. As the temperature increases the free-volume increases and the molecular motions become more rapid.

As well as the glass-rubber transition, amorphous polymers usually exhibit at least one secondary relaxation. These loss regions ( $\beta$ ,  $\gamma$ ,  $\delta$  relaxations) occur from motions in the glass-like state. The main chains are effectively frozen-in in this state such that large-scale rearrangements of the chains are not possible. Most polymers, though, contain side groups which are capable of undergoing hindered rotations independent of the main chain and most secondary transitions are ascribed to such rotations. However, these relaxations are also observed in certain linear polymers in which these rotations do not occur. Thus some limited local motions of the chain backbone may be possible in the glassy state. Two possible mechanisms

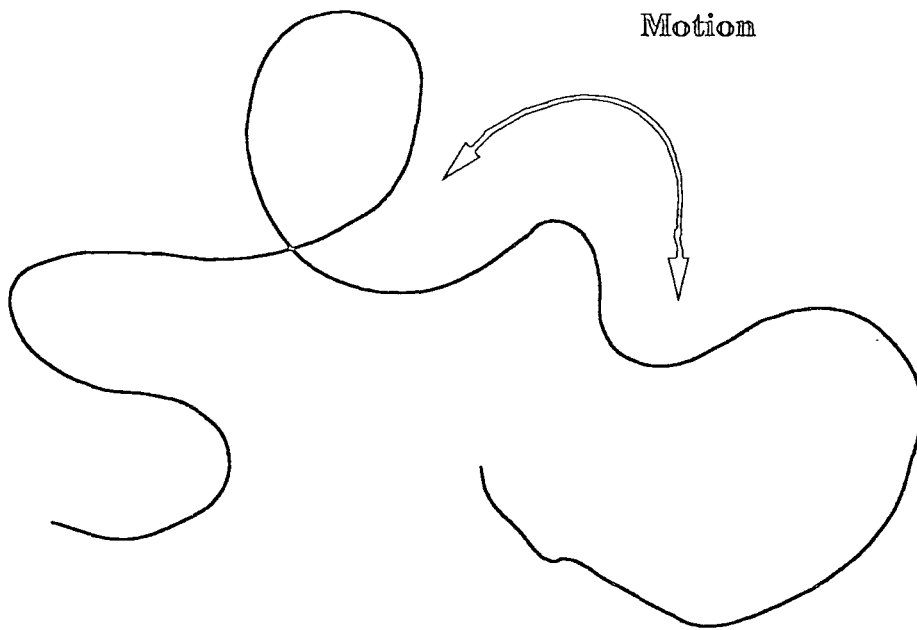


Figure 4.3 Reptation of a polymer chain during the glass transition.

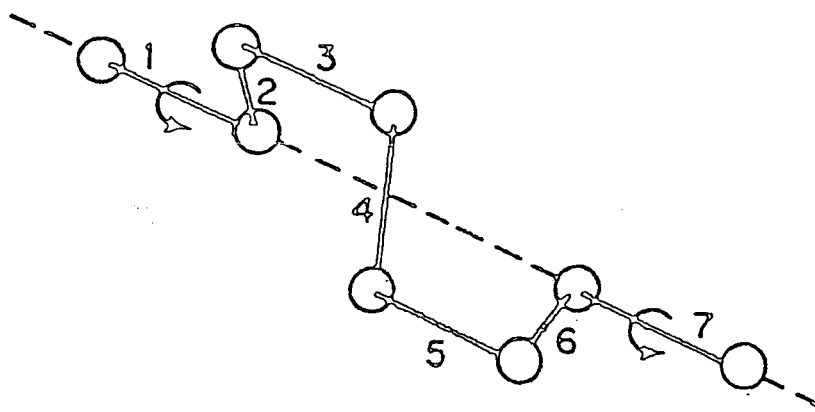


Figure 4.4 The crankshaft mechanism, due to Schatzki<sup>9</sup>, describing the secondary motion in linear polyethylene.

have been proposed for this type of motion, local mode theories<sup>8</sup> and the crankshaft mechanism of Schatzki<sup>9</sup>, see Figure 4.4.

Polystyrene, when produced by a free radical polymerisation, can be considered to have a classical amorphous structure. The DMTA  $\tan \delta$  spectrum for such a material, using the standard excitation frequency of 1Hz, is shown in Figure 4.5 and an interpretation<sup>3</sup> of this thermal spectrum can be made as follows

- 110°C      The  $\alpha_a$  or 'T<sub>g</sub> process' due to the onset of rotational freedom of the chain backbone.
  
- 20°C      Very broad  $\beta_a$  relaxation due to the torsional vibration of the phenyl ring about its axis to the main chain (this can be proved by analysis of the equivalent dielectric response).
  
- 240°C    Broad  $\delta_a$  transition, possibly associated with 'local mode' motion; co-operative torsional excursion about bonds without change in configuration.

Generally, though, the DMTA spectrum is different for different polymers and hence each requires its own molecular interpretation. Many amorphous polymers also show a  $\gamma$  process as well, which can be associated with angular chain co-operative motion giving rise to local configurational change or single bond flips.

Crystalline polymers e.g. polyesters, nylons, in general have a significant amorphous content, often in the region of 40%. The 'fringed micelle' or two-phase model, discussed more in chapter 6, is a basic approach used to describe the morphological structure. The amorphous phase undergoes its own set of motional transitions, largely the same as the completely amorphous materials. A slight perturbation of the transitions occurs though, due to constraints imposed by the crystalline phase, with the result that the glass transition may be shifted to higher temperatures and is always diminished in  $\tan \delta$  amplitude. Superimposed on these amorphous

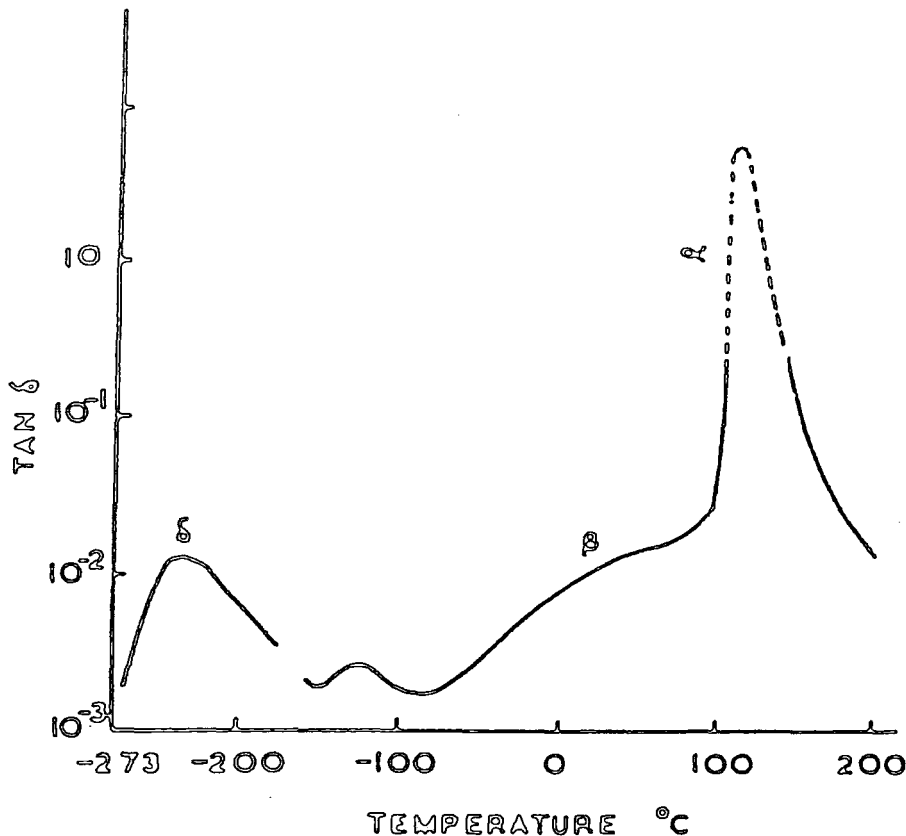


Figure 4.5 Dynamic mechanical relaxations in amorphous polystyrene measured at 1Hz.

transitions, as shown earlier in Figure 4.1, are the crystalline relaxations. The most notable contribution is the presence of a melting process, but the molecular origins of other ordered motions is tempered by the complicated and uncertain nature of the true physical structure. For example the  $\alpha_c$  process in polyethylene has been proposed as being due to motion in chain folded lamellae<sup>10</sup>, but also due to the motion of lattice defects<sup>11</sup>.

Besides homopolymers other polymeric systems may also be studied by DMTA. These include blends, copolymers and composites. A very interesting two-component system is that of a polymer and a plasticiser. The fundamental observation is that for compatible systems a single combined  $\alpha_a$  peak is observed, whose location is composition dependent.

Figure 4.6 illustrates data for polyvinyl chloride plasticised with various amounts of di(ethyl-hexyl) phthalate<sup>12</sup>. Clearly the added plasticiser lowers

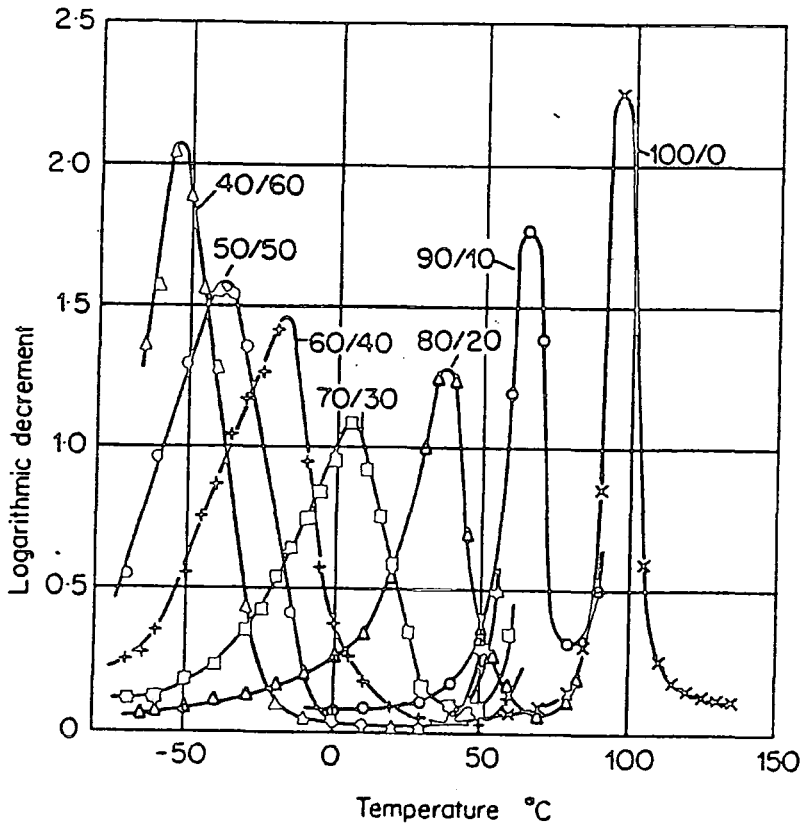


Figure 4.6 Logarithmic decrement ( $\pi \times \tan \delta$ ) of polyvinylchloride plasticised with various amounts of di(ethyl-hexyl) phthalate (after Wolf<sup>12</sup>).

the glass transition temperature enabling the material to be more easily processed in its softened state. For less compatible components, however, where the plasticiser has only a limited solubility in the polymer, the damping peak becomes very broad as shown in Figure 4.7. Diethyl phthalate is a relatively good plasticiser, dibutyl phthalate a poorer one and dioctyl phthalate a very poor plasticiser. In the limit of total incompatibility, each component exhibits its own characteristic relaxations.

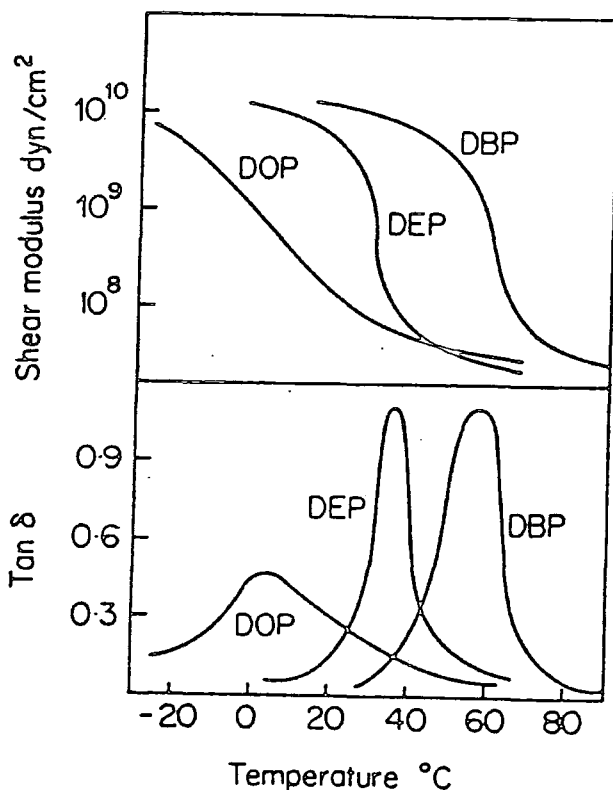


Figure 4.7 Shear modulus and loss factor,  $\tan\delta$ , for polyvinylchloride plasticised with diethyl phthalate (DEP), dibutyl phthalate (DBP) and n-dioctyl phthalate (DOP) after Gradin *et al*<sup>2</sup>.

Another important aspect measured by this technique is the effect of molecular weight and crosslinking. Molecular weight normally affects the mechanical behaviour above the glass transition, although the position of  $T_g$  in very low molecular weight materials is dependent on this property. High molecular weight chains are long enough to become temporarily entangled with one another, thereby forming physical crosslinks. These crosslinks prevent molecular flow and lead to rubber-like behaviour and a plateau in the modulus curve. On longer time scales or at higher temperatures, however, these crosslinks slowly disentangle.

Chemical crosslinking, on the other hand, raises the temperature of and broadens the glass transition and furthermore is permanent. This behaviour can be seen in Figure 4.8 for phenol formaldehyde crosslinked with different amounts of hexamethylene tetramine<sup>13</sup>. At a hardener concentration of 10% the material so highly crosslinked that no glass transition can be detected at all. The effects of chemical crosslinking are readily interpreted on the basis of free volume, where the crosslinking, by bringing adjacent chains closer together, reduces the free volume and hence raises  $T_g$ .

### 4.3 Dielectric Thermal Analysis

Dielectric thermal analysis<sup>1,14</sup> (DETA) is the electrical analogue of the mechanical DMTA and so is also a form of relaxation spectroscopy. However, the dielectric method detects only those molecular transitions involving dipolar activity or charge displacement. Thus DETA is a complimentary technique of great value in assigning or at the very least narrowing down the origins of molecular motion.

The basis of DETA is analogous to that of DMTA, previously discussed in detail. In the dielectric case a small sinusoidal electric field is applied to a suitable sample i.e. one that is not highly conducting. The charge  $Q$  is then assessed and normally followed via the current  $I$  since  $I = dQ/dt$ . The complex permittivity  $\epsilon^*$  is obtained from comparisons of the amplitudes, where

$$\epsilon^* = \epsilon' + i\epsilon'' \quad (7)$$

Phase measurement allows resolution of this complex parameter into a storage component, dielectric constant ( $\epsilon'$ ) and a loss component, the dielectric loss ( $\epsilon''$ ). The dielectric loss tangent,  $\tan \delta_E$ , is then described by





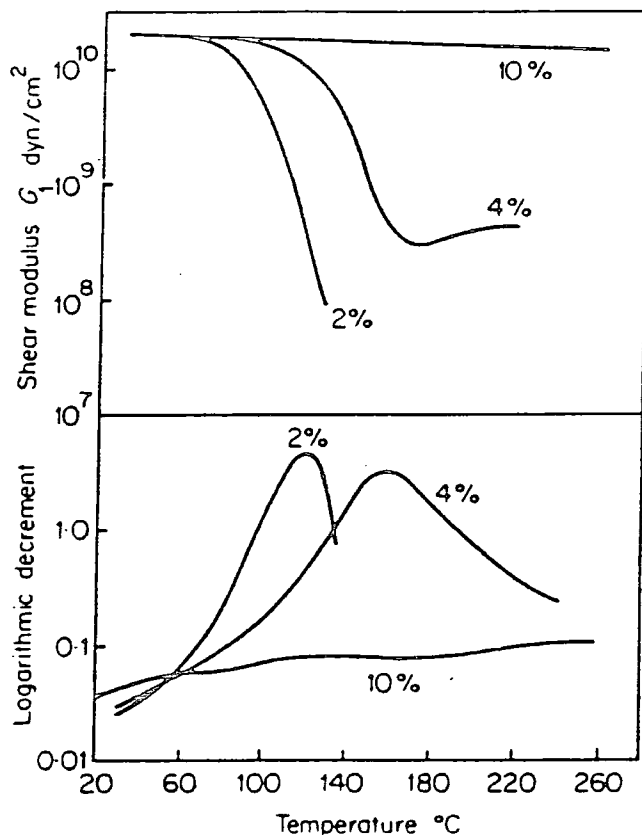


**Figure 4.8 Shear modulus,  $G_1$ , and logarithmic decrement ( $\pi \times \tan \delta$ ) of a phenol-formaldehyde resin crosslinked with hexamethylene tetramine at stated concentrations (after Drumm *et al*<sup>13</sup>).**

$$\tan \delta_E = \epsilon''/\epsilon' \quad (8)$$

as illustrated in the Argand diagram of Figure 4.9.

Dielectric data is represented in exactly the same format as DMTA, with plots of  $\tan \delta_E$  and  $\epsilon'$  versus temperature. However, the excitation frequency

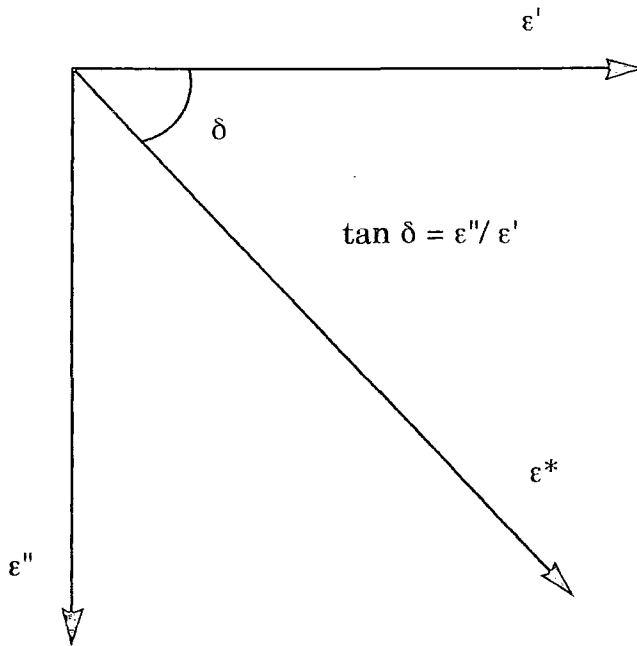


**Figure 4.9 Argand diagram showing the vector relationship between the dielectric constant ( $\epsilon'$ ) and dielectric loss ( $\epsilon''$ ).**

is much higher, typically 1 kHz is standard for dielectric measurements. Added to this the experimental frequency range is also much wider enabling frequency plane data to be more easily collected, if required. The strength of the dielectric process relates to the extent of freedom attained by the dipoles in that process<sup>15</sup>. Formally, the dielectric constant is equivalent to the mechanical compliance i.e. the dielectric experiment is measuring the ability of the system to move rather than to resist movement.

Nevertheless, the dielectric loss term correlates well in position with the loss modulus  $E''$  rather than the loss compliance  $G''$  as does  $\tan \delta_E$  with the DMTA  $\tan \delta$ . The reason for this is that the dielectric constant and the modulus are most affected by small-scale molecular motions, whereas compliance is weighted more towards large-scale molecular motions.

#### 4.4 Infrared Spectroscopy

Infrared (IR) spectroscopy is perhaps the most commonly-used method for the structural determination of polymers<sup>16,17</sup>. Although not regarded as a thermoanalytical technique, since the temperature control of a sample is trivial compared to the measurement of spectra, temperature dependent IR studies can reveal a wealth of structural information. Such results are particularly appropriate here because they can be correlated with the DMTA/DETA relaxations and can also provide further evidence as to the nature of thermal reactions.

As IR spectroscopy is such a fundamental analysis technique, it has been described in great detail and depth in the literature. As such no description will be given here, but if necessary the reader is referred to one of the many texts e.g.<sup>16,17</sup>. The control of temperature control, as mentioned, is quite simple and usually achieved by means of a sample heat stage. In this case an in-house accessory was utilised, as described in the experimental section.

#### 4.5 Thermomechanical Analysis

Thermomechanical analysis<sup>18</sup> (TMA) is a further technique which has been utilised. This method is a particularly sensitive technique for measuring dimensional changes in a sample as a function of temperature, or time isothermally. It can detect small changes associated with the onset of transitions within a polymer. In this study it has been used to probe the glass transition region.

The technique, also known as thermodilatometric analysis, monitors the linear expansion or contraction of a solid sample with temperature through a mechanical push-rod which rests lightly on the surface of the sample. The weight of the push-rod is compensated by a balancing support such that only a nominal weight of about 1g is exerted on the specimen. The movement of the rod is then monitored by a linear variable differential

transformer (LVDT). This one dimensional measurement may then be converted to a volume if the other dimensions remain constant.

#### 4.6 Experimental Section

The DMTA measurements were made using a Polymer Laboratories Mk II instrument belonging to the Helsby Technology Centre of BICC Cables Ltd. The machine was operated in tensile geometry as illustrated in Figure 4.10. The stress is proportional to the level of AC current fed to the drive coil from the tensile control unit and the frequency of oscillation may be varied between 0.01 and 200 Hz. The strain is proportional to the displacement of the drive clamps and is measured by a non-contacting eddy current transducer. The tensile head vibrator is mounted on a movable carriage, driven by a stepper motor, so that as the sample relaxes the force may be maintained. In addition a reducing force mode was applied for polyaniline samples such that the static tensile force is maintained at a constant ratio to the dynamic force. Under these conditions the strain is constant and sample creep minimised. The sample is covered by a oven (not shown) and the temperature controlled over the range -150-300°C by a temperature controller. The whole system was run under external computer control using a Compaq 386 machine. Various analysis routines in the software (PL V500 V5.20) allowed the experimental results to be manipulated.

The following experimental conditions were employed for standard scans at a frequency of 1Hz: static force, 1N; reducing force, on; strain, 32µm peak to peak displacement; thermal scan, -130 to 300°C; heating rate, 3°C /min. Sample dimensions, typically 12 x 5 x 0.06 mm, were kept approximately constant throughout so as to ensure reproducibility. The results are shown as plots of log storage modulus, ( $\log E'$  (Pa)) and mechanical damping ( $\tan \delta$ ) versus temperature. In addition variable frequency scans at 0.3 and 3 Hz were also measured under the same conditions.

DETA measurements were also recorded on a Polymer Laboratories instrument by Mr G. Foster, applications specialist of Polymer Laboratories Ltd, Loughborough. Samples, in the form of flat circular discs of 35mm

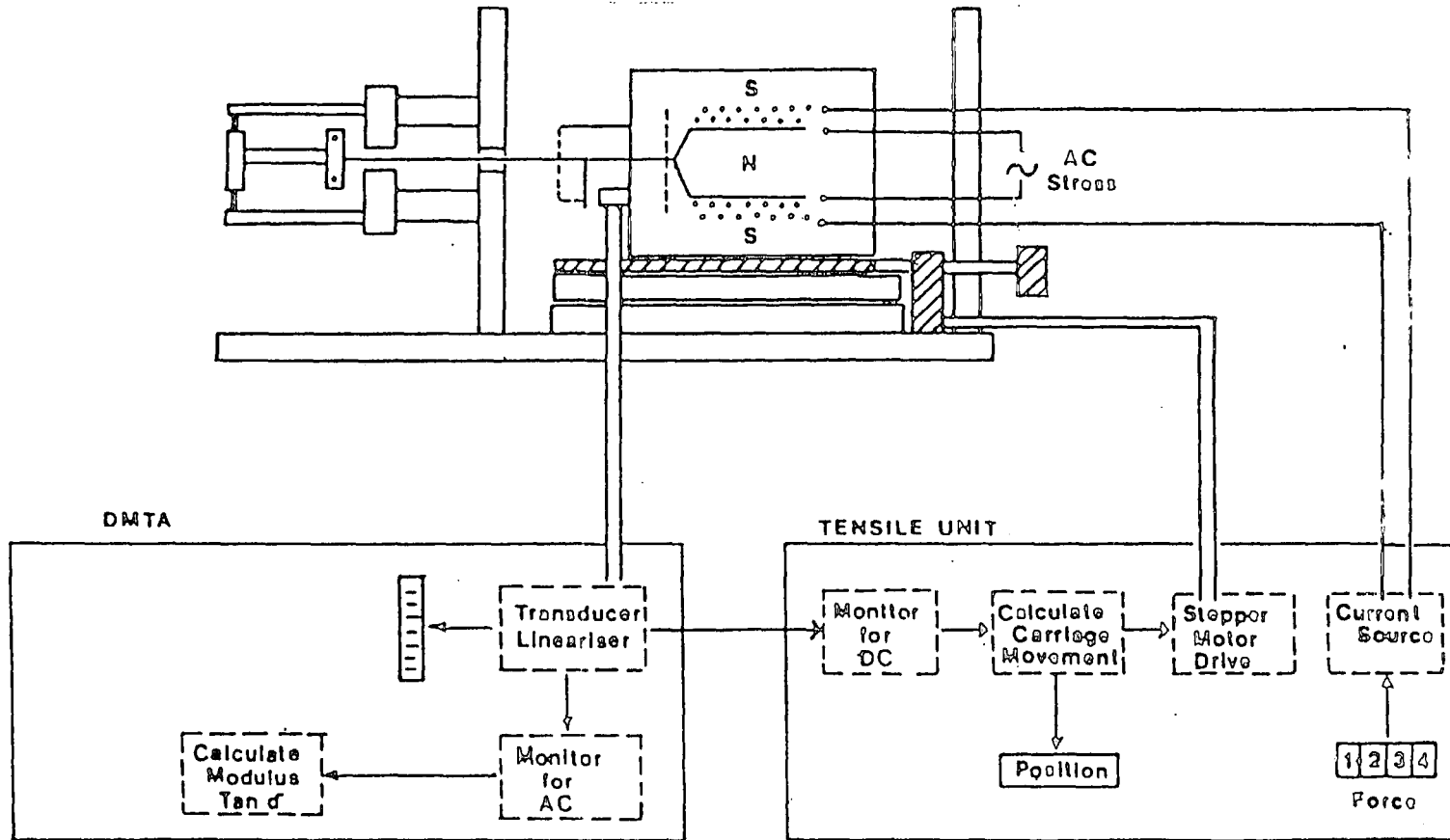


Figure 4.10 Schematic diagram of the DMTA operating in tensile mode.

diameter, were sandwiched between two metal electrodes. With this technique it is only possible to examine base films since doped samples are found to be too highly conducting. An excitation frequency of 1 kHz was used with the same temperature range and heating rate as for DMTA experiments. Thermograms are shown as plots of permittivity, ( $\epsilon'$ ) and dielectric damping ( $\tan \delta$ ) versus temperature. Similarly, the DETA was under computer control.

IR data was recorded on a Perkin-Elmer 580B spectrophotometer operating at  $3 \text{ cm}^{-1}$  resolution. This wavelength dispersive instrument, shown in Figure 4.11, was kindly donated to our group at Durham by BICC Cables Ltd, Helsby Technology Centre. Spectra were recorded over the range  $4000\text{-}400 \text{ cm}^{-1}$  under a dry-air purge. Free-standing films were measured in transmission using samples of less than  $20 \mu\text{m}$  in thickness. Spectra were also recorded in reflection using thin (ca.  $5 \mu\text{m}$ ), homogeneous films cast on an aluminium coated glass slide, mounted on an in-house designed reflection accessory. Such samples could be studied at elevated temperature by the coupling of a resistive heater, incorporating a Pt thermocouple, to the reverse side of the slide. The sample temperature was controlled in the range R.T. to  $250^\circ\text{C}$  using a Cal 9000 temperature controller.

The thermomechanical analysis was also carried out at the thermal analysis suite of BICC Cables Ltd, Helsby Technology Centre. The instrument used was a Stanton-Redcroft 792 model TMA, as illustrated in Figure 4.12. Specimens, in the form of 5 mm diameter discs, were monitored under a nitrogen atmosphere over the range R.T.- $300^\circ\text{C}$  with a heating rate of  $5^\circ\text{C min}^{-1}$ . A nominal push-rod weight of 5g was used. A chart recorder was used to record the data.

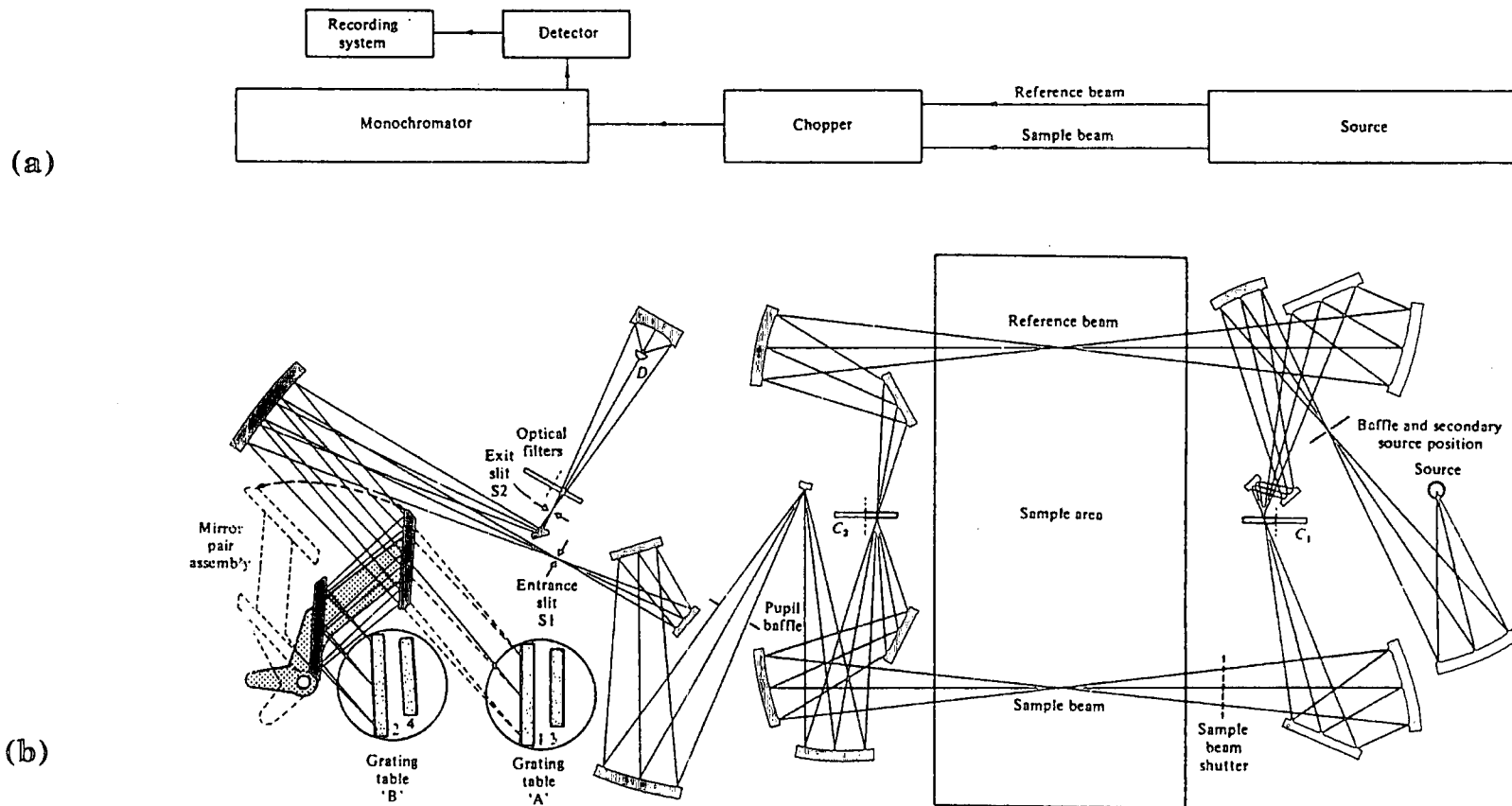


Figure 4.11 The dispersive infrared spectrophotometer; (a) block diagram, (b) optical diagram of a double-beam Perkin Elmer instrument.  $C_1$  is a rotating chopper/reflector which generates the sample and reference beams. The action of this chopper is synchronised with another chopper,  $C_2$ , and allows the radiation emitted by the materials in the sample and reference beams to be corrected for. There are four diffraction gratings, which are used for different regions of the spectrum and are brought into use automatically by rotation of the tables A or B or the mirror assembly. The detector, D, is a thermocouple.

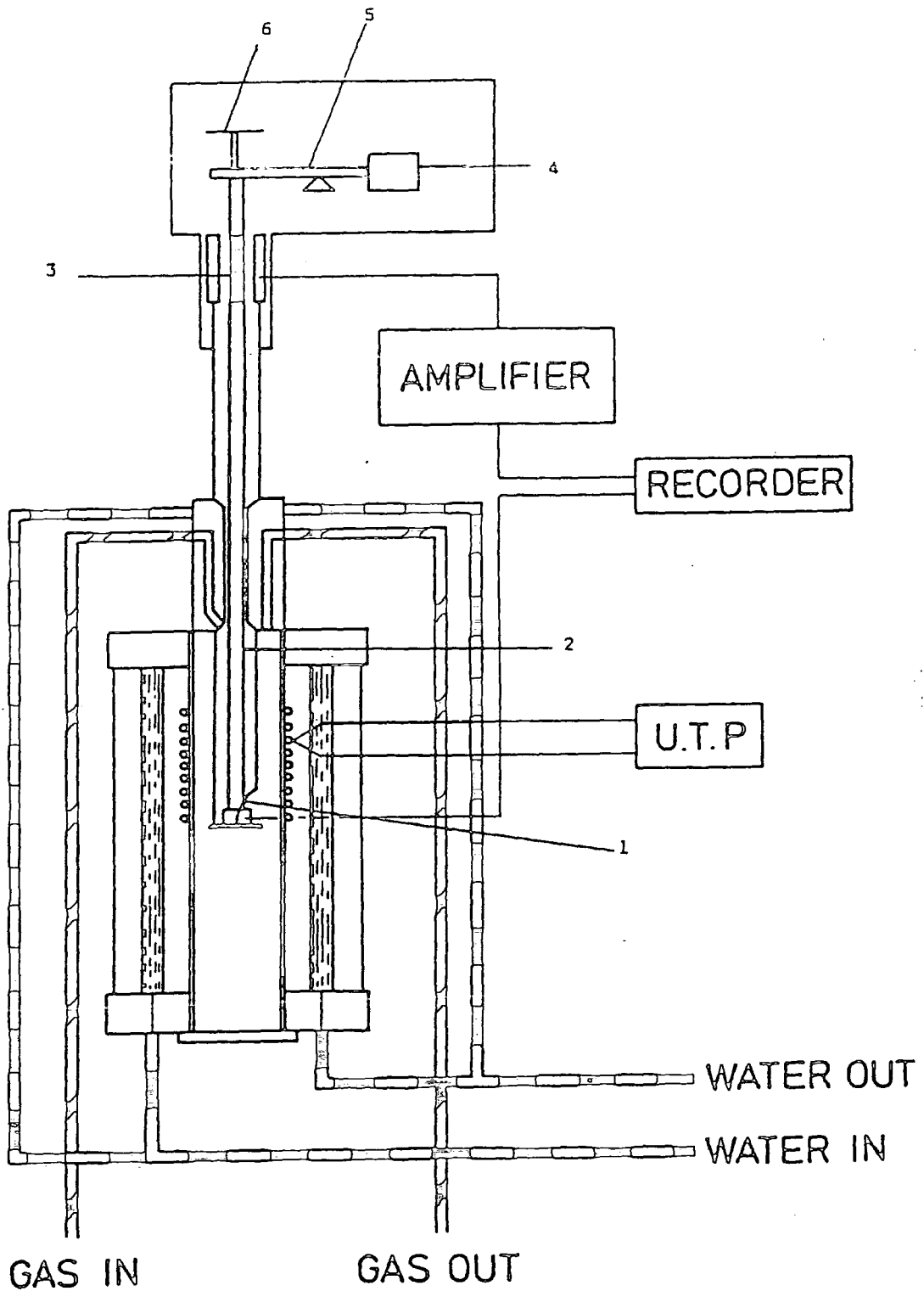


Figure 4.12 Schematic diagram of the Stanton-Redcroft model 792 TMA; (1) sample thermocouple, (2) quartz probe, (3) linear variable differential transducer (LVDT), (4) adjustable counter weight, (5) frictionless balance arm, (6) weight platform.



## 4.7 Results and Discussion

### 4.7.1 Mechanical Analysis

A typical thermal spectrum of an as-cast EB film is shown in Figure 4.13. The  $\tan \delta$  spectrum is dominated by an extremely broad relaxation feature incorporating two transitions, a peak at 180°C and a shoulder at approximately 100°C. From TGA analysis (reported in the previous chapter) these transitions are associated with loss of NMP solvent molecules. The 100°C transition coincides with a decrease in storage modulus from  $10^9$  to  $10^7$  Pa and can thus be assigned to a film softening or glass ( $T_g$ ) transition. It is through this glass-rubber transition, involving co-operative thermal motion of individual chain segments along the polymer backbone, that samples can be stretch aligned.

The residual 25% NMP is known to act as a 'plasticiser', the  $T_g$  transition shifting to higher temperatures with decreasing weight fraction of solvent<sup>19</sup>. However, the main constraint for a plasticiser is permanence. In this respect NMP is very poor as it is thermally removed during the transition. The width of the relaxation feature reflects the plasticisation criterion; since it is extremely broad in this case, polymer and solvent do not form a single solid phase. NMP remains essentially in the liquid state and is thus more volatile than the polyaniline component. It is this solvent volatility which is responsible for the glass transition. The 'spaces' produced by removal of NMP molecules act as a free volume around the chains, giving them rotational freedom.

However, this free volume exists for only a finite time. As the temperature rises beyond  $T_g$  the storage modulus increases to  $10^9$  Pa and the sample hardens. This process is characterised by the peak in  $\tan \delta$  at 180°C. Hardening occurs because sample compaction reduces the free volume to such an extent that chains become extensively entangled (i.e. physical crosslinking). This collapse in sample dimensions has been observed using thermomechanical analysis and is shown in Figure 4.14.

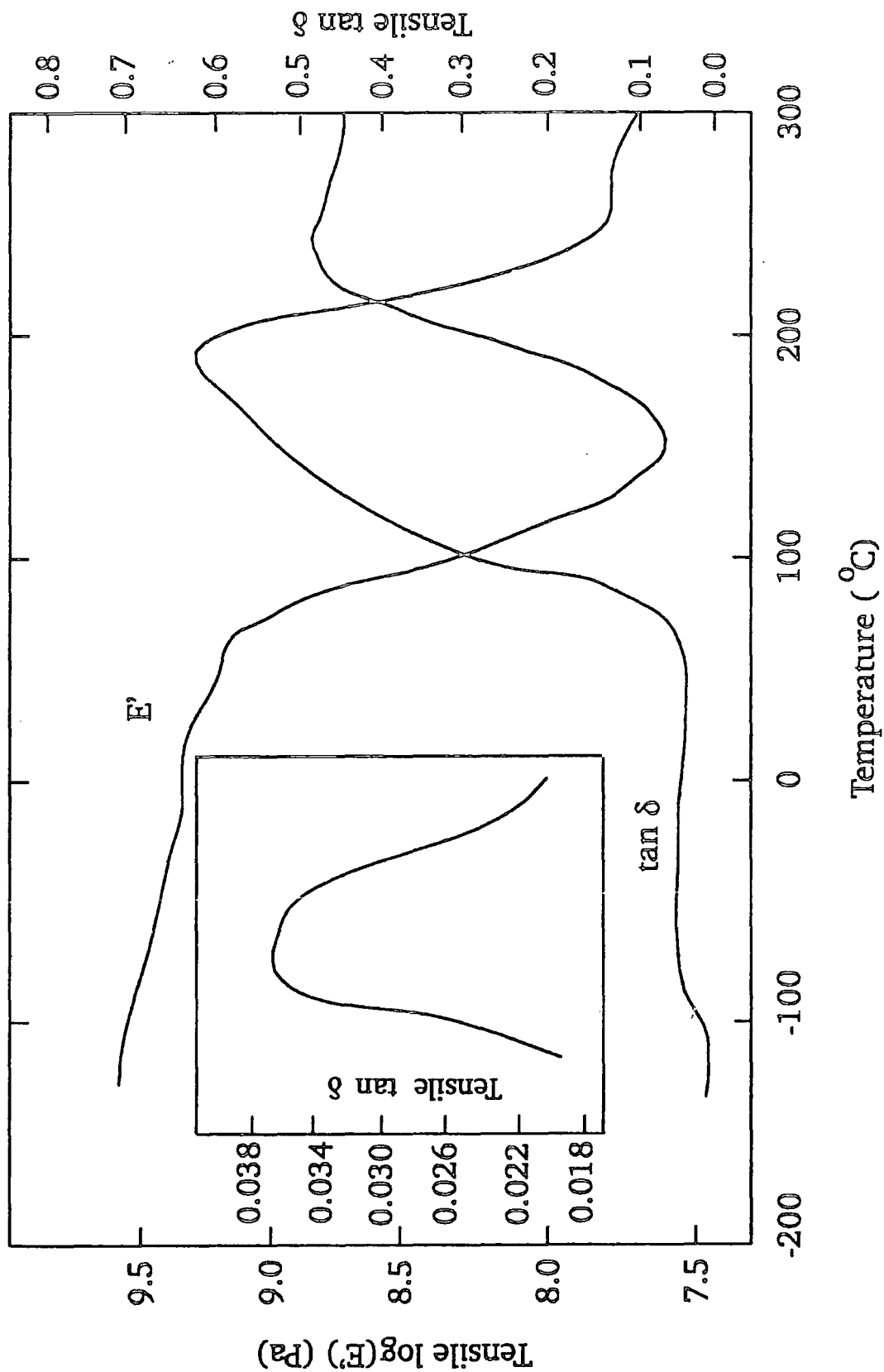


**Figure 4.13** DMTA thermogram (1Hz) of an as-cast EB film. The inset is an expansion of the  $\tan \delta$  curve.

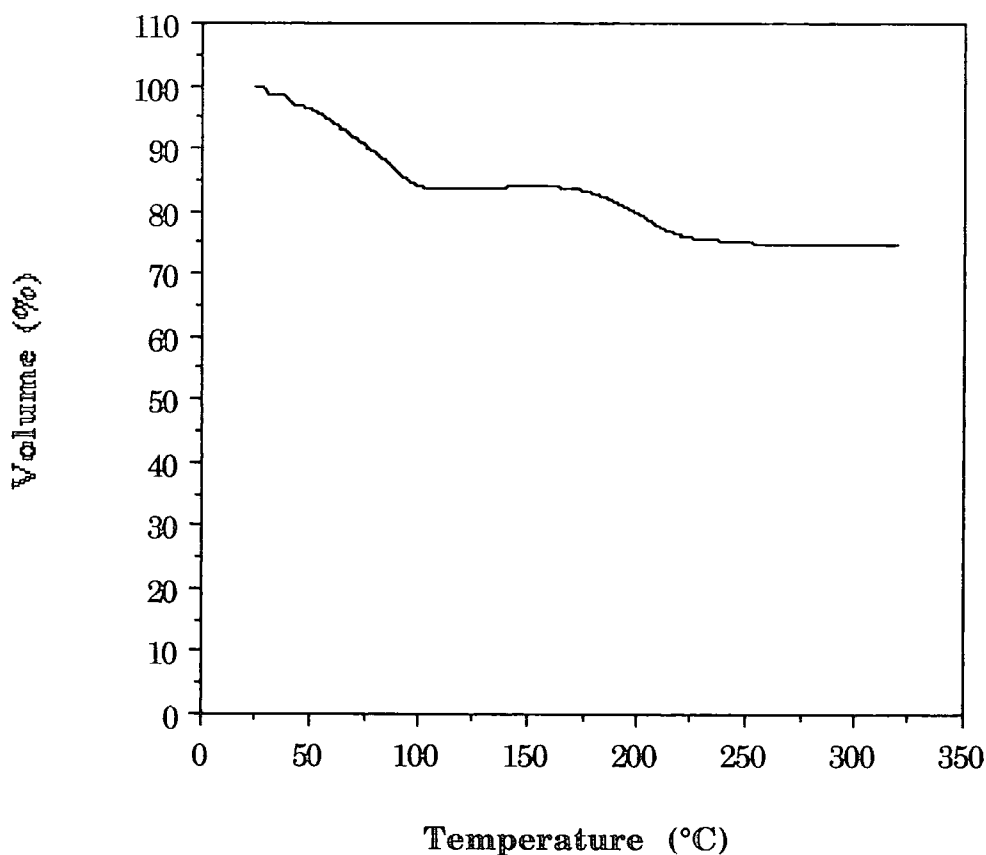


**Figure 4.14** The collapse in sample dimensions of an as-cast EB film with temperature as measured by thermomechanical analysis.

It seems clear that hardening involves a high degree of chain entanglements, but several pieces of evidence indicate a chemical crosslinking process (involving bonding between chains) occurs as well. Firstly, both chemical and physical crosslinks are indistinguishable on a short time scale<sup>3</sup>, but if only the latter are present the material should soften with time. However, an isothermal scan at 180°C, Figure 4.15, showed no such storage modulus decrease. Secondly, a similar rise in modulus due to hardening is exhibited during the cure of epoxy resins<sup>14</sup> and other synthetic polymers<sup>1</sup>. Furthermore, polyaniline samples heated through this hardening regime are totally intractable in NMP whereas as-cast samples are appreciably re-soluble.

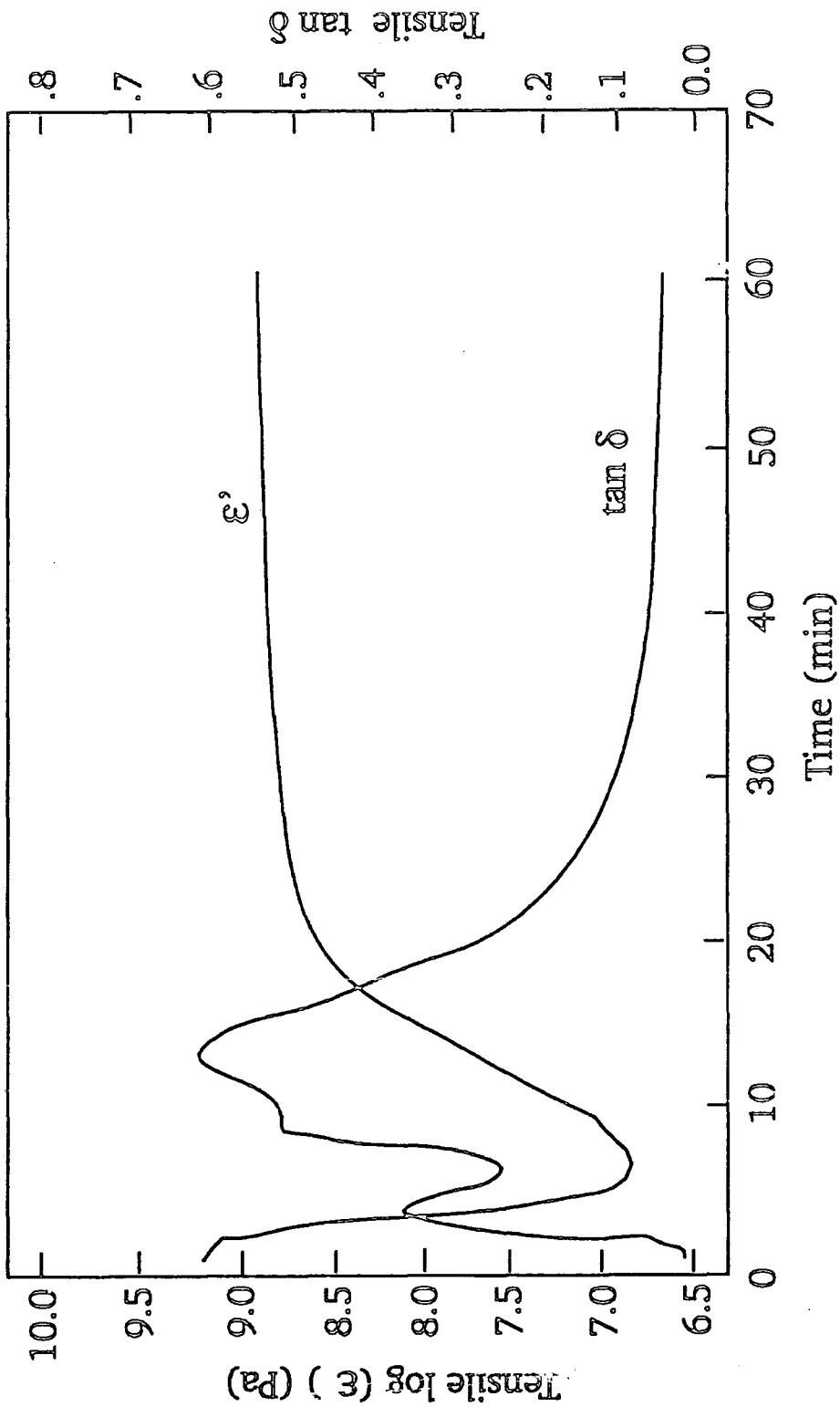


Figure 4.15

Isothermal DMTA scan for 1 hr at 180°C of an as-cast EB film.

The nature of possible chemical crosslinking processes is not evident from this data - this question is addressed using IR spectroscopy. What is clear is that to avoid crosslinking, samples must be thermally processed below the 180°C transition temperature. The hardening reaction is highly detrimental to the physical properties of the material. For example a crosslinked EB film is extremely brittle, mechanically weak, and cannot be stretch aligned. Added to this its conductivity when doped (1M HCl) is approximately one hundred times smaller than the 60-70 S cm<sup>-1</sup> of an as-cast doped film.

Another feature of the results for as-cast EB films is the presence of an asymmetric relaxation at approximately -80°C as shown on the expanded tan  $\delta$  curve of Figure 4.13. This transition is believed to be due to phenyl ring twisting. This type of ring motion plays a key role in the electronic properties of the polyaniline<sup>20,21</sup> and has been identified in low temperature NMR studies<sup>22</sup>. Using transition state theory the activation energy,  $\Delta H^*$ , of this peak is estimated to be 11 kcal mol<sup>-1</sup>, derived from peak positions at three different frequencies (0.3, 1, 3 Hz). There appears to be no similar calculation for polyaniline ring twisting in the literature with which to assess this value. However, a similar ring relaxation has been observed for polyethylene terephthalate (PET), a polymer which also contains a phenyl ring in the chain backbone<sup>1</sup>. For PET the activation energy for this motion is calculated to be 17 kcal mol<sup>-1</sup>, but also contains a contribution from an ester group in the structure. Therefore, a  $\Delta H^*$  value of 11 kcal mol<sup>-1</sup> for polyaniline ring twisting seems reasonable.

Further molecular information has been gained from the rescanning of an as-cast film. Such a sample, having been heated up to 300°C, is crosslinked, but is also solvent-free. Hence the observed transitions can only be attributed to the polymeric material with no effects due to NMP. Such a thermogram is shown in Figure 4.16. This spectrum was then reproducible on subsequent thermal scanning. It must be noted that in this crosslinked state films are extremely brittle and need very careful handling. Despite this, many specimens were found to fracture even with application of only a minimal stress.

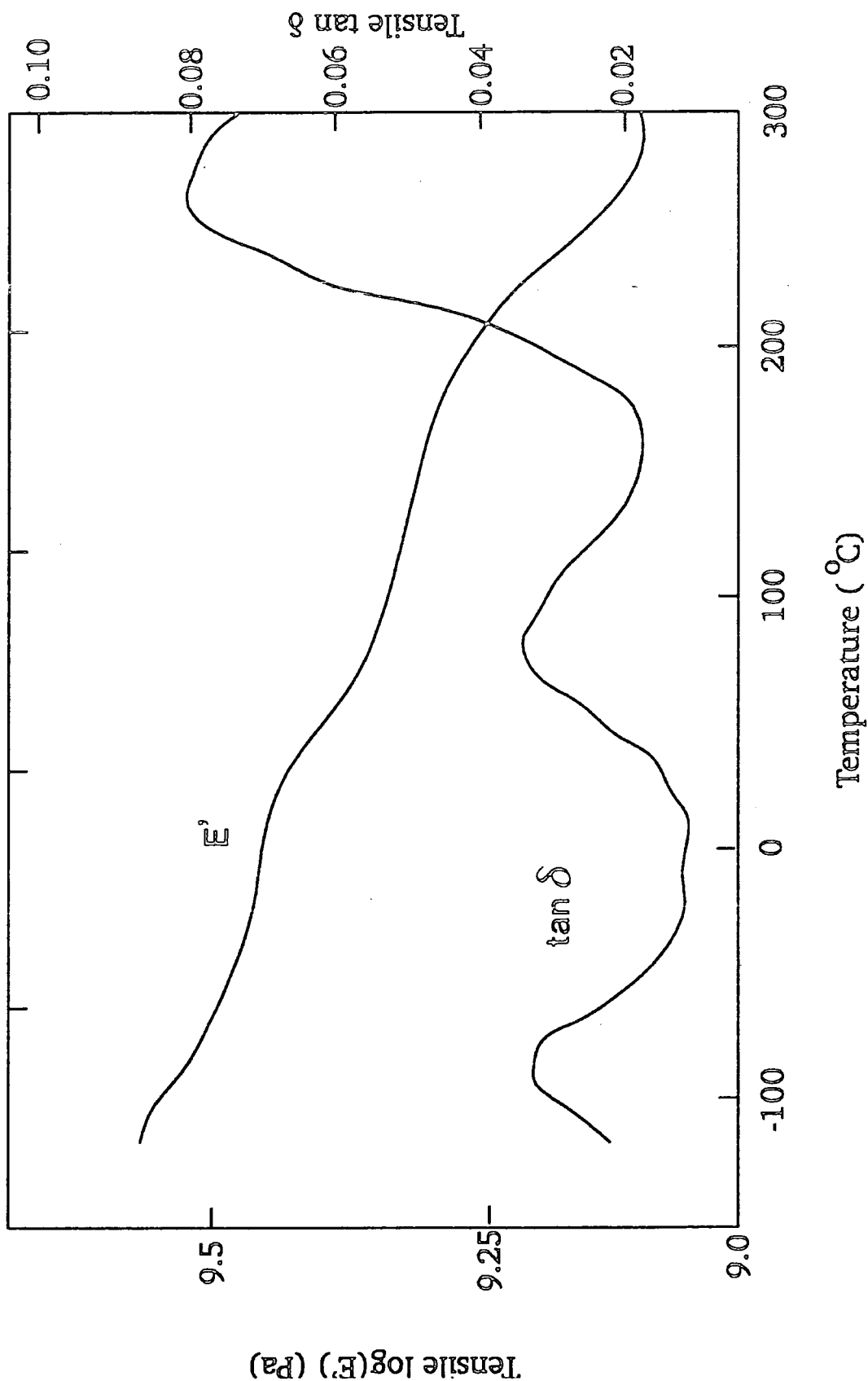


Figure 4.16

Rescan (1Hz) of the DMTA data (Figure 4.13) for an as-cast EB film.

The most obvious difference between the rescan and the initial scan is the loss of both the  $T_g$  transition at 100°C and the film hardening transition at 180°C. This is easily explained through the absence of NMP. Three damping peaks are observed though. Firstly, the -80°C transition is still present with the same magnitude in  $\tan \delta$  as for the as-cast film, although more symmetric in shape. This relaxation has also been observed in stretch aligned and doped samples as well. Secondly, a new damping peak is seen in  $\tan \delta$  at approximately 85°C. Its origin is difficult to assess using only this data but is discussed more in the following sections.

Lastly, a high temperature transition is observed at approximately 265°C. This can be ascribed to a  $T_g$ -like transition of the solvent-free, polymeric material. The large increase in temperature over the as-cast material for this peak position is predicted from the plasticisation effect of NMP. Also the magnitude of the peak in  $\tan \delta$  must be noticed. Relative to Figure 4.13, it has been reduced by a factor of nearly 10 (with only a minor decrease in modulus). This is because polymer chains are now crosslinked and so conformational motion of the backbone is severely suppressed. Similar behaviour is exhibited by many thermosetting resins and chemically crosslinked thermoplastics<sup>2</sup>.

Turning to doped ES films, the reason why such samples cannot be stretch aligned is because they contain no NMP (see TGA results chapter 3 section 3.3.2). The DMTA scan of Figure 4.17 clearly does not indicate the presence of a glass relaxation, although there is a small  $\tan \delta$  peak centred at ca. 60°C. Thus there is no free volume which can be produced around the chains allowing them rotational freedom. Indeed due to this lack of a 'plasticiser', these samples are considerably weaker than an as-cast film, but not as brittle as a crosslinked specimen. This mechanical weakness is the factor why doped films invariably fracture during DMTA experiments as can be seen in Figure 4.17.

It should be pointed out that all the above molecular relaxations result from amorphous regions. This lack of crystalline transitions is not surprising though, since as-cast films have only a small crystalline content (see XRD results in chapter 6). The effects of chain order have been studied, but it was

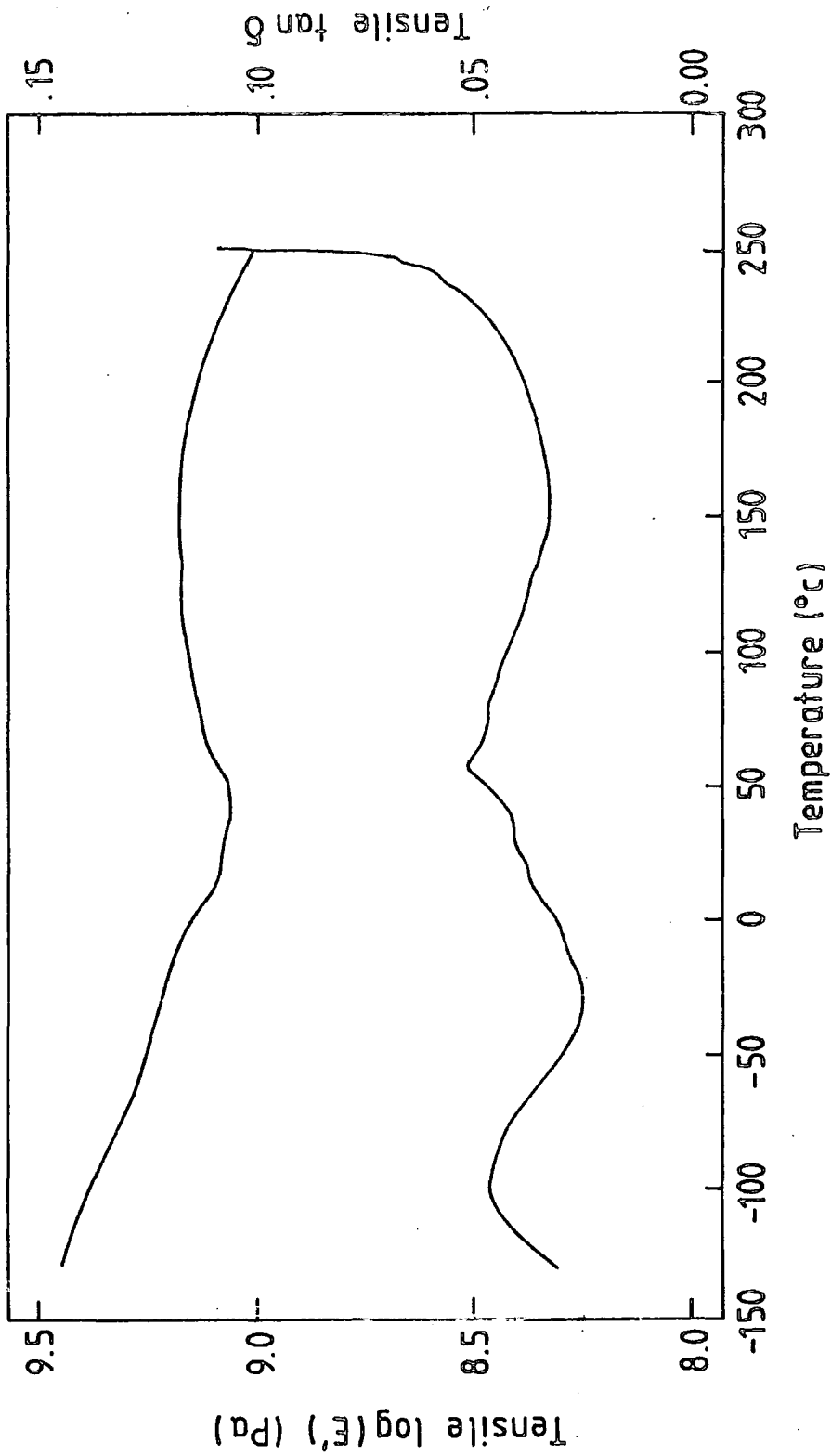


Figure 4.17

DMTA scan (1 Hz) for an as-cast ES film doped in 1M HCl.



found that no crystalline transitions were observed below the maximum temperature, 300°C, of the instrument. Furthermore, highly stretched films were often found to fracture, presumably because removal of most of the NMP during the alignment process had left them quite rigid and inflexible. This frequent fracture of specimens, both stretched and doped, rather limits the applicability of this DMTA technique.

However, it was possible to study some stretched samples allowing the transitions below around 150°C to be analysed. A typical result, illustrated in Figure 4.18, for a sample extended by 180% shows both the low temperature  $\tan \delta$  peak at -80°C and also a weak relaxation at around 85°C, the same as that observed for the rescanned unstretched sample mentioned previously. Above 150°C the  $\tan \delta$  curve rises to a point where film fracture occurs. This feature appears to be the onset of the glass transition peak, which is expected to appear at higher temperatures due to the loss of NMP induced by the thermal orientation procedure. However, the most interesting observation concerning the thermal spectrum is the fact that the -80°C peak has been reduced in magnitude relative to that observed for an as-cast sample. This empirical result confirms an amorphous assignment to the low temperature relaxation, since stretching, as revealed by XRD, increases the effective crystallinity in the films.

#### 4.7.2 Dielectric Analysis

Dielectric analysis of an as-cast EB film, shown in Figure 4.19, clearly reveals both the  $T_g$  and the crosslinking transitions (peak  $\tan \delta$  100°C and 160°C respectively). The correlation of peak positions with DMTA is good despite the difference in measurement frequencies. Both transitions are very strong dielectrically - the 160°C damping peak has a magnitude of over 4. This value is also similar to that observed for epoxy resins during cure and thus might imply chemical crosslinking involving dipolar species, though the removal of polar NMP molecules must have a contributing effect. The glass-rubber transition is prominent dielectrically since it involves rotations of the dipolar chains. For polyaniline the extent of freedom attained by the dipoles, as shown by the variation in  $\epsilon'$ , reaches a

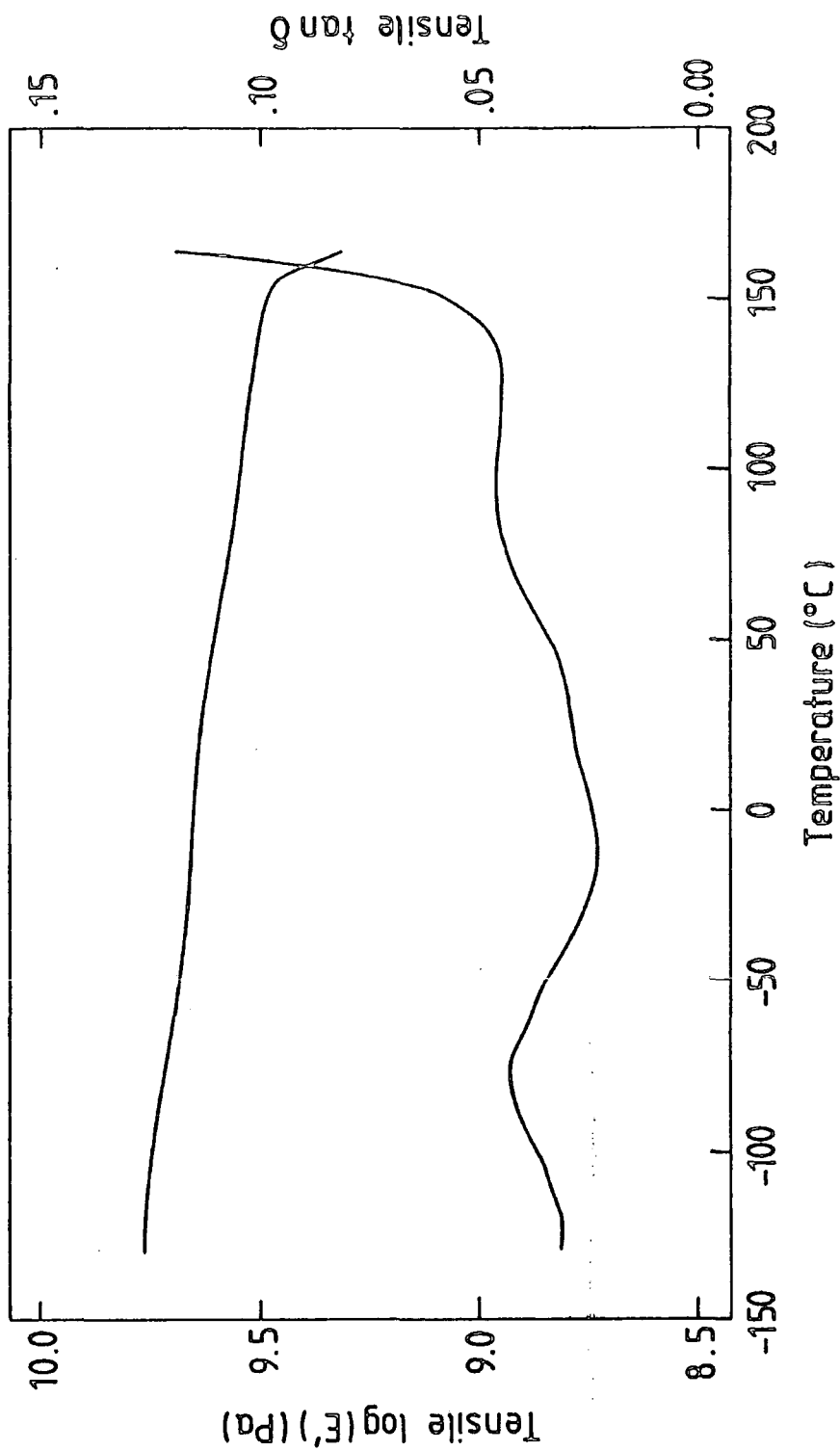


Figure 4.18 DMTA scan (1 Hz) for an as-cast EB film elongated by 180%.

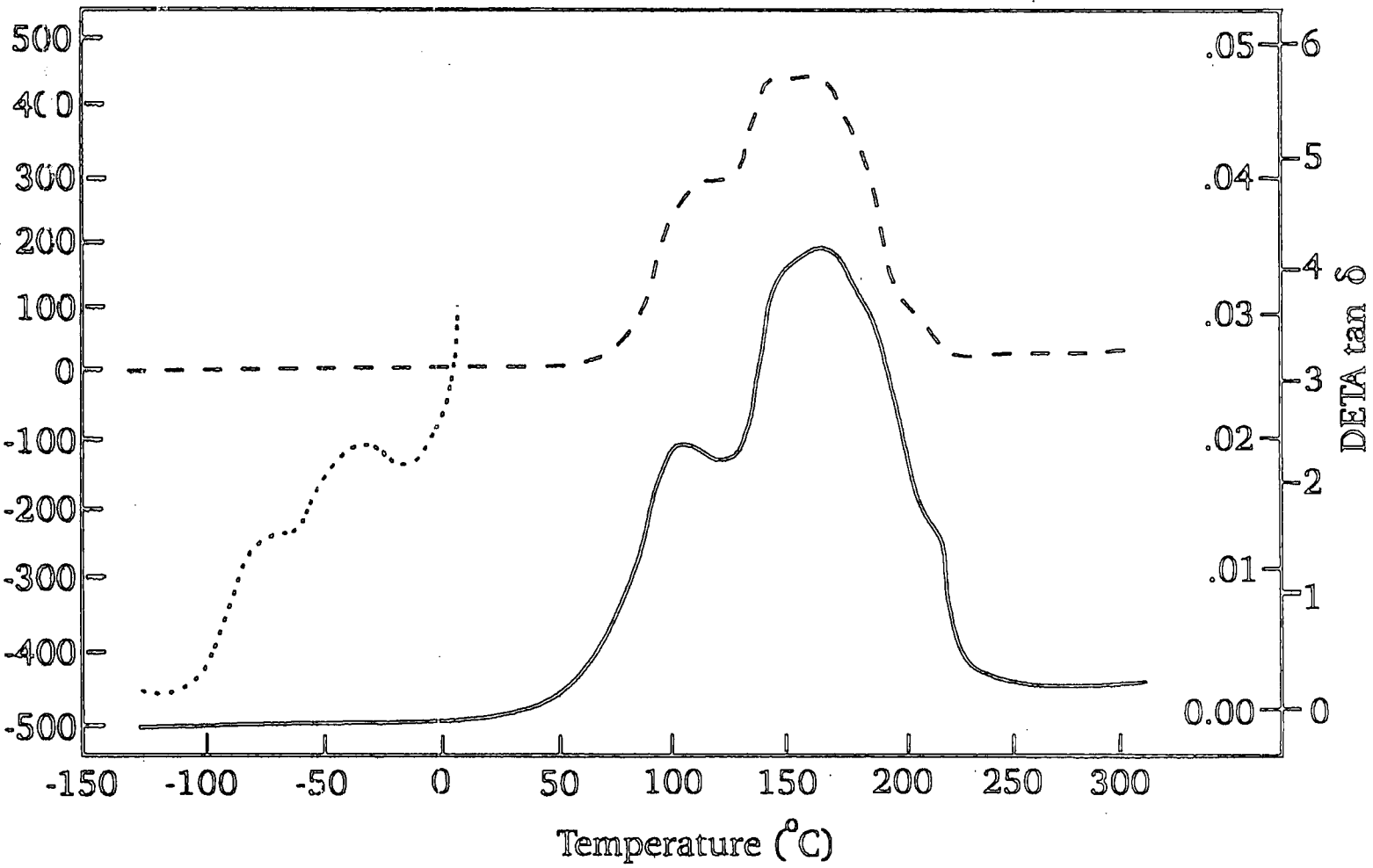


Figure 4.19  
 3 Aylward  
 DETA thermogram (1kHz) of an as-cast EB film.  
 The dotted line is an expansion of the tan  $\delta$  plot  
 corresponding to the inner y-axis.

maximum during  $T_g$  and then, as expected, decreases due to the hardening process.

The low temperature feature from the DMTA data is also seen, now possibly consisting of a double transition. This relaxation is very weak dielectrically because the relative intensity of this peak to either of the other relaxations is much smaller in DETA than DMTA. This precludes any polar activity and compounds the original assignment to a librational ring motion.

The DETA rescan, shown in Figure 4.20, is dominated by the 85°C transition of the mechanical analogue. As the DETA technique only detects motions of charged or dipolar species this strong molecular motion must therefore involve polar activity. The ring relaxation can also be observed although it is rather swamped by the main 85°C relaxation. The upswing on the high temperature side of the main transition is likely due to sample conductivity effects<sup>14</sup>.

### 4.7.3 Infrared Spectroscopy

An absorption spectrum for a typical as-cast EB film is shown in Figure 4.21(a). In this study we are concerned with the changes which may occur at elevated temperatures, but clearly the first stage must be an assignment of the vibrational bands. Such an analysis has been made in detail in the next chapter. Therefore, the reader is directed to section 5.5.1, for the detailed vibrational assignments.

Next, an as-cast specimen was heated to 200°C, cooled and the spectrum retaken - Figure 4.21(b). This treatment, as indicated by the DMTA and DETA results, removes the solvent and crosslinks the polymer chains. Hence, we can now evaluate this hypothesis using IR spectroscopy.

Comparing Figures 4.21(a) and 4.21(b) below 2000  $\text{cm}^{-1}$ , the most striking difference is the loss of the NMP carbonyl band at 1675  $\text{cm}^{-1}$  for the heat treated film. As mentioned previously in chapter 5, this is due to removal of the solvent. A small band does appear at 1705  $\text{cm}^{-1}$  which could be a

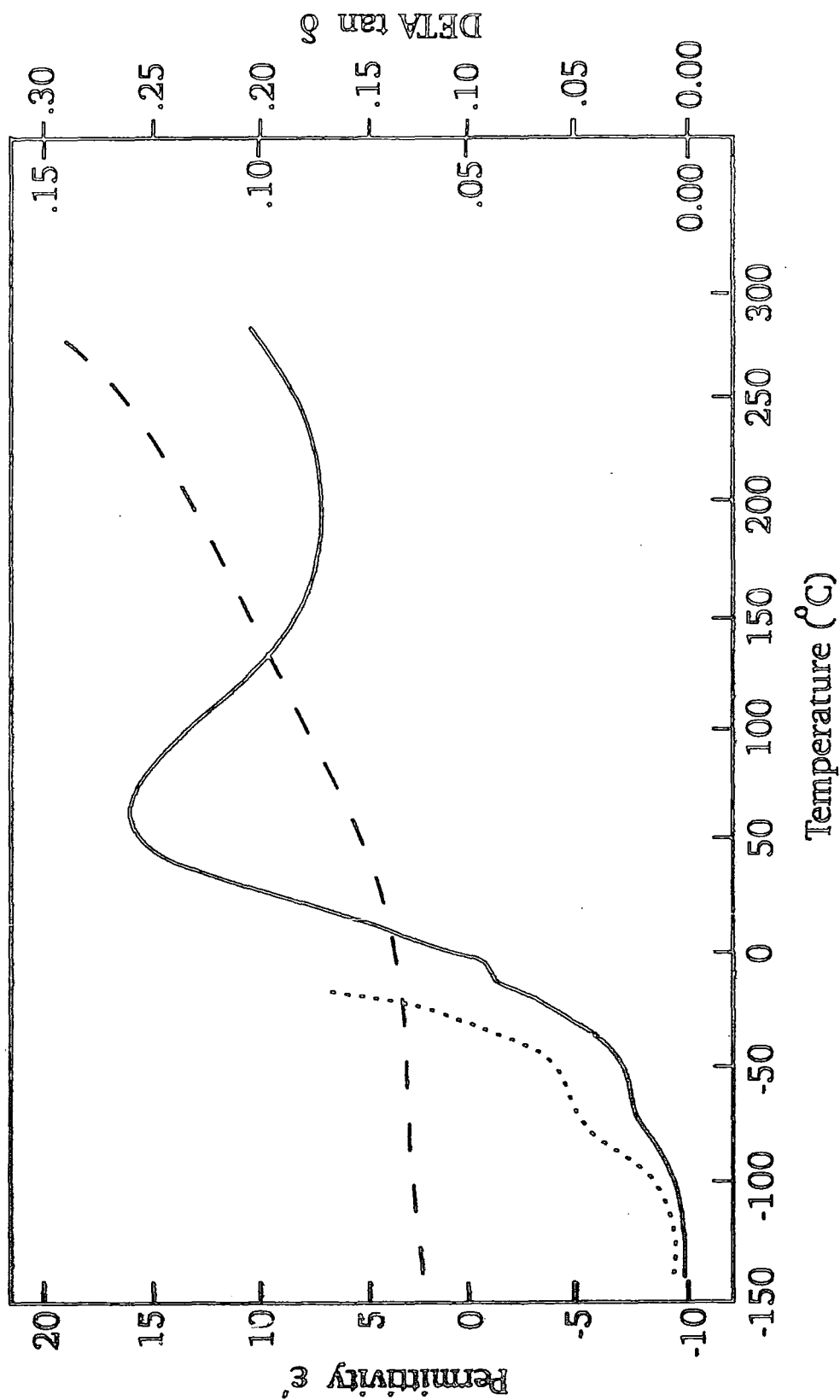


Figure 4.20

Rescan (1kHz) of DETA data for an as-cast EB film (Figure 4.19). The same notation applies.

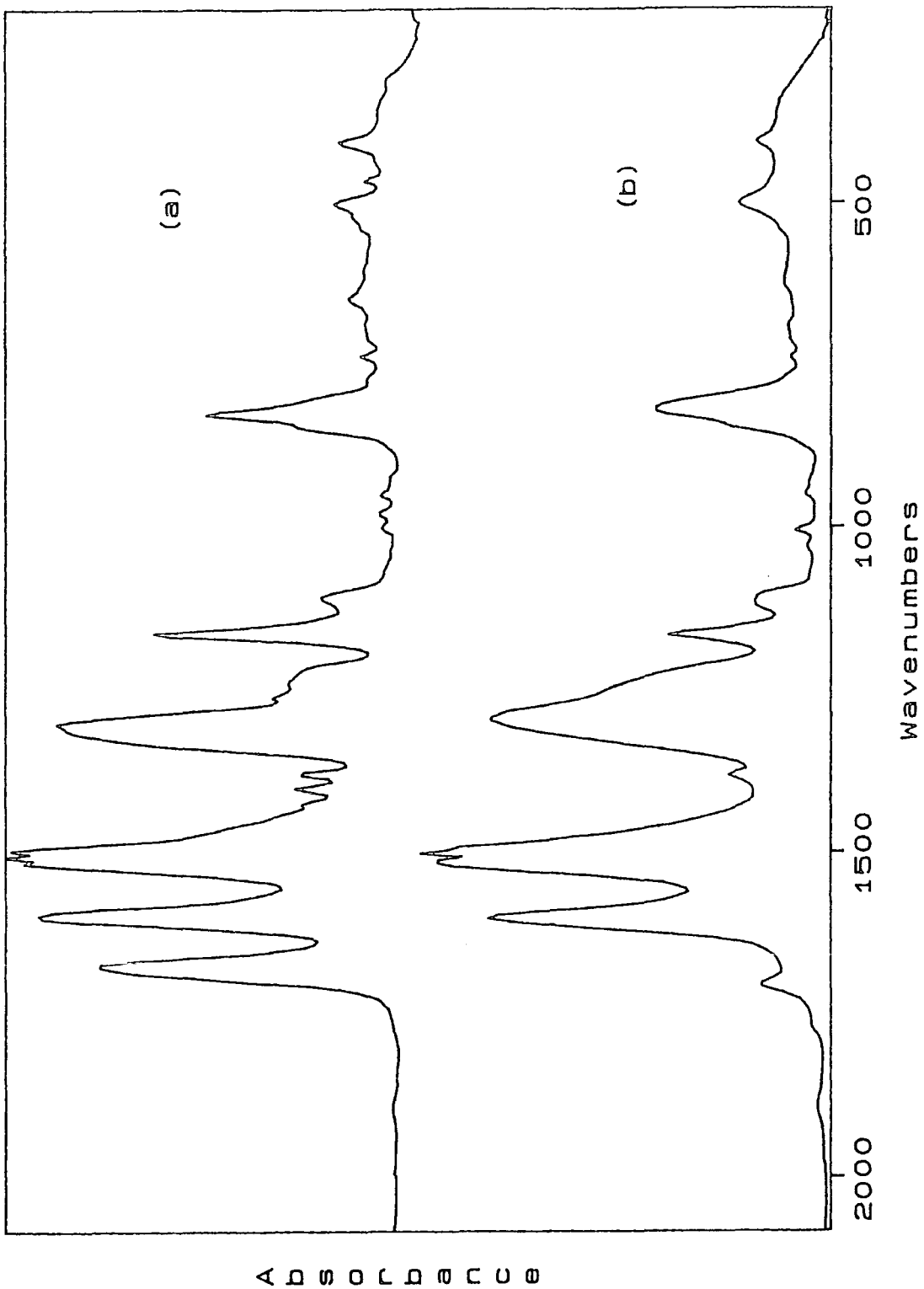


Figure 4.21

Transmission IR spectra of an EB film between 2000-200  $\text{cm}^{-1}$ ; (a) as-cast, (b) having been heated to 200°C.

quinoid-imine stretching mode or a C=O stretch due to slight sample oxidation. Examining the spectrum more closely, all the remaining absorption bands have an increased width. Such broadening can be attributed to increased interaction of vibrational modes through a high degree of chain entanglements i.e. physical crosslinking.

It is also noticeable, though, that significantly more broadening occurs in the region between 1300-1100  $\text{cm}^{-1}$ . Specifically this involves the secondary (2) $^\circ$  amine stretching vibration which exhibits a considerable shoulder to the low frequency side of the mode, lowering the peak by some 10  $\text{cm}^{-1}$ . The 1160  $\text{cm}^{-1}$  vibration broadens to a lesser extent, but is also much reduced in intensity. These changes occur on top of the broadening ascribed to chain entanglement and thus may indicate chemical bonding as well. A possible chain bonding process, suggested by MacDiarmid *et al*<sup>23</sup>, is the formation of nitrogen bridges between two quinoid-imine units. However, the reaction is believed to only proceed at 300 $^\circ\text{C}$  under an inert atmosphere. Furthermore there is no experimental evidence to suggest that this process actually occurs.

However, the possibility also exists that chain defects and impurities are responsible for chemical crosslinking. These are present in levels of only a few percent (elemental analysis in experimental section) but the change in  $\nu(\text{CN})$  is small and therefore characteristic of a change in only a few percent, perhaps about 5%, of the nitrogen linkages. Relatively few crosslinks are required to render a polymer structure extremely rigid. Furthermore, bands at around 1105  $\text{cm}^{-1}$  and 645  $\text{cm}^{-1}$  are observed in the as-cast spectrum of Figure 4.21(a) which correlate with reported modes for sulphonate residues in polyaniline powder<sup>24</sup>. These modes shift in frequency and disappear respectively in Figure 4.21(b), the heat treated film. Therefore, contaminant involvement in the hardening transition can be proposed. This topic is discussed further in the next section.

Another useful area where IR spectroscopy has been used is in the identification of the certain DMTA/DETA relaxation features. For this work, the reflection accessory was used so that spectra could be taken at elevated

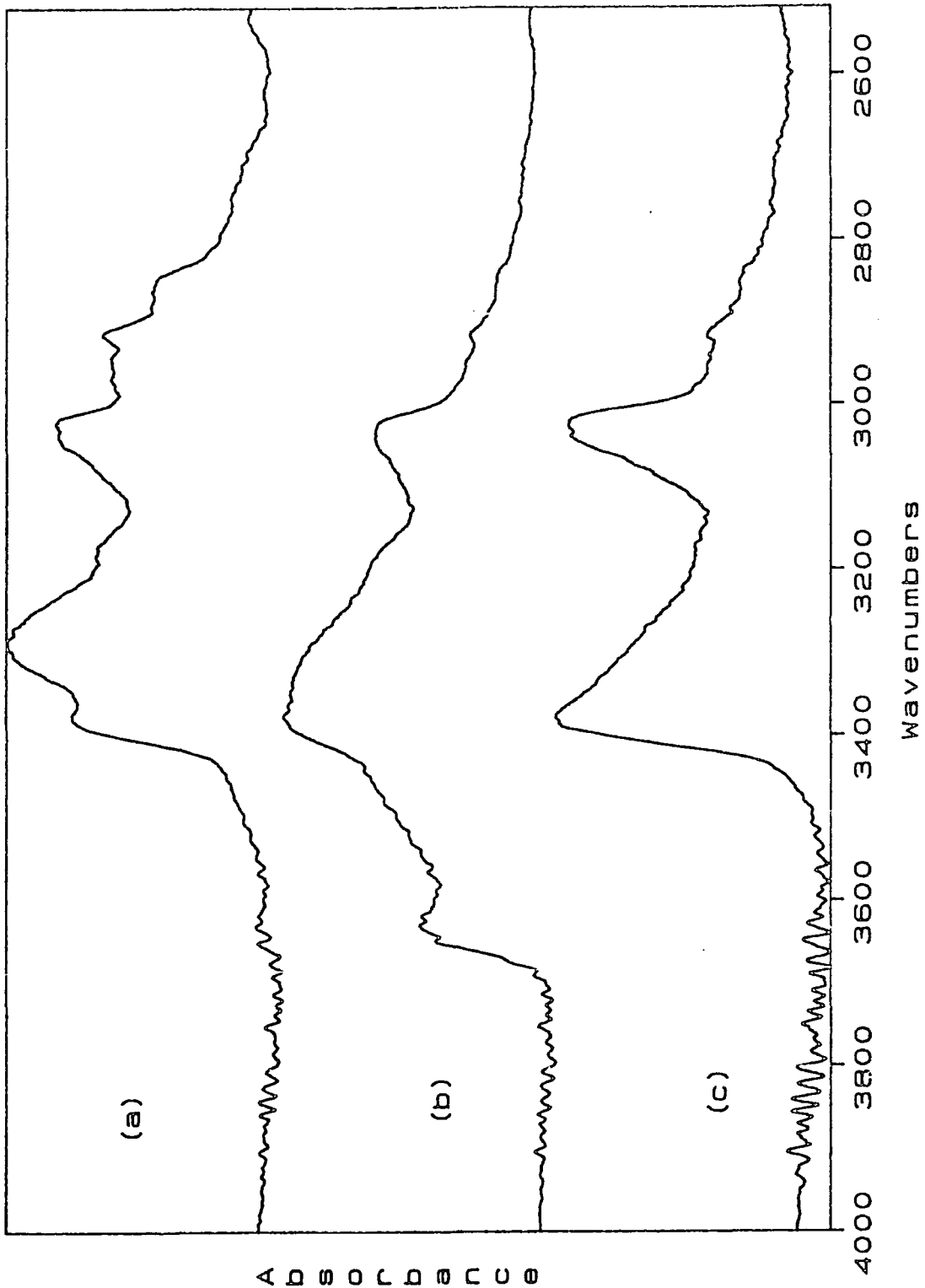


**Figure 4.22** Reflectance IR spectra between 4000-2600  $\text{cm}^{-1}$ ; (a) an as-cast EB film, (b) the same film having been heated to 200°C and (c) the heat treated film at 100°C.



temperatures. Figure 4.22 shows the spectra of an EB film in several different states, (a) as-cast, (b) solvent-free and (c) the solvent-free sample at 100°C. The loss of NMP has already been probed, but a very interesting difference occurs in the N-H region between spectra (b) and (c). In the former the peak at 3380 cm<sup>-1</sup> is very broad with a new band, relative to the as-cast state, at around 3600 cm<sup>-1</sup>. These underlying features can be identified as OH stretching bands of absorbed water molecules - the polar nature of the amine units effectively traps water molecules through hydrogen (H-) bonding.

Yet if the spectrum is taken at 100°C, as in Figure 4.21(c), the N-H band is much sharper and the OH vibrations disappears. This indicates that water vapour is lost above this temperature and furthermore corresponds to the relaxation peak at 85°C in both the DMTA and DETA thermograms of solvent-free films. Therefore this 85°C relaxation can be assigned to the breaking of H-bonds between absorbed water and amine groups. Also, if the sample is cooled back to room temperature the spectrum returns to that of Figure 4.22(b), so that thermal cycling involves the loss and recapture of water molecules.

#### 4.7.4 Further Discussion

A lot of recent interest in polyaniline has involved work on 'gels'<sup>25</sup>, formed from polyaniline (EB)/NMP solutions. Such materials are produced by simply allowing the polymer/solvent system to stand and over a length of time a gel forms. An essential feature of such gels is the connectivity of chains as a result of crosslinks<sup>26</sup>. Indeed, films cast from such gels have been proposed as being physically crosslinked<sup>27</sup>. Gel formation is observed for the 8 wt% EB/NMP solutions used in this study, after a period of about 24 hrs at room temperature. This process is rapid, however, if the solution is heated. Gelation times at room temperature increase for decreasing polymer concentration down to a level of about 1 wt%, below which no gelation occurs.

However, with one batch of EB powder it was noticed that gelation occurred at a faster rate and to a higher extent for a given concentration in NMP. An elemental analysis of the powder revealed an increase in contaminants (total S, Cl, O content 7.89 wt%), traced to inadequate purification. This information strongly suggests that crosslinking is associated with such contaminants. Increased sulphonate and chloride residues, both free ions and ring substitution defects, are likely responsible for the raised level in this second batch (spectroscopic data was unfortunately not conclusive). Both types of impurity are reactive species, however, and will chemically bond forming crosslinks. Heating the samples increases the reactivity of these species and the rate of gelation. Analogous chemical crosslinking reactions occur in other synthetic polymers when heated with additives such as sulphur and peroxides<sup>1</sup>. Therefore, polyaniline/NMP solutions and hence films appear to crosslink both physically and chemically.

All these results thus prove the need for precise control of polyaniline synthesis and processing. Only a slight variation in chemical synthesis has produced a considerable effect on the crosslinking reaction (gelation) of the polymer in NMP solution. Moreover, the central role of chain defects and impurities in such a crosslinking process has been highlighted. The quality of polyaniline is thus a crucial factor in determining the physical properties of the material.

#### 4.8 Summary

Dynamic mechanical and dielectric thermal analyses have revealed a wealth of new information about the thermal transitions which occur in the amorphous regions of polyaniline films. First of all a glass transition,  $T_g$ , has been identified at around 100°C for as-cast EB films. This co-operative thermal motion of chain segments is made possible by the removal of volatile NMP molecules at elevated temperatures because a 'free volume' is created around the chains. The  $T_g$  transition is critically dependent on the amount of NMP in the film and shifts to higher temperatures with decreasing solvent content. In the case of as-cast EB films this NMP content has been estimated to be ca. 25% as measured by thermomechanical

analysis. It is because of this  $T_g$  transition that EB films can be stretch aligned, whereas doped ES films, which contain no NMP, cannot.

The chain mobility, though, only exists for a finite time and at a temperature of 180°C films start to harden. This collapse in free volume has been monitored by thermomechanical analysis and the hardening reaction is thus initially due to chains becoming highly entangled or physically crosslinked. However, the nature of the data and the permanence and brittleness of thermally hardened films also suggests a chemical crosslinking reaction occurs as well. This inference has been compounded by infrared spectroscopy and also by relation to polyaniline/NMP gels. This latter material consists of a highly crosslinked polymer network, whose degree of crosslinking is greatly increase by the presence of residual contaminants in the polyaniline. These contaminants, beside being free anion impurities, also occur as sulphonate and chloride ring substituents, species which are highly reactive at elevated temperatures and will likely chemically bond i.e. form chemical crosslinks. As such chemical bonding in polyaniline films cast from NMP can be proposed. This reaction imposes an upper limit on the processing temperature of specimens since it results in mechanically weak, low conductivity (when subsequently doped) films.

Many of the wide variety of often conflicting experimental results can be explained by subtle differences in polyaniline synthesis giving rise to different amounts of contaminants. Chemical crosslinking is just one example of how these contaminants can drastically effect the physical properties of the polymer. Polyaniline thus needs to be precisely synthesized and processed so as to remove both impurities and chain defects.

Another important feature of the mechanical and dielectric data is the presence of a low temperature transition at -80°C, which has been identified as a phenyl ring twisting motion. This relaxation has been calculated to have an activation energy of 11 kcal mol<sup>-1</sup>, which is a particularly useful result in light of the fact that such motion plays a central role in the electronic transitions of polyaniline. Also, the ability of solvent-free specimens to absorb water by hydrogen bonding to amine units has been identified by infrared analysis. This water vapour, however, is lost above

100°C; this feature occurs as a transition at around 85°C in the rescanned mechanical and dielectric thermograms. Furthermore, this is a reversible process so that thermal cycling involves the loss and capture of water molecules.

## References

- 1 N. G. McCrum, B. E. Read and G. Williams, *Anelastic and Dielectric Effects in Polymeric Solids*, Dover Publications, (1991).
- 2 P. Gradin, P.G. Howgate, R. Selden and R.A. Brown in *Comprehensive Polymer Science*, Volume 2, ed. G. Allen, Pergamon Press, 1989, pp 533-569.
- 3 R. E. Wetton in, *Developments in Polymer Characterisation - 5*, ed. J. V. Dawkins, Elsevier Applied Science Publishers, (1986), pp 179-229.
- 4 P.G. de Gennes, *J. Chem. Phys.*, **55**, (1971), 572.
- 5 V.A. Kargin and G.L. Solninskii, *Zh. Fiz. Khim*, **23**, (1949), 526.
- 6 J.G. Kirkwood and R.M. Fuoss, *J. Chem. Phys.*, **9** (1941), 329.
- 7 S.Glasstone, K.J. Laidler and H. Eyring, *The Theory of Rate Processes*, McGraw-Hill, New York, 1941.
- 8 S. Saito, *Kolloid Z.*, **189**, (1963), 116.
- 9 T.F. Schatzki, *Polymer Preprints*, **6**, (1965), 646.
- 10 M. Takayanagi, *Mem. Fac. Eng. Kyushu Univ.*, **23**, (1963), N° 1, p 1.
- 11 W. Pechold, S. Blasenbury and S. Woerner, *Kolloid Z.*, **189**, (1963), 14.
- 12 K. Wolf, *Kunststoffe*, **41**, (1951), 89.
- 13 M. F. Drumm, C.W.H. Dodge and L.E. Nielsen, *Ind. Eng. Chem.*, **48**, (1956), 76.
- 14 R. E. Wetton, M. R. Morton and A. M. Rowe, *American Laboratory*, **18**, (1986), 91.
- 15 *Theory of Dielectrics*, H. Frolich, Oxford University Press, London, 1958.
- 16 *The Vibrational Spectroscopy of Polymers*, eds. D. I. Bower and W. F. Maddams, Cambridge University Press, (1989).
- 17 W. Klopffer, *Introduction to Polymer Spectroscopy*, Springer-Verlag, Berlin, 1984.

- 18 J.N. Hay in *Analysis of Polymer Systems*, eds. L.S. Bark and N.F. Allen, Applied Science Publishers, London, 1982, Chapter 6.
- 19 Y. Wei, G. Jang, K. F. Hseuh E. M. Scherr, A. G. MacDiarmid and A. J. Epstein, *Polymer*, **33**, (1992), pp 314-322.
- 20 J. L. Bredas in *Proceedings of the Nobel Symposium on Conjugated Polymers and Related Materials*, ed. W. R. Salaneck, Oxford University Press, 1992.
- 21 A. J. Epstein, R. P. McCall, J. M. Ginder and A. G. MacDiarmid, in *Spectroscopy of Advanced Materials*, Volume 19, eds. R. J. H. Clark and R. E. Hester, John Wiley and Sons Ltd, 1991, pp 355-392.
- 22 S. Kaplan, E.M. Cornwell, A.F. Richter and A.G. MacDiarmid, *Macromolecules*, **22**, (1989), 1669.
- 23 E. M. Scherr, A. G. MacDiarmid, S. K. Manohar, J. G. Masters, Y. Sun, X. Tang, M. A. Druy, P. J. Glatkowski, V. B. Cajipe, J. E. Fischer, K. R. Kromack, M. E. Jozefowicz, J. M. Ginder, R. P. McCall and A. J. Epstein, *Synth. Met.*, **41-43**, (1991), 735.
- 24 T. Ohsaka, Y Ohnuki, N Oyama, G. Katagiri and K. Kamisako, *J. Electroanal. Chem.*, **161** (1984), 399.
- 25 K. Tzou and R. V. Gregory, *Synth. Met.*, *Proceedings of ICSM 1992*.
- 26 M. J. Miles in *Developments in crystalline polymers-2*, ed. D.C. Basset, Elsevier Applied Science, 1984.
- 27 A. G. MacDiarmid, Y. Min, E. J. Oh, E. M. Scherr, X. Tang, J. G. Masters and A. J. Epstein, *Synth. Met.*, **55-57**, (1993), 677.

## Chapter 5

### Infrared Orientation Studies

This Chapter concentrates on the use of polarised infrared spectroscopy to probe the molecular orientation in stretch aligned films. The results are discussed with respect to the observed anisotropy in conductivity and also in the light of similar results obtained for other conductive polymers. Further, very useful information has been derived concerning the torsional angle of C<sub>6</sub> rings along the polymer chain.

#### 5.1 Introduction

Infrared spectroscopy provides a convenient and relatively simple method with which to measure orientation in stretched polymer films. The technique involves recording the IR absorption spectrum of the sample with polarised radiation in two orthogonal directions. Dichroic behaviour of specific absorption band can then be observed. Such measurement provide information on the type and degree of chain orientation. Furthermore, it is also possible to obtain information about the chemical and geometrical structure of an individual polymer chain.

#### 5.2 Orientation and Infrared Dichroism

For a normal mode of vibration of a chemical group to be IR active it must have a change in dipole moment, or transition moment associated with it<sup>1</sup>. Considering a particular vibration, such as the N-H stretching motion of an amine group, the atoms oscillate along the chemical bond such that this bond direction becomes the direction of the transition moment. If it were possible to analyse this single amine unit with polarised light in various directions a strong absorption band would be seen for the electric field vector of the radiation parallel to the N-H bond (direction of transition moment). Conversely, for light polarised at right angles to the bond, no absorption band would be recorded at all. A measure of such differences in

absorption for the various polarisations is known as the dichroic behaviour of the particular band in question.

In practice it is not possible to observe an amine group individually. The absorption band is a macroscopic measurement, a superposition of all the individual units in the sample. For an isotropic sample these units would be randomly distributed with respect to molecular orientation so that in fact no dichroic behaviour would be observable in the N-H stretching band. This is the case for an as-cast polyaniline film since the sample consists of a random distribution of polymer chains.

However, by uniaxial stretching it is possible to produce some degree of chain alignment or orientation in the polymer film. Such a processing procedure results in chains which are preferentially aligned parallel to the stretching direction. The exact extent of chain order depends on the polymer itself and the stretching conditions; for example, a polyethylene sheet can be elongated by several hundred percent at 120°C resulting in all the chains becoming oriented within  $\pm 10^\circ$  of the stretch direction<sup>2</sup>. Polymers with more complex chemical structures, such as PANi, would not be expected to show such high chain alignment, but in general some orientation can be achieved.

Partial alignment of a polymer renders the sample anisotropic and in turn orients the individual groups associated with the chain backbone. If the IR absorption spectrum is now recorded with light polarised parallel and perpendicular to the stretch direction, then for any particular absorption band there will be a net difference in total intensity,  $I$ , between the two spectra. The ratio of these intensities for the two polarisation directions is called the dichroic ratio,  $R$ , and can be defined as

$$R = \frac{I_{\perp}}{I_{\parallel}} \quad (1)$$

N.B. This definition is somewhat arbitrary and in some cases the inverse ratio is called the dichroic ratio<sup>2</sup>.

If the geometrical orientation (transition moment) of all the groups in a partially aligned sample were known the expected dichroic ratio of an absorption band could be calculated. Since this is not possible a model has to be assumed for a certain orientation distribution and only then can the dichroic behaviour be analysed. The most appropriate model for the chain alignment resulting from 1-D elongation is that of partial axial orientation. For this type of orientation the dichroic ratio of an absorption band is dependent on two main parameters:

- the degree of chain orientation,
- the angle between the molecular chain axis and the direction of the transition moment.

In the case of the latter parameter a certain amount of care must be taken. It is often assumed that the direction of the transition moment is known relative to the chemical bond direction. This relation can be defined with some certainty for specific stretching vibrations such as C-H, N-H and S-H bands and also those of the CH<sub>2</sub> group. For the former vibrations the change in dipole moment lies along the bond<sup>2</sup>. However, for many other vibrations the transition moment cannot be unequivocally established. Most notable is the C=O stretch for which<sup>2</sup> the angle between the transition moment and bond direction can vary between 10 and 20° depending on the chemical environment.

Analysis of dichroic data using the partial axial model has been reported for oriented films of the conductive polymers PPV<sup>3,4</sup> and PA<sup>5</sup>. Although these polymers possess rather simpler chemical structures than PANi, the results constitute a yardstick for this work and are hence a very useful reference point.



### 5.3 Theoretical Analysis

Two differing analyses are notably followed in the literature, those due to Read<sup>5</sup> and Zbinden<sup>2</sup>. Both give consistent results and contain numerous references to IR dichroic studies of polymeric materials. The latter method, although involving a more detailed interpretation, also provides a very good account of the underlying principles behind dichroic ratio analysis. For this reason the analysis of Zbinden has been followed in this work and is outlined below.

#### 5.3.1 Partial Axial Orientation

The partial axial orientation model describes polymer chains preferentially aligned along the stretch direction, but randomly distributed with regards to rotation about their chain axis. For this type of orientation, Figure 5.1, a polymer chain is considered whose axis is denoted  $c$  in the molecular coordinate system ( $a, b, c$ ). Associated with the chain is a transition moment  $M$  (of a particular chemical bond) at an angle  $\theta$  with respect to  $c$ . The system is chosen so that  $M$  lies in the  $ac$  plane. The axis  $c$  is at an angle  $\gamma$  with respect to the  $z$ -axis, the stretch direction in the sample coordinate system ( $x, y, z$ ). The angle  $\gamma$  can vary between  $0$  and  $\pi$ . The number of chains pointing in a certain direction is defined by a distribution function  $f(\gamma)$  which is rotationally symmetrical about the  $z$ -axis. Thus  $f(\gamma)d\gamma$  is a partially integrated distribution function which defines the number of chains pointing in the shaded angle element shown in Figure 5.2.

The sample coordinate system is fixed in space when the film is mounted in the spectrometer, but the ( $a, b, c$ ) system is not and assumes various directions according to the orientation of the individual chains. To determine the expected absorption intensity along the sample axes the components of the transition moments must be related in the two systems. This is achieved, in general terms, by a coordinate transformation of the following form:

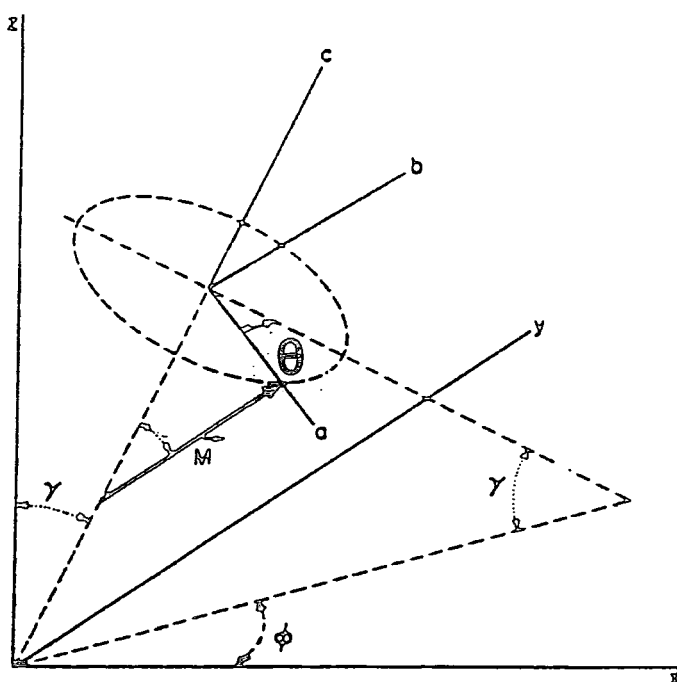


**Figure 5.1 Partial axial orientation.**  $M$  is a dipole moment, associated with a specific chemical bond, which forms an angle  $\theta$  with the chain axis  $c$ . This chain axis itself forms an angle  $\gamma$  with the stretch direction, denoted by the  $z$ -axis.

$$\begin{pmatrix} M_x & M_y & M_z \end{pmatrix} = \begin{pmatrix} T_{11} & T_{12} & T_{13} \\ T_{21} & T_{22} & T_{23} \\ T_{31} & T_{32} & T_{33} \end{pmatrix} \begin{pmatrix} M_a \\ M_b \\ M_c \end{pmatrix} \quad (2)$$

Mathematically, this formula is a matrix vector multiplication such that the component  $M_x$ , for example, is given by

$$M_x = T_{11}M_a + T_{12}M_b + T_{13}M_c$$

The transformation may be written in a reduced format

$$M_{x,y,z} = (T) M_{a,b,c} \quad (2a)$$

where (T) represents a transformation matrix.

The matrix components are trigonometric functions but their form depends on the individual chain orientation and the choice of the molecular coordinate system. In the case of partial axial orientation the transformation matrix is given by

$$(T) = \begin{pmatrix} \cos\theta \cos\gamma \cos\phi + \sin\theta \sin\phi & \sin\theta \cos\gamma \cos\phi - \cos\theta \sin\phi & \cos\phi \sin\gamma \\ \cos\theta \cos\gamma \sin\phi - \sin\theta \cos\phi & \sin\theta \cos\gamma \sin\phi + \cos\theta \cos\phi & \sin\phi \sin\gamma \\ -\sin\gamma \cos\theta & -\sin\gamma \sin\theta & \cos\gamma \end{pmatrix} \quad (3)$$

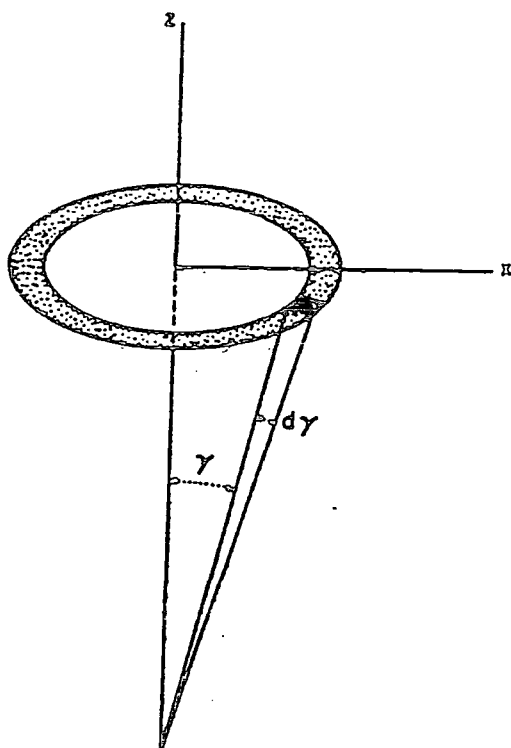


**Figure 5.2** The partially integrated orientation function  $f(\gamma)d\gamma$  represented by the shaded area.

### 5.3.2 The Dichroic Formula

For light polarised with its electric field vector along the x direction the absorption will only depend on the  $M_x$  component of the transition moment. Hence the intensity is proportional to the square of the component and by integrating over all the individual transition moments the total intensity along the sample axis may be obtained. Similarly the intensities along y and z are obtained from the  $M_y$  and  $M_z$  respectively.

In general it can be shown that, with certain restrictions placed on the distribution function, the absorption intensities for all polarisation directions can be described by an equation representing an ellipsoid. Such an 'intensity ellipsoid' allows the dichroic ratio to be completely defined by only three parameters, the intensities in the directions of the main ellipsoid axes. It is important to realise, though, that since the observed dichroism is obtained by integration over all chain orientations no direct information can be derived about the distribution function. Thus several intensity distributions could lead to the same intensity ellipsoid. This is why it is necessary to assume an orientation type - partial axial orientation.

For partial axial orientation the axes of the intensity ellipsoid correspond to the following integrations

$$I_x = \frac{1}{4\pi^2} \int_{\gamma=0}^{\pi/2} \int_{\psi=0}^{2\pi} \int_{\theta=0}^{2\pi} M_x^2(\gamma, \theta, \psi) f(\gamma) d\theta d\psi d\gamma$$
$$I_y = \text{same integral over } M_y^2 \tag{4}$$
$$I_z = \text{same integral over } M_z^2$$

Using the transformation matrix (3) and integrating over the angles  $\theta$  and  $\psi$  leads to the following expressions

$$I_x = I_y = \frac{M^2}{2} \left( \sin^2\theta \int_0^{\pi/2} (2-3\sin^2\gamma)f(\gamma)d\gamma + \int_0^{\pi/2} 2\sin^2\gamma f(\gamma)d\gamma \right) \quad (5)$$

$$I_z = \frac{M^2}{2} \left( \cos^2\theta \int_0^{\pi/2} (2-3\sin^2\gamma)f(\gamma)d\gamma + \int_0^{\pi/2} 2\sin^2\gamma f(\gamma)d\gamma \right)$$

The z-axis denotes the stretch direction so that the dichroic ratio can be then be defined with the use of (1). Generally it is expressed in the following form<sup>7</sup>,

$$R = \frac{I_{\perp}}{I_{\parallel}} = \frac{\sin^2\theta + S}{2\cos^2\theta + S} \quad (6)$$

where S is an orientation parameter and  $\theta$  the angle between transition moment and molecular chain axis, c. S is subsequently defined by

$$S = \frac{F}{N - \frac{3}{2}F} \quad (7)$$

where

$$F = \int_0^{\pi/2} \sin^2\gamma f(\gamma)d\gamma \quad N = \int_0^{\pi/2} f(\gamma)d\gamma \quad (8)$$

The distribution function  $f(\gamma)$  is usually normalised so that  $N = 1$  by definition and hence

$$S = \frac{F}{1 - \frac{3}{2}F} \quad (9)$$

The orientation parameter  $S$  itself depends only on the shape of the distribution function  $f(\gamma)$ . Usually, however, the explicit form of  $f(\gamma)$  is not known. Therefore at least one  $\theta$  value must be known for  $S$  to be calculated. Once  $S$  is known  $\theta$  can be measured, so that the geometrical structure of the polymer chain can be assessed. The latter analysis, however, assumes that the degree of orientation is the same for all bands which requires that the sample be homogeneous with respect to its physical state. If the polymer contains ordered as well as unordered regions though, the crystalline and amorphous components of the spectra need to be separated so that each phase can be treated separately. However, this is not always an easy task for such semi-crystalline polymers, particularly for those with complex chemical structures so that for simplicity  $S$  usually defines an average orientation for the two fractions.

Specific distribution functions may be assumed, though, which can be integrated allowing  $S$  to be visualised. For example, in the case where all chains are perfectly aligned along the  $z$ -axis, this distribution function is of such a form that using (7) and (8)  $F=0$  and hence  $S=0$ . A corresponding function for a random distribution of chains leads to  $F=2/3$  so that  $S=\infty$ . Thus  $S$  varies from 0 to  $\infty$  by going from a perfectly oriented sample to a random chain distribution. Other models lying between these two limiting cases also may be developed and are discussed in the results section.

#### 5.4 Experimental Details

Dichroic data was recorded using a Mattson Sirius 100 FTIR instrument belonging to Dr J. Yarwood of the Chemistry Department. The spectrometer was computer controlled using FIRST software. The polariser, consisting of a gold wire grid deposited on a KRS-5 substrate, was

housed in a free-standing rotatable mount. Samples, in the form of single (stretched) films were positioned behind the polariser with their stretch axis vertical. Absorption spectra were recorded over 200 scans with a resolution of  $4\text{ cm}^{-1}$ . Since the spectrometer is a single beam instrument it was also necessary to record a background scan with the polariser in the beam and subtract this from the sample scan.

The FTIR spectrometer<sup>7</sup>, the basis of which is the well known Michelson interferometer shown schematically in Figure 5.3, has several notable advantages over a conventional wavelength dispersive instrument. Since radiation of the whole range of wavelengths passes through the system at all times the intensity falling on the detector is much higher than in the

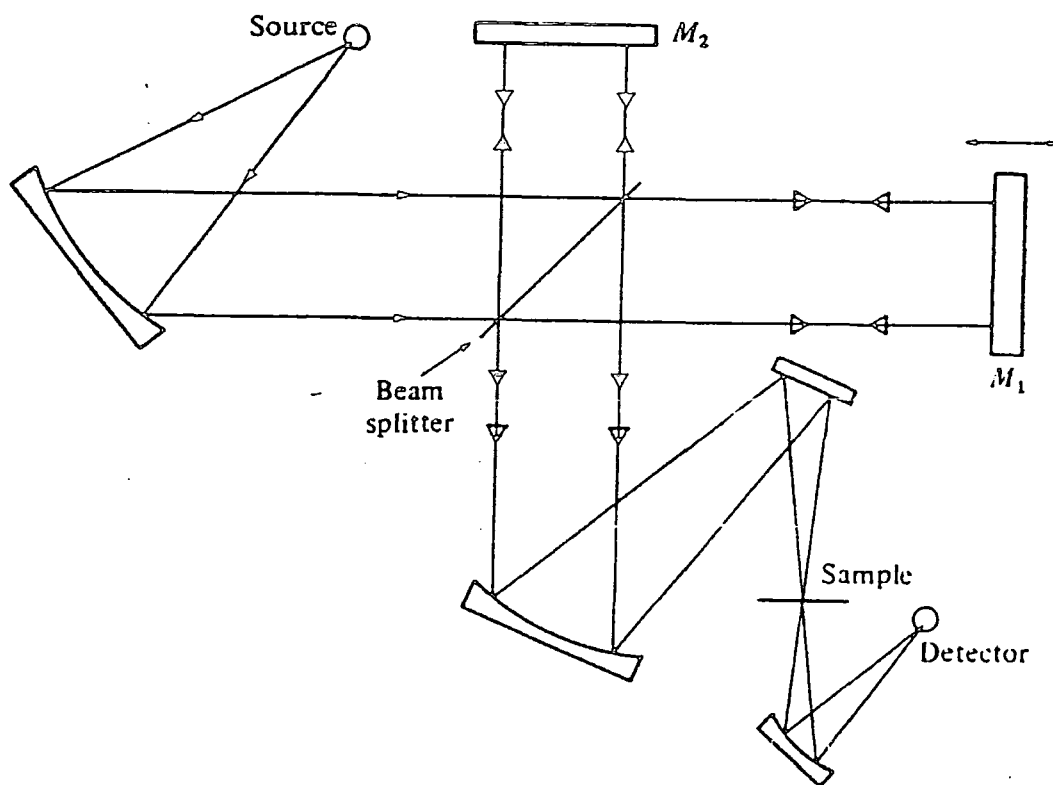


**Figure 5.3 Schematic diagram of a Fourier Transform infrared spectrometer based on a Michelson interferometer.**

dispersive case. This difference, a combined effect of the multiplex and throughput factors, results in a very much higher signal-to-noise ratio. As a result it is possible to record data of similar quality much more rapidly using the FTIR technique. Furthermore, it also permits the study of more highly absorbing samples and so provides a greater range of options for specimen thickness.

This latter point is particularly advantageous for this analysis since the stretched polyaniline films used have a minimal thickness of about 15 $\mu$ m. If samples are extended further, lowering this value, fracture occurs.

Using a dispersive spectrophotometer (the Perkin-Elmer 580B described in the previous chapter) it was found that band absorbances observed for parallel polarisation of even 15 $\mu$ m films were beyond the practical limit of the instrument (about 3 absorbance units). Using unpolarised radiation good quality spectra for such specimens were recorded, thus illustrating the further reduction in intensity caused by the polariser.

With the FTIR instrument film thicknesses of 15 $\mu$ m and higher could be readily used. Even so there was still found to be a threshold thickness limit for polarised FTIR spectra. This is particularly disabling since high elongations can only be achieved for relatively thick films. As a consequence films extended by more than 250% are not suitable for examination by IR dichroism. Clearly the only way to overcome this problem is to produce highly extended films of lower thickness. This is an area of research currently being studied at Durham. A further problem is introduced by the fact that protonated, i.e. conducting films, are highly absorbing due to their 'metallic' nature so that these samples also cannot be examined (even in reflection, the protonated spectrum was extremely weak and totally unusable).

Dichroic ratios are often estimated, for practicality, using peak band intensities in the perpendicular and parallel polarisations. However, more strictly the ratio is defined by the integrated intensities of a band. The former approximation is highly justified when the band shape of the two polarisations is the same, but errors may be introduced if this is not the



case. So, in this study both methods were tested. For such analyses it is necessary to construct a baseline for a particular peak, as outlined in Read<sup>6</sup>. For the peak intensity method, this baseline gives a measure of the background intensity and also defines the limits when integrating. Data processing of this type was carried out using routines incorporated in the FIRST software.

Errors may be introduced in a dichroic analysis if bands are broad and/or overlap, so creating uncertainty in the position of a baseline. In the case of polyaniline spectra, broad bands are observed and so this may be the case. However, the error introduced is not as serious as in the determination of a single band intensity since it is likely that errors in the perpendicular and parallel spectra will be similar and cancel to some extent. A number of other factor, such as polariser efficiency and beam convergence (as discussed by Zbinden<sup>2</sup>) may also affect the dichroic ratio, but these are normally minor and so have been neglected here.

## 5.5 Results and Discussion

The first stage in any spectroscopic analysis is the assignment of vibrational bands, but the depth of interpretation depends on the nature of the information being sought. An empirical analysis is sufficient if the spectrum is to be used on a 'finger-print' basis but for a molecular orientation study as detailed an understanding as possible, involving modes of vibration, is required.

### 5.5.1 Assignment of Vibrational Bands

In the IR absorption spectrum of an as-cast EB film two distinct groups of broad bands are seen between about 2000-200  $\text{cm}^{-1}$  and 3600-2800  $\text{cm}^{-1}$  as shown in Figures 5.4 (a) and (b) respectively. Many workers have published similar data for polyaniline in a variety of forms and oxidation states. However, spectral assignments are not often attempted, undoubtedly due to the structural and stereochemical complexity of the polymer. Notable

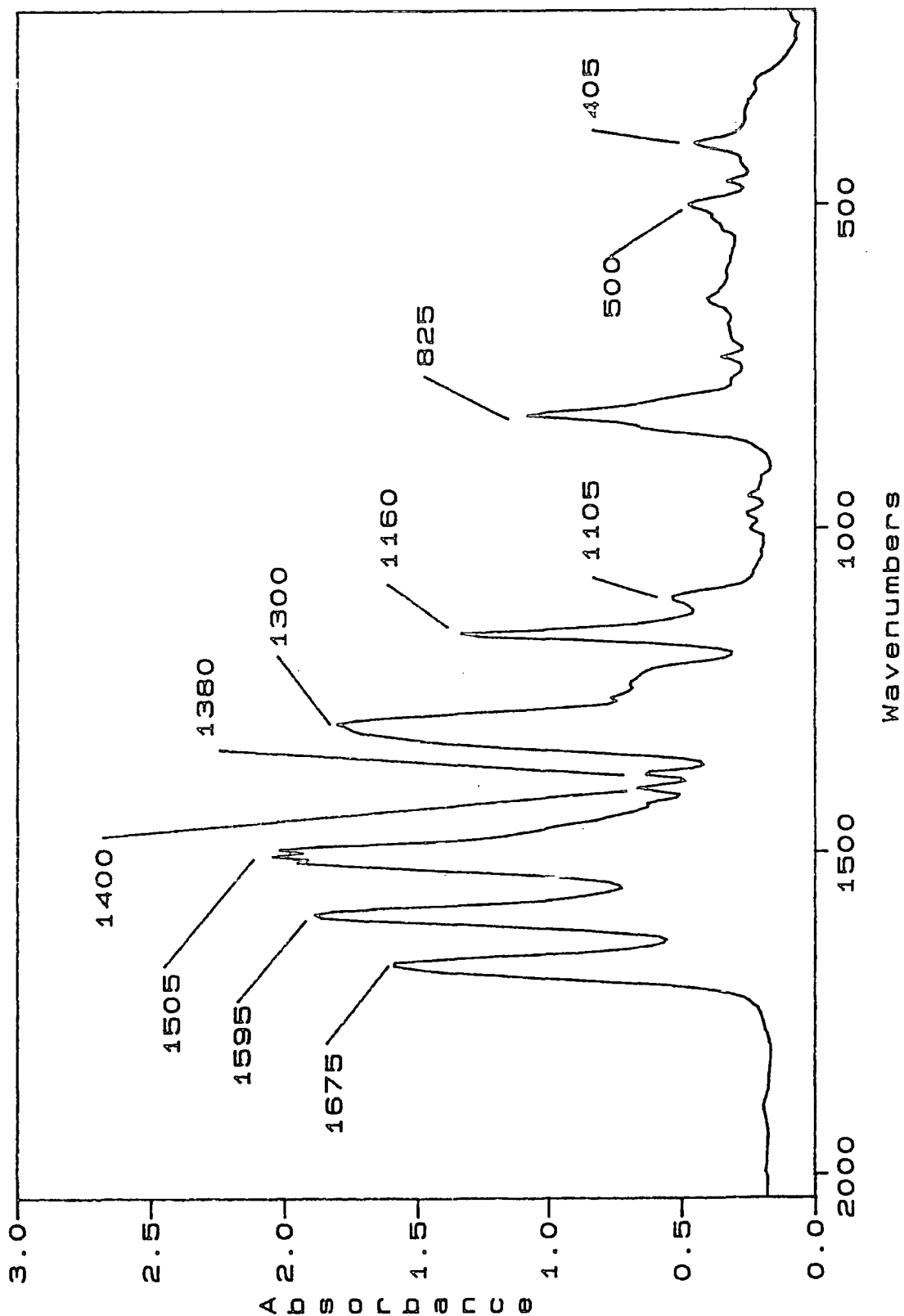


**Figure 5.4(a)** IR absorption spectrum between 2000-200  $\text{cm}^{-1}$  of an as-cast EB film. The spectrum was recorded using the Perkin-Elmer 580B described in chapter 4.

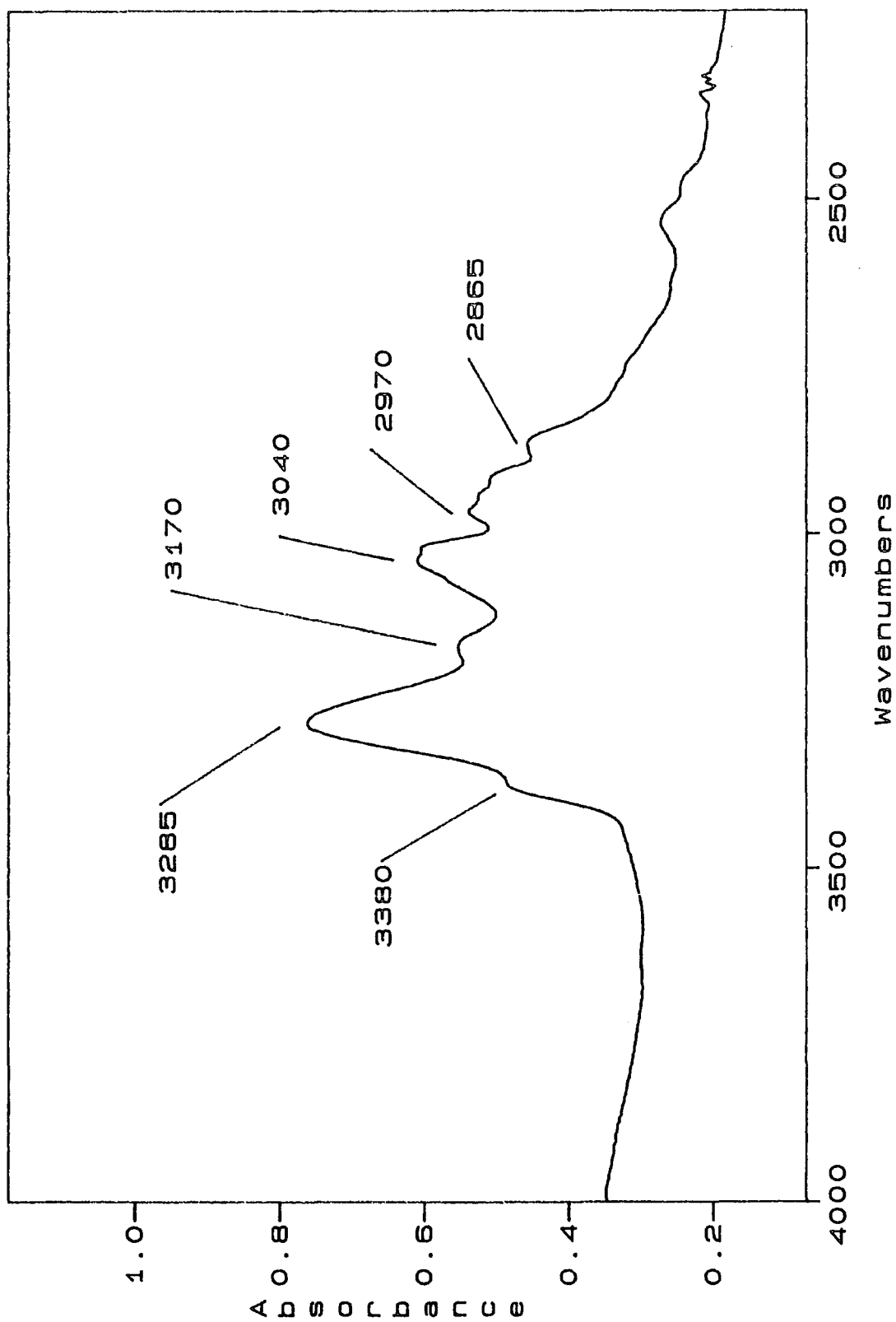


**Figure 5.4(b)** IR absorption spectrum between 4000 -2400  $\text{cm}^{-1}$  of an as-cast EB film. The spectrum was again recorded using the Perkin-Elmer 580B instrument.

exceptions though include papers by Tang *et al*<sup>8</sup> based on analysis of THF soluble i.e. low  $M_w$  polyaniline, Ohira *et al*<sup>9</sup> (KBr powder pellets) and a few reports by MacDiarmid *et al*<sup>10,11</sup> (pellets and films). Perhaps the most comprehensive interpretations result from the work of Furukawa *et al*<sup>12,13</sup>. Here both Raman and infrared data are compared for a variety of polyaniline samples, including isotopically substituted derivatives, in an attempt to establish oxidation states. The results pertain to electrochemically synthesised material though, which is generally understood to have rather different physical properties to chemically synthesised material e.g. a much shorter chain length.

Clearly a detailed interpretation of the vibrational spectrum for an EB (chemically synthesised) solvent-cast film is far from trivial. However, using the available data, together with correlation charts and further related spectral information, an assignment of vibrational bands has been made here. The results are tabulated in Table 5.1, but are discussed in more detail below.

Below  $2000\text{ cm}^{-1}$ , two strong bands occur at  $1595$  and  $1505\text{ cm}^{-1}$  which are characteristic of aromatic polymers and can be assigned to non-symmetric  $C_6$  ring stretching modes. The higher frequency vibration is reported to be mainly due to quinoid ring units<sup>10</sup>. The relative intensity of these two bands thus gives an indication of the oxidation state of the material. The  $1300\text{ cm}^{-1}$  vibration is in the C-N stretching region and is indicative of secondary ( $2^\circ$ ) aromatic amine group. This band also has a broad shoulder to lower frequency. The  $1160\text{ cm}^{-1}$  mode and the weaker  $1110\text{ cm}^{-1}$  vibration are assigned to an in-plane C-H bending motion of the aromatic rings, although others have suggested a C-N stretching mode<sup>8</sup>. The strong peak at  $825\text{ cm}^{-1}$  is an out-of-plane C-H bending mode. The position of this peak is characteristic of para-disubstituted aromatic rings and the absence of other out-of-plane bending vibrations in the region implies that the polymer backbone consists of para-linked  $C_6$  rings, in agreement with  $^{13}\text{C}$  NMR findings (Chapter 3). The weaker features at  $525$  and  $405\text{ cm}^{-1}$  are also consistent with out-of-plane C-H bends.

Frequency (cm <sup>-1</sup> )	Relative Strength <sup>a</sup>	Assignment <sup>b</sup>	Comment
3380	w	N-H stretch	
3285	m	N-H stretch	H-bonding to NMP
3170	w	N-H stretch	
3040	m	aromatic C-H stretch	
2970	w	C-H stretch	NMP
2865	w	C-H stretch	NMP
1675	vs	C=O stretch	NMP
1595	vs	C=C ring stretch	mainly quinoid
1505	vs	C=C ring stretch	benzenoid
1400	m	asymmetric CH <sub>3</sub> deformation	NMP
1380	m	unknown	
1300	vs	C-N stretch	
1160	s	i/p C-H bend	possible coupling to C-N stretch
1105	w	i/p C-H bend	
825	s	o/p C-H bend	1,4 - disubstituted aromatic rings
525	vw	o/p C-H bend	
405	vw	o/p C-H bend	

<sup>a</sup> Relative strength: vs very strong; s strong; m medium; w weak; vw very weak

<sup>b</sup> Assignment: i/p in-plane; o/p out-of-plane

Table 5.1 Assignment of IR vibrational bands, shown in Figure 5.4, for an as-cast EB polyaniline film.

All the above vibrations are assigned to groups of the polymer chain. However, there is also a strong absorption at  $1675\text{ cm}^{-1}$  which is undoubtedly a characteristic stretching vibration of a carbonyl (C=O) group. Such a group only occurs in NMP and this characteristic vibration is clearly visible in the IR spectrum of the pure solvent, Figure 5.5. The interaction between solvent and polymer reduces the frequency of this vibration slightly since in the pure NMP spectrum the carbonyl band actually occurs at around  $1700\text{ cm}^{-1}$ . The intensity of this C=O peak is thus a measure of the amount of residual solvent in the EB film. Other solvent peak may be assessed with the help of Figure 5.5, but as with the carbonyl band polymer/solvent interactions tend to shift the peak positions. One such solvent band which may be identified though is a  $\text{CH}_3$  asymmetric stretching mode at  $1400\text{ cm}^{-1}$ . Solvent peaks reduce in intensity if the film is thermally processed because the relatively volatile NMP is eliminated (this is perhaps a more intuitive way to assign NMP peaks). However, heating samples to beyond a critical temperature has a drastic effect on the whole structure of the film, inducing an irreversible and highly detrimental crosslinking reaction. The changes to the spectrum under these circumstances have been described in detail in the preceding chapter.

It is also instructive to examine the spectrum of a deuterated (d-EB) film, Figure 5.6. Deuterated samples were prepared for neutron diffraction studies described in chapter 7. The spectrum itself is rather complicated since the material, as discussed in section 7.3.2, appears to be only partially deuterated. However, some interesting features can be observed, the most notable of which is an aromatic C-D stretching band at  $2249\text{ cm}^{-1}$ . Some change is also discernable in the main bands below  $2000\text{ cm}^{-1}$ . All have been shifted down in frequency to some extent, except the  $1160$  and  $1105\text{ cm}^{-1}$  vibration (these latter bands occur at  $1186$  and  $1120\text{ cm}^{-1}$  respectively and are also much reduced in intensity). Such shifts may indicate a strong coupling between group frequency modes in this region which perhaps explain the different assignments between groups of the  $1160\text{ cm}^{-1}$  peak in the undeuterated spectrum .

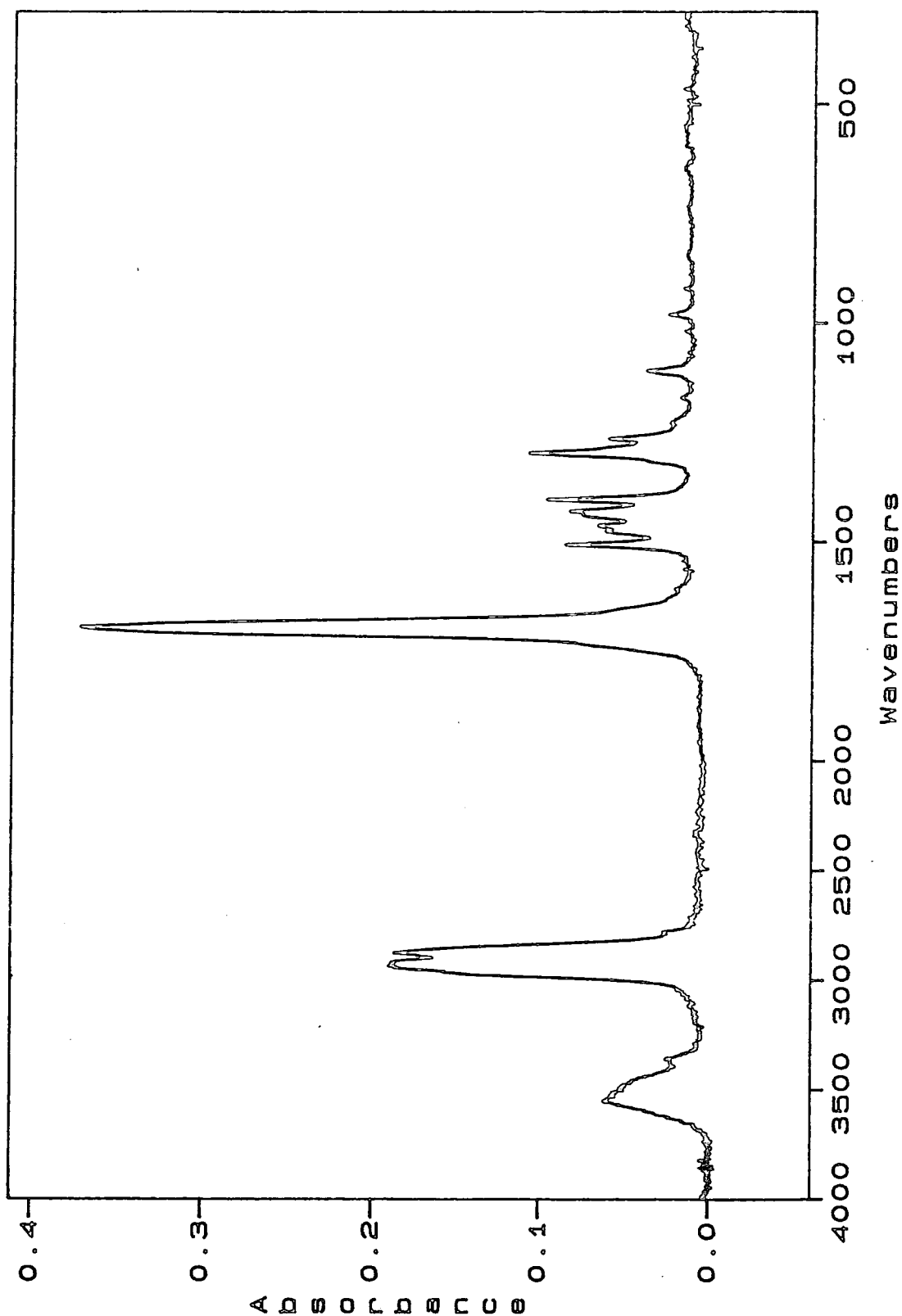
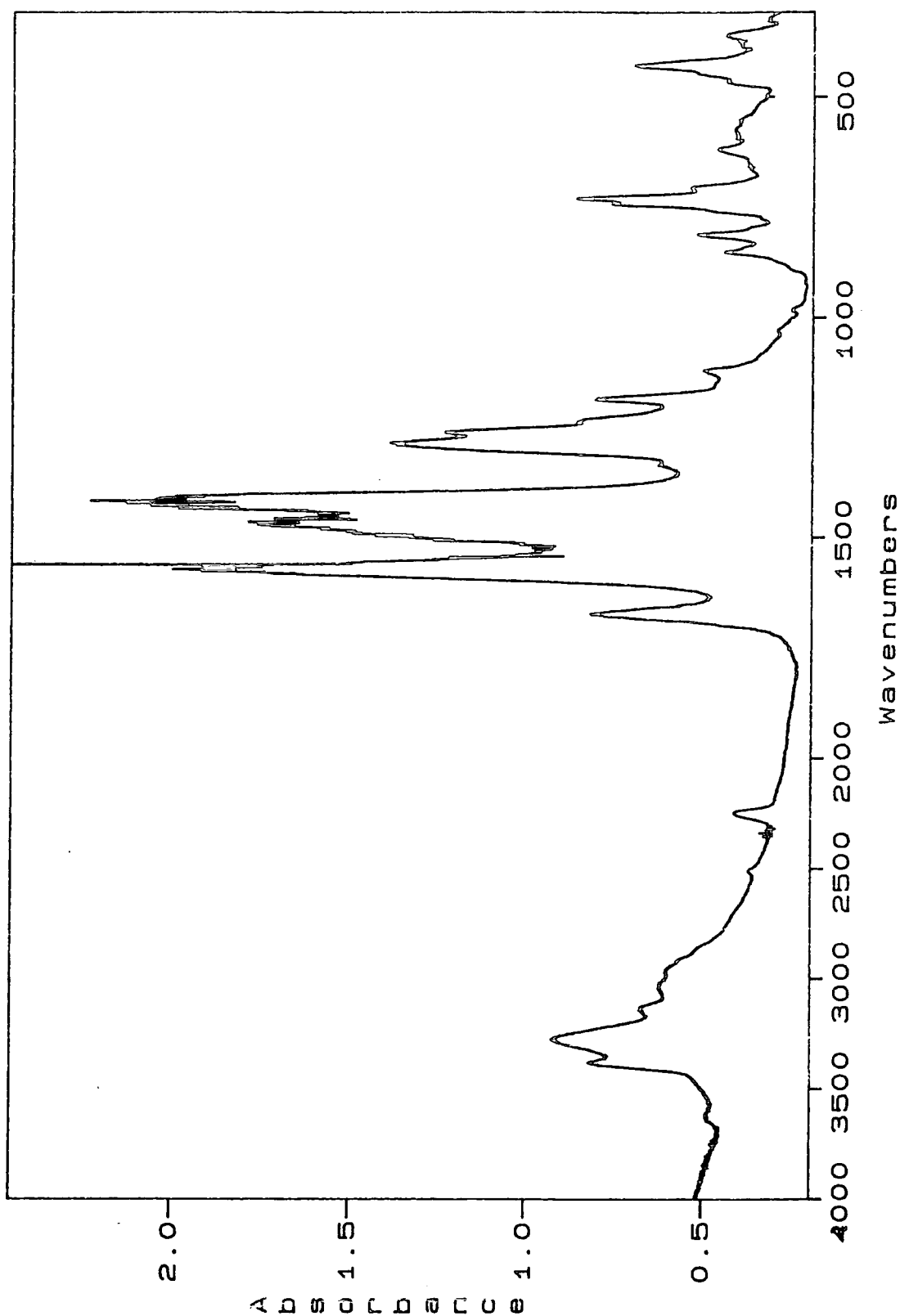


Figure 5.5 IR absorption spectrum of pure NMP. The spectrum shows the strong carbonyl band at ca.  $1700\text{ cm}^{-1}$  and was recorded (Perkin-Elmer 580B) on a polished KBr disc substrate. The absorption band at around  $3570\text{ cm}^{-1}$  is due to water vapour.



**Figure 5.6** IR absorption spectrum of an as-cast deuterated (d-EB) polyaniline film illustrating the C-D stretching band at  $2249\text{ cm}^{-1}$ . This spectrum was also recorded using the Perkin-Elmer 580B spectrophotometer.



As well as the fingerprint region, bands are also seen in the N-H and C-H stretching regions between about 3600-2800  $\text{cm}^{-1}$  as shown in Figure 5.4(b). This part of the spectrum has received rather less attention in the literature and so has been investigated further here. The aromatic  $\nu(\text{CH})$  is easily identifiable above 3000  $\text{cm}^{-1}$  as a peak at 3040  $\text{cm}^{-1}$ . The weaker features at lower frequency are  $\text{CH}_2$  stretches of NMP. At higher wavenumbers a N-H vibration is observed at 3285  $\text{cm}^{-1}$  with a shoulder at approximately 3380  $\text{cm}^{-1}$ . For diphenylamine, which we can consider to represent the benzenoid-amine part of the polyaniline chain, a sharp peak is observed at around 3380  $\text{cm}^{-1}$  which is indicative of  $\nu(\text{NH})$  for the 2° amine units<sup>14</sup>. This clearly identifies the shoulder in the polyaniline spectrum.

The main N-H band, however, occurs at 3285  $\text{cm}^{-1}$ . This peak shift indicates hydrogen (H-) bonded amine groups. For example<sup>7</sup>, H-bonding in the polyamide Nylon 6,6 shifts  $\nu(\text{NH})$  from 3450  $\text{cm}^{-1}$  down to about 3300  $\text{cm}^{-1}$ . We can further identify that this H-bonding involves NMP molecules bonding to the polar amine groups, since this band disappears in conjunction with the solvent carbonyl band when the sample is heated to 200 °C (see Figure 4.22). It is this H-bonding that gives the polymer a degree of solubility in NMP, since the highly polar solvent molecules are able to attract amine units in lieu of other amine units. This reduces the strong chain-chain H-bonding and induces solvation.

### 5.5.2 Orientation Measurements

Figure 5.7 shows the parallel and perpendicularly polarised IR spectra of an EB film stretched by 230% over the range 4000-400  $\text{cm}^{-1}$ . The thickness of the sample was about 15 +/- 2  $\mu\text{m}$  as measured by a micrometer. The two main groups of bands between 3600-2800  $\text{cm}^{-1}$  and 2000-400  $\text{cm}^{-1}$  are shown more clearly in Figures 5.8(a) and (b) respectively. It is apparent that there is considerable dichroism for specific vibrations below 2000  $\text{cm}^{-1}$ . An interesting observation is that for the parallel polarisation a band is resolved from under the low frequency C-N shoulder. The C-H and N-H stretching regions also show some anisotropy. However, the N-H bands are rather convoluted and furthermore subject to H-bonding and solvent

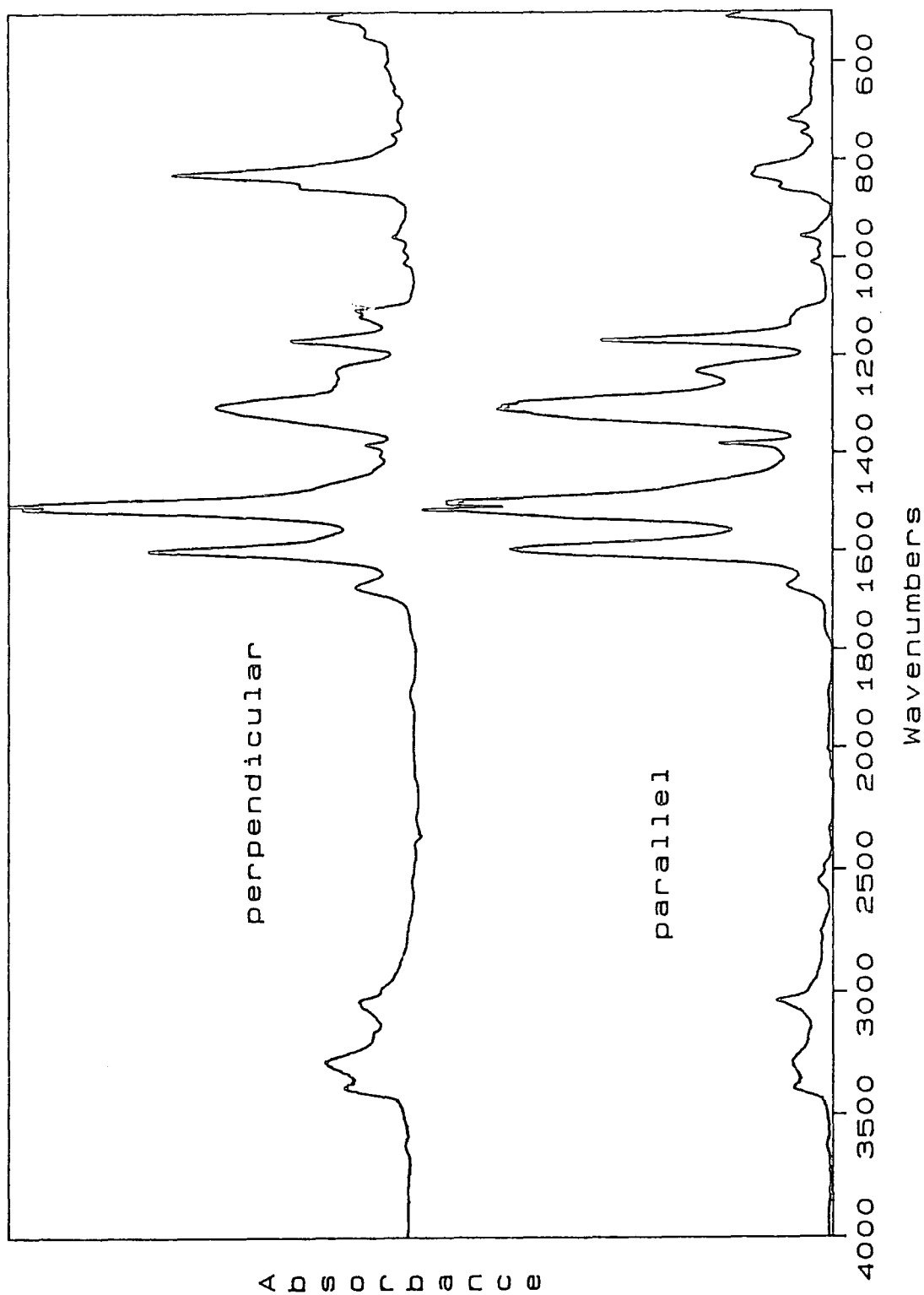
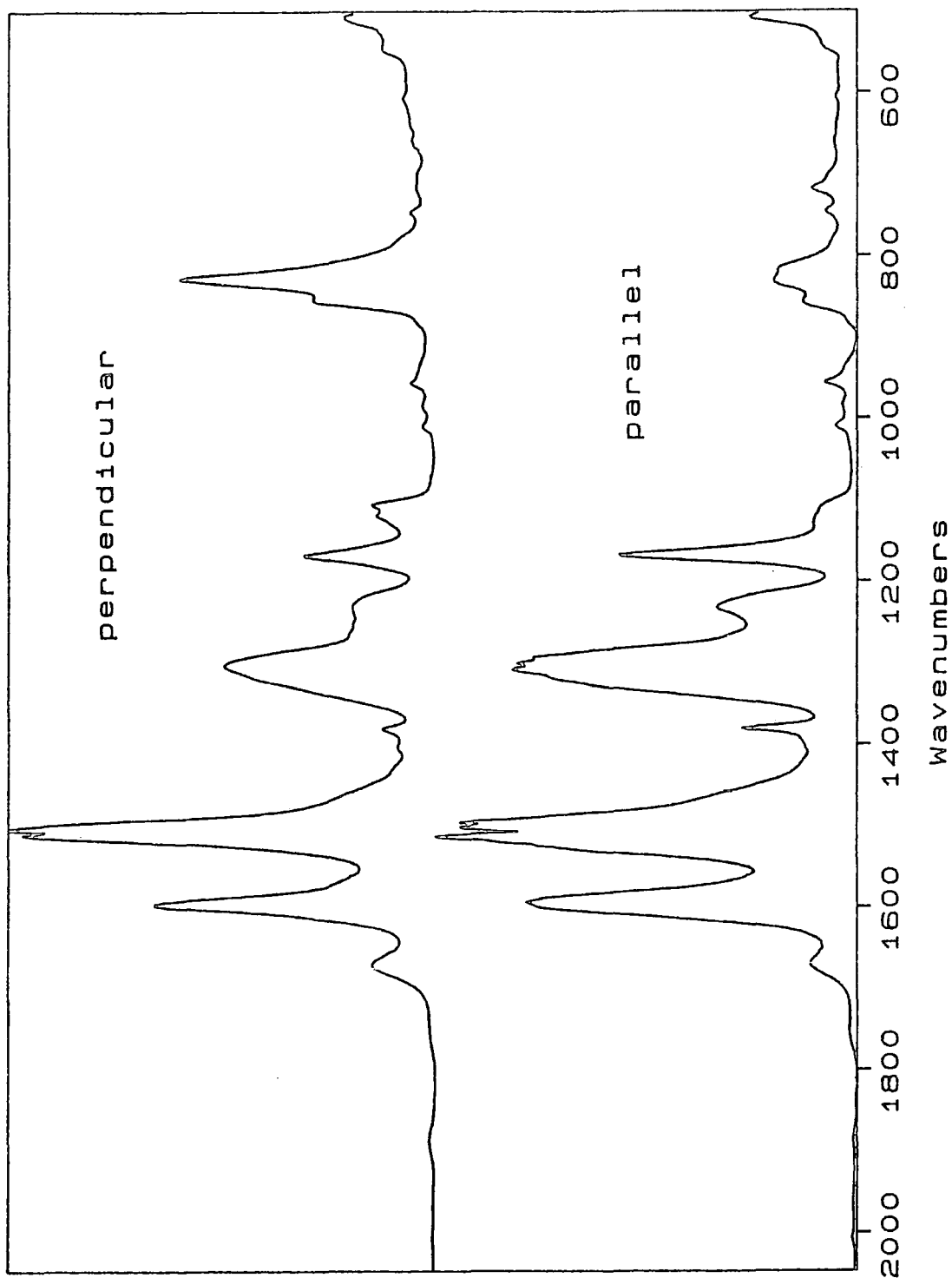


**Figure 5.7** Polarised IR absorption spectra of an oriented EB film with the incident electric field vector perpendicular (top) and parallel (bottom) to the stretch direction.



4 0 0 0 0 0 0 0 0 0

Figure 5.8(a) The polarised IR absorption spectra of Figure 5.7 showing the bands between 2000-200  $\text{cm}^{-1}$  in detail.

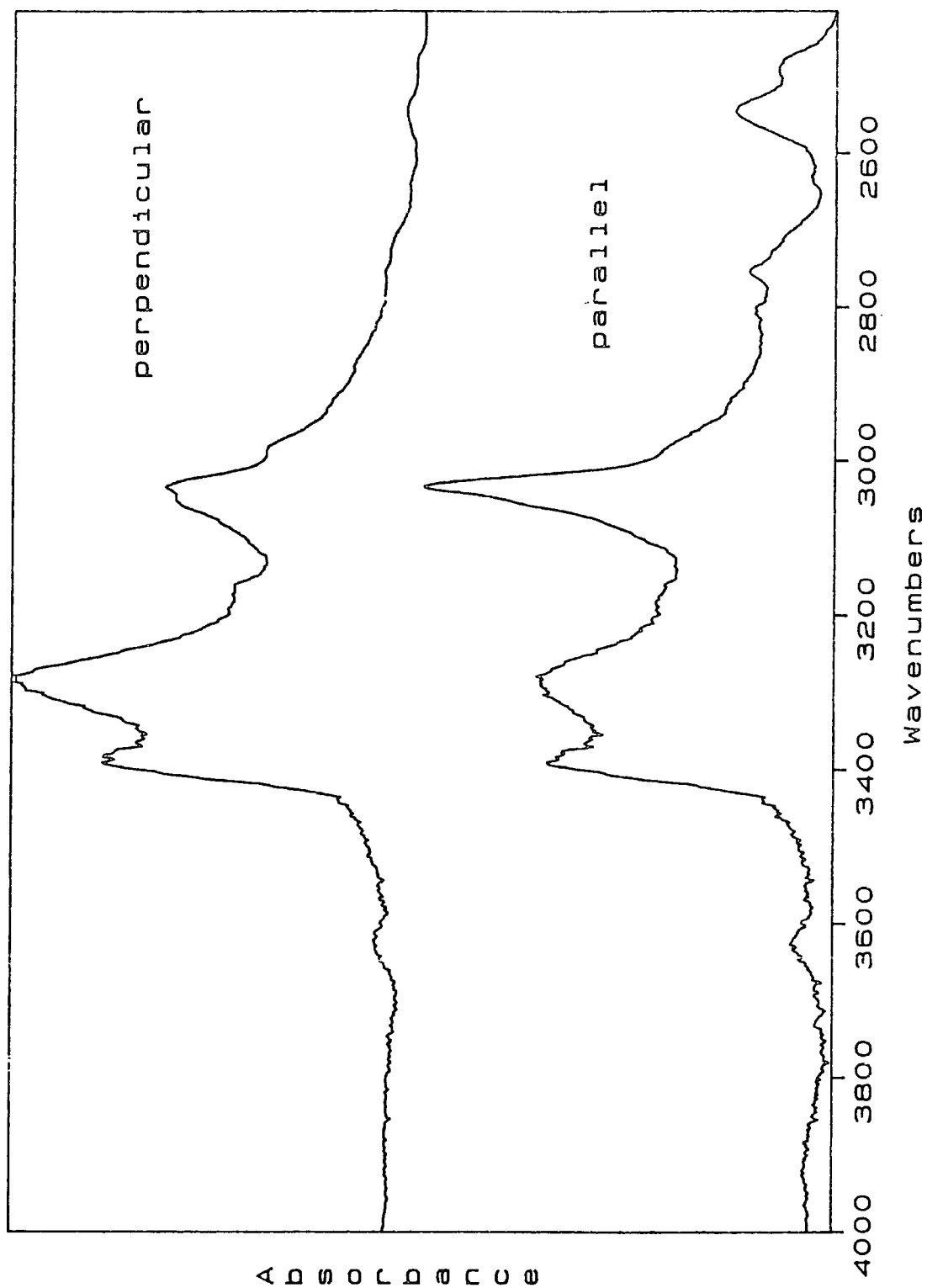


**Figure 5.8(b)** The polarised IR absorption spectra of Figure 5.7 showing the bands between 4000-2800  $\text{cm}^{-1}$  in detail.

interactions. These effects mask the true dichroic behaviour, making analysis very difficult. This is unfortunate since the vibration has a well specified transition moment direction<sup>2</sup>. Despite this, very useful data can still be obtained from the other bands.

The dichroic ratio for the main vibrational bands are shown in Figure 5.9 for films of various extensions. These results were calculated using integrated oscillator intensities as discussed in the experimental section, but it was found that peak intensity values gave very similar results. The 825 cm<sup>-1</sup> mode shows quite a strong perpendicular polarisation for highly stretched samples, in agreement with the assignment to an out-of-plane ring bending mode. All other vibrations, except the C=O stretch at 1675 cm<sup>-1</sup>, exhibit a very similar, moderately strong, parallel dichroism effect which tends to saturation at large extensions. The carbonyl band, however, shows no dichroic behaviour within experimental error. Thus the residual solvent, i.e. that not removed during thermal stretch alignment, is not oriented along with the polymer chains.

To determine the degree of chain orientation it is first necessary to decide upon a specific vibration for which the transition moment direction is known. The C-H stretch is a good example, but the band is a composite of all the individual groups and hence all the directions on a specific aromatic ring. A more suitable vibration, however, is the C-N stretch at around 1300 cm<sup>-1</sup>. For this stretching vibration it seems reasonable to assume that the change in dipole moment lies along the axis of the chemical bond (no evidence was found to disprove this assumption). Based on such an assumption the degree of chain orientation can be calculated provided the angle this C-N bond makes with the molecular chain axis is known.

This latter parameter may be conveniently derived from the idealised geometrical chain structures proposed from theoretical studies<sup>10,15</sup> and oligomeric structure determinations<sup>16</sup> (as discussed in chapter 2). To recap, the basis of these models is a plane of nitrogen atoms, in a zigzag along the chain axis. However, each individual C-N bond is constrained to lie at an angle of approximately 30° with respect to this axis and this information can therefore be used in this analysis.

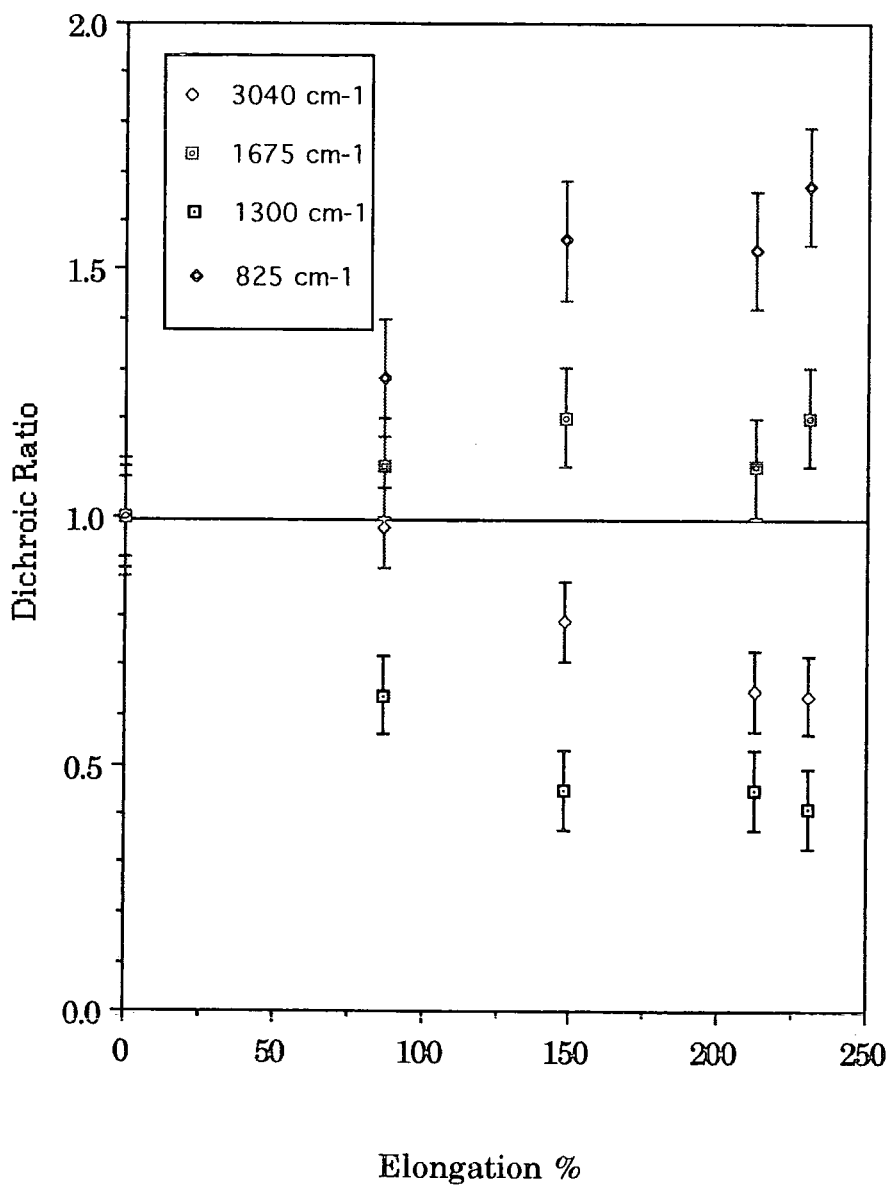


**Figure 5.9** Dichroic ratio versus elongation for various absorption bands of EB films. Although not shown, the 1595, 1505 and 1160  $\text{cm}^{-1}$  bands exhibit an almost exact behaviour to the 1300  $\text{cm}^{-1}$  mode.

From Figure 5.9 the 1300  $\text{cm}^{-1}$  dichroic ratio for the 230% elongated film is around 0.41. Using this value for R and the corresponding  $\theta$  value of  $30^\circ$  in the dichroic formula (6), the orientation parameter, S, is determined as 0.58. Values of S may be similarly derived for the other extensions using the

relevant dichroic ratio. It is important to remember, though, that this is an average value over all morphological phases of the sample. As stated earlier  $S$  depends on the distribution function  $f(\gamma)$  and although the form of this function is not specifically known certain distributions may be assumed which help to visualise the degree of orientation. If the sample is considered to consist of a fully oriented chain fraction,  $f$ , and a randomly oriented fraction,  $(1-f)$ , then  $f(\gamma)$  takes a form<sup>17</sup> such that

$$S = \frac{2}{3} \frac{(1-f)}{f}$$

Although this is rather an unrealistic model it is particularly useful since it may be shown<sup>18</sup> that the randomly oriented fraction,  $(1-f)$ , is equal to the Hermans orientation function. This is a parameter which can be derived from X-ray diffraction experiments as a measure of orientation. and such an analysis is infact reported in the next chapter. So using  $S = 0.58$  yields  $f = 0.53$  and hence  $(1-f) = 0.47$ . Before commenting on this value it is also useful to discuss another distribution function for this type of orientation, which is usually regarded as the most realistic.

Such a distribution function may be derived from a deformation scheme proposed by Kratky<sup>19</sup>, originally to describe orientation of crystallites in semicrystalline materials. It is also sometimes known as the pseudo-affine deformation model<sup>20</sup>. Briefly, the model describes molecular orientation of chain segments corresponding to the macroscopic deformation of a sample and during orientation these rigid chain segments rotate in an equivalent manner to lines joining points on the bulk material. If the sample volume remains constant during stretching then a distribution can be derived dependent on the sample extension. A detailed discussion is given by Zbinden<sup>2</sup> but suffice to say here that for a film extended by 230% an  $S$  value of around 0.70 is expected. Clearly, in reality, the orientation process in polyaniline is not so efficient as that described by Kratky. However, this might have been expected since normally the model defines an upper limit for orientation. Factors such as viscous flow and the non-rigidity of structural units for an amorphous phase lower the molecular ordering.

Furthermore, in the case of polyaniline films, the assumption of a constant deformation volume is rather invalid as significant sample compaction occurs during stretching due to removal of volatile NMP molecules (see TMA results in previous chapter).

The opposite is true, though, for stretch aligned PPV films. It is reported<sup>2</sup> that for these samples the orientation process is more efficient than the Kratky model. This enhanced orientation is considered to relate to the fact that PPV samples are stretched during an elimination process which is presumed to plasticise the films, much in the same way as the removal of NMP does for polyaniline. However, the elimination reaction produces conjugated units on the chain, since PPV is synthesised and processed in a non-conjugated, precursor form. This increase in unsaturation is an added driving force for orientation.

In spite of this difference it is very interesting to compare the conductivities of the two polymers. Although, in both cases, the orientation analyses relate to non-conducting forms and doping requires some molecular reorganisation, the relevant conductivities for similarly stretched films may be compared. For polyaniline a 230% stretched EB film has an orientation value,  $S$ , of 0.58 and if protonated in 1 M HCl may be expected to have a parallel conductivity of around  $250 \text{ S cm}^{-1}$  (see Figure 2.12). In the case of  $\text{AsF}_5$ -doped PPV<sup>3</sup>, a film of similar elongation shows a parallel conductivity of less than  $100 \text{ S cm}^{-1}$  with a corresponding undoped  $S$  value of about 0.75. Thus oriented ES films exhibit a conductivity over twice as large as similarly elongated  $\text{AsF}_5$ -doped PPV films .

The assessment of the degree of orientation also allows information to be derived about the geometrical structure of the polymer chain. One of the most important considerations in this respect is the torsional angle between neighbouring  $\text{C}_6$  rings along the polyaniline chain. In general it is predicted<sup>11,16</sup> that for benzenoid units this angle is approximately  $50\text{-}60^\circ$ , or equivalently an angle of  $25\text{-}30^\circ$  between the plane of the rings and the N-N zigzag plane. The more rigid quinoid-imine units, though, are expected to lie almost in the nitrogen plane. These values refer to a base chain - in the protonated state an average ring torsional angle is defined which



constrains the rings to be as near to planarity as steric hinderance will allow, in accordance with increased electron delocalisation in this form of the material. Using the orientation parameter, the extent of ring rotations may be assessed if we consider the base chain to be an idealised, average structure, i.e. there is no difference between benzenoid and quinoid rings. The justification for this may be somewhat tenuous, but the analysis does yield sensible results, in light of the true complexity of the chain structure.

The method again makes use of the dichroic equation (6) and also the fact that the out-of plane aromatic C-H vibration at  $825\text{ cm}^{-1}$  has a well-defined transition moment in a direction normal to the plane of the ring. If it is assumed that the same value of  $S$  as for the C-N stretch also applies to this band i.e. a homogeneous sample, the value of  $\theta$  can be obtained. Using  $S = 0.58$  for the 230% film and the  $825\text{ cm}^{-1}$   $R$  value of 1.67 gives  $\theta = 68^\circ$ . Now the geometry requires that with the plane of the ring perpendicular to the N-N plane  $\theta$  will be  $30^\circ$ . Correspondingly, with both the planes concentric,  $\theta$  takes the value of  $90^\circ$ . Using this information a  $\theta$  value of  $68^\circ$  is equivalent to an average angle of  $33^\circ$  between the ring and nitrogen planes. This is certainly a result in very good agreement with the other reports of torsional angles. It is also interesting to note that a very similar value is derived if the dichroic behaviour of the in-plane C-H bending band at  $1160\text{ cm}^{-1}$  is used, with a transition moment in the plane of the ring. This mode was not automatically chosen here since the assignment was rather disputed in other reports<sup>8</sup>. However, the agreement of the ring torsional angle suggest that the assignment given in this work is particularly justified.

## 5.6 Summary

Infrared orientation studies of stretched EB films have revealed detailed information about the molecular orientation produced during macroscopic stretching of a sample. A specimen stretched by 230% was shown to have an degree of orientation equivalent to 53% of the polymer chains aligned with the stretch direction. Upon protonation in 1M HCl such a film exhibits a conductivity in the range of  $250\text{ S cm}^{-1}$ . This value is over twice as large as that obtained for similarly elongated  $\text{AsF}_5$ -doped PPV films. Also, the extent

of orientation in such PPV samples corresponds, typically, to over 75% of chains perfectly oriented. Therefore, intrinsically, polyaniline is much the better conductor. Further analysis has probed the geometrical structure of an EB chain and has determined an average ring torsional angle between the C<sub>6</sub> and the nitrogen-nitrogen planes of 33°. This result is in very good agreement with theoretical and oligomeric crystal structure studies.

## References

- 1 C.N. Banwell, *Fundamentals of Molecular Spectroscopy*, Second Edition, McGraw-Hill, 1972.
- 2 R. Zbinden, *Infrared Spectroscopy of High Polymers*, Academic Press, New York, 1964.
- 3 D.D.C. Bradley, R.H. Friend, H. Lindenberger and S. Roth, *Polymer*, **27**, (1986), 1709.
- 4 D.R. Gagnon, F.E. Karasz, E.L. Thomas and R.W. Lenz, *Synth. Met.*, **20**, (1987), 85.
- 5 P.D. Townsend, C.M. Pereira, D.D.C. Bradley, M.E. Horton and R.H. Friend, *J. Phys. C*, **18**, (1985), L283.
- 6 B.E. Read in *Structure and Properties of Oriented Polymers*, ed. I.M. Ward, Applied Science Publishers, London, 1975.
- 7 *The Vibrational Spectroscopy of Polymers*, eds. D.I. Bower and W. F. Maddams, Cambridge University Press, (1989).
- 8 J. Tang, X. Jing, B. Wang and F. Wang, *Synth. Met.*, **24**, (1988), 231.
- 9 M. Ohira, T. Sakai, M. Takeuchi, Y. Kobayashi and M. Tsuji, *Synth. Met.*, **18**, (1987), 347.
- 10 A.J. Epstein, R.P. McCall, J.M. Ginder and A.G. MacDiarmid in *Spectroscopy of Advanced Materials*, Volume 19, eds. R.J.H. Clark and R.E. Hester, John Wiley & Sons Ltd, 1991.
- 11 K.R. Kromack, M.E. Jozefowicz, J.M. Ginder, A.J. Epstein, R.P. McCall, G. Du, J.M. Leng, K. Kim, C. Li, Z.H. Wang, M.A. Druy, P.J. Glatkowski, E.M. Scherr and A.G. MacDiarmid, *Macromolecules*, **24**, (1991), 4157.
- 12 Y. Furukawa, T. Hara, Y. Hyodo and I. Harada, *Synth. Met.*, **16**, (1986), 189.

- 13 Y. Furukawa, F. Ueda, Y. Hyodo, I. Harada, T. Nakajima and T. Kawagoe, *Macromolecules*, **21**, (1988), 1297.
- 14 *Aldrich Library of Infrared Spectra*, Edition 3, ed. C.J. Pouchert, Aldrich Chemical Co, Inc.
- 15 J.L. Bredas in *Proceedings of the Nobel Symposium on Conjugated Polymers and Related Materials*, ed. W.R. Salaneck, Oxford University Press, 1992.
- 16 L.W. Shacklette, J.F. Wolf, S. Gould and R.H. Baughman, *J. Chem. Phys.*, **88**, (1988), 3955.
- 17 R.B.D. Fraser, *J. Opt. Soc. Am.*, **43**, (1953), 929.
- 18 B. Jasse and J.L. Koenig, *J. Macromol. Sci.-Rev. Macromol. Chem.*, **C17**, (1969), 71.
- 19 O. Kratky, *Kolloid-Z*, **64**, (1933), 401.
- 20 I.M. Ward in *Structure and Properties of Oriented Polymers*, ed. I.M. Ward, Applied Science Publishers, London, 1975.

## Chapter 6

### X-ray Diffraction Studies

This chapter reports on the results of X-ray Diffraction (XRD) experiments on polyaniline films. The aim of these studies was to elucidate the sample morphology and to characterise structural changes due to stretch alignment and also protonation. The experiments were performed using the X-ray facilities of BICC Cables Ltd, Wrexham Technology Centre. The equipment at Wrexham was run by Dr. J Jutson.

#### 6.1 Introduction to X-ray Diffraction

X-ray diffraction is a fundamental technique used in the determination of the atomic structure of a crystal or crystalline material. Detailed discussions of background topics such as crystallography, the properties of X-rays and diffraction theory, can be found in most solid state physics books. Only a basic introduction of these ideas will be provided here. The reader wishing to be informed in further detail is referred to one of the numerous texts<sup>1,2</sup>.

The phenomenon of X-ray diffraction results from a process where X-rays are scattered by the electrons of the atoms in a crystal, without change in wavelength. This is known as coherent or Bragg scattering. A diffracted beam is produced corresponding to scattering from a certain set of crystallographic planes (hkl), but only when certain geometric conditions are satisfied. This criterion is defined by the Laue conditions and also by the familiar Bragg equation,

$$\lambda = 2 d_{hkl} \sin\theta \quad (1)$$

where  $\lambda$  is the X-ray wavelength,  $d_{hkl}$  the inter-planar spacing and  $2\theta$  the scattering angle. The planes are oriented so that their normal bisects the angle between the incident and diffracted beams.

If a single crystal in an arbitrary orientation is illuminated with monochromatic radiation it is unlikely to have any set of planes oriented in a position to fulfil the diffraction geometry. Thus diffraction will not normally occur. Diffraction methods, therefore, have to ensure that these planes satisfy the diffraction conditions. The moving crystal technique involves rotating the crystal into appropriate orientations for it to diffract radiation. This is the basis of the diffractometer, used in this work. A most useful method for defining the geometrical conditions for diffraction is the Ewald sphere construction, see Figure 6.1. The concept involves the use of the reciprocal lattice representation, where a set of planes is defined as a lattice point, which lies a distance  $1/d_{hkl}$  along a line normal to the planes. A vector AB, length  $1/\lambda$ , is drawn parallel to the incident beam direction and ending at any reciprocal lattice point B. If the sphere centred on A of radius  $1/\lambda$  intersects another lattice point such as C, then it can be shown that the diffraction conditions (i.e. Bragg law) for this set of planes are satisfied. Rotating the crystal is equivalent to rotating the reflecting sphere about B, so that other lattice points will intersect its surface and thus be brought into the appropriate reflecting positions.

The resulting diffraction pattern, combining both the position and intensities of the diffraction effects (Bragg peaks), is a fundamental physical property of the crystal. The information can be utilised as a rapid method for sample identification, but also as a means to elucidate the crystal structure. Analysis of the position of the Bragg peaks leads to a knowledge of the size, shape and orientation of the constitutive unit cell. However, to determine the spatial coordinates of the atoms (in term of some fixed origin in the cell) relative to a given set of planes, the intensities of the diffracted beams must be measured and analysed. The most important factor in the intensity equation is the crystal structure factor  $F(hkl)$  given by

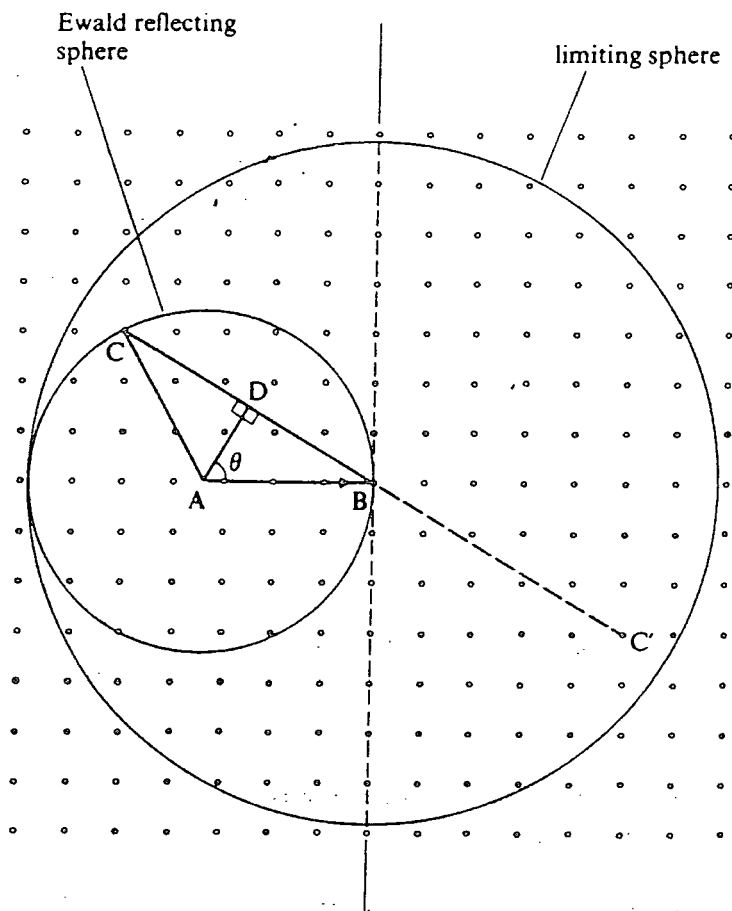


**Figure 6.1 The Ewald sphere construction.** Reciprocal lattice points are represented by dots and point B is taken as the origin of reciprocal space. The vector  $|AB| = 1/\lambda$  is in the direction of the incident beam. All reciprocal lattice points lying on the Ewald sphere give rise to reflections. Also shown is the limiting sphere of radius  $2/\lambda$ , within which the lattice points lie (from <sup>1</sup>).

$$F(hkl) = \sum_i^N f_i \exp [2\pi i (hx_i + ky_i + lz_i)] \quad (2)$$

where  $x$ ,  $y$  and  $z$  represent the fractional coordinates of the  $i$ th atom in the unit cell, containing  $N$  atoms, and  $f_i$  is the atomic scattering factor or structure factor. Equation (2) can be expressed in trigonometric terms as

$$F(hkl) = \sum_i^N f_i [\cos 2\pi (hx_i + ky_i + lz_i) + i \sin 2\pi (hx_i + ky_i + lz_i)] \quad (3)$$

If the real and imaginary terms are represented by A and B respectively then the magnitude or modulus of F is

$$|F(hkl)| = (A^2 + B^2)^{1/2} \quad (4)$$

The term  $|F(hkl)|^2 = A^2 + B^2$  may be regarded as the ideal intensity of the reflection (hkl) and can be determined directly from the experimental intensity. The phase relationship of  $|F(hkl)|$ , however, given by  $\phi = \tan^{-1}(B/A)$  cannot be derived - this is the so-called phase problem. A number of experimental factors<sup>1</sup> modify the ideal intensity to give that actually observed, I(hkl):

$$I(hkl) = pLmAK|F(hkl)|^2 \quad (5)$$

where p is the polarisation factor, L the Lorentz factor, m the multiplicity, A the absorption factor and K is the scale factor.

## 6.2 Diffraction by Polymers

### 6.2.1 The 'Fringed Micelle' Model

The previous section outlined diffraction by referring to the classical case of a macroscopic single crystal, consisting of a regular periodic lattice. Long chain molecules such as synthetic polymers, however, have an inherently different structure. The basic chemical repeat unit for these

macromolecules is a covalently connected array in a zigzag arrangement lying along the molecular chain axis. In other directions less ordered bonding arrangements occur so that there is no continuous or exact periodic structure in three dimensions. This spatial bonding pattern creates a texture which suppresses the overall crystallinity. Order exists only locally with amorphous regions separating the crystalline domains.

The 'fringed micelle' or two-phase model, see Figure 6.2, first proposed by Hermann (see Ward<sup>5</sup>) represents the organisation of long chain molecules. Amorphous regions are characterised by a random tangle of polymer chains. The crystalline regions, or crystallites, consist of highly ordered segments of chains which are bound together by van der Waals forces. Such forces operate only at close distances so that the extent of the crystallites reflects the ability of the polymer to line up in a regular and close packed way. Thus high-density (linear) polyethylene is highly crystalline, but



Figure 6.2 The 'fringed micelle' or two-phase model for polymers representing ordered regions, or domains, in a less well ordered matrix.



polymers such as poly(methyl methacrylate), with sterically hindering substituent groups on the chain, are essentially amorphous.

In the case of high-density polyethylene a one-phase model has been found to be more appropriate<sup>4</sup>. Here the solid consists of an entirely crystalline phase with chain-folded or lamellar-like crystals. Structural distortions (e.g. branching, atactic disorder) and grain boundaries cause crystal imperfection. Such a paracrystalline model is a limiting case for highly crystalline polymers. However, in the case of semi-crystalline materials the use of the two-phase model is generally well justified.

Usually polymers are oriented by drawing or stretching. In such cases the two regions respond separately. For uniaxial stretching chains tend to align along the stretch direction or fibre axis as mentioned in the previous chapter. Crystalline regions orient along this axis producing long slender crystallites with often many repeat units along the chain axis. Amorphous regions also align with the stretch direction, but less readily and with no sign of 3-D order. This is not true, however, for amorphous polyethylene terephthalate<sup>5</sup>. Here stretching produces both molecular orientation and regions of 3-D order. The simplest explanation of this behaviour is that orientation processes have brought chains into adequate position so that they may crystallize.

### **6.2.2 Structural Analysis**

For an unoriented semi-crystalline polymer the diffraction information will be spherically averaged due to the totally random distribution of crystallites. Thus for an X-ray photograph we might expect a series of circular (Debye-Scherrer) rings typical of a polycrystalline material. This overlay of crystallite signals severely limits the structural information which can be obtained from such materials. Further complications are added by superimposed Compton (incoherent) scattering from amorphous regions. This kind of scattering has no consistent phase relationship to the incident X-rays and generally consists of a band of wavelengths centred at slightly longer wavelength than the incident beam. The effect contributes to the

diffuse background of an X-ray pattern. Therefore, it is necessary to separate the incoherent and coherent scattering patterns since only the latter relate to structural features. This cannot be achieved experimentally, but the modified scattering may be calculated with considerable accuracy by subtraction of the incoherent term from the experimental data.

The diffraction information is much improved, however, for stretch aligned samples<sup>6</sup>, although the amorphous scattering still remains. The pattern, though, is still of poorer quality than that obtained in single crystal diffraction. Figure 6.3 shows an X-ray diffraction photograph for a typical uniaxially oriented semi-crystalline polymer.

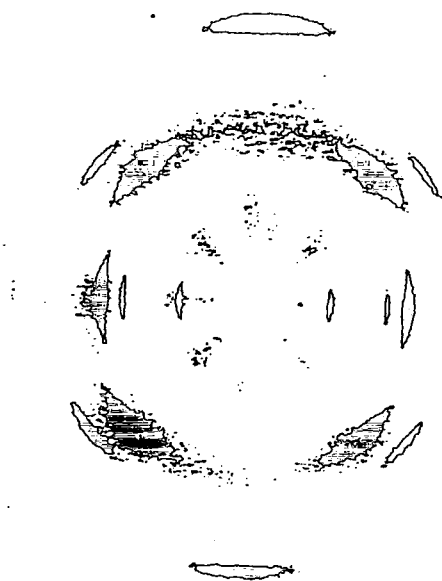


**Figure 6.3** An X-ray diffraction photograph of uniaxially oriented isotactic polystyrene, with the stretch direction vertical (from Atkins<sup>10</sup>).

Arcing of the diffraction signals is seen due to imperfect crystallite alignment as there is only preferential alignment along the fibre axis. Furthermore the crystallites exist in random orientations about this axis. Arcing is intermediate between the Debye-Scherrer rings observed for a

polycrystalline or unoriented sample and the point-like signals of a signal crystal. Diffraction photographs allow a qualitative measure of crystallite misalignment. A more quantitative measure of the distribution can be obtained from the circular (azimuthal) intensity distribution around a (h00), (0k0) or (00l) arc (if such signals exist). Data can then be presented in the form of a pole figure<sup>7</sup> or used to calculate the Hermans orientation function<sup>8</sup> defined as

$$f_{hkl} = \frac{3 \langle \cos^2 \varphi \rangle_{hkl} - 1}{2} \quad (6)$$

where  $\langle \cos^2 \varphi \rangle_{hkl}$  is the full width at half maximum (FWHM) of the intensity distribution along the arc. This is also a function that may be derived from IR orientation studies. Comparison of the two results is useful since the X-ray function defines only crystalline orientation whereas the IR function is usually an average of both amorphous and crystalline fractions.

Another feature of the diffraction signal is a broadening effect which, assuming no variation in lattice dimensions, is attributable to an effective crystallite size. Broadening is readily recorded by the radial intensity distribution of an (hkl) arc as a function of  $2\theta$ . Upon correcting for instrumental broadening the Scherrer formula<sup>9</sup> may be used to calculate the coherence length,  $L_{hkl}$ , where

$$L_{hkl} = \frac{K\lambda}{\Delta(2\theta) \cos\theta} \quad (7)$$

K is a constant of proportionality very close to 1,  $\theta$  the Bragg angle and  $\Delta(2\theta)$  is the angular FWHM of the intensity profile in radians.

Stretch aligned samples are invariably used in the crystal structure determination of polymers<sup>10</sup>. Each  $d_{hkl}$  spacing for an arc on a photograph can be easily deduced knowing the specimen to film distance,  $D$ ;

$$d_{hkl} = \lambda / 2 \sin^{-1} [ \tan^{-1} (R/D) / 2 ] \quad (8)$$

where  $R$  is the radius of the circle upon which the specific  $(hkl)$  arc lies.

Indexations can then be made using a suitable unit cell structure. Equatorial signals correspond to  $(hk0)$  reflections while layer lines gives information for successive values of  $l$ . Those lying on the meridian must have a  $00l$  indexation. Lattice parameters can thus be derived. As mentioned previously, intensity measurements are then required to place atoms in the unit cell. In some cases, e.g. polymers with simple repeat units such as polyethylene, structural determinations of this kind are very successful. Usually, however, even detailed diffraction data is not sufficient to establish unequivocally the spatial coordinates of the atoms.

This problem is generally overcome by augmenting the diffraction data with reliable stereochemical and rigid-body constraints. Crystal structures of oligomeric samples provide good reference points. Density measurements give valuable information on the number of chain segments in the unit cell. Computerised modelling of possible structures is also an integral part of the analysis. A flow chart outlining procedures used for structural determination is shown in Figure 6.4.

### 6.3 Polyaniline Diffraction Data

For a polymer such as polyaniline, a detailed crystal structure determination using X-ray methods is affected by several factors. First of all the emeraldine oxidation state is far from simple. Furthermore, the assumed repeat unit of Figure 2.3(c) is rather idealised since <sup>13</sup>C NMR analysis reported in this thesis has identified small amounts of sulphonate and chloride impurities occurring as ring substituents on the backbone.

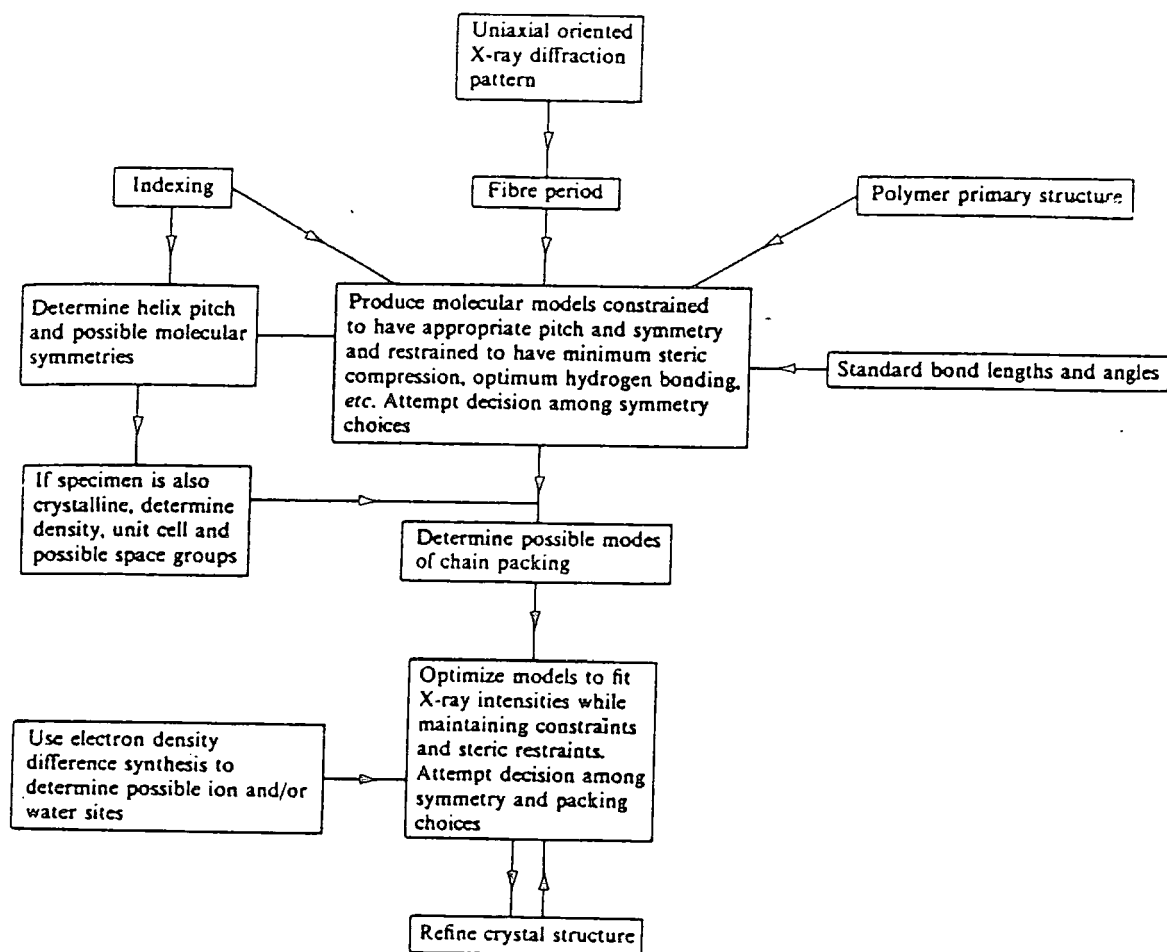


**Figure 6.4** A flow chart illustrating the procedure for structural determination of polymeric X-ray diffraction data (from Atkins<sup>10</sup>).

Another important point highlighted by the NMR studies is the ability of the chain to adopt a large number of different conformations. Clearly this variation in stereochemistry limits the analysis. Added to this the experimental X-ray diffraction data is not well resolved - only a handful of Bragg peaks are observed. Thus, crystal structure determination is fraught with many difficulties.

Several groups have strived to derive this information for polyaniline using X-ray results. Pouget *et al*, in particular, have completed some very detailed

work<sup>11,12</sup>. They postulate an orthorhombic unit cell, called EB II, for base films and also give possible structures for protonated samples. However, the results are heavily based on polyphenylene oxide (PPO) and polyphenylene sulfide (PPS) single crystal structures. These materials are isoelectronic with the fully reduced form of polyaniline, LEB, and thus are somewhat inappropriate for the emeraldine oxidation state. Further indication of the inadequacies of X-ray analysis is then provided when the authors turn to increasingly confusing discussions concerning the existence of different crystalline phases for seemingly endless variations of the form of the emeraldine oxidation state.

Rather than add to the conjecture, the crystal structure of polyaniline, despite being a vital concern, has not been assessed in this X-ray analysis. Instead results concentrate on other structural aspects of the polymer. However, the question of crystal structure has not remained unaddressed. In the following chapter, what is believed to be the first neutron diffraction results on polyaniline are presented. This analysis has provided a further dimension to X-ray diffraction data, such that crystal structures may be put forward with much more certainty.

## 6.4 Experimental Details

### 6.4.1 The Diffractometer

The main experimental tool used for X-ray studies was a Siemens D500 diffractometer. The technique involved the use of monochromatic cobalt  $K\alpha$  radiation ( $\lambda = 1.788\text{\AA}$ ) with scanning in a step-wise fashion over a  $2\theta$  range from  $5\text{-}80^\circ$  utilising a step size of  $0.010^\circ$ . The counting time for each step was 15 seconds. Diffraction data was recorded in reflection using single film samples which were aligned with their stretch direction parallel to the diffracting plane. A perpendicular film geometry was also employed in certain cases.

The diffractometer utilises the Bragg-Brentano para-focusing geometry<sup>9</sup>, illustrated in Figure 6.5. X-rays diverge from point A to strike the specimen

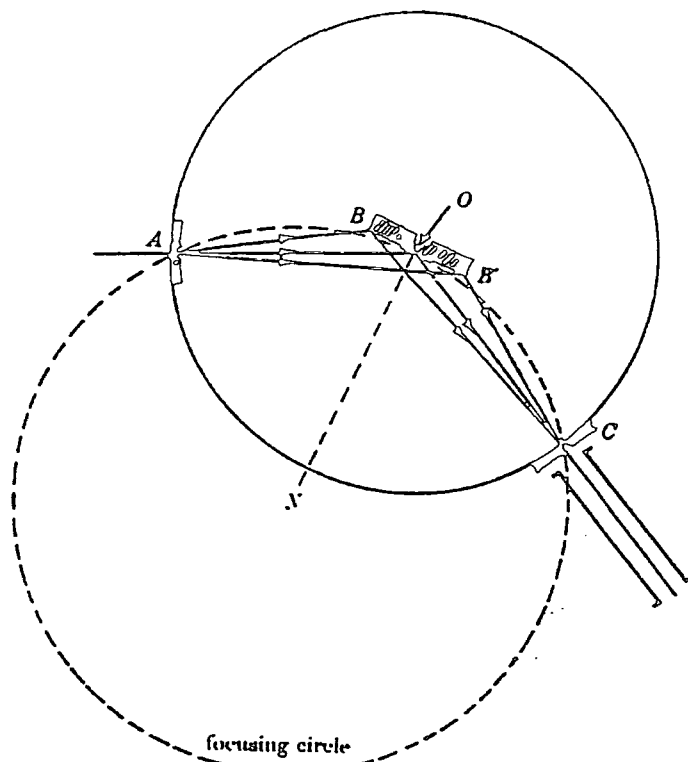


Figure 6.5 The Bragg-Brentano focusing geometry, as discussed in the text.

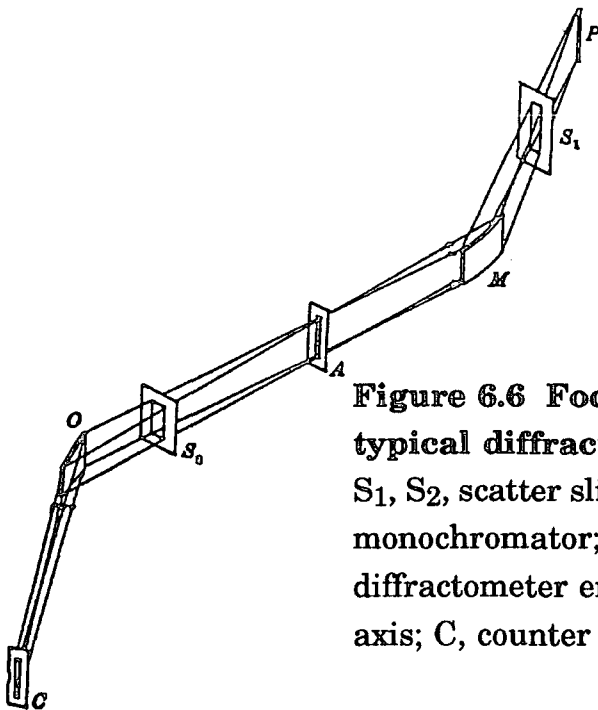


Figure 6.6 Focusing arrangement of a typical diffractometer. P, X-ray tube line focus; S<sub>1</sub>, S<sub>2</sub>, scatter slits; M, curved-crystal monochromator; A, monochromator focus and diffractometer entrance slit; O, diffractometer axis; C, counter entrance slit.

which is moved along the focusing circle AOC (OA and OC are equal). The detector C (Geiger-counter) is mounted on an arm which is pivoted at O. The specimen is rotated at half the angular speed of C so that ON, the normal to the sample, always bisects angle AOC. Thus the condition for diffraction, as described by the Ewald sphere construction mentioned previously, is met. Since the specimen is flat, not curved, and merely tangential to the focusing circle, true focusing is not achieved. However, provided the beam divergence is kept small, the error due to this approximation to true focusing is also small. This can be achieved by using a slit and monochromator arrangement as shown in Figure 6.6. Here P is the X-ray tube focus, M the monochromator and O and C, as before, the specimen axis and the counter entrance slit respectively. S<sub>1</sub> and S<sub>2</sub> are scatter slits. The focus of the monochromator is at A and it is usual to also have a slit at this point to further filter the beam. The case illustrated in Figure 6.6 is known as the parallel arrangement due to the parallel nature of the direction of the line focus, the diffractometer axis and the monochromator axis. The effect of the monochromator is to reduce the vertical divergence of the X-ray beam, since only incident beams of slight divergence will be reflected by the curved crystal. Using this type of arrangement the typical angular beam is around 0.5°.

#### **6.4.2 Data Processing and Analysis**

The diffractometer data was analysed by computer using Diffract 500 software. A fit program enables profile fitting to the experimental line shapes. For incoherent scattering (amorphous) a Lorentzian function was used incorporating a baseline level if necessary. Bragg peaks were fitted using Gaussian or Cauchy profiles. These latter profiles represent 'simplified methods' for expressing the true line shape<sup>9</sup>. The real crystalline profile is neither true Gaussian or true Cauchy; in the case of a diffractometer the diffraction geometry causes the experimental profile to depart from these assumed line shapes and become unsymmetrical. More accurate Fourier-transform<sup>13</sup> and iterative-folding<sup>14</sup> methods are also used, but these are much more complex and difficult to handle. Therefore, when



only relative and order-of-magnitude numerical results are needed, Gaussian and Cauchy crystal profiles are routinely employed.

The percentage crystallinity,  $X_c$ , in a specimen can be estimated by comparison of the integrated areas under 'crystalline' and 'amorphous' peaks. For undoped specimens the strong (110) and (200) Bragg peaks were integrated together with an amorphous signal centred at 4.7Å. In the case of emeraldine salt films only three crystalline curves at low d spacing were compared to the amorphous halo since a high sloping background at low scattering angles did not enable a suitable fit to the high d value Bragg peak (8.9Å) to be made. The values of  $X_c$  are only relative, however, since it is necessary to assume a constant of proportionality equal to unit for the amorphous term.

The width of the Bragg peaks was measured by comparison to a standard, hexamethylene tetraamine, to account for instrumental broadening. This standard has an orthorhombic crystal structure, similar to that used for emeraldine base, and also a similar transparency. The resulting widths may then be considered to derived from finite crystal size (the coherence length, L) if it is assumed that lattice dimensions do not vary.

### 6.4.3 Flat-Film Photographs

A texture goniometer, required for orientation measurements, is only a very recent addition to the accessories of the Siemens 500 Diffractometer at Wrexham. Due to limitations of time, and also money, it was not possible to use this piece of equipment during this analysis. However, a number of flat film X-ray photographs were taken so that specimen orientation could be probed. This was achieved using a set-up as illustrated in Figure 6.7. Samples were mounted with their fibre (stretch) axis vertical with a specimen to film distance, D, of 60mm and utilising copper  $K\alpha$  radiation (1.544 Å). Long exposure times (24 hrs) were tried at first, in anticipation of relatively weak coherent scattering signals. Although the latter was found to be the case, the background intensity was discovered to mask much of the information so that a compromise time of 2-3 hrs was used.

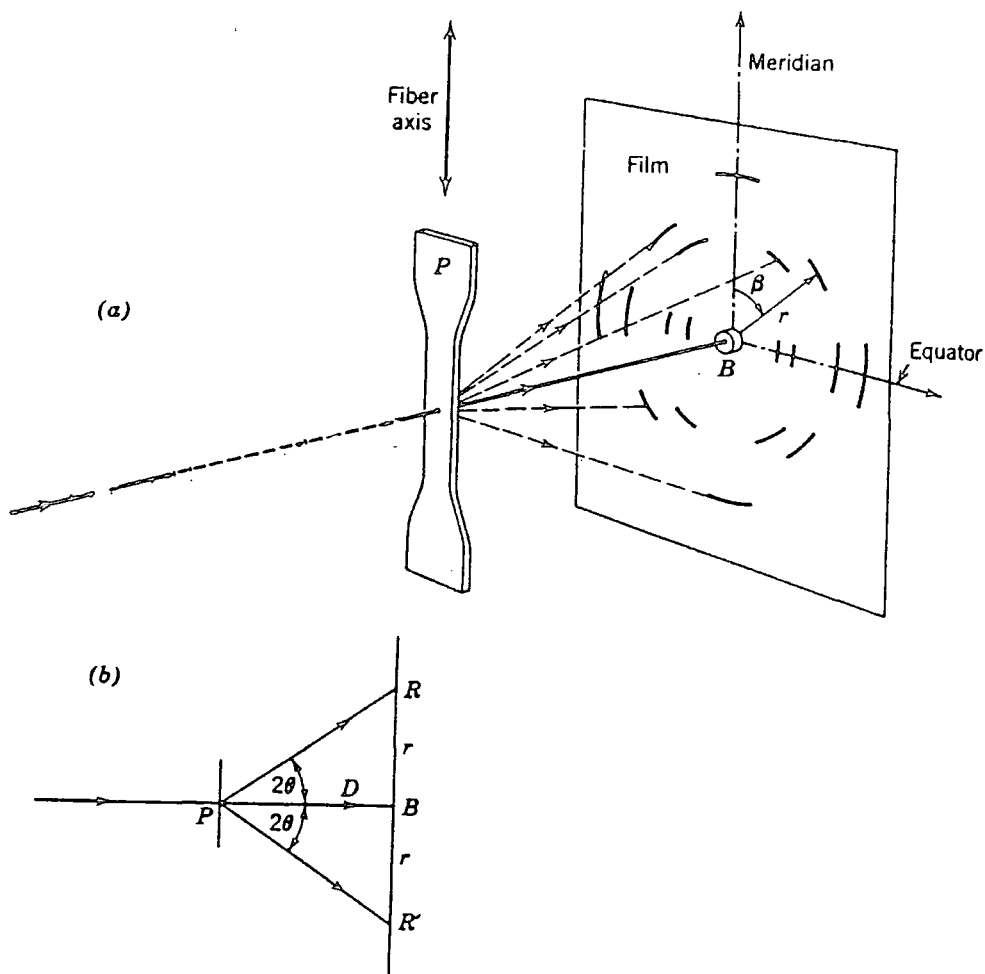


**Figure 6.7 The flat-film photographic technique for an uniaxially oriented polymer film: (a) schematic perspective; (b) dimensional relationships.**

The resulting arced diffraction patterns (for stretched films) enable a visual interpretation of orientation to be made, but it is also desirable to measure the intensity profile of the arcs more accurately. To do this a Joyce Loebel 3CS microdensitometer was used. However, this instrument is only designed to measure intensity in a linear profile i.e. along the radius of the arcs. Therefore, to record the circular intensity distribution it was necessary to assume that an arc approximated to a straight line over the region probed. This approximation is valid when as large a part of the arc as is necessary is scanned and also if those of largest diameter are used. Thus for undoped,

stretched films the signal at 3.9Å was utilised while for conducting samples that at 3.5Å was probed. It is still the case that the error in any derived value of the Hermans orientation function is far from negligible, but this method does give a reasonable estimate within the experimental limitations.

## 6.5 Experimental Results

Selected experimental diffraction data are shown in this section for both doped and undoped stretch aligned samples, Figures 6.8 to 6.12. Also included are examples of profile fitting of amorphous and crystalline line shapes using the Diffract 500 software as outlined in the data processing and analysis section. Figures 6.13, 6.14 and 6.15 are contact prints of flat-film X-ray photographs. These patterns have been used in the determination of crystallite orientation.

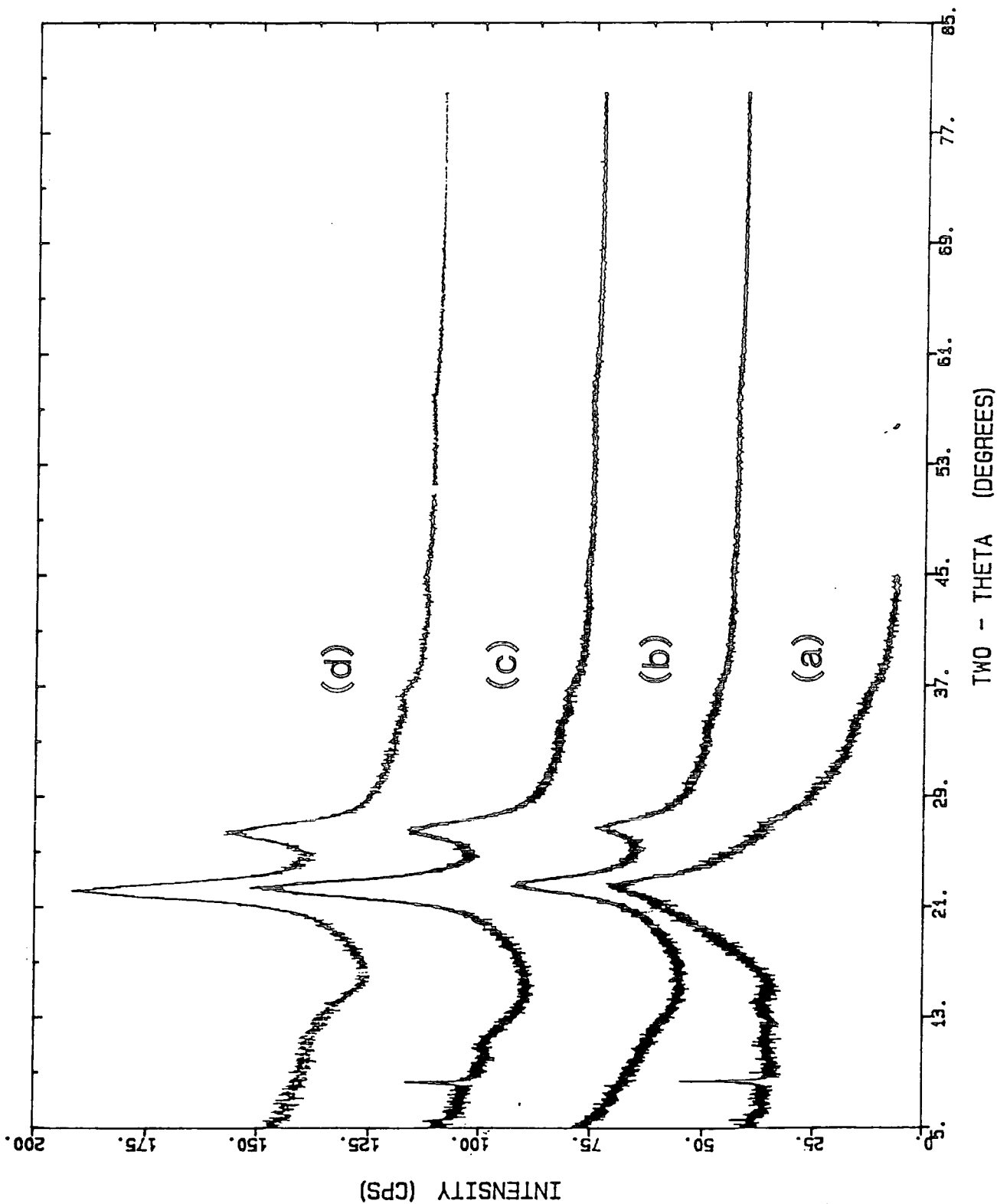


**Figure 6.8** Diffractometer scans for stretched EB films: (a) no extension; (b) 100% extension; (c) 180% extension; (d) 230% extension.

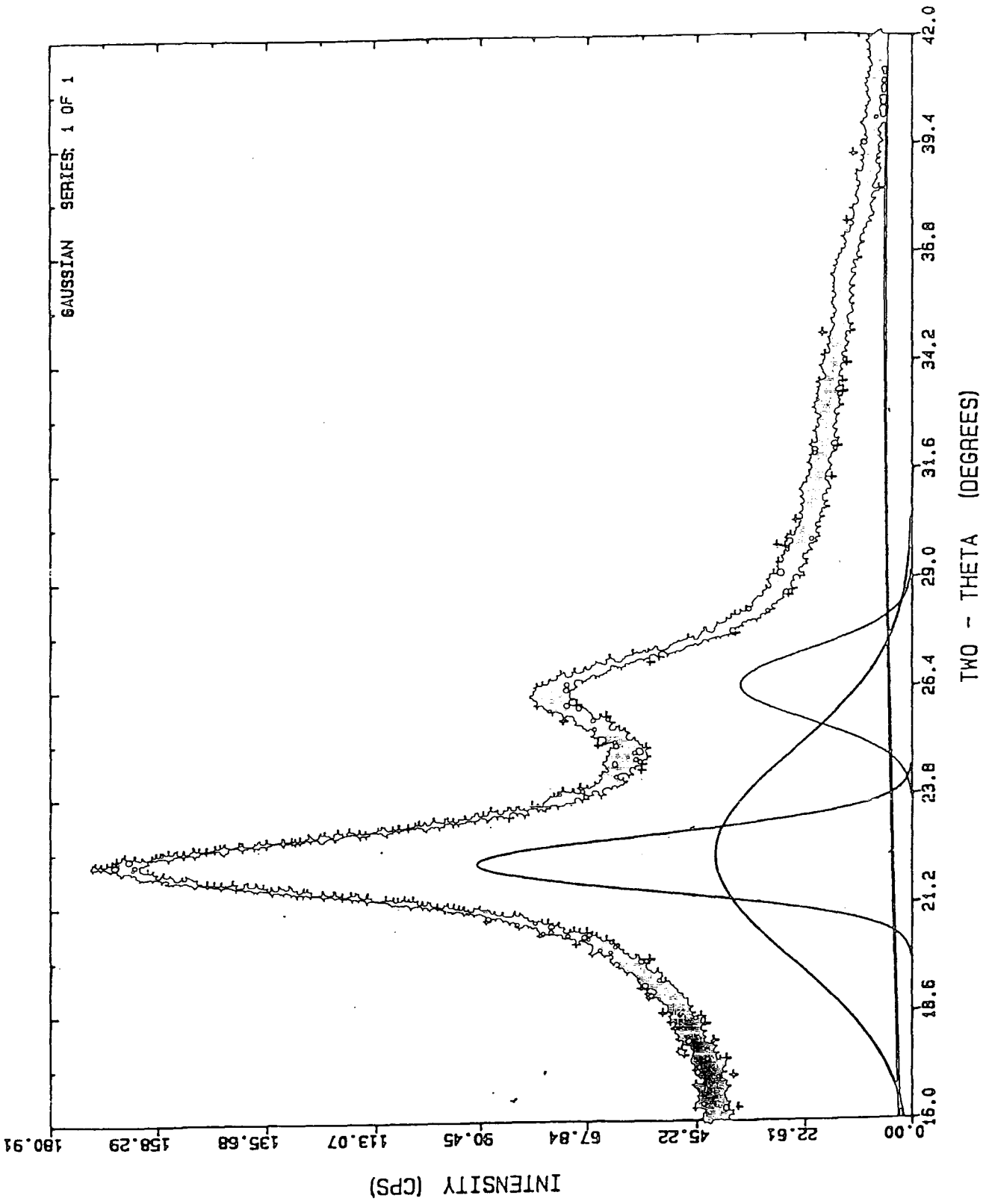
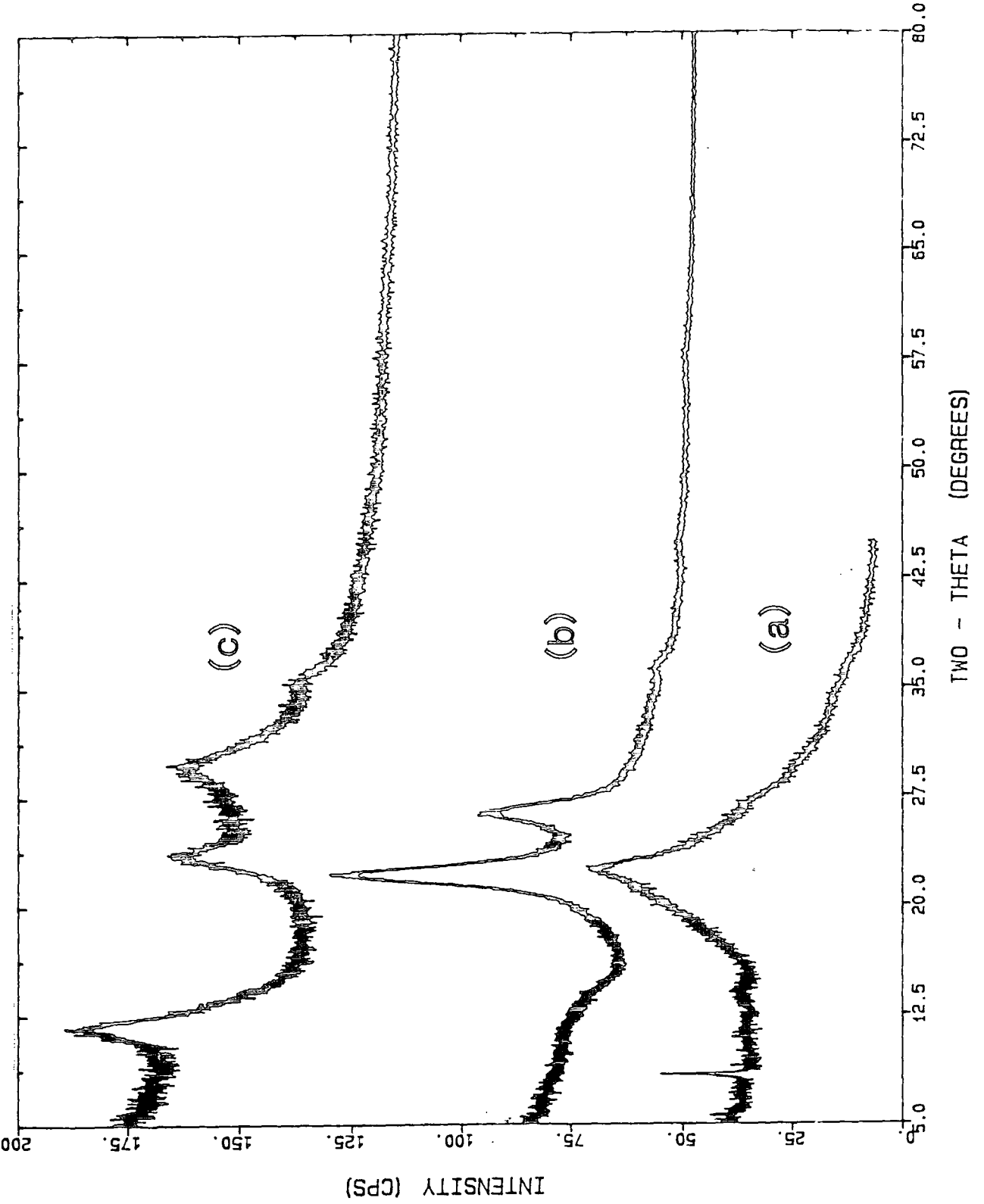


Figure 6.9 Profile fit for a 230% elongated EB film. The amorphous scattering consists of a broad Lorentzian curve together with a baseline level.



**Figure 6.10** The shift in peak positions for doped ES films: (a) unstretched EB film; (b) 230% extended EB film; (c) 240% extended ES film.

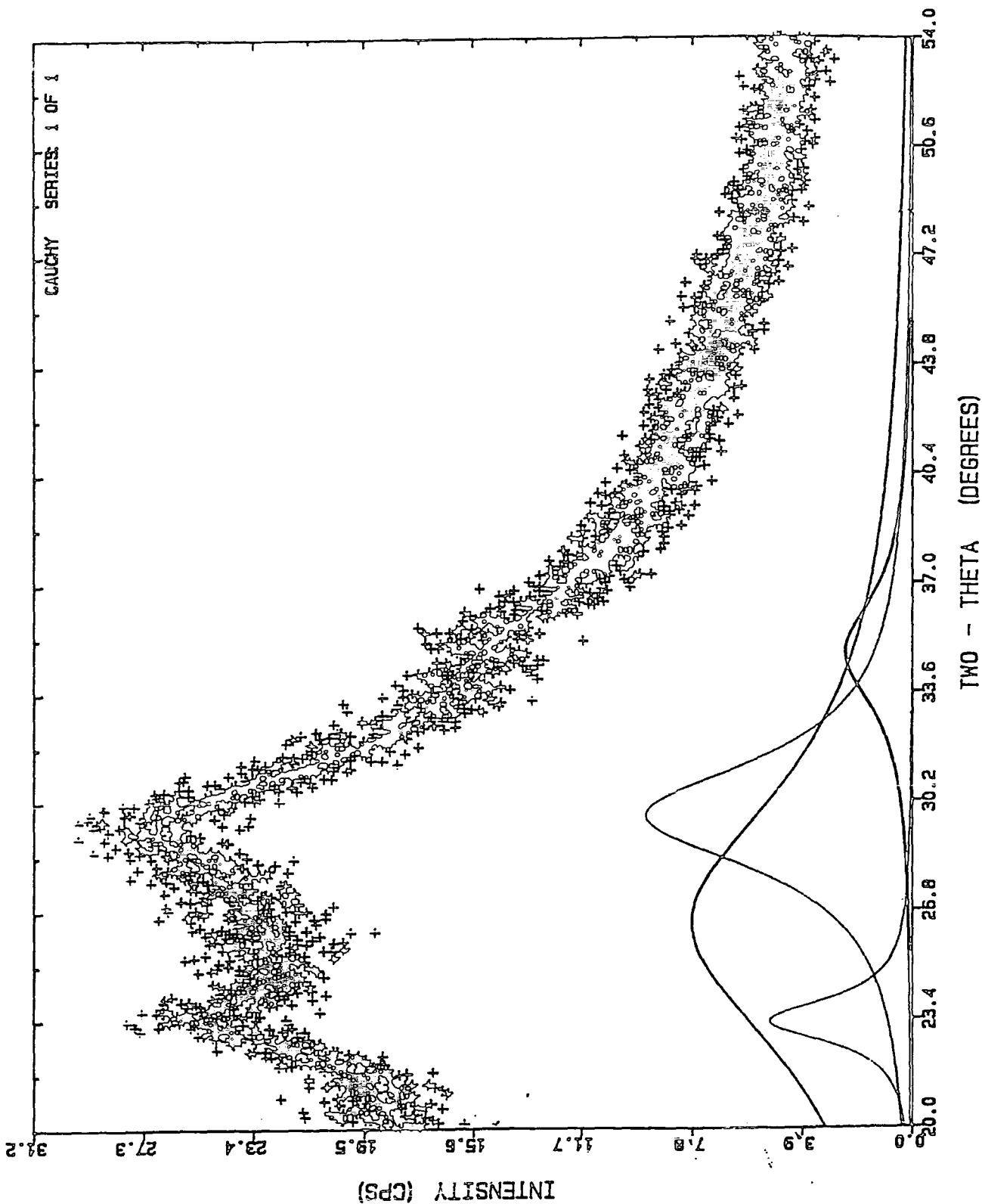


Figure 6.11 Profile fit for a 115% elongated ES film. The Bragg peak at  $8.9\text{\AA}$  ( $2\theta = 11.5^\circ$ ) is not shown.

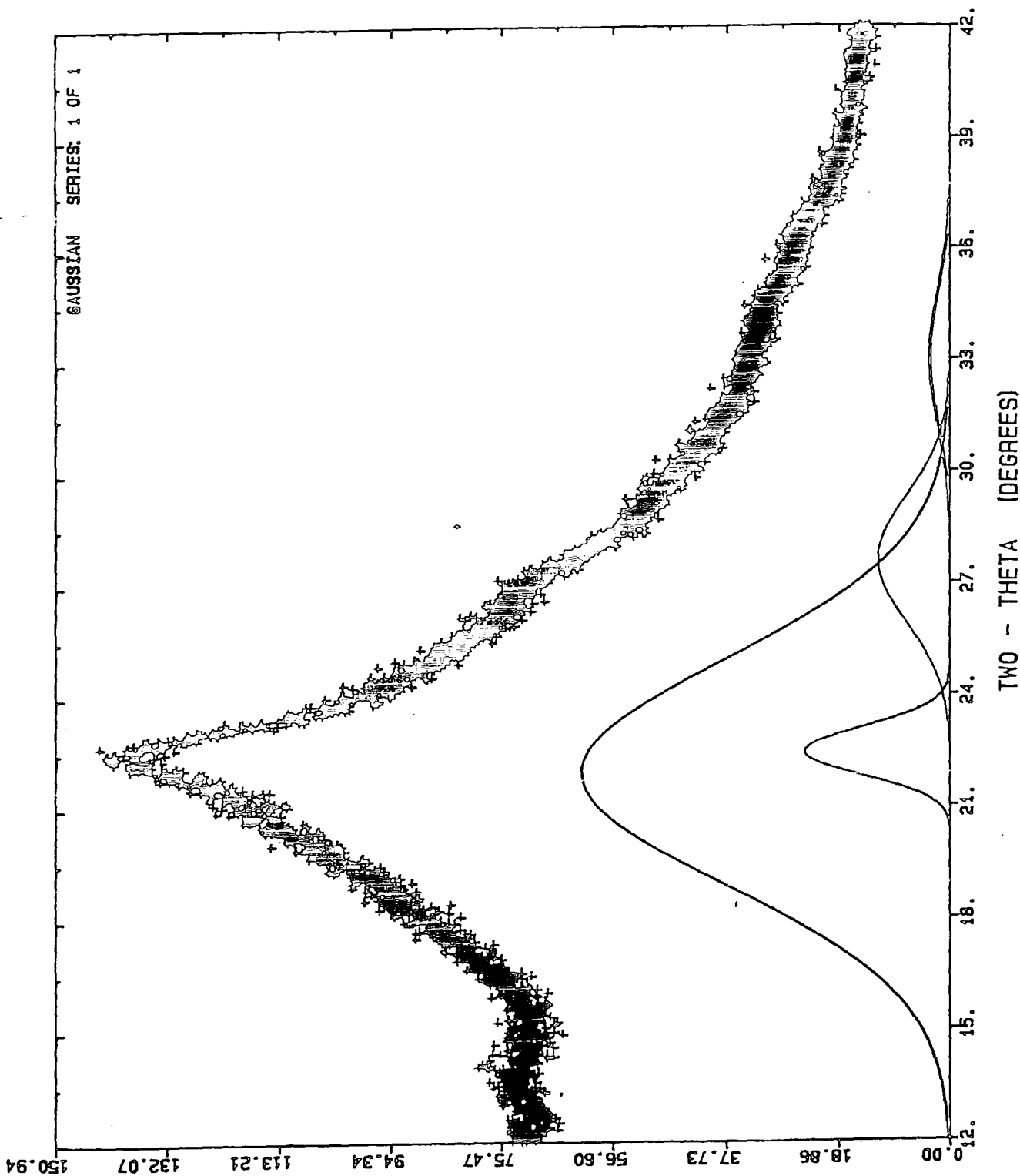
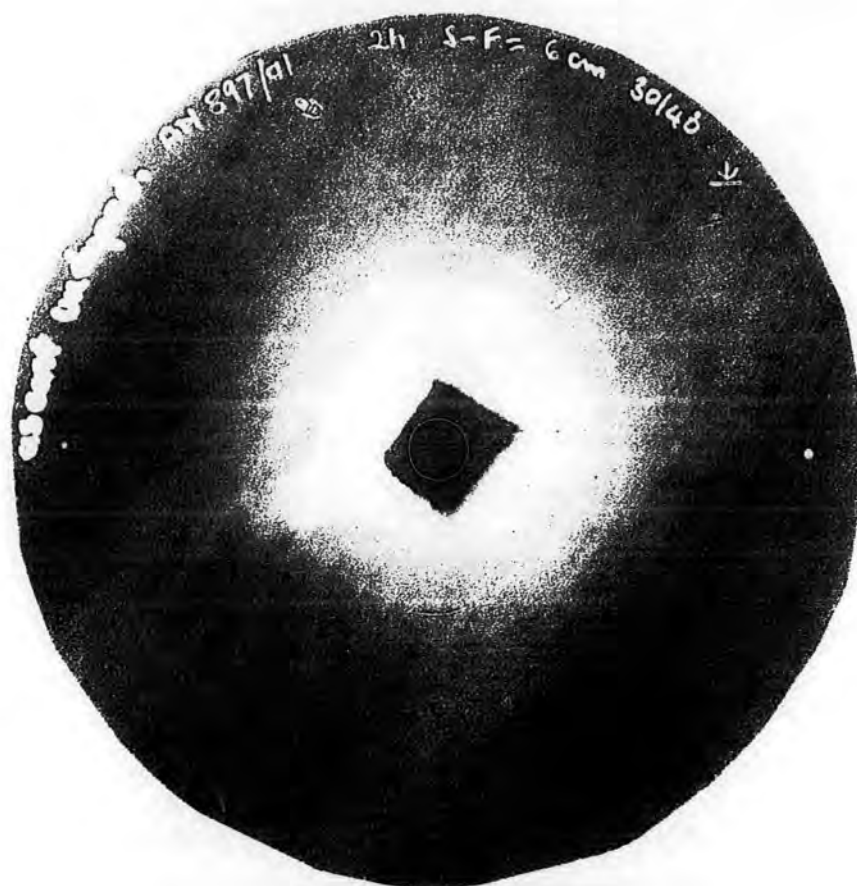


Figure 6.12

Profile fit for an unstretched EB film, showing the weak structural features under the broad amorphous curve.





**Figure 6.13** Flat-film X-ray photograph of an unstretched EB film. The figure shows two circular diffraction signals, in accordance with the unoriented nature of the specimen.



**Figure 6.14** Flat-film X-ray photograph of an 230% elongated EB film with the stretch direction vertical. The two circular diffraction signals seen in Figure 6.13 are now observed as arcs along the equator.



**Figure 6.15** Flat-film X-ray photograph of an 170% elongated **ES** polyaniline film with the stretch direction **vertical**. Again, arced diffraction signals are clearly visible along the equator.

## 6.6 Discussion of Results

The diffractometer scans of Figure 6.8 for EB films clearly shows increasingly crystalline structure evolving with elongation. For highly stretched films three Bragg peaks are discernible. A typical profile fit is shown in Figure 6.9 for the two major features of the 230% elongated film. Using this data information on the positions and relative intensities of individual peaks can be derived and is tabulated in Table 6.1.

Peak type	Relative strength <sup>a</sup>	2 $\theta$ / degrees	d spacing / Å	(hkl) indexation <sup>b</sup>
amorphous	m	22.0	4.7	-
crystalline	vs	22.5	4.6	(110)
crystalline	s	26.5	3.9	(200)
crystalline	vw	35.5	2.9	(020)

<sup>a</sup>Relative strengths: vs very strong; s strong; vw very weak

<sup>b</sup>Indexation according to an orthorhombic unit cell structure derived from neutron diffraction

Table 6.1 Peak types, relative intensities and positions for stretched EB films.

As mentioned previously, since only three Bragg peaks are seen it is not feasible to determine a unit cell structure. The crystalline peaks are, however, to a first approximation compatible with an orthorhombic unit cell with 2-D dimensions  $a = 5.7\text{Å}$ ,  $b = 7.8\text{Å}$ . This and other possible structures have been determined from neutron diffraction analysis and are all reported in the next chapter.

Figure 6.10 demonstrates the change in crystal structure which occurs on doping in 1 M HCl (unstretched base film also shown for comparison). A change in d spacings is evident and also a further Bragg peak at a higher d value. A profile fit for part of a 115% stretched doped film is depicted in Figure 6.11. The information for these protonated structural features is

similarly displayed in Table 6.2. Bragg peaks for ES samples are significantly less intense than their undoped counterparts and also masked by high background scattering. This reduction in structural detail in turn does not allow for an accurate determination of a crystal structure, even using neutron diffraction. A reasonable fit using the neutron technique, however, was found to be a pseudo-orthorhombic structure, unit cell dimensions  $a = 7.9\text{\AA}$ ,  $b = 7.1\text{\AA}$ . But even so the (hkl) indexations are still somewhat uncertain.

Peak type	Relative Strength <sup>a</sup>	$2\theta$ / degrees	d spacing / $\text{\AA}$	(hkl) indexation <sup>a</sup>
crystalline	s	11.5	8.9	(010)
crystalline	w	23.5	4.4	(012)?
amorphous	m	26.0	4.0	-
crystalline	m	29.5	3.5	(200)
crystalline	vw	34.5	3.0	?

<sup>a</sup>Relative strengths: s strong; m medium; w weak; vw very weak

<sup>b</sup>Indexation according to a pseudo-orthorhombic unit cell described in text; question marks indicate uncertain or unknown indexations

**Table 6.2** Peak types, relative intensities and positions for stretched ES films.

Using the experimental diffraction data it is possible to define the percentage crystallinity in the samples,  $X_c$ , by comparing the areas under the crystalline and amorphous fitted curves. This procedure has been described in the data analysis and processing section. It must be realised, though, that the values are only relative not absolute. The results are shown in Figure 6.16. It can be shown that base films show a smooth increase in  $X_c$  with increasing elongation, with an unstretched film containing around 10% crystallinity. It is interesting to note that for a film of 230% elongation  $X_c$  has a value of 0.55. This is almost identical to the value of molecular orientation obtained for the same film through IR orientation

measurements. Therefore, it can be concluded that the distinction between molecular orientation and crystallinity is perhaps rather artificial for this material.

A similar increase in crystallinity has also been reported, but only qualitatively, by MacDiarmid *et al*<sup>15</sup>. These workers also suggest<sup>16</sup>, on the basis of several assumptions, that unstretched film have an  $X_c$  of no more than 4%. This disparity may well be explained by the simplified approach to true line shapes used here and also inaccuracies in the fit for an unstretched film (due to the very small degree of structure), see Figure 6.12. Another recent report<sup>17</sup> concludes that the the order between crystalline and amorphous regions are similar on a local scale and only differ by the spatial range of structural correlations. The inference is that it is not surprising that virtually amorphous films can be stretched producing structured regions since the short range order between the two phases is so similar. More simply, this is a reiteration of the connection between the concepts of crystallinity and molecular order introduced previously.

Unlike base films, conductive ES samples do not exhibit a linear increase in  $X_c$  with stretch ratio. The behaviour is rather variable but may be generalised as an approximately constant crystallinity value independent of sample elongation. A possible cause for the large scatter of values is the exclusion of the crystalline peak at 8.9Å in the calculations - an acceptable curve fit could not be produced due to the high sloping background. The general trend cannot readily be explained, but it is clear that doping, through inclusion of counter-ions, induces a distinct change on a microscopic level. It must also be pointed out that an anomaly occurs for an unstretched, doped film. Here, the diffraction pattern is observed to be virtually unstructured and so  $X_c$  must be close to 0%.

Another calculation performed on the diffraction data was the estimation of a coherence length or crystalline block size from the width (FWHM) of the Bragg peaks. The method, described in the experimental section, accounted for instrumental broadening through the use of a standard, hexamethylene tetraamine, and further assumed that no lattice striations were present. Thus the peak widths could be ascribed only to finite crystalline size. It was

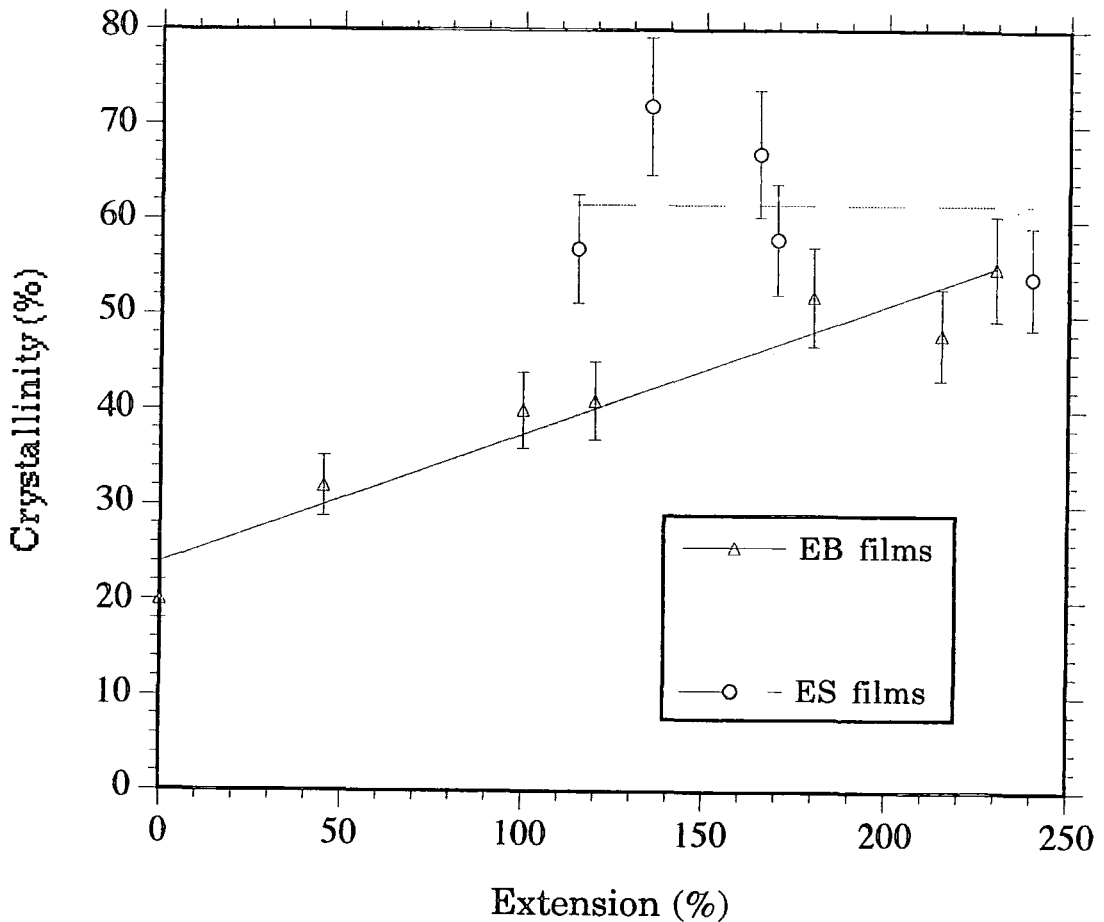


**Figure 6.16** Variation in crystallinity,  $X_c$ , with extension for EB and ES films. Note that an anomaly occurs for an unstretched ES film where  $X_c \sim 0\%$ ; this data point is not shown on the graph.

found these fitted widths did not vary with stretch ratio (within experimental error). Values were calculated to be 60-70Å for the two main (110) and (200) peaks in undoped samples. If it is assumed that the unit cell c-axis is aligned with the stretch direction, which will be discussed later on in this section, this measurement defines the extent of crystallinity perpendicular to the stretch direction. ES films exhibit a slightly smaller block size, 50-60Å, measured from the 4.4 and 3.5Å peaks. It is not clear if

these values also pertain to a perpendicular direction due to the uncertainty in the (hkl) indexation.

The coherence lengths for the (110) and (200) base peaks can be compared with those for low density polyethylene (LDPE), which also possesses an orthorhombic crystal structure. For this material typical values for  $L^{18}$  are 95Å along the [110] direction and 150Å along the [200] direction. Thus the crystalline domain size is much larger in LDPE and the lack of order in polyaniline may again be traced to the complexity of its stereochemistry. Clearly only very small segments of the polyaniline chain have the right conformations to allow crystallisation to become energetically favourable.

Analysis of crystallite orientation has also been studied, using flat-film X-ray photographs. Figure 6.13 shows that for an as-cast polyaniline film. Two distinct signals are clearly visible, occurring as rings due to the unoriented nature of the specimen. From the diffraction geometry and the previous data it is possible to intuitively assign the outer ring to a d spacing of 3.9Å and the inner one a value of 4.6Å. These values were also checked by substituting the appropriate parameters into (8). A more interesting case, though, can be seen in the photograph for a 230% stretched film, Figure 6.14. Here, although the rings are still seen, the signals are clearly arced along the equator. Since these diffraction features have (110) and (200) indexations for an orthorhombic EB unit cell, it can be concluded that the a and b axes of the cell are preferentially oriented perpendicular to the stretch direction. Correspondingly, the c axis must be aligned parallel to this direction. It is also clear, though, that as no signals are observed along the meridian, there is no distinct periodicity along the stretch axis. Furthermore, the absence of discrete layer-line reflections indicates there is considerable axial translational disorder and the lack of higher-order equatorial signals suggest the lateral order is only small. This must be contrasted with PPV and PA films<sup>19</sup> which despite being elongated to a higher extent also exhibit a considerable degree of order.

The photograph of a 170% stretched, doped film, Figure 6.15, also exhibits a number of equatorial, arced reflections. The 3.5Å reflection, whose (hkl) indexation of (200) was assigned with the most degree of certainty, shows



that the a axis is aligned in a perpendicular manner. Similarly, if the 8.9Å arc is believed to be the (010) reflection, the b axis must also be aligned in this direction in analogy with base specimens. This tends to indicate that the speculated assignment of (012) to the 4.4Å signal in Table 6.2 is erroneous, since this would mean that the c axis is also perpendicularly aligned, which is not possible. Again, though, there is no evidence of any longitudinal or axial order in this doped specimen.

Microdensitometer tracings for both Figures 6.14 and 6.15 have enabled the degree of crystallite orientation to be assessed. At this stage it is important to bear in mind the limitations in this analysis as outlined in Section 6.4.3. For the undoped, 230% stretched sample the scan along the 3.9Å (200) arc revealed an intensity distribution with a FWHM of approximately 18°. Substituting this value into (7) yields a crystallite Hermans orientation function of 0.86. For the doped, 170% stretched film the 3.5Å (200) reflection gave a FWHM of around 9°, corresponding to an orientation function of 0.96. Thus it appears that protonation induces a further degree of crystallite orientation along the stretch direction. This effect is not as yet understood, but again it is possible to cite the introduction of counter-ions into the unit cell as being directly responsible.

The Hermans value of 0.86 for the base film can be compared with that of 0.53 derived from IR orientation measurements. This is not a surprising result, however, since the latter value is an average of both amorphous and crystalline phases, whereas the former only describes crystalline orientation. Indeed, from the previously mentioned connection between molecular orientation and crystallinity, this behaviour might have been expected. The preferential alignment of chain along the stretch direction should only allow crystallites to nucleate in an oriented fashion. It is also clear from these photographs that crystalline order does not extend over large distances, particularly along the stretch direction. This conclusion is in agreement with the small experimentally determined coherence lengths and also with recent small-angle X-ray scattering data<sup>20</sup>.

## 6.7 Summary

X-ray diffraction studies have probed the crystalline fraction of polyaniline films. Due to the nature of the data (only 2-3 discernable Bragg peaks are seen) it has not been possible to determine possible unit cell structures. However, this fundamental concern has been addressed using neutron diffraction, reported in the next chapter. The results have indicated, though, a linear increase in relative crystallinity,  $X_c$ , with elongation for EB films. An unstretched film is estimated to have an  $X_c$  of around 0.10 while a 230% stretched film exhibits an  $X_c$  of around 0.55. This latter value is very similar to the orientation parameter derived from IR measurements and indicates that crystallinity and molecular orientation are closely related. For doped ES specimens a change in  $d$  spacings is observed, but there is no distinct pattern between crystallinity and elongation for these samples.

The widths of the Bragg peaks, for all samples, indicate a very small crystalline block size of around 50-60Å. This result may be interpreted by acknowledging the complex stereochemical structure of the chain. Only very short segments have the correct geometry to make crystallisation energetically favourable. Furthermore, the Bragg widths do not vary with stretch ratio, indicating that the increase in crystallinity is due to nucleation of new crystallites rather than growth of pre-existing ones.

Orientational analysis has shown a slight lateral order in stretched EB films. The results are consistent with the  $a$  and  $b$  axes of an assumed orthorhombic unit cell being preferentially aligned perpendicular to the stretch direction, so that the  $c$  axis must be oriented in a parallel manner. However, in other directions and particularly along the stretch axis, very little periodicity is evident. The Hermans orientation function for a 230% extended sample was found to be 0.86, significantly larger than the IR derived value of 0.53. This is generally expected, though, since the X-ray value describes only crystalline orientation whereas the IR technique defines an average i.e. crystalline and amorphous case. The interpretation for a 170% doped specimen is very similar to that for base films. However, an even higher Hermans parameter of 0.96 was measured indicating that protonation induces a further degree of crystallite orientation.

## References

- 1 P.J. Brown and J.B. Forsyth, *The Crystal Structure of Solids*, Edward Arnold Publishers Ltd, 1973.
- 2 C. Kittel, *Introduction to Solid State Physics*, 5th edition, John Wiley and Sons, 1976.
- 3 O. Gerngross, K. Hermann and W. Abitz, *Z: Phys. Chem.*, **B10**, (1930), 371.
- 4 H.A. Stuart, *Ann. N. Y. Acad. Sci.*, **83**, (1959), 1.
- 5 I.M. Ward, *Mechanical properties of Solid Polymers*, Wiley-Interscience, 1971, Chapter 1.
- 6 L.E. Alexander, *X-ray Diffraction Methods in Polymer Science*, Wiley-Interscience, 1969.
- 7 R.S. Stein and G.L. Wilkes in *Structure and Properties of Oriented Polymers*, ed. B.E. Read, Applied Science Publishers, 1975.
- 8 J.J Hermans, P.H. Hermans, D. Vermaas and A. Weidinger, *Rec. Trav. Chim. Pays-Bas*, **65**, (1946), 427.
- 9 H.P Klug and L.E. Alexander, *X-ray Diffraction Procedures for Polycrystalline and Amorphous Materials*, Second Edition, Wiley-Interscience, 1974.
- 10 E.D.T. Atkins in *Comprehensive Polymer Science*, Volume 2, ed. G Allen, Pergamon Press, 1989.
- 11 M.E. Jozefowicz, R. Laversanne, H.H.S. Javadi, A.J. Epstein, J.P. Pouget, X. Tang, and A. G. MacDiarmid, *Phys. Rev. B*, **39**, (1989), 12958.
- 12 J.P. Pouget, M.E. Jozefowicz, A.J. Epstein, X. Tang and A.G. MacDiarmid, *Macromolecules*, **24**, (1991), 779.
- 13 L.P. Smith, *Phys. Rev.*, **46**, (1934), 343; A.R. Stokes, *Proc. Phys. Soc. (London)*, **A61**, (1948), 382.
- 14 H.C. Burger and P.H. van Cittert, *Z. Phys.*, **79**, (1932), 722; S. Ergun, *J. Appl. Crystallogr.*, **1**, (1968) 19.
- 15 E. M. Scherr, A. G. MacDiarmid, S. K. Manohar, J. G. Masters, Y. Sun, X. Tang, M. A. Druy, P. J. Glatkowski, V. B. Cajipe, J. E. Fischer, K. R. Kromack, M. E. Jozefowicz, J. M. Ginder, R. P. McCall and A. J. Epstein, *Synth. Met.*, **41-43**, (1991), 735.

- 16 J.E. Fischer, X. Tang, E.M. Scherr, V.B. Cajipe and A.G. MacDiarmid, *Synth. Met.*, 41-43, (1991), 661.
- 17 M. Laridjani, J.P. Pouget, E. M. Scherr, A.G. MacDiarmid, M.E. Jozefowicz and A.J. Epstein, *Macromolecules*, 25, (1992), 4106.
- 18 J. Jutson, BICC Cables Ltd, personal communication, 1993.
- 19 D.D.C. Bradley, R.H. Friend, T. Hartmann, E.A. Marseglia, M.M. Sokolowski and P.D. Townsend, *Synth. Met.*, 17, (1987), 473.
- 20 B.K. Annis, J.S. Lin, E.M. Scherr and A.G. MacDiarmid, *Macromolecules*, 25, (1992), 429.

## Chapter 7

### Neutron Diffraction Studies

This chapter reports on the results of neutron diffraction studies carried out at the ISIS facility, Rutherford-Appleton Laboratories, U.K.

#### 7.1 Introduction

In the previous chapter X-ray diffraction studies of polyaniline films were presented. While a great deal of valuable information was derived from these studies, a very important aspect could not be addressed, namely unit cell structures of the crystalline fractions. This inability to probe the crystalline structure arose not only because of the nature of the ordered phase (crystallites are extremely small), but also because of certain limitations imposed by the experimental technique. However, these constraints, discussed more in the following section, can be overcome by the use of a complimentary technique, neutron diffraction. Using this latter method has enabled this most crucial structural aspect of polyaniline to be investigated.

#### 7.2 Aspects of Neutron Diffraction

The determination of crystal structure by neutron diffraction utilises an identical equation to that which applies to X-ray diffraction. This is the structure factor equation, present again below, upon which the intensity of a Bragg (hkl) reflection critically depends.

$$F(hkl) = \sum_i^N f_i \exp [2\pi i (hx_i + ky_i + lz_i)]$$

where  $x$ ,  $y$  and  $z$  represent the fractional coordinates of the  $i$ th atom in the unit cell, containing  $N$  atoms, and  $f_i$  is the atomic scattering factor or structure factor.

However, there are a number of very important differences which allow neutron diffraction to supplement X-ray analysis. In the case of X-ray scattering the fundamental scattering body is the electron. Therefore the scattered wave from an atom, quantified by the X-ray atomic scattering factor,  $f_x$ , will consist of the contributions from all the extra-nuclear electrons, which are equal in number to  $Z$ , the atomic number. Thus it is clear that X-ray scattering will be strongest for heavy atoms, so that for polymers, which typically constitute of the lighter elements, the scattering is weak. This is particularly apparent for the hydrogen atom. Furthermore, the electronic cloud of an atom extends over a region of space comparable to the wavelength of the incident X-rays (typically  $1\text{\AA}$ ). So as the Bragg angle,  $\theta$  increases the amplitude of scattering, which is initially proportional to  $Z$ , starts to decrease rapidly. For a given atom the rate of fall of  $f_x$  depends on  $(\sin\theta)/\lambda$ , as shown in Figure 7.1 for potassium, using data given in the International Tables for X-ray Crystallography. The result is that X-ray scattering is diminished at high scattering angles.

The neutron scattering factor,  $f_n$ , on the other hand shows no regular or rapid increase with atomic number and also does not vary with  $\theta$ . This isotropic nature of scattering results from the fact that neutrons are scattered by the nucleus of the atom<sup>1</sup>. Nuclei, unlike the surrounding electronic cloud, are small in comparison to the wavelength of neutrons (also typically  $1\text{\AA}$ ). Consequently, in Figure 7.1 the neutron scattering factor,  $f_n$ , is a straight line. The interaction of a neutron beam with a specific nucleus is characterised by the total scattering cross-section,  $\sigma$ . This parameter is the sum of the coherent scattering cross-section i.e. that which is coherent with other nuclei and can thus produce interference and the incoherent scattering cross-section. These two terms are affected if the spin of the nucleus is non-zero; a scattering nucleus with a spin  $I$  may combine with a neutron, of spin  $\frac{1}{2}$ , to form one of two alternative compound nuclei, having spins of  $I + \frac{1}{2}$  and  $I - \frac{1}{2}$  respectively. Furthermore, a specific element may naturally occur as a mixture of several different isotopes, each

with a defined abundance. Each isotope will have its own characteristic value of  $f_n$ , as well as having different spin values.

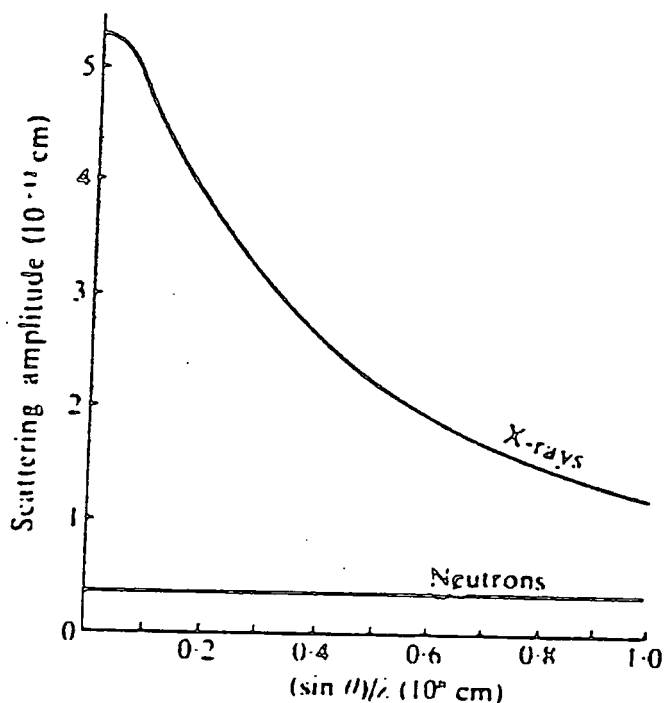


Figure 7.1 The variation of X-ray and neutron scattering factors with  $(\sin \theta)/\lambda$  for a potassium atom (from Bacon<sup>1</sup>).

The neutron scattering factor,  $f_n$ , is also sometimes called the coherent scattering amplitude and denoted by  $b$ . This parameter is the mean scattering length of the element in question, averaged over the various possible isotopes (which constitute the element) and also where necessary the different spin combination of a particular isotope. Table 7.1 compares  $f_x$  and  $b$  for some typical elements and isotopes found in polymer structures.

Element	Atomic Number	Specific Nucleus	Nuclear Spin	b (10 <sup>-12</sup> cm)	f <sub>x</sub> <sup>a</sup> (10 <sup>-12</sup> cm)
H	1	H	1/2	-0.374	0.02
		H	1	0.667	0.02
C	6	C	0	0.665	0.48
		C	1/2	0.60	0.48
N	7	N	1	0.94	0.53
		N	1/2	0.65	0.53
O	8	O	0	0.580	0.62
		O	5/2	0.578	0.62
		O	0	0.600	0.62
S	16	S	0	0.28	1.9
Cl	17	Cl	3/2	1.18	2.0
		Cl	3/2	0.26	2.0

<sup>a</sup> f<sub>x</sub> measured at  $(\sin \theta) / \lambda = 0.5 \text{ \AA}^{-1}$

Table 7.1 A comparison of X-ray and neutron scattering data for various elements and isotopes (taken from Bacon<sup>1</sup>).

A negative sign means that neutron scattering is accompanied by a reversal of phase, so that such a nucleus appears as a negative peak in a neutron diffraction Fourier map, as opposed to positive peaks for the normal atoms.

It is clear from Table 7.1 just how weakly hydrogen atoms, because of their low electron density, scatter X-rays. It is possible to locate such atoms if the X-ray scattering data is good, but the standard deviation of the positions is always high. With neutron diffraction hydrogen atoms can be found with almost the same precision as carbon or oxygen atoms. Even greater accuracy can be obtained if the hydrogens are substituted by deuterium atoms, not only because of their increased scattering length but also because hydrogen atoms give rise to a significant amount of incoherent scattering. Using deuterium this latter problem is eliminated.



The advantages of neutron diffraction, though, are somewhat counter-balanced by specific disadvantages; the experimental technique is much more difficult than X-ray diffraction and hence much more expensive. The flux of a typical beam of monochromatic thermal neutrons is much less than that of an X-ray beam and neutrons are more difficult to record or count (there is no suitable photographic method for recording neutrons). Thus neutron structural analysis can only be carried out at a high power reactor, of which there are relatively few world-wide. Because of this scarcity 'beam time' is much sought after and allocated only if the experiments are deemed suitable and important. At first this resulted in neutron analysis being seldomly used by polymer scientists, particularly because high quality, often single crystal materials were a prerequisite. Now, however, with constant improvement to the technique, polymeric materials are being regularly studied by neutron analysis. In this chapter neutron diffraction has been used in structural determination of polyaniline, in what is believed to be the first such experiment of its kind on the polymer. The results reveal conclusive evidence that this technique provides a great improvement on standard X-ray diffraction data and hence allows a much more detailed analysis of polyaniline crystal structure.

### 7.3 Experimental Section

These studies were carried out using the ISIS facility at the RAL in conjunction with Dr N.R. Bernhoeft, formerly of the Physics Department, Durham University and with the help of Dr A.C. Hannon, instrument scientist on LAD.

#### 7.3.1 The LAD Diffractometer

The LAD<sup>2</sup> instrument (the Liquids and Amorphous Diffractometer) is shown in Figure 7.2. This facility is optimised for the study of amorphous solids and liquids so that structure factors may be measured over a wide range of momentum transfer. However, it is also suitable for structural determination in semi-crystalline polymers. The instrument comprises

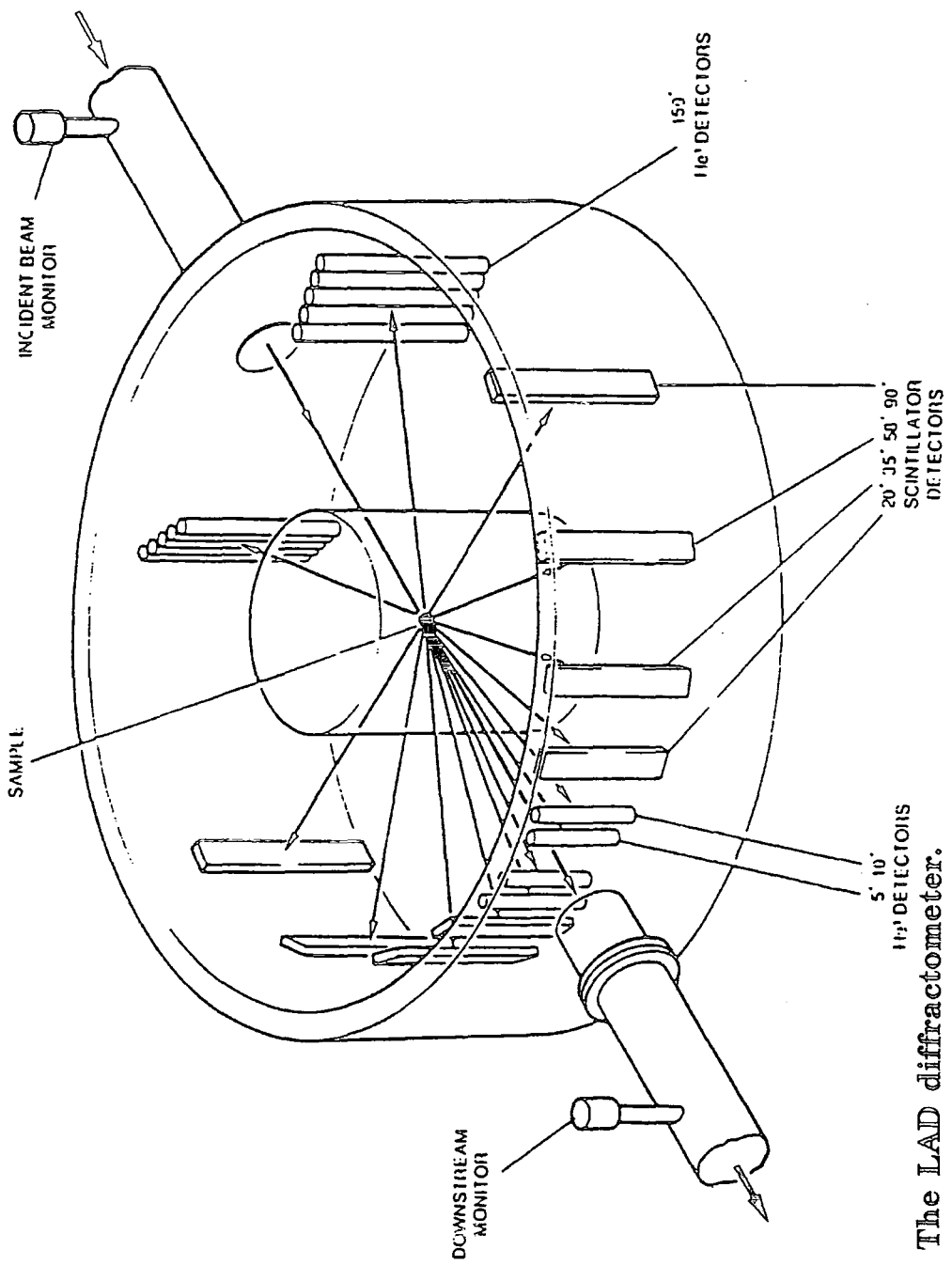


Figure 7.2 The LAD diffractometer.

seven banks of detectors ( $\text{He}^3$  and scintillator) positioned in the horizontal plane at various different scattering angles ranging from  $5^\circ$  to  $150^\circ$ . The detectors at low  $2\theta$  values enable diffraction features up to a d spacing of around  $80\text{\AA}$  to be seen. The backward angle detectors, i.e. those at high  $2\theta$  values only have a small maximum d-spacing (below  $5\text{\AA}$ ), but have high resolution. The incident beam may have a wavelength in the range  $0.25\text{-}6.5\text{\AA}$  and is  $40\text{mm}$  high and  $20\text{mm}$  wide. A  $\text{CH}_4$  moderator at  $100\text{K}$  is used to collimate the beam and the sample is positioned approximately  $10\text{m}$  from the moderator. Data was acquired on a vaxstation 3200 and analysed using the ATLAS<sup>3</sup> - Analysis of Time-of-Flight Diffraction Data from Liquid and Amorphous Samples - data analysis suite.

### 7.3.2 Samples

For the neutron experiments deuterated emeraldine base (d-EB) was prepared, so that the position of hydrogen atoms could be more readily established. This material was synthesised in an analogous procedure to standard polyaniline (see section 3.2), but using aniline- $\text{d}_7$  (99 atom % d, MSD Isotopes) dissolved in  $1\text{M}$   $\text{DCl}$ . Ammonium persulfate was still used as the oxidant and after deprotonating in ammonium deuterioxide the product was washed with quantities of  $\text{D}_2\text{O}$ . The yield of deuterated emeraldine base was 80%. Following the procedure given in 3.3.2 the molecular weight,  $\overline{M}_p$ , of this material was determined as  $7.4 \times 10^4$  which corresponds to around 780  $\text{C}_6\text{D}_{4.5}\text{N}$  repeat units. This value is over twice as large as that determined for normal EB using the same synthesis procedure. The deuterated powder was then used to make free standing films in exactly the same way as outlined in section 3.4.1. In this procedure non-deuterated NMP was used though, since it is not possible to obtain this solvent in deuterated form. Samples were stretched and some subsequently doped in  $1\text{M}$   $\text{DCl}$ , to give the deuterated ES form.

An outcome of the use of non-deuterated NMP is that the polyaniline chains are only partially deuterated. This can be seen in chapter 5 from the IR absorption spectrum of a d-EB film, Figure 5.5. Although there is a peak at  $2239\text{ cm}^{-1}$ , which is associated with a C-D stretch, the corresponding C-H

stretch at around  $3040\text{ cm}^{-1}$  is also observable. If it is assumed that the powder material was fully deuterated, then it is possible that some degree of proton exchange may have occurred between the NMP solvent and the polymer C-H groups. In an effort to prove such a theory a KBr powder spectrum was recorded. Unfortunately, the quality of spectra from a powder pellet is not good and this, combined with a high sloping background above  $2000\text{ cm}^{-1}$ , did not allow the extent of deuteration in the powder to be established. It is also clear from Figure 5.5 that the amine units remain undeuterated since the N-H peaks above  $3000\text{ cm}^{-1}$  still occur with no evidence of corresponding N-D bands. The proposed exchange mechanism may also be responsible for this effect. In any case, the fact that only certain hydrogen positions have been isotopically substituted in d-EB films must be recognised and allowed for in the structural analysis.

These samples were mounted in the diffractometer using a picture frame type holder inclined at  $90^\circ$  to the incident beam, as illustrated in Figure 7.3. The holder was made of aluminium, a metal which scatters neutrons only weakly. In order to observe any diffraction signals at all, it was found that a number of films stacked together had to be used. Furthermore, the holder needed to be shielded with cadmium, which has a high absorption cross-section for neutrons, so as to eliminate spurious scattering from the aluminium. For stretched base samples a montage of four films was used with an average elongation of 185%. Doped films had a slightly lower, but still comparable, average extension of 150%. In addition to stretched films a sample of six unstretched, base films was also examined. All the data was collected at room temperature. It was also hoped that further information could be collected below ambient temperature, since the sample compartment is contained in a cryostat. However, the limited timescale of the experiment, incorporating 2 days of beam time, did not allow for this further analysis.

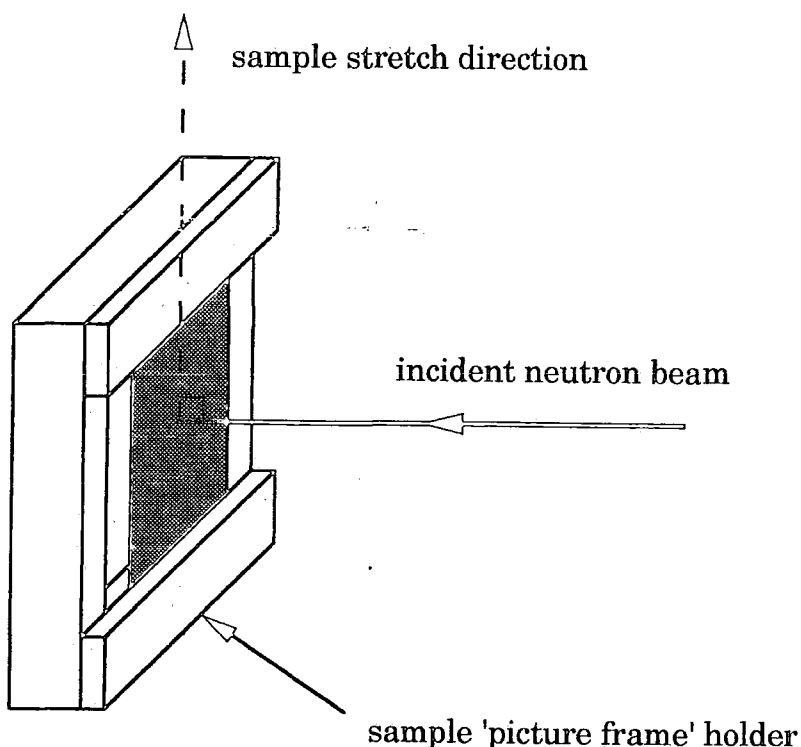


Figure 7.3 A schematic diagram of the aluminium 'picture frame' holder used to mount samples in the diffractometer.

#### 7.4 Results and Analysis

From the outset it is clear that neutron scattering can provide an extra level of diffraction information above the X-ray technique. This is immediately apparent from the form of the neutron data as typically some 10-20 diffraction peaks are observable for stretched samples. To assess possible unit cell structures it is necessary to complete a rigorous structural analysis. Due to the sample and diffractometer arrangement though, the data presented here can only provide scattering information perpendicular to the stretch direction; the crystallites, as deduced from X-ray analysis, are highly aligned along this elongation axis. This 'a-b' plane scattering hence only allows a two dimensional unit cell to be derived. While further beam time has now been allocated to address this imbalance these experiments

are, rather unfortunately, not within the time limit of this thesis. Therefore, this work is only the first stage of the investigation, but the further investigations will be an on-going concern for our group at Durham.

To model the neutron scattering a detailed chain structure for polyaniline, both in the base and salt forms, was first required. However, such geometrical structures have not yet been reported in the literature, no doubt as a consequence of the true stereochemical complexity of the emeraldine oxidation state (as described in section 3.3.1). In order to circumvent this problem it was decided, as a first approximation, to represent an emeraldine chain, as viewed along the chain axis, by a double-headed arrow or dipole. This dipole may be viewed as a 'motif', consisting of two 'effective' atoms, each assigned to an arbitrary scattering length, at each end of the dipole. While such an representation is undoubtedly only a crude approximation, a much more rigorous calculation (involving a 'motif' consisting of a detailed 2D projection of a oligomeric chain structure) gave very similar results, so that such a dipole representation is not so unreasonable. The results, based on this initial dipolar approximation, will now be presented and then the more detailed model discussed.

Using the dipole projection as the basic building block for a unit cell, various cell structures were then examined. The procedure involved the comparison of calculated intensities for these unit derived cells to those observed experimentally. The scattering from an assumed cell was modelled in reciprocal space using a Gaussian distribution function to represent the finite crystallites. A Gaussian profile, as described in section 6.4.2 for XRD analysis, is a commonly-used approximation for representing crystalline line shapes. The Gaussian peaks were all set to an equal width, with the crystallite size, in real space (assuming no variation in lattice dimensions) given by  $2\pi$  upon the Gaussian width. The widths in reciprocal space were also corrected for instrumental broadening by subtracting a derived spectrometer resolution function. The results were then displayed in real space with the relative heights of the Bragg peaks determined by the (hkl) structure factors. This analysis procedure was carried out in collaboration with Dr N.R. Bernhoeft using the facilities at SPSMS, Grenoble, France.

From a qualitative assessment of the diffraction data it is evident that the observed Bragg peaks are not very intense and are also rather broad e.g. the resolved peak at 4.6Å in the stretched emeraldine base scattering has a width (FWHM) of about 5Å. These features reiterate the findings of X-ray analysis, namely that the crystalline percentage is only moderate and the crystallites themselves have very small dimensions. Thus, despite the large number of Bragg reflections observed, there are likely to be a number of assumed structures which yield a good fit to the experimental data.

As a result it was first decided to assess an orthorhombic unit cell, known as EB II, as proposed by Pouget et al<sup>4,5</sup> from X-ray structural analysis. As previously mentioned the X-ray technique gives very little structural detail so that any assumed unit cell will be only a basic assessment. Indeed this EB II cell is primarily based on the unit cells of single crystals of polyphenylene sulfide<sup>6</sup> and polyphenylene oxide<sup>7</sup>, materials which in fact more closely represent the fully reduced leucoemeraldine base form. However, despite this reliance on analogous data, an EB II type cell with dimensions  $a = 7.78 \text{ \AA}$ ,  $b = 5.70 \text{ \AA}$ , as shown in Figure 7.4(a), was found to be quite a good approximation to the neutron diffraction data for stretched EB films. The best fit to the experimental data was achieved with the edge dipole 'motifs' oriented at a setting angle of  $20^\circ$  to the b-axis, with the centre dipole orthogonal to the outer ones. The scattering for this model is compared with that observed experimentally in Figure 7.5. The width of the modelled gaussian scattering in reciprocal space had a standard deviation of  $0.07 \text{ \AA}^{-1}$ , which corresponds to a finite crystalline block size of about  $100 \text{ \AA}$ . This is comparable with the value of around  $60 \text{ \AA}$  determined from X-ray analysis of Bragg peak widths using the Scherrer formula.

The scattering from the montage of six unstretched EB films was found to be virtually unstructured in the range of d-spacings also covered by X-ray diffraction. However, the lower d value range probed by neutron diffraction was found to show some similar features to the stretched film data. Thus the unstretched base scattering was modelled, see Figure 7.6, using the cell structure previously derived but altering the spatial extent (i.e. distribution) of the cells. From such an analysis the standard deviation of the Gaussian widths in reciprocal space was estimated to be  $0.55 \text{ \AA}^{-1}$ , which is equivalent

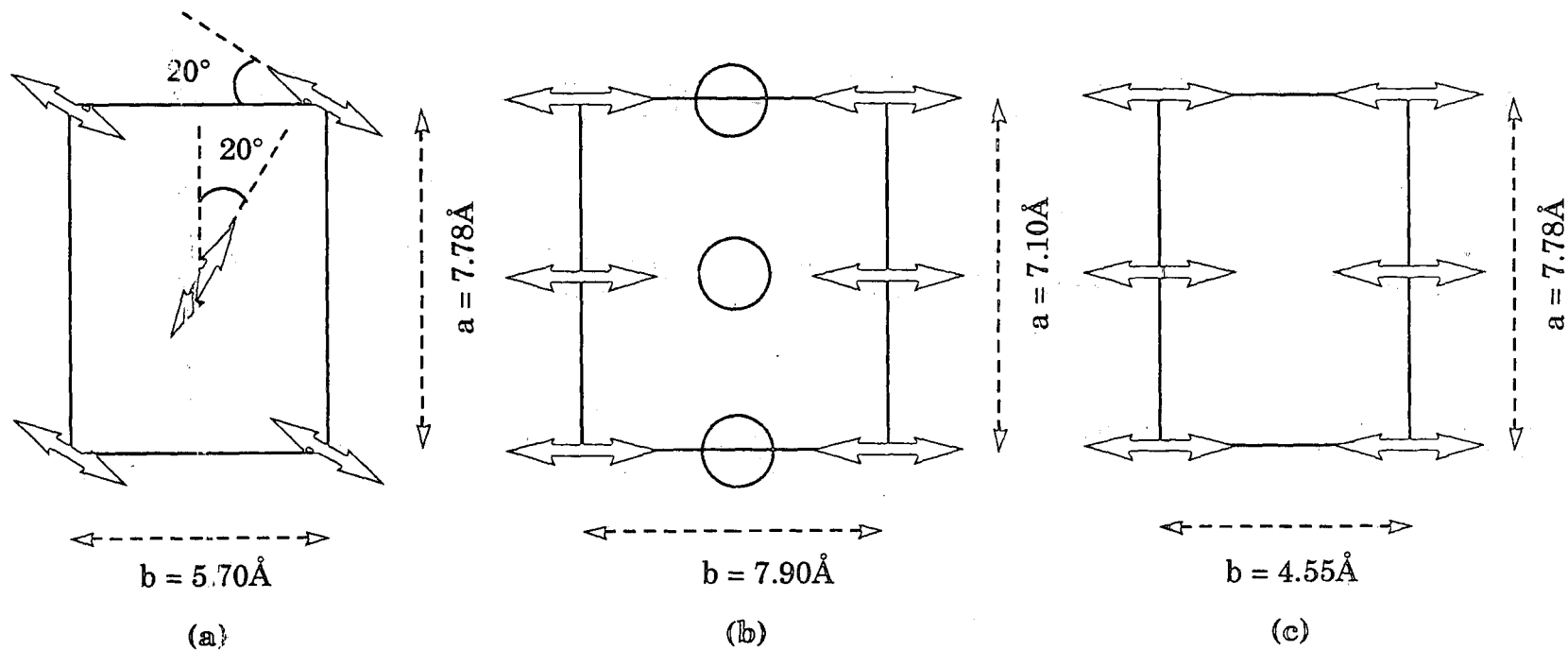


Figure 7.4 2D unit cell structures fitted to the neutron diffraction data for polyaniline films using the dipolar approach, as discussed in the text. The dipoles represent segments of polymers chains as viewed along the chain axis and the circles represent chloride counter-ions. Structure (a) is an EB cell modelled on a structure proposed by Pouget<sup>4,5</sup>; (b) is the proposed unit cell for ES i.e. doped films; (c) is the alternative unit cell investigated for base samples.



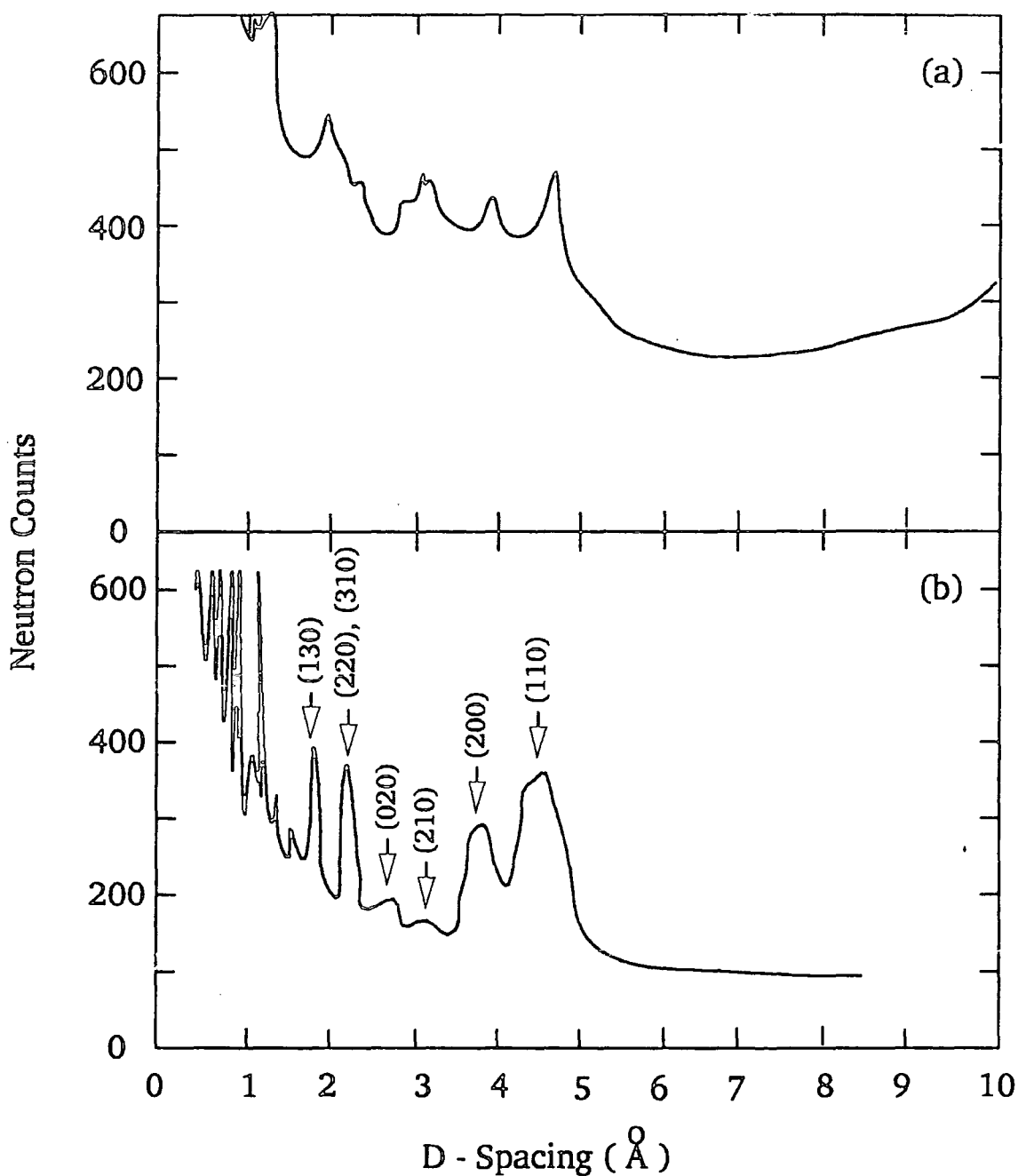
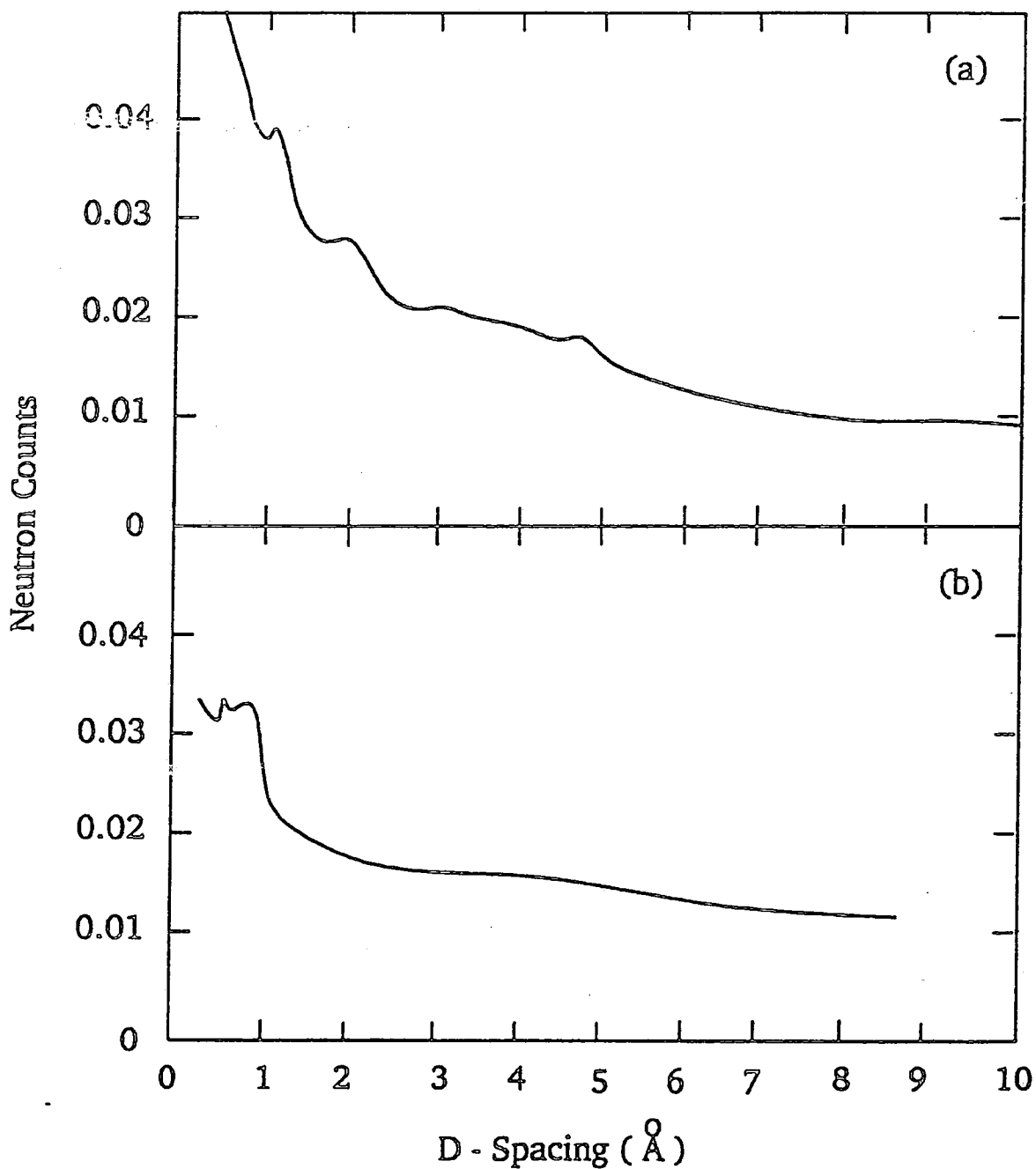


Figure 7.5 Neutron diffraction data for stretched EB films, (a), with an average extension of 185%. The scattering is modelled in (b) with the orthorhombic unit cell of Figure 7.4(a) using the dipolar approach, as discussed in the text.



**Figure 7.6** Experimental neutron diffraction data for unstretched EB films, (a). Despite being virtually unstructured the scattering has been approximated in (b) with the dipolar derived orthorhombic unit cell of Figure 7.4(a) but with a crystalline block size of only 10Å.

to a diffracting object with a spatial extent of only  $10\text{\AA}$ . This is in effect just one unit cell length and reflects the minor degree of order in unstretched samples, as discussed for the X-ray analysis.

The experimental diffraction data from the stretched ES i.e. doped films show much less well resolved structural features than for base samples. To model this scattering, though, the pseudo-orthorhombic unit cell of Figure 7.4(b) has been adopted, and the diffraction data are shown in Figure 7.7. The dopant  $\text{Cl}^-$  ions are assumed to sit midway between the polymer chains with a scattering length of approximately one tenth of the dipoles or chain projections, which are aligned along the b axis. Again the finite unit cell size is modelled in Gaussian fashion in reciprocal space with a standard deviation of  $0.2\text{\AA}^{-1}$ , approximately  $30\text{\AA}$  real space. Given the 2D unit cell dimensions of  $a = 7.1\text{\AA}$ ,  $b = 7.9\text{\AA}$ , this means 3-4 unit cells to each crystallite at an elongation of 150%. This coherence length may be viewed as the width of a conducting particle or 'fibre' since the crystallites are nominally aligned with the stretch direction.

Based on this initial dipole analysis there is quite a difference between the postulated unit cell structures for base and salt samples. This seems to imply that upon doping there must be considerable molecular rearrangement. In light of the fact that such a doping transformation must be energetically favourable, an alternative structure was investigated for base specimens. This unit cell is illustrated in Figure 7.4(c) and is structurally very similar to the ES unit cell with the  $\text{Cl}^-$  ions removed. The simulated diffraction pattern for this cell is given in Figure 7.8 and is also in reasonable agreement with the experimental data. The lattice parameters are  $a = 7.78\text{\AA}$  and  $b = 4.55\text{\AA}$  with the dipoles aligned along the b axis and a structural block of  $100\text{\AA}$  as determined by the widths of the peaks. Such a structure would permit an easy mechanism for inclusion of dopant  $\text{Cl}^-$  ions by simple displacement of the chains.

To assess the validity of this simplified dipole approach, the scattering from the stretched EB films was also modelled using a far more detailed building block 'motif', based on the structure of a four ring oligomer of leucoemeraldine base, derived by Bredas<sup>8</sup>. This model has been described in

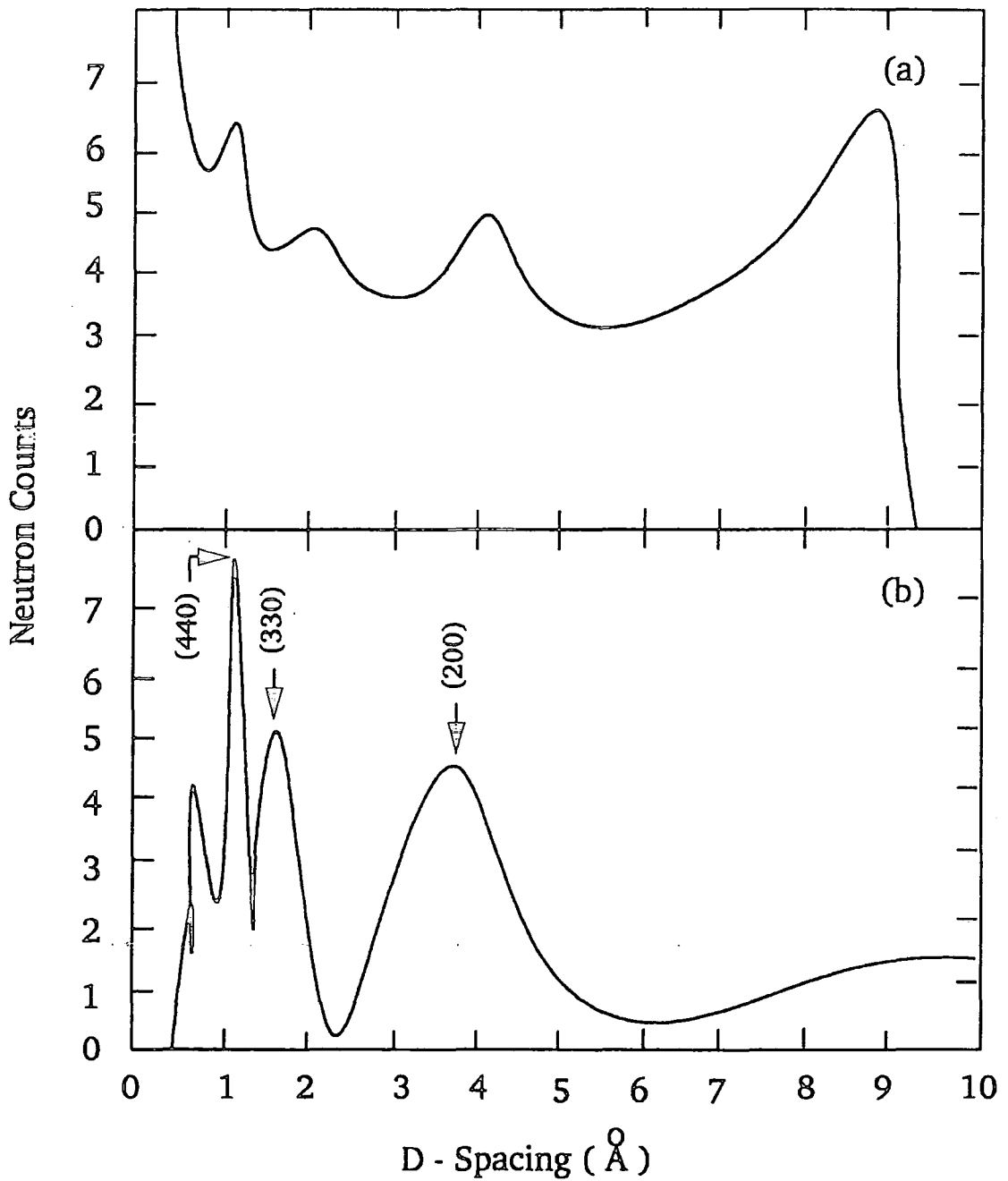


**Figure 7.7** The experimental neutron data for stretched ES films, (a), with an average of extension 150%, modelled in (b) with the pseudo-orthorhombic unit cell of Figure 7.4(b), using the dipolar approach.

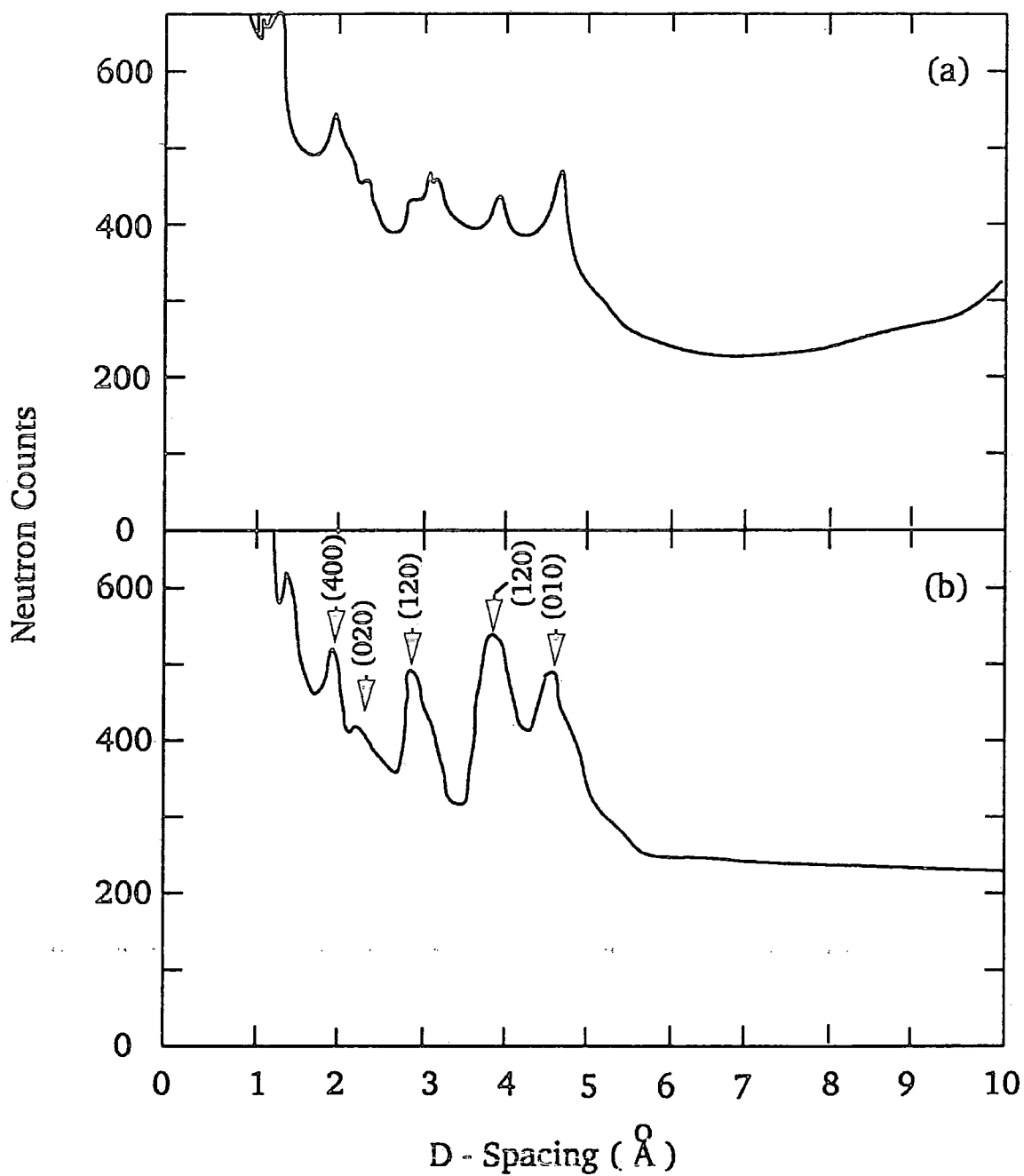


**Figure 7.8** The experimental neutron data for stretched (185%) EB films (a) simulated in (b) with the alternative base unit cell depicted in Figure 7.4(c) using the dipolar approach.

detail in 2.3.2, but to recap the basis is a nitrogen-nitrogen zigzag plane, with each C<sub>6</sub> ring unit twisted alternately by +/- 26° out of this plane. It is important to realise though that such a segment only represents an average chain structure i.e. there is no distinction between benzenoid and quinoid or amine and imine units. At first sight this seems to be a rather poor system to model. However, this model has been used because it represents the most detailed available in light of the extensive conformational complexity of the emeraldine polymer chain. Having computed the atomic positions in 3D, each atom was then projected onto a 2D basal plane and assigned to the relevant neutron scattering length (see Table 7.1). This projection consists of four ring-nitrogen units or 48 atoms, but it is evident that the structure has a symmetry plane every 24 atoms along the chain axis. This 'motif', illustrated in Figure 7.9, has also been represented, for simplicity, as a double-headed arrow or dipole. Since this projection, unlike the previous dipole one, has 'width' and takes up a considerable volume of a unit cell, the resulting interference is much more complicated; the re-radiation from each atom in each 'motif' in a cell can interfere and this must be calculated for.

Using this detailed chain projection to model the stretched EB diffraction data, the simplest possible unit cell, a rectangular 2D net, was assessed. Each projection of the chain segment was placed at the corner of a rectangle (dimensions  $a = 4.8\text{\AA}$  and  $b = 3.9\text{\AA}$ ) and allowed to rotate at an angle  $\theta$ , the setting angle, to the b axis. From the data a value of approximately 40° was found to be appropriate for  $\theta$ . Adding a smooth background term allowed a good fit to the scattering data, as illustrated in Figure 7.10, so that the simplest possible stacking of chains appears to be consistent with the data. The corresponding unit cell structure is depicted in Figure 7.11. Such a structure is basically the same as the alternative cell derived from the dipole approximation (Figure 7.4(c)) only with the b-axis cut in half i.e.  $7.8\text{\AA} / 2 = 3.9\text{\AA}$  and the 'motifs' rotated. Therefore, the dipole 'motif' approach does seem to be a reasonably good and furthermore mathematically simple way to model polyaniline neutron diffraction data. The stretched ES scattering data presented here is not sufficiently resolved or detailed to allow for a similar rigorous analysis, but hopefully when further experiments have been completed (which will

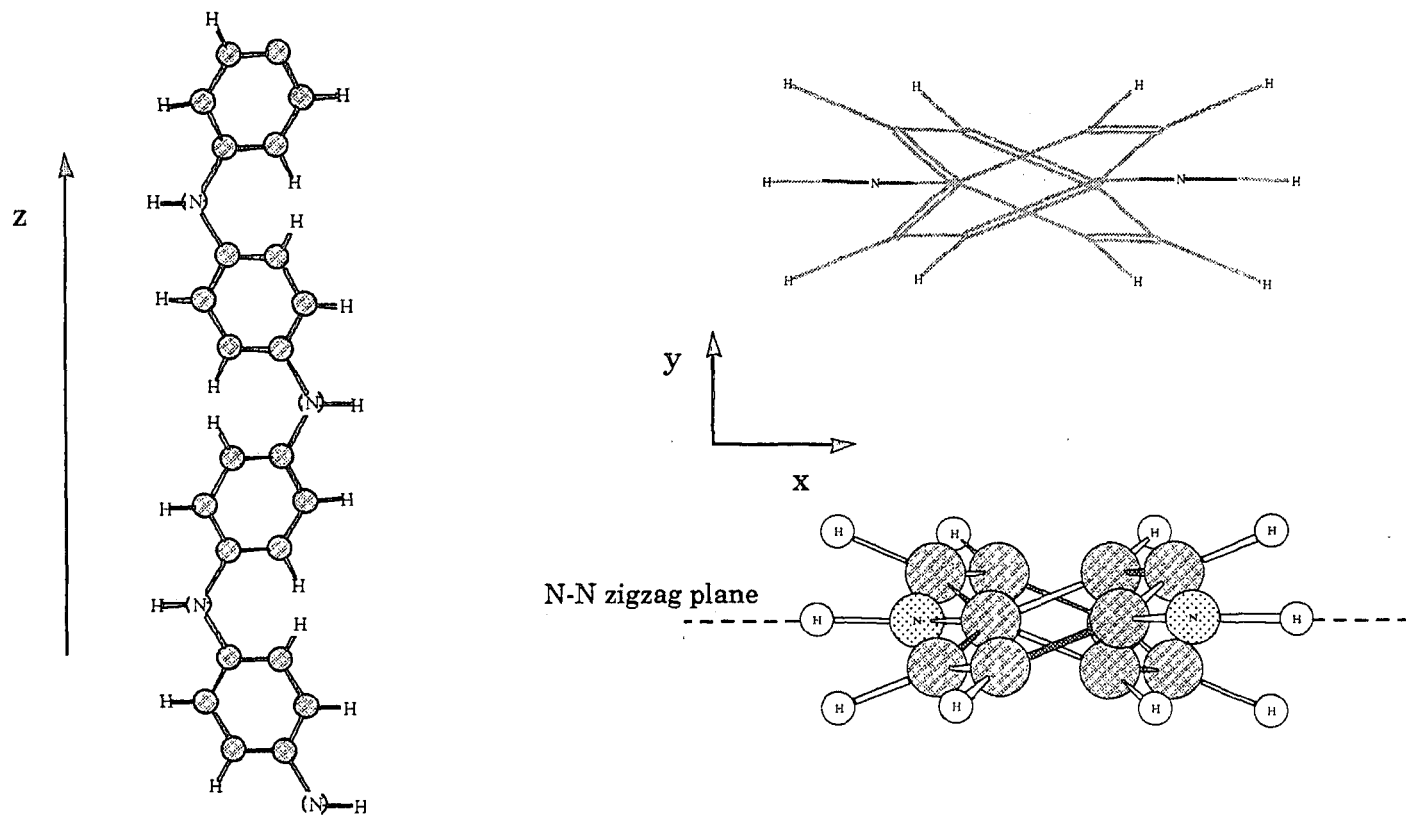


Figure 7.9 The segment of a four ring aniline oligomer, on the left, taken from Bredas<sup>8</sup>, has been used as a model for an EB chain. Each atom has been projected onto a basal (x,y) plane, bottom right, to give a detailed 2D view along the chain axis. The top right illustration is a wire frame 2D model which shows more clearly the torsional angles of the C<sub>6</sub> ring units. This 2D projection has also, for simplicity, been represented in the unit cell structure of Figure 7.11 as a dipole.

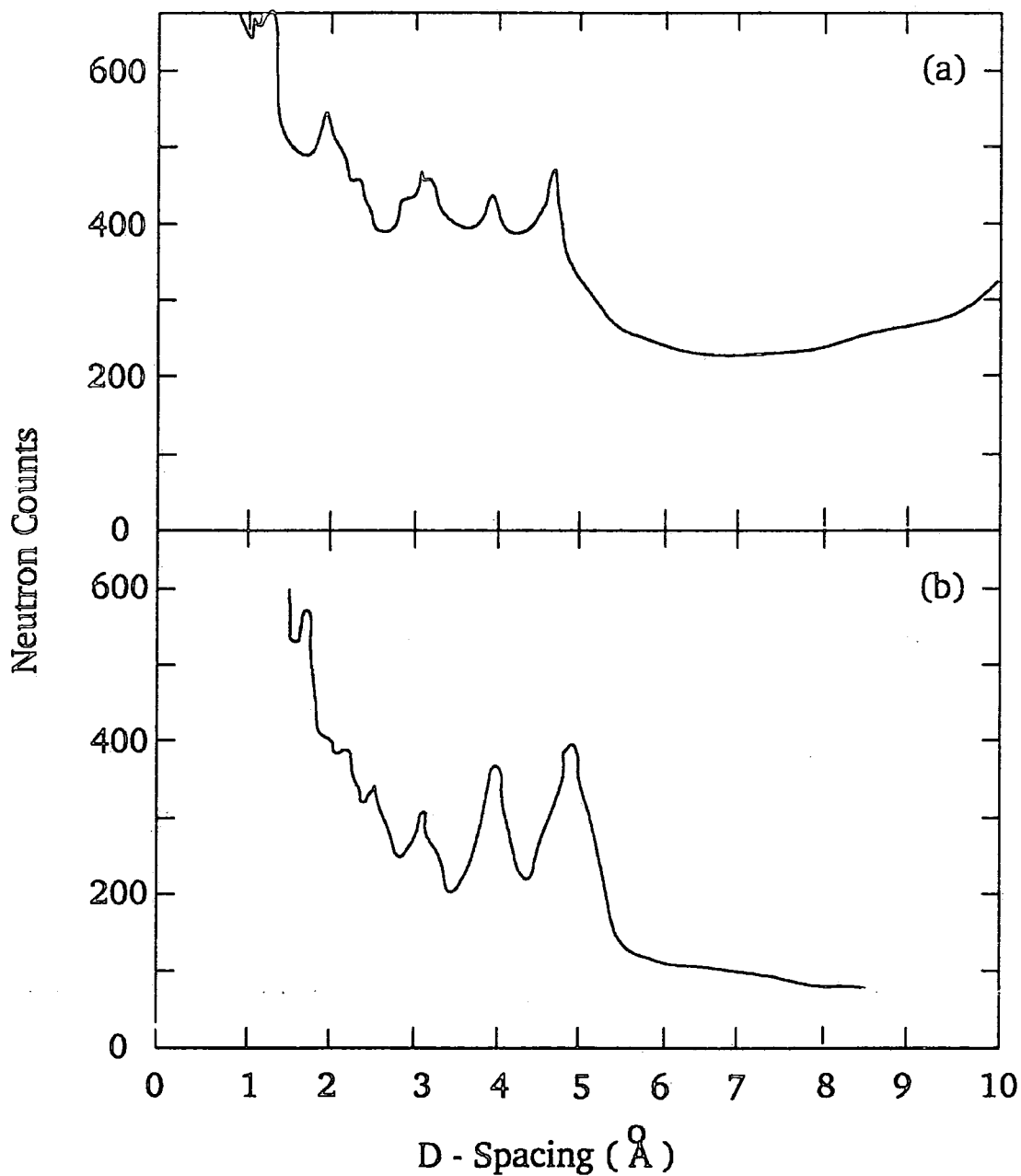


Figure 7.10

The experimental neutron data for stretched (185%) EB films,(a), simulated in (b) with the unit cell of Figure 7.11 using the detailed 2D chain projection as illustrated in Figure 7.9



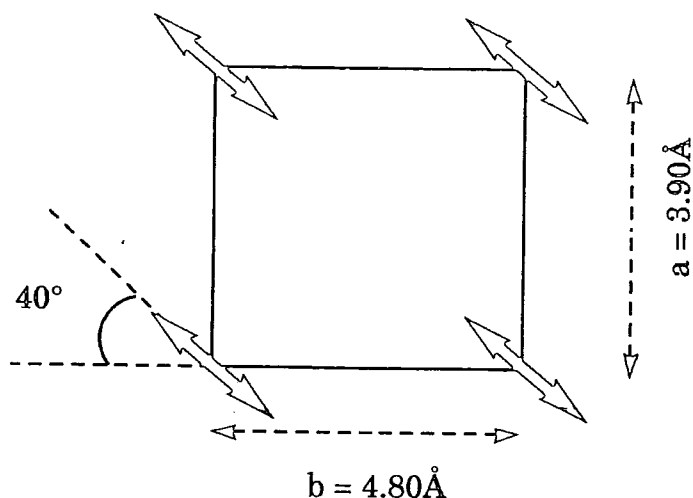


Figure 7.11 The 2D unit cell structure for EB derived using a detailed chain projection model as outlined in Figure 7.9. The structure is basically the same as the alternative cell derived from the dipolar approximation (Figure 7.4(c)) only with the b-axis cut in half i.e.  $7.8\text{\AA} / 2 = 3.9\text{\AA}$  and the 'motifs' rotated.

use significantly higher aligned films due to improvements in processing) such an analysis will be possible. It is confidently expected though, that such an approach will be able to give further back-up to the ideas presented here.

## 7.5 Summary

Neutron diffraction has been used to assess the structure of the crystalline fraction of polyaniline films. Such structural analysis is made possible because many more Bragg peaks are seen for neutron scattering data than are observed using XRD. For these studies deuterated EB and ES polyaniline samples have been prepared. The results represent the initial stages of an ongoing study using this technique and as such the experimental data presented in this thesis has only allowed for 2D (a and b

axes) unit cell structures to be derived. For this analysis a simple dipole model, incorporating 'two' effective atoms, has been used to represent the cross-sectional view along the polymer chain. Although at first sight this may seem a rather crude and too simple approximation, this approach has been justified by the good agreement with a much more rigorous analysis method, using a 2D chain segment projection incorporating 48 atoms.

This dipole analysis has shown that there is more than one possible 2D unit cell structure which fits the scattering data for EB films, within the limits of experimental error. These include an orthorhombic type structure containing five dipoles 'motifs' i.e. 2D projections along a chain axis, Figure 7.4(a) (four at the corners of a rectangular unit cell with one in the centre) and a more symmetrical one, Figure 7.4(c) containing six such dipole 'motifs' (four at the corners with the remaining two half way along the a-axes). The model proposed for a salt unit cell though, Figure 7.4(b), derived from ES scattering data, is similar to the latter EB unit cell but with three interstitial chloride counter-ions placed along the the line of symmetry bisecting the b-axes. As a result of this analysis, it has been proposed that the latter EB cell, Figure 7.4(c), is the more likely because it more closely resembles the derived ES cell structure. Such a proposal is based upon simple energy arguments since upon doping the chloride counterions can easily be accomodated (to give the ES cell) with the minimum amount of molecular rearrangements. The former EB structure, on the other hand, would require much more severe and hence energetically unfavourable molecular rearrangements. The soon to be completed results and analysis of further neutron diffraction studies, also incorporating c-axis measurements, will doubtless help to elucidate the results presented so far.

## References

- 1 G.E. Bacon, *Neutron Diffraction*, Third Edition, Clarendon Press, 1975.
- 2 *ISIS Experimental Facilities*, edited and compiled by B. Boland and S. Whapham, December 1992.

- 3 A.K. Soper, W.S. Howells and A.C. Hannon, *ATLAS - Analysis of Time-of-Flight Diffraction Data from Liquid and Amorphous Samples*, RAL Report RAL-89-046, (1989).
- 4 M.E. Jozefowicz, R. Laversanne, H.H.S. Javadi, A.J. Epstein, J.P. Pouget, X. Tang, and A. G. MacDiarmid, *Phys. Rev. B*, **39**, (1989), 12958.
- 5 J.P. Pouget, M.E. Jozefowicz, A.J. Epstein, X. Tang and A.G. MacDiarmid, *Macromolecules*, **24**, (1991), 779.
- 6 B.J. Tabor, E.P. Magre, J. Boon, *Eur. Polym. J.*, **7**, (1971), 1127.
- 7 J. Boon and E.P. Magre, *Makromol. Chem.*, **126**, (1969), 130.
- 8 J. L. Bredas in *Proceedings of the Nobel Symposium on Conjugated Polymers and Related Materials*, ed. W. R. Salaneck, Oxford University Press, 1992.

## Chapter 8

### Conclusions

#### 8.1 Overall Summary

This thesis has assessed some of the many structural aspects of the conductive polymer, polyaniline, based primarily on the analysis of free-standing film samples. Whilst polyaniline is undoubtedly a very complex and intriguing material, the results presented here have revealed a wealth of information about the polymer, although perhaps even more remains to be discovered! The findings of this thesis are now summarised below.

A number of important aspects concerned with sample preparation have been studied, from the synthesis of polyaniline to the stretch alignment and subsequent doping of free-standing films cast from the solvent N-methyl-2-pyrrolidinone (NMP). Starting with the polymer synthesis, a procedure has been described and analysed. The emeraldine base powder (EB) produced has been assessed for chemical composition using elemental analysis and  $^{13}\text{C}$  solution state NMR and for molecular weight using gel permeation chromatography (g.p.c.). The NMR results have unequivocally established that the product is indeed EB polyaniline. However, the polymer has also been shown to possess a high degree of stereochemical complexity. This complexity is likely responsible for many of the further problems encountered with detailed characterisation studies. Furthermore, the polymer was also found to contain a small fraction, ca. 5%, of contaminants, some of which may be associated with chain defects (as discussed later on). Through gel permeation chromatography, using poly (2-vinylpyridine) (PVP) as a calibration standard, the molecular weight of the polymer was determined to be typically  $\overline{M}_p = 3.2 \times 10^5$ . The choice of PVP as a standard has allowed the molecular weight to be estimated with a high degree of accuracy since, unlike previously used polystyrene standards, PVP displays good solubility in NMP. Through these analysis techniques it has also been shown that only slight variation in synthesis procedure can greatly alter the chemical and in turn physical properties of the polymer. The

importance of precise control of polyaniline synthesis is therefore strongly emphasised.

The fabrication of polyaniline films has been described using the solvent N-methyl-2-pyrrolidinone (NMP). These samples have been assessed for quality and also for composition using thermogravimetric analysis (TGA). This latter technique has indicated that as-cast EB films typically contain some 25% residual NMP. However, conducting specimens, i.e. those protonated by aqueous HCl, contain no NMP and furthermore tend to lose dopant molecules at elevated temperatures. The orientation of polyaniline films has also been described in some detail, in particular in relation to the alignment of other conducting polymers and common thermoplastics such as polyethylene. Stretching can only be achieved for as-cast EB films and is crucially dependent on the residual NMP in the material. The stretching process itself depends on a wide number of variables and was found to be rather difficult to control. Nevertheless, a procedure was developed through which polyaniline samples with extensions of up to 300% could be produced on a quite reproducible scale.

After processing these base samples can be protonated to the emeraldine salt (ES), i.e. conducting form by doping films in 1M HCl. Unstretched, ES films have a conductivity of typically  $60\text{-}70\text{ S cm}^{-1}$ . However, extended samples display a remarkable increase in conductivity when measured parallel to the stretch direction. For maximally stretched films i.e. 300% this parallel conductivity is some  $350\text{ S cm}^{-1}$ , with an anisotropy (parallel divided by perpendicular conductivity) of around 24. These conducting samples have also been studied using thermopower analysis, the results of which have enabled the mechanism of conduction to be assessed. The magnitude of the thermopower implies conduction in extended states i.e. metallic conductivity, but the temperature variation of this parameter indicates that variable range hopping dominates the conduction mechanism. A likely possible cause of this deviation from metallic behaviour is the presence of defect structures along the chain backbone.

The results of various thermal analysis experiments have revealed a wealth of new information about the thermal properties of polyaniline, much of which also allows the orientation process of the polymer to be rationalised. Through dynamic mechanical thermal analysis (DMTA) and dielectric thermal analysis (DETA) a number of important thermal transitions pertaining to amorphous film regions have been observed. First of all a glass transition,  $T_g$ , has been identified at around 100°C for as-cast EB films. This co-operative thermal motion of chain segments is made possible because the relatively volatile NMP molecules are removed at elevated temperatures. This, in turn, creates a 'free volume' around the chains. This  $T_g$  transition is critically dependent on the amount of NMP in the films and shifts to higher temperatures with decreasing solvent content. In the case of as-cast EB films this NMP content has been estimated to be ca. 25% as measured by thermomechanical analysis. It is because of this  $T_g$  transition that EB films can be stretch aligned, whereas doped ES films, which contain no NMP, cannot.

The chain mobility, though, only exists for a finite time and at a temperature of around 180°C, films start to harden. This collapse in free volume has been monitored by thermomechanical analysis and the hardening reaction is thus initially due to chains becoming highly entangled or physically crosslinked. However, the nature of the data and the permanence and brittleness of thermally hardened films also suggests a chemical crosslinking reaction occurs as well. This inference has been compounded by infrared spectroscopy and also by relation to polyaniline/NMP gels. This latter material consists of a highly crosslinked polymer network, whose degree of crosslinking is greatly increase by the presence of residual contaminants in the polyaniline. These contaminants, beside being free anion impurities, also occur as sulphonate and chloride ring substituents, species which are highly reactive at elevated temperatures and will likely chemically bond, i.e. form chemical crosslinks. As such chemical bonding in polyaniline films cast from NMP can be proposed. This reaction imposes an upper limit on the processing temperature of specimens since it results in mechanically weak, low conductivity (when subsequently doped) films.

Many of the wide variety of often conflicting experimental results can be explained by subtle differences in polyaniline synthesis giving rise to different amounts of contaminants. Chemical crosslinking is just one example of how these contaminants can drastically effect the physical properties of the polymer. Again, the need for precise material synthesis and also processing is highlighted in order to remove both impurities and chain defects.

Another important feature of the mechanical and dielectric data is the presence of a low temperature transition at  $-80^{\circ}\text{C}$ , which has been identified as a phenyl ring twisting motion. This relaxation has been calculated to have an activation energy of  $11 \text{ kcal mol}^{-1}$ , which is a particularly important result in light of the fact that such motion plays a central role in the electronic transitions of polyaniline. Also, the ability of solvent-free specimens to absorb water by hydrogen bonding to amine units has been identified by infrared analysis. This water vapour, however, is lost above  $100^{\circ}\text{C}$ ; this feature occurs as a transition at around  $85^{\circ}\text{C}$  in the rescanned mechanical and dielectric thermograms. Furthermore, this is a reversible process so that thermal cycling involves the loss and capture of water molecules.

Infrared orientation studies of stretched EB films have revealed detailed information about the molecular orientation produced during macroscopic stretching of a sample. A specimen stretched by 230% has been shown to have an degree of orientation equivalent to 53% of the polymer chains aligned with the stretch direction. Upon protonation in 1M HCl such a film exhibits a conductivity in the range of  $250 \text{ S cm}^{-1}$ . This value is over twice as large as that obtained for similarly elongated  $\text{AsF}_5$ -doped PPV films. Also, the extent of orientation in such PPV samples corresponds, typically, to over 75% of chains perfectly oriented. Therefore, intrinsically, polyaniline is much the better conductor. Further analysis has probed the geometrical structure of an EB chain and has determined an average ring torsional angle between the  $\text{C}_6$  and the nitrogen-nitrogen planes of  $33^{\circ}$ . This result is in very good agreement with theoretical and oligomeric crystal structure studies.

X-ray diffraction (XRD) studies have been used to probe the crystalline fraction of polyaniline films. Due to the nature of the data (only 2-3 discernable Bragg peaks are seen) it has not been possible to determine possible unit cell structures. However, this fundamental concern has been addressed using neutron diffraction. The results have indicated though a linear increase in relative crystallinity,  $X_c$ , with elongation for EB films. An unstretched film is estimated to have an  $X_c$  of around 0.10 while a 230% stretched film exhibits an  $X_c$  of around 0.55. This latter value is very similar to the orientation parameter derived from IR measurements and indicates that crystallinity and molecular orientation are closely related. For doped ES specimens a change in d spacings is observed, but there is no distinct pattern between crystallinity and elongation for these samples.

The widths of the Bragg peaks, for all samples, indicate a very small crystalline block size, around 50-60Å. This result may be interpreted by acknowledging the complex stereochemical structure of the chain. Only very short segments have the correct geometry to make crystallisation energetically favourable. Furthermore, the Bragg widths do not vary with stretch ratio, indicating that the increase in crystallinity is due to nucleation of new crystallites rather than growth of pre-existing ones.

Orientational analysis of the X-ray data has shown a slight lateral order in stretched EB films. The results are consistent with the a and b axes of an assumed orthorhombic unit cell being preferentially aligned perpendicular to the stretch direction, so that the c axis must be oriented in a parallel manner. However, in other directions and particularly along the stretch axis, very little periodicity is evident. The Hermans orientation function for a 230% extended sample was found to be 0.86, significantly larger than the IR derived value of 0.53. This is generally expected, though, since the X-ray value describes only crystalline orientation whereas the IR technique defines an average i.e. crystalline and amorphous case. The interpretation for a 170% doped specimen is very similar to that for base films. However, an even higher Hermans parameter of 0.96 was measured indicating that protonation induces a further degree of crystallite orientation.



As mentioned earlier, neutron diffraction (ND) has been used to assess the structure of the crystalline fraction of polyaniline films. Such structural analysis is made possible because many more Bragg peaks are seen for ND data than are observed using XRD. For these studies deuterated EB and ES polyaniline samples have been prepared. The results represent the initial stages of an on-going study using this technique and as such the experimental data presented in this thesis has only allowed for 2D (a and b axes) unit cell structures to be derived. For this analysis a simple dipole model, incorporating 'two' effective atoms, has been used to represent the cross-sectional view along the polymer chain. Although at first sight this may seem a rather crude and too simple approximation, this approach has been justified by the good agreement with a much more rigorous analysis method, using a 2D chain segment projection incorporating 48 atoms.

This dipole analysis has shown that there is more than one possible 2D unit cell structure which fits the scattering data for EB films, within the limits of experimental error. These include an orthorhombic type structure containing five dipole 'motifs' i.e. 2D projections along a chain axis (four at the corners of a rectangular unit cell with one in the centre) and a more symmetrical derivative containing six such dipole 'motifs' (four at the corners with the remaining two half way along the a-axes). The ND model proposed for a salt unit cell though, derived from ES scattering data, is similar to the latter EB unit cell but with three interstitial chloride counter-ions placed along the the line of symmetry bisecting the b-axes. As a result of this analysis, it has been proposed that the latter EB cell is the more likely because it more closely resembles the derived ES cell structure. Such a proposal is based upon simple energy arguments since upon doping the chloride counter-ions can easily be accommodated (to give the ES cell) with the minimum amount of molecular rearrangements. The former EB structure, on the other hand, would require much more severe and hence energetically unfavourable molecular rearrangements. The soon to be completed results and analysis of further ND studies, also incorporating c-axis measurements, will doubtless help to elucidate the results presented so far.

## 8.2 Suggestions for Further Work

Clearly there is a great deal of further work that can be carried out on polyaniline. In particular, with regards to the studies presented in this thesis, a number of important aspects may be highlighted. Firstly the move towards synthesis optimisation, in terms of (ultra-)high molecular weight material and removal of all defect structures, is very important and a subject which is already receiving much attention. As a result of this the true properties of the polymer and not those due to impurities, will become manifest. The processing of polyaniline has also raised many questions. Whilst good quality films can be cast using N-methyl-2-pyrrolidinone (NMP) as a solvent, the stretch alignment of these samples is perhaps a rather crude and somewhat uncontrollable process, relying on removal of the NMP molecules to enable the polymer chains to gain enough flexibility to be oriented. Although a major improvement in the reproducibility and extent of stretch alignment has since been made, also here in Durham, it would be highly desirable to incorporate a permanent plasticiser into film samples. Such a development would undoubtedly widen the scope for processing, particularly with regards to commercial applications.

It would be highly desirable to process the polymer in the conducting emeraldine salt state. The samples described in this thesis may only be processed in the insulating emeraldine base form and so must be subsequently converted to the salt derivative. This topic is already quite a major area of research, with the use of functionalised acid dopants to induce solubility in common organic solvents. Perhaps the main goal of all these processing improvements would be to achieve levels of conductivity in the polymer much closer to those of metals, so as to eventually develop a cheap 'plastic alternative' for currently used conductors such as copper. Indeed, although startling improvements in conductivity have been observed for the highly extended samples mentioned in the last paragraph over those measured in this work, it is unlikely that polyaniline will ever achieve this aim. Further complications arise from the moderate stability of the conducting form at elevated temperatures and worries concerning the health and safety aspect of the polymer, especially on disposal.

This development of film orientation though will enable further studies to be undertaken using the techniques discussed in this thesis. The use of highly aligned samples can only enhance the results of infrared orientational and X-ray diffraction analyses to give more in-depth structural information. Such specimens will also allow neutron diffraction studies to develop a more detailed view of the nature of the crystalline phases in polyaniline. Another possible area for further work is the fabrication of stretch aligned films thin enough to be studied using (polarised) optical absorption spectroscopy. This type of analysis would enable detailed examinations of the microscopic electronic properties of the polymer to be made and in particular the importance of both intra-chain and inter-chain interactions to be assessed.

Thus, there remains many aspects and questions concerning polyaniline to be investigated and resolved. To this end, polyaniline will undoubtedly remain at the forefront of conductive polymer research.

Appendix  
Publications

# Solution-state carbon-13 nuclear magnetic resonance studies of polyaniline

A. M. Kenwright\* and W. J. Feast

*IRC in Polymer Science and Technology, University of Durham, South Road, Durham DH1 3LE, UK*

and P. Adams

*University of Durham Industrial Research Laboratories, Mountjoy Research Centre, South Road, Durham DH1 3LE, UK*

and A. J. Milton and A. P. Monkman

*Department of Physics, University of Durham, South Road, Durham DH1 3LE, UK*

and B. J. Say

*Department of Chemistry, University of Durham, South Road, Durham DH1 3LE, UK*  
(Received 9 December 1991; accepted 18 February 1992)

Solution-state  $^{13}\text{C}$  nuclear magnetic resonance spectra are presented for the emeraldine base and leucoemeraldine base forms of polyaniline. The bulk of the leucoemeraldine base sample gives a simple two-line spectrum, which is readily assignable. The emeraldine base samples give spectra of much greater complexity, showing many more lines than there are carbons in the postulated chain repeat unit. This is rationalized in terms of slow interchange of the many conformers available to the emeraldine base form. A quantitative 'region assignment' is made. Gel permeation chromatography measurements show that interconversion between the two forms is achieved without either significant crosslinking or chain scission. The minor peaks in the spectrum of the leucoemeraldine base form due to chain defects (including chain ends) are compared with chemical shift values calculated for postulated structures, and some structures can be rejected on the basis of this.

(Keywords: conducting polymers; polyaniline;  $^{13}\text{C}$  nuclear magnetic resonance; conformations)

## INTRODUCTION

Polyaniline is the generic term given to the products of the oxidative coupling of aniline. This reaction has been known for about 150 years<sup>1,2</sup>, and it is recognized that the properties of the material produced can be changed by further oxidation or reduction, as well as by protonation by strong acids. Trivial names have been associated with several of the forms produced in this way and structures have been postulated for them<sup>3,4</sup>, some of which are shown in *Figure 1*, but little hard evidence has been produced to support these postulated structures.

In the past decade there has been an explosion of interest in polyaniline because of its conductivity and processing properties, and many papers have appeared concerning the preparation and characterization of the various forms. The bulk of the characterizations have relied on some combination of elemental analysis, molecular-weight determination (by, for example, gel permeation chromatography (g.p.c.)), identification of functional groups present (by, for example, vibrational spectroscopy<sup>5</sup>), identification of chromophores by ultra-violet/visible (u.v./vis) spectroscopy and determination of oxidation state (by, for example, redox titrations). Others

have concentrated on the characterization of low-molecular-weight 'model' compounds<sup>6-8</sup>, or the synthesis of polymers under more controlled conditions<sup>9</sup> whose properties could be compared with the conventionally produced polyanilines. While these techniques go some way towards characterizing the material, they provide relatively little in the way of detailed information on the structure of the polymer chains. Solid-state  $^{13}\text{C}$  and  $^{15}\text{N}$  nuclear magnetic resonance (n.m.r.)<sup>10-16</sup> have been used in an effort to characterize the materials structurally and have yielded spectra that could be explained in terms of the postulated structures. Unfortunately, the available resolution, particularly in the case of the  $^{13}\text{C}$  spectra, was insufficient to allow the positive identification of the postulated structures, or indeed of any other structures that might have been present. In this work we have used solution-state  $^{13}\text{C}$  n.m.r. to examine polyaniline samples, and find the available resolution considerably increased, allowing a much greater insight into the possible structures present.

## EXPERIMENTAL

The 'emeraldine base' form of polyaniline was prepared as follows. Aniline (0.1 mol) was added to hydrochloric

\* To whom correspondence should be addressed

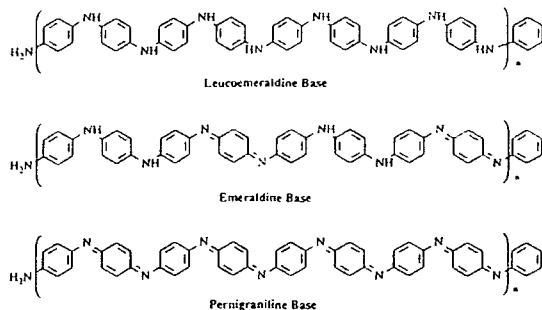


Figure 1 Postulated structures for various oxidation states of polyaniline

acid solution (100 ml, 3.5%, ca. 0.1 mol HCl) in a 250 ml beaker, and mixed using a magnetic stirrer to give a solution with a final pH between 1 and 2, as measured by indicator paper. Ammonium persulphate (0.1 mol) was dissolved in distilled water (60 ml), and this was added to the stirred reaction mixture. The mixture turned a dark blue/green colour and the reaction was observed to be slightly exothermic over a period of about 10 min. The mixture was left to stir for a total of about 6 days, after which it was filtered and washed with two lots of water, methanol (to remove any low-molecular-weight species) and finally with more water. The filter cake was added to an ammonia solution (100 ml, 35%) and stirred for 7 h before filtering and repeatedly washing with water, occasionally interspersed with washing with isopropanol. At this point the filtrate was colourless. The filter cake was then dried under vacuum at 323 K for 24 h to give a brown/purple product, which was crushed using a mortar and pestle. Elemental analysis showed that the material contained small residual amounts of chlorine (0.50 wt%) and sulphur (0.38 wt%). Some 4.69 wt% was not accounted for and is ascribed to oxygen, possibly associated with the chlorine or sulphur, or with trapped solvent species (water, methanol or isopropanol). Indeed, isopropanol was subsequently positively identified in the  $^{13}\text{C}$  spectra. Chlorine and sulphur residues are normally found in the products of such preparations and they remain largely unchanged by attempts to wash them out, suggesting that they may be present as ring substituents.

The 'leucoemeraldine base' form of polyaniline was prepared from emeraldine base (2.0 g), which was placed in a 250 ml beaker with high-performance liquid chromatography (h.p.l.c.)-grade *N*-methyl-2-pyrrolidone (NMP) (20.0 g) and stirred. The beaker was then placed in an ultrasonic bath for about 15 min to disperse the emeraldine base before phenylhydrazine (2.50 g) was added and the mixture stirred for 24 h at room temperature, by which time the solution had turned dark brown. This was transferred to a nitrogen-atmosphere glove-box and toluene was added with vigorous stirring to precipitate the leucoemeraldine base, which was recovered by filtration, washed four times with toluene, and left to dry on the Buchner funnel before transferring to a vacuum desiccator. The desiccator was evacuated in the glove-box and then taken out of the box and subsequently kept under dynamic vacuum for 2 days in an effort to remove the toluene residues. (In spite of this, traces of toluene were still evident in the  $^{13}\text{C}$  n.m.r. spectra—see below.) The desiccator was then returned to the glove-

box and the leucoemeraldine base ground using a mortar and pestle to give a light-tan coloured powder.

A sample of the leucoemeraldine base was subsequently reoxidized as follows. Leucoemeraldine base (1.09 g) was added to a solution of  $\text{FeCl}_3 \cdot 6\text{H}_2\text{O}$  (0.812 g, 0.003 mol) in aqueous hydrochloric acid (50 ml, 2 M), and the mixture was stirred vigorously for 24 h under air in a fume hood. The product was recovered by filtration and washed several times with water before being added to ammonia solution (50 ml, 35%) and stirred for a further 6 h. It was filtered again and washed several times with water before being dried under vacuum at 323 K for 24 h.

Gel permeation chromatography (g.p.c.) measurements (Polymer Labs PL-gel mixed column, NMP + 0.1% LiCl) carried out on all three samples gave identical responses, showing that the interconversion from one form to another did not result in significant amounts of either chain scission or crosslinking.

N.m.r. samples were prepared by adding powdered polyaniline (0.4 g) to an approximately 50/50 v/v mixture of NMP and perdeuterated dimethylsulphoxide ( $d_6$ -DMSO) (4 g) with stirring. The mixture was then placed in an ultrasonic bath for about 15 min to ensure dispersion of the polyaniline, after which it was transferred to a 10 mm diameter n.m.r. tube, which was capped and sealed with 'para-film'. The  $^{13}\text{C}$  spectra of the polyaniline samples were obtained on a Bruker AMX-500 spectrometer at an operating frequency of 125.77 MHz, and a nominal probe temperature of 303 K. The  $^{13}\text{C}$  spectra of model compounds were run in  $d_6$ -DMSO on a Varian VXR400-S spectrometer at an operating frequency of 100.577 MHz, and at ambient probe temperature (about 293 K). All chemical shift values are quoted relative to tetramethylsilane (TMS), although referencing was done via the  $d_6$ -DMSO peak, which was taken to be at +39.5 ppm.

## RESULTS AND DISCUSSION

Our initial objective was to see whether or not it was possible to obtain reasonable-quality solution-state  $^{13}\text{C}$  spectra of polyaniline samples, since we could find no record of other workers having done this. We looked first at the 'as-made' emeraldine base sample, and found that we could observe relatively high-quality spectra without undue difficulty. The region of interest from the normal proton-decoupled  $^{13}\text{C}$  spectrum and d.e.p.t.-90 $^{17}$  spectrum (distortionless enhancement by polarization transfer) are shown in Figure 2. The effect of the d.e.p.t.-90 sequence is to select only those carbons having one directly bonded proton, and it is therefore a very valuable assignment tool in this case. From these spectra we can readily identify the quaternary (in the sense of non-proton-bearing) carbons, and observe that there are peaks in all the spectral regions we would expect for the postulated structure. However, it is also immediately evident that the spectrum is considerably more complicated than might be expected from naive consideration of the postulated structure as drawn in Figure 1. It is therefore not possible to make an immediate assignment on the basis of these spectra alone.

We next looked at the sample of leucoemeraldine base prepared by reduction of the emeraldine base using phenylhydrazine. A normal proton-decoupled  $^{13}\text{C}$  spectrum of this material is shown in Figure 3, together with a vertical expansion showing the minor peaks in the

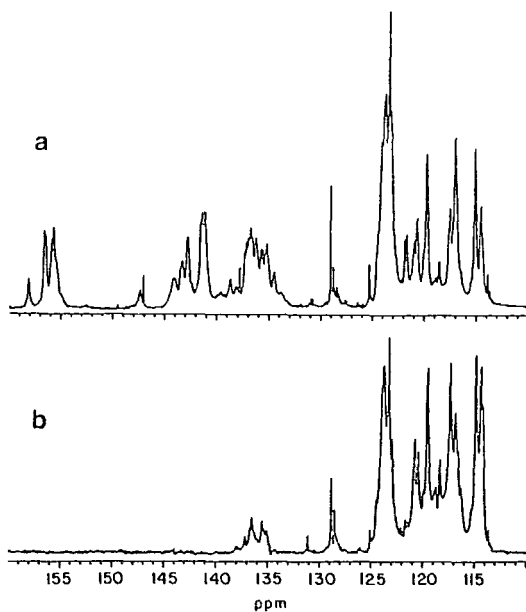


Figure 2 Emeraldine base as made. (a)  $^{13}\text{C}\{^1\text{H}\}$ : 5 s recycle,  $90^\circ$  pulse, 0.47 s acquisition, 40 000 transients, continuous decoupling. (b) D.e.p.t.-90: 1 s recycle, 0.47 s acquisition, 38 000 transients

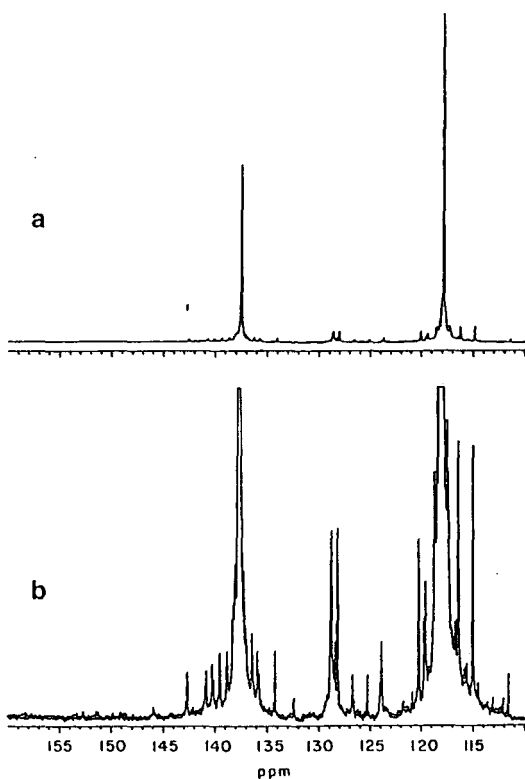


Figure 3 Leucoemeraldine base. (a)  $^{13}\text{C}\{^1\text{H}\}$ : 5 s recycle,  $90^\circ$  pulse, 0.47 s acquisition, 10 000 transients, continuous decoupling. (b) Vertical expansion

baseline. It is immediately obvious that the major features in the region of interest are just two lines at 117.84 and 137.44 ppm. When a spectrum of this sample is recorded under quantitative conditions (decoupler gated off during 30 s recycle), the two peaks have an intensity ratio of 2:1 within experimental error, and the two peaks account for more than 95% of the intensity in the 110 to 160 ppm region of the quantitative spectrum when the peaks due to residual toluene (125.3, 128.2 and 128.8 ppm—quarternary at  $\sim 137.5$  ppm presumed under the major peak) have been eliminated. In a d.e.p.t.-90 spectrum only the peak at 117.84 ppm is seen, while a  $^1\text{H}$  spectrum recorded on the decoupler coil of the 10 mm probe, while not of optimal resolution, clearly showed two broad peaks centred at 6.98 and 7.51 ppm having an intensity ratio of 4:1 within experimental error. All of the above is completely consistent with the postulated structure and, when taken in conjunction with the other available data on the sample, is proof that the vast majority of the sample has the structure postulated for leucoemeraldine base. We will return to the question of the minor peaks later.

We then looked at the sample prepared by reoxidation of the leucoemeraldine base. The proton-decoupled  $^{13}\text{C}$  spectrum of this material is shown in Figure 4, together with a spectrum of the original emeraldine base run under similar conditions for comparison. It can be seen that the two spectra are practically identical, except that the linewidth is possibly slightly greater in the reoxidized material. This may be due to the presence of paramagnetic residues following the treatment with  $\text{FeCl}_3$ . The fact that these two spectra are so similar, together with the evidence from g.p.c. showing that neither chain scission nor crosslinking occurred during these reactions,

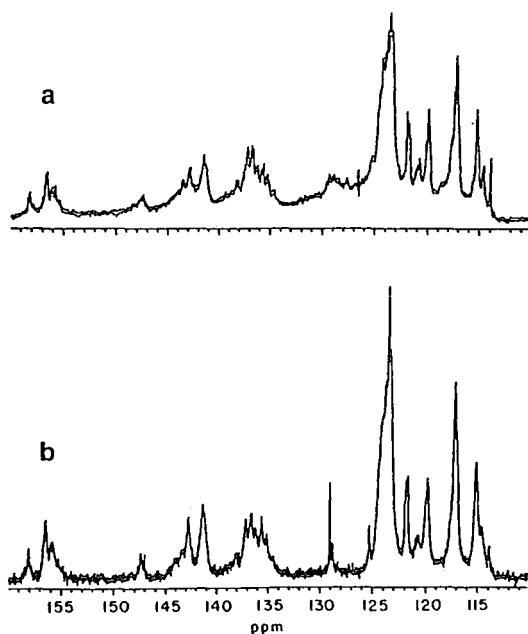


Figure 4 Emeraldine base  $^{13}\text{C}\{^1\text{H}\}$ . (a) Reoxidized from leucoemeraldine using  $\text{FeCl}_3$ : 1 s recycle,  $90^\circ$  pulse, 0.47 s acquisition, 11 000 transients, continuous decoupling. (b) As made: 1 s recycle,  $30^\circ$  pulse, 0.47 s acquisition, 1 000 transients, continuous decoupling

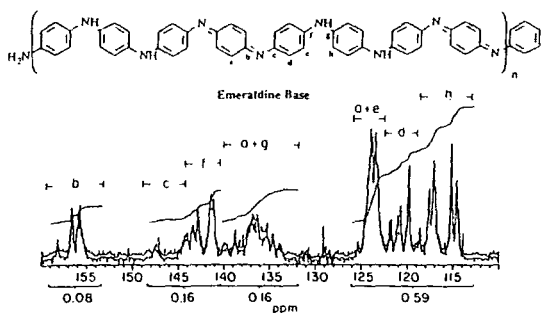


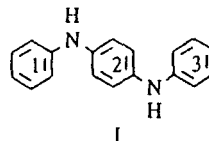
Figure 5 Emeraldine base as made,  $^{13}\text{C}\{^1\text{H}\}$  under quantitative conditions: 30 s recycle,  $90^\circ$  pulse, 0.47 s acquisition, 4750 transients, decoupler gated off during recycle

is of key importance, since it clearly shows that the changes involved in going from emeraldine base to leucoemeraldine base are fully reversible, and almost certainly do not involve any major structural changes. It therefore follows that, since we have already shown the leucoemeraldine base sample to be almost entirely composed of phenylene rings connected by *para*-substituted nitrogens, the emeraldine base sample must have the same skeletal structure. This is entirely consistent with the postulated structure for emeraldine base, and would seem to be the first unequivocal confirmation of the structure.

With this in mind, we can turn to consider in more detail the spectrum of emeraldine base. We have previously identified the quaternary carbons in this spectrum from the d.e.p.t.-90 experiment. On the basis of this, studies of model compounds<sup>2,13</sup> (see also below) and the integrations from a spectrum obtained under quantitative conditions, the region assignments shown in Figure 5 could be made. These assignments are in quantitative agreement with the postulated structure, confirming the assignments previously made by Kaplan *et al.*<sup>14</sup> on the basis of solid-state  $^{13}\text{C}$  n.m.r., and correcting our earlier assignments of solid-state spectra<sup>15</sup>. It should be noted that it is possible to make much more definite assignments based on the solution-state data because the linewidths are reduced by more than an order of magnitude, and also because it is possible to obtain solution-state spectra under quantitative conditions.

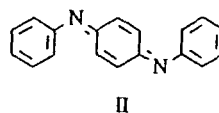
We are still left, however, with many more peaks than assignable carbons in the spectra of emeraldine base, suggesting a wealth of conformational effects, or a reduction in ring symmetry, or both. This is in marked contrast to the extreme simplicity of the leucoemeraldine base spectra. We must try to explain why this might be the case, even if we cannot as yet make a detailed assignment of each peak. X-ray crystallographic data on model compounds of polyaniline<sup>7</sup>, as well as on other systems where two *para*-substituted phenylene rings are linked via one (essentially tetrahedral) atom, such as bisphenol derivatives and aromatic polyethers, show that on average the torsion angle between the phenylene rings is non-zero, the angle between the bridging bonds and the ring axes being fixed. This means that the two rings are effectively skewed with respect to each other. In principle, this renders the two sides of the rings inequivalent although this inequivalence is generally not seen in solution-state n.m.r. spectra because of the rapid

ring-flipping motion ( $180^\circ$  jumps) characteristic of *para*-substituted phenylene rings in polymer chains<sup>18,19</sup>, which has the effect of averaging the inequivalence on the n.m.r. timescale. It is important to note that, in solution, a number of conformational possibilities exist resultant on the fact that the two bonds to the bridging atom allow rotational isomerism. For any given relative orientation of the two rings (angle of skew) there are four possible orientations of the bond from the bridge to ring 2 for any given orientation of the bond from ring 1 to the bridge. In the case of two phenylene rings these positions would be equivalent by virtue of being symmetry-related, but in the case of three phenylene rings, such as in the model compound *N,N'*-diphenyl-*p*-phenylenediamine (I):



this means that there are four possible orientations of the 1,4-axis in ring 3 for any given orientation of the 1,4-axis in ring 1. Interchange between these orientations is, of course, possible by rotation about the carbon-nitrogen bonds. If we therefore consider the chain in leucoemeraldine base to be composed of short stiff segments (the phenylene rings) coupled by rotational junction points (the nitrogens), we can easily envisage that relatively rapid conformational interchange could occur in solution via the normal types of chain motional behaviour. Taking this in conjunction with the averaging due to phenylene ring flipping, the simple two-line spectrum obtained for leucoemeraldine base becomes fully understandable. Rapid conformational interchange would not be expected in solid samples below  $T_g$ , however, and this doubtless goes a long way towards explaining the very much broader lines observed for leucoemeraldine base in solid-state  $^{13}\text{C}$  spectra<sup>14</sup>.

Turning to emeraldine base, the obvious chemical difference is the inclusion of quinoid-imine rings. This not only gives rise to more lines by reducing the structural symmetry of the chain, but also has several other effects by virtue of its bonding. First, because the carbon-nitrogen bonds in the quinoid-imine system are double bonds, there is no possibility of ring flipping and therefore differences may be observed between the two sides of the ring. This is clearly demonstrated in studies<sup>6</sup> on the model compound *N,N'*-diphenyl-2,5-cyclohexadiene-1,4-diimine (II):



and these effects are reproduced in the observed spectra of emeraldine base, with peaks corresponding to the proton-bearing carbons of the quinoid-imine ring being observed in both the 134 to 137 ppm and 122 to 125 ppm ranges. Since the carbon-nitrogen bonds are constrained to be coplanar with the quinoid-imine ring and the double bonds are effectively rotationally locked, the whole quinoid-imine system shows *cis-trans* isomerism, which presumably affects the shifts not only of the



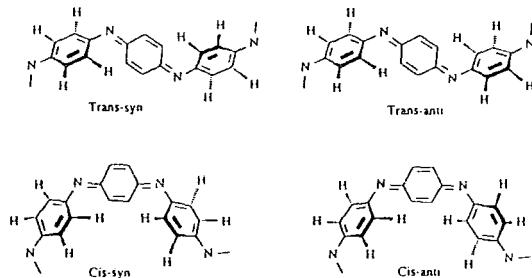


Figure 6 Possible chain conformations about the quinoid-imine ring

quinoid-imine ring but also of the two phenylene rings attached to it, and indeed the amine-bonded ring beyond that (which would be subject to two such sets of effects, one from either direction down the chain), since it has been shown in the case of other poly(*para*-linked phenylenes) that substituent and other effects at a given site can be detected up to three rings away<sup>20</sup>. It is also the case that, since phenylene ring flips are believed to be at least partially cooperative in the cases where more than one ring is involved, another effect of having the quinoid-imine locked with respect to its substituents would be to block, or at least considerably slow, the ring flipping of the phenylene groups attached to it. If this were the case then differences across the phenylene rings might be apparent in the spectra, and added conformational complexity would be expected because of the relative orientation of the skewed phenylene rings with respect to each other. This is illustrated in Figure 6, where *cis/trans* refers to the geometry of the phenylene rings in relation to the fixed quinoid-imine ring, and *syn/anti* refers to the relative orientations of the phenylene ring hydrogens.

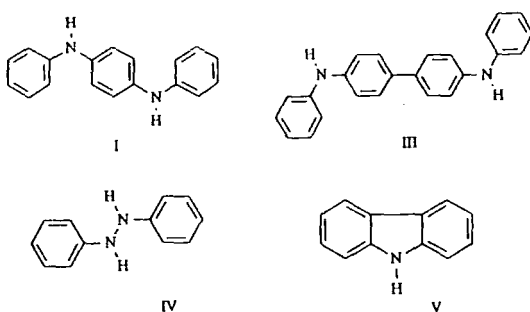
In terms of chain dynamics the introduction of quinoid-imine rings would be expected to have two important effects. First, it halves the number of rotational junctions in the chain, and secondly, it doubles the average length of stiff segment between the rotational junctions (stiff segments are now the doubly amine-bonded phenylene group (one ring), and the quinoid-imine group with its directly bonded phenylenes (three rings)—see Figure 1). These two effects would be expected to make the chain significantly stiffer and thus reduce the rate of conformation interchange. This is not to suggest that there is little or no motion in the chain; obviously motion is present otherwise relatively high-resolution spectra would not be obtained. Nevertheless, it seems that certain configurational properties of the chain may be relatively long-lived on the n.m.r. timescale, giving rise to distinct and characteristic signals.

It is not possible to predict how many peaks should be observed in the emeraldine base spectrum on the basis of the above since the size of some of the effects is not known (or indeed if they are present at all), but it is possible to be convinced that the greatest number of peaks that might be observed for such a structure is in excess of one hundred. Thus, the complexity of the observed spectrum is consistent with the postulated structure for emeraldine base.

Before leaving this subject, there are two additional points that should be made. First, the quantitative spectrum shows that one in four of the rings is a

quinoid-imine, but it cannot be claimed that it shows the quinoid-imine rings are entirely regularly distributed as every fourth ring on the chain. From the spectrum, it would seem that the majority of the rings follow this pattern, but the possibility of occasional disruptions (which would give rise to additional spectral complexity) cannot be ruled out. Secondly, minor peaks due to end-groups, minor substituents, solvent residues and the products of various possible side-reactions were identifiable in the spectrum of leucoemeraldine base and should therefore be expected in the emeraldine base spectrum but will be of too low an intensity for identification.

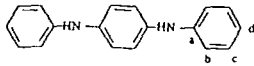
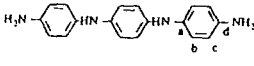
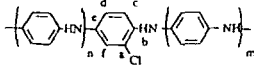
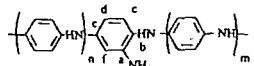
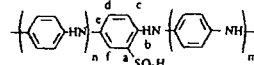
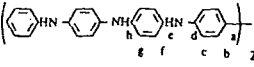
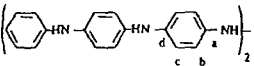
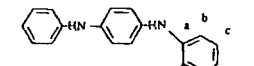
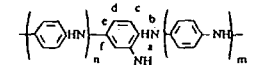
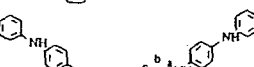
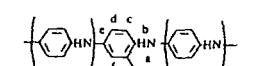
In order to try to evaluate some of the possible structures that might be giving rise to the minor peaks in the spectrum of leucoemeraldine base (Figure 3), the spectra of a series of model compounds were recorded. The model compounds were *N,N'*-diphenyl-*p*-phenylenediamine (I), *N,N'*-diphenylbenzidine (III), *N,N'*-diphenylhydrazine (IV) and carbazole (V):



These were used in conjunction with the measured chemical shift values for the major peaks in the leucoemeraldine base spectrum and published values for phenyl substituent effects<sup>21</sup> to calculate chemical shift values for postulated structures, the results of some of which are given in Table 1. While the quoted values are the result of a fairly crude procedure and should not be regarded as accurate to better than  $\pm 1$  ppm, they do serve to make some interesting points when these calculated shifts are compared with the minor peaks observed in the spectrum of leucoemeraldine base (Figure 3). First, the presence of both types of end-groups (phenyl-capped and amine-capped) is consistent with the observed spectrum, as are chloride and sulphonate as substituents on the chain. The presence of benzidine and diphenylhydrazine type structures in the chain cannot be excluded, neither can the presence of *ortho*-substituted (rather than *para*-substituted) rings in the chain and carbon-carbon bonded branching points, but branching points due to amine-bonded rings seem unlikely, as do carbazole type structures in the chain and amine ring substituents, since no peaks are observed below 110 ppm. More sophisticated models will be required before definite assignments of the minor peaks can be made.

Finally, it was observed during the course of these investigations that the rate of dissolution of the emeraldine base in the solvent system was quite slow even following ultrasonic dispersion. Freshly prepared samples were of relatively low viscosity, but gave low signal-to-noise ratios in the spectra and fewer discernible features than in the normal emeraldine base spectrum presented in Figure 2. An example of these effects can be seen in Figure 4, where both spectra were obtained within

Table 1 Calculated shifts for postulated structures

Structure	Shifts (ppm)	Comments
	a = 144.9 b = 115.1 c = 129.1 d = 118.3	Observed
	a = 134.9 b = 115.9 c = 116.9 d = 136.5	Calculated for $\text{NH}_2$ substituent <sup>21</sup>
	a = 124.1 b = 137.8 c = 119.2 d = 115.9 e = 138.8 f = 118.2	Calculated for Cl substituent <sup>21</sup>
	a = 136.0 b = 124.0 c = 118.6 d = 107.8 e = 138.2 f = 104.4	Calculated for $\text{NH}_2$ substituent <sup>21</sup>
	a = 132.3 b = 134.7 c = 118.6 d = 121.1 e = 138.2 f = 115.1	Calculated for $\text{SO}_3\text{H}$ substituent <sup>21</sup>
	a = 131.5 b = 126.2 c = 116.7 d = 142.0 e = 133.2 f = 118.5 g = 115.8 h = 136.0	Calculated for substituent derived from (I)
	a = 142.4 b = 112.5 c = 115.4 d = 133.7	Calculated for substituent derived from (I)
	a = 131.5 b = 115.7 c = 118.9	Calculated for substituent derived from (I)
	a = 134.2 b = 124.0 c = 118.4 d = 107.6 e = 138.0 f = 104.4	Calculated for substituent derived from (I)
	a = 134.9 b = 107.7 c = 123.0 d = 129.5 e = 110.7 f = 112.1	Calculated for substituent derived from (I)
	a = 131.5 b = 134.5 c = 116.7 d = 116.6 e = 136.3 f = 114.9	Calculated for substituent derived from (III)

a few hours of sample preparation. Over a period of about 12 h, the viscosity of the sample increased, but the number of resolvable features in the spectra increased also. After this time the samples apparently remained stable for several days. We interpret this as being due to

the slow dissolution of material originally present mainly as finely dispersed solid, so that at short times after sample preparation the concentration of polymer actually in solution would be relatively low (low viscosity and low signal-to-noise ratio), but chain mobility for the material in solution would be relatively high, leading to rapid conformational interchange. As the concentration of material in solution increased, the viscosity and signal-to-noise ratio would increase also, but the rate of conformational interchange would decrease, giving rise to a greater number of distinct features in the spectrum. We report this here because we believe that it may be significant to other workers in, for example, the production of solvent-cast films.

## CONCLUSIONS

We have shown that it is possible to obtain high-quality solution-state  $^{13}\text{C}$  n.m.r. spectra of polyanilines, and that the information content of these spectra is very much greater than that of solid-state spectra. We have shown that the vast majority (>95%) of the material present in a sample of leucoemeraldine base has the postulated structure (*para*-substituted phenylene rings linked by amine groups). We have shown that emeraldine base has the same skeletal form as leucoemeraldine base (*para*-substituted six-membered rings linked by nitrogens), and that the observed spectrum is consistent with the postulated structure despite its considerable complexity. It is also clear from the data that there are defects in the structure, and although these cannot be identified with certainty they may be present at a concentration of up to 5 mol% of the repeat units. The evidence does not favour branching at amine-bonded ring sites but does not exclude branching at carbon-carbon bonded ring sites, or trisubstituted nitrogens. End-groups form part of the 'defect' resonances, but do not account for all of them.

## ACKNOWLEDGEMENTS

We would like to thank Mrs J. M. Say for technical assistance.

## REFERENCES

- 1 Runge, F. F. *Ann. Phys. (Lpz.)* 1834, 31, 513
- 2 Fritzsche, J. *J. Prakt. Chem.* 1840, 20, 453; 1843, 28, 198
- 3 Willstatter, R. and Moore, C. W. *Chem. Ber.* 1907, 40, 2665
- 4 Green, A. G. and Woodhead, A. E. *J. Chem. Soc.* 1910, 97, 2388; 1912, 101, 1117
- 5 Furukawa, Y., Ueda, F., Hyodo, Y., Harada, I., Nakajima, T. and Kawagoe, T. *Macromolecules* 1988, 21, 1297
- 6 Sandberg, M. and Hjertberg, T. *Synth. Met.* 1989, 29, E257
- 7 Shacklette, L. W., Wolf, J. F., Gould, S. and Baughman, R. H. *J. Chem. Phys.* 1988, 88, 3955
- 8 Wu, F. L., Wudl, F., Nowak, M. and Heeger, A. J. *J. Am. Chem. Soc.* 1986, 108, 8311
- 9 Wudl, F., Angus, R. O., Lu, F. L., Allemand, P. L., Vachon, D. J., Nowak, M., Liu, Z. X. and Heeger, A. J. *J. Am. Chem. Soc.* 1987, 109, 3677
- 10 Devreux, F., Bidan, G., Syed, A. A. and Tsintavis, C. *J. Physique* 1985, 46, 1595
- 11 Hjertberg, T., Salaneck, W. R., Lundstrom, I., Somasiri, N. L. D. and Macdiarmid, A. G. *J. Polym. Sci., Polym. Lett. Edn.* 1985, 23, 503
- 12 Menardo, C., Nechtschein, M., Rousseau, A., Travers, J. P. and Hany, P. *Synth. Met.* 1988, 25, 311

*Solution-state <sup>13</sup>C n.m.r. of polyaniline: A. M. Kenwright et al.*

- |    |   |    |   |
|----|---|----|---|
| 13 | Hagiwara, T., Yamaura, M. and Iwata, K. <i>Synth. Met.</i> 1988, 26, 195  | 17 | Bendall, M. R. and Pegg, D. T. <i>J. Magn. Res.</i> 1983, 53, 272   |
| 14 | Kaplan, S., Conwell, E. M., Richter, A. F. and Macdiarmid, A. G. <i>J. Am. Chem. Soc.</i> 1988, 110, 7467   | 18 | Spiess, H. W. <i>Colloid Polym. Sci.</i> 1983, 261, 193   |
| 15 | Monkman, A. P. and Adams, P. <i>Synth. Met.</i> 1991, 41-43, 891  | 19 | Schaefer, J., Stejskal, E. O., McKay, R. A. and Dixon, W. T. <i>Macromolecules</i> 1984, 17, 1479               |
| 16 | Richter, A. F., Ray, A., Ramanathan, K. V., Manohar, S. K., Furst, G. T., Opella, S. J., Macdiarmid, A. G. and Epstein, A. J. <i>Synth. Met.</i> 1989, 29, E243 | 20 | Abraham, R. J., Haworth, I. S., Bunn, A. and Hearmon, R. A. <i>Polymer</i> 1990, 31, 728 and references therein |
|    |   | 21 | Kalinowski, H.-O., Berger, S. and Braun, S. 'Carbon-13 NMR Spectroscopy', Wiley, Chichester, 1988, p. 313       |

in 'Electronic Properties of Polymers', eds.  
M Kojmany, M Melnyk + S Roth, Springer Verlag  
Series in Solid State Sciences, 107 (1992) p 255.

Properties of solution cast films of polyaniline and the effects of orientation

A. P. Monkman, F. Hampson and A. J. Milton

Molecular Electronics Group,  
School of Engineering and Applied Science,  
University of Durham, South Road, Durham, DH1 3LE, U.K.

**Abstract.** The electronic properties of free standing films of polyaniline (PANi) and the subsequent effects of orientation upon the films will be discussed. Film conductivity of the order  $70 \text{ Scm}^{-1}$  unoriented, and up to  $350 \text{ Scm}^{-1}$  in the oriented state have been measured along with anisotropies up to 24:1. To examine the nature of the charge carriers in these films we have employed thermoelectric measurements. These reveal room temperature values of  $S = -18.3 \text{ uVK}^{-1}$ , and that  $S \propto T^{0.7}$ . These results will be compared to the two widely accepted theories for conduction mechanisms within conducting polymers, namely variable - range hopping and metallic conductivity.

## 1. Introduction

We have spent a great deal of time optimising the chemical synthesis and handling procedures during the preparation of polyaniline (PANi). In order to understand the physical phenomena involved in the mechanisms of conduction in conductive polymers it is important to produce repeatable samples of high integrity with aligned polymer chains.

It has been shown for polyacetylene [1,2] and polyparaphenylene vinylene [3] that stretch alignment of the precursor polymer before conversion to the conjugated form leads to vast improvements in conductivity and mechanical properties. In these oriented materials, high degrees of anisotropy in physical properties have also been measured, such as conductivity anisotropy ratios greater than 1000:1 in polyacetylene [4] and highly anisotropic optical absorption [5].

As can be seen, it would be very desirable to orient films of polyaniline (PANi) in such a way as to increase the measured conductivity and, with a high degree of order between chains, probe the true conduction mechanism and optical absorption properties of the polymer. MacDiarmid *et al.* have recently shown that PANi is moderately soluble in N-methyl-2-pyrrolidone (NMP), a solvent commonly used to dissolve azo dyes [6] thus, leading to a route to produce free-standing PANi films via casting films of chemically prepared PANi from NMP. Subsequent stretch alignment by the application of uniaxial stress at elevated temperatures forms films of high electrical conductivity, up to maximum  $350 \text{ Scm}^{-1}$  and anisotropies in both conductivity and optical reflection spectra [7,8]. This shows that the chains are being aligned and that the processes of energy transfer parallel and perpendicular to chain alignment directions have at least different energy barriers, if not different mechanisms. Throughout the chemical preparation of our samples, due care and attention is taken when handling materials in case small amounts of benzidine are present. To produce the films the chemically prepared PANi powder is washed

several times in various solvents. This should remove any benzidine present in the material.

In addition to the conductivity measurements on our films we have further characterised PANi films using thermopower measurements. These measurements yield information about carrier sign and the nature of the density of states close to the Fermi level.

## 2. Experimental Section

Full details of sample preparation can be found elsewhere [7]. Briefly, emeraldine salt was synthesised via the oxidative coupling of aniline. The salt, after careful washing, was neutralised with ammonia. The resulting base could then be dissolved in N-methyl-pyrrolidone (NMP) and subsequent films could be cast from this solution. After removal of NMP, the films could be removed from the substrate. These films could further be processed by the application of uniaxial stress, to produce oriented films showing a good degree of anisotropy [8].

Electrical measurements were made on samples using the standard 4 point probe Montgomery method [9] employing Keithley 196 DVM, 619 electrometer and a 220 current source. Thermopower measurements were made on a system based around an Oxford Instruments liquid nitrogen cryostat and temperature controller. Sample heaters were driven by a high current ramp generator (in house) and sample voltages measured (after amplification) on Keithley 195 and 196 DVM's. The electrical circuit for measuring thermopower can be seen in Fig. 1. For such an experimental system it can be seen that

$$v_s = A. [S(T_1 - T_2) + S_{cu} (T_{ref} - T_1) + S_{cu} (T_2 - T_{ref})]$$

$$\therefore v_s = A [(S - S_{cu}) \Delta T] \quad \text{where } \Delta T = T_1 - T_2$$

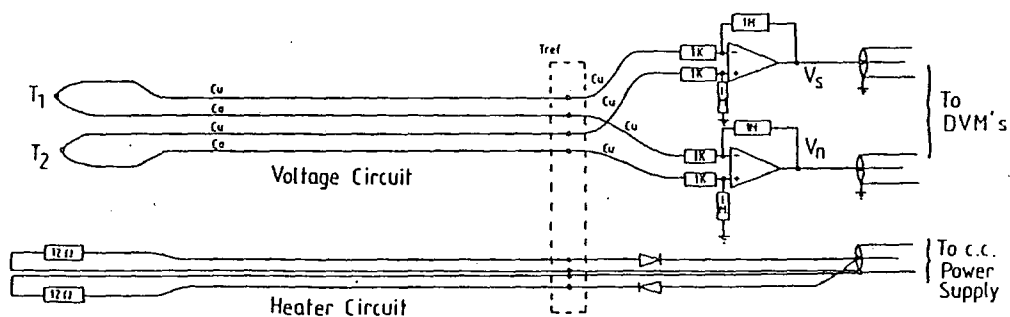


Figure 1 : Electronic circuit diagram for thermopower measurements  $T_1$  and  $T_2$  are the temperatures at the sample ( $T_1 - T_2 =$  thermal gradient). Cu = copper wire, Co = constantine wire and  $T_{ref}$  = reference temperature.

similarly  $V_n = A[(S - S_{co}) \Delta T]$

thus  $S = (S_{cu} - S_{co}) \cdot \chi + S_{cu}$  with  $\chi = \frac{S - S_{cu}}{S_{cu} - S_{co}}$

where  $S =$  thermopower of sample.

Thus the thermoelectric power of PANi,  $S$ , can be measured with minimum electrical (and hence thermal) contact. Thermopowers at specific temperatures ranging from 300 - 77°K where measured using  $\Delta T = 1^\circ K$ . This method also takes into account the temperature dependence of the thermopower of the contact wires. In all cases, temperature dependent results are normalised such that this factor is removed, yielding true values of the thermopower of PANi at any temperature, and hence the correct temperature dependence.

### 3. Results

As previously reported [8] the electrical conductivity of as "prepared" PANi films is an order of magnitude higher than that of pressed pellet samples, being typically 70-80 S cm<sup>-1</sup>. This figure is repeatable if care and control is exercised in the

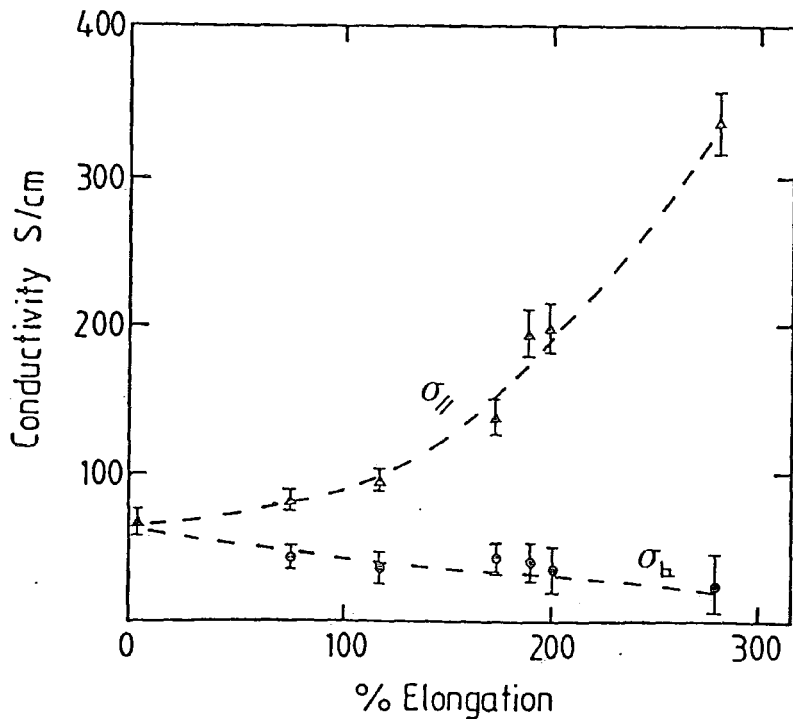


Figure 2 : Dependence of the measured conductivity of PANi as a function of elongation ratio  $\sigma_{||}$  is the conductivity measured parallel to the stretch direction,  $\sigma_{\perp}$  the conductivity perpendicular to the stretch direction.

chemical synthesis of the polymer. After stretching the samples we find a further increase in the conductivity. At present the maximum we have been able to attain is  $350 \text{ Scm}^{-1}$  in the parallel direction. Figure 2 shows the behaviour of the conductivity in both the parallel and perpendicular direction as a function of stretch ratio. As can be seen the maximum anisotropy ratio so far attained is 24:1.

As previously reported [8], the maximum stretch ratio attained is 650%, however we have found that (i) reproducibility of results above stretch ratios of ca 350-400% is poor, and (ii) doping of such highly stretched materials becomes difficult leading to a concomitant low value of conductivity.

The thermoelectric properties of a highly conducting unoriented film  $\sigma_{RT} \sim 80 \text{ Scm}^{-1}$ , can be seen in Fig. 3. Here we find that  $S_{RT} = -18.3 \text{ uV/K}$ , and a temperature dependence of thermopower from 300K to 77K, which shows a non linear behaviour, as would be expected for metallic conduction.

#### 4. Discussion

From our previous work [7,8] and data presented here, it can clearly be seen that PANi, in the form of free standing cast films, made from chemically prepared PANi, is a much better material than previously examined i.e., previous results on electrochemically prepared material [10,11] can be put into their proper context, as representing data on short chain polymer. The conductivity of the as cast films is an order of magnitude higher than that typically reported for previous PANi and in the case of the oriented materials another order of magnitude increase is achieved. These results, along with optical data [8], indicate a far higher degree of conjugation, commensurate with either increased chain length or a higher degree of chain perfection and more probably both. With orientation of the films, one begins to observe macroscopic anisotropy, in both electrical and optical properties.

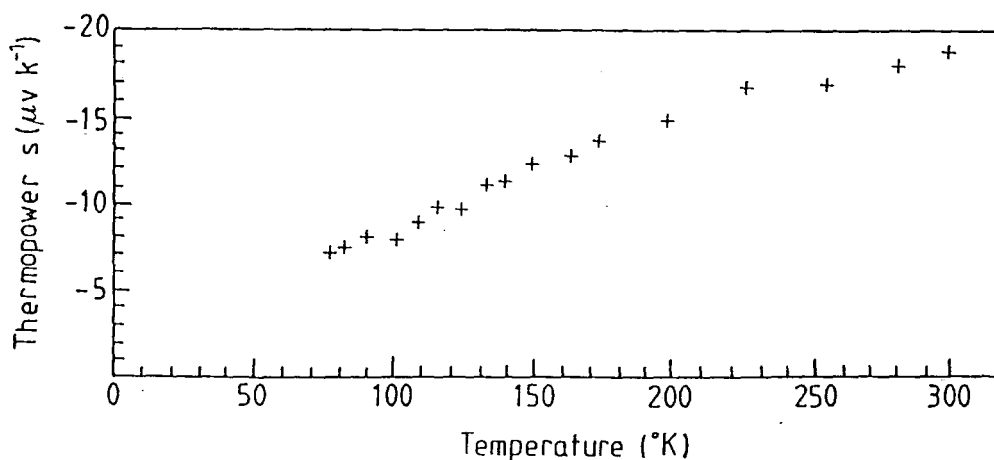


Figure 3 : The temperature dependence of the thermopower of a polyaniline film doped with HCl to a conductivity of  $80 \text{ Scm}^{-1}$ .

Maximum observed electrical anisotropy of 24:1 at an elongation ratio of 350% shows that interchain hopping must have a low probability in PANi, suggesting a very small interchain overlap integral. However, one should also note that at higher elongation ratios, it becomes progressively more difficult to dope the films. This can be ascribed as either being due to an increased crystallinity of the material [12] or this may also be due to an increased degree of H-bonding between polymer chains. The role of H-bonding in PANi is little known at present, but must be a key ingredient to the system as a whole. One of the reasons why PANi is intractable in all but NMP (and a few related solvents) is the strength of the H-bonding between chains, only NMP is a stronger H-bonder than PANi so it can break the interchain bonds and form NMP-PANi H-bonds, and thus "solvate" the chains. It should also be noted that in the doped form, the delocalisation of the nitrogen lone pair charge may lead to increased H-bonding. This would lead to surface doping of the films instead of homogeneous bulk doping.

The thermopower data for the cast films is consistent for that previously reported by Shacklette *et al* [13]. At room temperature, the value of thermopower is -18.3  $\mu\text{V}/\text{K}$ . One can chose two scenarios to describe transport in PANi either a variable - range hopping picture [14] where

$$S = \frac{k^2}{2e} (T_0 T)^{1/2} \left( \frac{d \ln N(E)}{dE} \right)_{E-E_F}$$

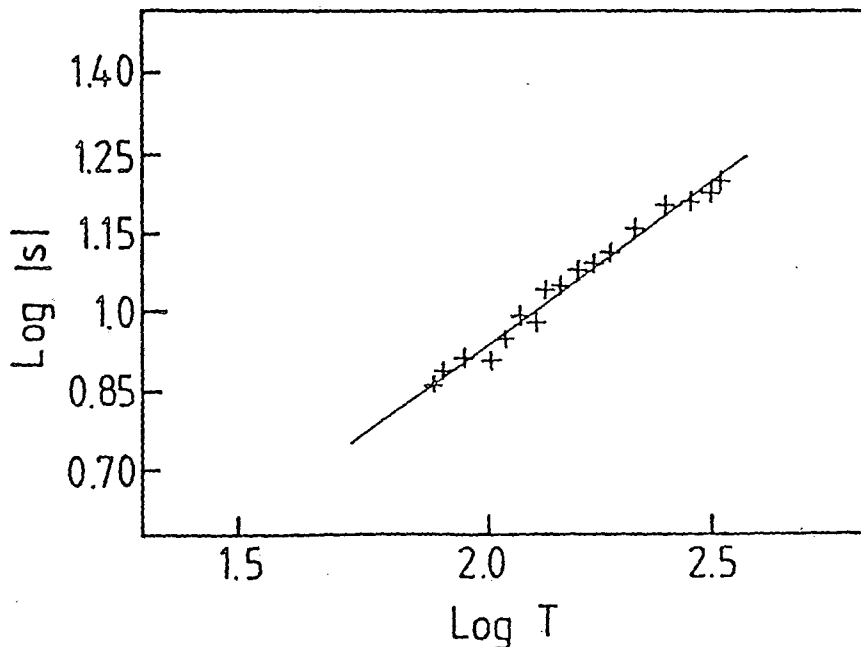


Figure 4: Fit of thermopower data. Best straight line yields a  $T^{0.7}$  dependence.



or as a metallic system where

$$S = \frac{\pi^2}{3} \frac{k^2 T}{e} \left( \frac{\partial \ln \sigma(E)}{\partial E} \right)_{E=E_F}$$

where  $\sigma(E) \propto (N(E))^2$ .

In both cases the negative sign of the thermopower would imply negative charge carriers, i.e. electrons, not holes. However, in the VRH case,  $S \propto T$  whereas in the metallic case  $S \propto T$ . Figure 4 shows a log plot of  $S$  vs  $T$ . The best fit to the data occurs with  $S \propto T^{0.7}$  midway between the two.

Further from our results, it can be seen that the experimental data can be extrapolated to  $S = 0$  at  $T = 0$ , and that  $S$  remains small and negative down to 77K there is no sign reversal. The small magnitude of  $S$  implies that the carriers giving rise to conduction (NB. thermopower is a measure of conductivity at zero applied field), come from states only a few kT from the Fermi level, implying a density of states at or close to the Fermi level. Similarly since  $S$  is non zero, the density of states at the Fermi level must be non stationary. From this one has to deduce that conduction is by carriers in extended states. As pointed out by Mott [14], in this type of regime the sign of  $S$  is denoted by the behaviour of the density of states at the Fermi level, e.g. if  $N(E)$  is decreasing around  $E_F$ ,  $S$  will be negative. However, the data is still not totally consistent with this metallic picture, as  $S \propto T^{0.7}$ , and not linearly dependent on  $T$ . Such behaviour is seen in Iodine doped polyacetylene, whereas when  $\text{AsF}_5$  is used as a dopant, there is a true linear  $T$  dependence [15]. One should note in the polyacetylene case that the  $\text{I}_3$  samples had a  $\sigma_{RT} = 40 \text{ Scm}^{-1}$  whereas the  $\text{AsF}_5$  samples were an order of magnitude higher, at  $640 \text{ Scm}^{-1}$ . Thus one could deduce that our PANi samples are still not conducting enough or chemically "defect" free enough to show true metallic behaviour, and that the conduction mechanism, even in our aligned samples is still dominated by hopping, noting that the localised states must be within a few kT of the Fermi level. The negative sign of the carriers being explained by the previous model proposed by Shacklette et al [13].

## 5. Summary

To conclude, processing PANi into films yields improvements to the mechanical and physical properties of the polymer. We have successfully shown that these films can be oriented to some degree, and that conductivity can be increased to  $350 \text{ Scm}^{-1}$ , with an electrical anisotropy of 24:1. We have found that in these oriented films, doping becomes more difficult, due to increased sample crystallinity and/or increased H-bonding. From thermoelectric power measurements, we have found that  $S_{RT} = -18.3 \text{ uVK}^{-1}$ . This value indicates a metallic type of transport by negative charge carriers, i.e. electrons. However, the temperature dependence of the thermopower is not linear, rather  $S \propto T^{0.7}$  suggestive of a more VRH-like transport. This contradiction may imply that at present our PANi samples are at the border line between conduction in extended states and conduction via hopping, perhaps a sign of remaining chain imperfections, or that conduction in PANi is truly VRH and that in the oriented samples the dimensionality is less than 3. Thus more work is still required.

## References

1. H. Naarmann and N. Theopilou, *Synth. Met.*, **22**, (1987), 1.
2. K. Akagi, M. Shimomwa and Y. Tanabe, *Synth. Met.*, **28**, (1989), D1.
3. D. D. C. Bradley, *J. Phys. D : Appl. Phys.*, **20**, (1987), 1389.
4. H. Naarmann in "Conjugated Polymeric Materials", ed. J. L. Bredas and R. R. Chance, NATO ASI series E. Applied Physics, Vol. 182, Kulwer, 1990, p11.
5. G. Leising, *Synth. Met.*, **28**, (1989), D215.
6. M. Anegelopoulos, G. E. Asturias, S. P. Emer, A. Ray, E. M. Scherr, A. G. MacDiarmid, M. Akhtar, Z. Kiss and A. J. Epstein, *Mol. Cryst. Liq. Cryst.*, **160**, (1988), 151.
7. A. P. Monkman and P. Adams, *Synth. Met.*, **40**, (1991), p87.
8. A. P. Monkman and P. Adams, *Solid State Comm.*, **78**, (1991), 29.
9. M. C. Montgomery, *J. Appl. Phys.*, **42**, (1971), 2971.
10. A. P. Monkman in "Conjugated Polymeric Materials", ed. J. L. Bredas and R. R. Chance, NATO ASI series E : Applied Physics, vol. 182, Kulwer, 1990, p273.
11. F. Wudl, R. O. Angus Jr., F. L. Lu, P. M. Allemand, D. J. Jackson, M. Nowak, Z. Y. Lui and A. J. Heeger, *J. Am. Chem. Soc.*, **109**, (1987), 3677.
12. J. Pouget, M. E. Jozefowicz, A. J. Epstein, X. Tang and A. G. MacDiarmid, *Macromolecules* **24** (1991) 779.
13. Y. W. Park, Y. S. Lee, C. Park, L. W. Shacklette, R. H. Baughman, *Solid State Comm.* **63** (1987) 1063.
14. *Electronic Processes in Non Crystalline Materials* by N. F. Mott and E. A. Davies, 2nd Edition Clarendon Press, Oxford, 1979.
15. Y. W. Park, A. Denenstein, C. K. Chiang, A. J. Heeger and A. G. MacDiarmid, *Solid State Comm.*, **29**, (1979), 747.

# A comparative study of polyaniline films using thermal analyses and IR spectroscopy

A J Milton and A P Monkman

Organic Electro-active Materials Research Group, Department of Physics,  
University of Durham, South Road, Durham DH1 3LE, UK

Received 5 February 1993, in final form 7 June 1993

**Abstract.** We have used dynamic mechanical and dielectric thermal analyses together with infrared spectroscopy to identify molecular motions in polyaniline films cast from emeraldine base powder dissolved in the solvent N-methyl-2-pyrrolidinone (NMP). These relaxations include a librational ring motion at around  $-80^{\circ}\text{C}$  and a glass transition ( $T_g$ ) centred at  $100^{\circ}\text{C}$ . We have also observed a permanent film hardening process at around  $180^{\circ}\text{C}$  which is ascribed to polymer chain crosslinking, both physical (associated with chain entanglements) and more importantly chemical (chain–chain chemical bonding). Chemical crosslinking can be further identified with chain defects and residual impurities in the polymeric material. The importance of precise control of polyaniline synthesis and processing is therefore strongly emphasised. These results have clear implications for the thermal orientation process in polyaniline.

## 1. Introduction

Dynamic mechanical thermal analysis (DMTA) and dielectric thermal analysis (DETA) are both forms of relaxation spectroscopy which are well suited to the study of polymeric materials [1]. In the mechanical technique essentially all structural transitions and changes in molecular motions are detected, but in the dielectric case only those relaxations involving dipolar or charged species are detected. Although both excitation frequency and temperature can be altered for these techniques, the latter is the major variable. Hence samples are usually thermally scanned at a discrete frequency—1 Hz and 1 kHz being standard for DMTA and DETA respectively. A limited frequency range is, however, required for the determination of activation energies. The information gained from these techniques is particularly invaluable in the case of polyaniline since a fundamental property of this material, when in as-cast film form, is the ability to orient the polymer chains at elevated temperatures.

Additional structural detail can be observed using infrared (IR) spectroscopy. Absorption bands are seen corresponding to vibrations of specific bonds within the material structure. By following the band changes with changing temperature, information can be obtained which helps to identify further the origin of the observed mechanical/dielectric relaxations in polyaniline films. The DMTA measurements have been briefly reported in a

previous paper [2], but are discussed in more detail here in conjunction with DETA and IR spectroscopy.

Implicit in all three of these techniques and indeed in any experiment is the precise chemical structure of the sample material being studied. For polymeric materials such as polyaniline this not only includes molecular weight, but also chain defects, chain branching/crosslinking and impurities, as well as effects due to solvents. Therefore, details of synthesis and processing become of the utmost importance and always need to be reported. In the field of polyaniline research this has not always been the case, and the wide range of varied and often conflicting experimental results are testament to this argument.

## 2. Experimental section

Polyaniline was chemically synthesized in the emeraldine base form (figure 1), by our usual multi-step addition of the oxidant ammonium persulphate to an aqueous solution of aniline hydrochloride [3]. The reaction was carried out at room temperature, stirred for 24 h, filtered and then washed with two 100 ml amounts of water. The filtered material was deprotonated in aqueous ammonia solution for a minimum of 4 h, refiltered and washed with  $2 \times 100$  ml of water and then washed with enough propanol so as to remove all low molecular weight material. The product was then dried under vacuum at  $70^{\circ}\text{C}$

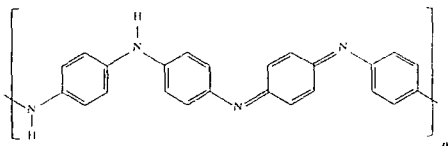


Figure 1. Idealized repeat unit for emeraldine base.

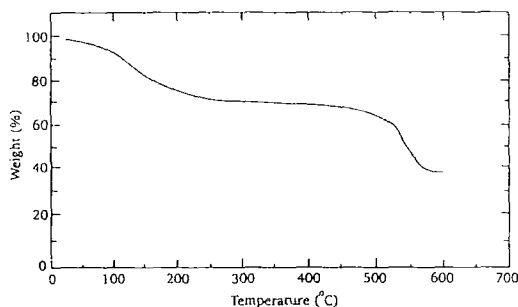


Figure 2. TGA thermogram (Stanton-Redcroft TG-770 thermobalance) of an as-cast film under nitrogen purge using a heating rate of  $20^{\circ}\text{C min}^{-1}$ . The weight loss ( $\sim 25\%$ ) up to  $\sim 250^{\circ}\text{C}$  can be assigned to NMP solvent.

for 24 h to give a dark purple powder, emeraldine base, with a typical yield of 80–85%.

The molecular weight of this base polymer was determined as approximately  $3 \times 10^4$  by gel permeation chromatography using an NMP/LiCl solution and polyvinylpyridine standards [4]. Elemental analysis revealed a carbon, nitrogen and hydrogen content consistent with the emeraldine base repeat unit (C 75.97%, N 14.56%, H 4.99%), but with small amounts of residual sulphur (0.38 wt%) and chlorine (0.50 wt%). The remaining 3.60 wt% was ascribed to oxygen. Some of these impurities are due to free ions which can be removed by further washing of the powder. However, some residues still remain even after extensive purification and hence must be associated with defect structures in the idealized chain repeat unit. Indeed sulphonate and chloride ring substituents have been identified in emeraldine base through NMR studies here in our laboratory at Durham [5].

Free standing films were cast from a homogeneous, 8 wt% solution of emeraldine base dissolved in NMP. Excess solvent was removed at  $70^{\circ}\text{C}$  under vacuum until the samples were dry. These samples were then peeled from the substrate to give as-cast films with a typical NMP content of 25% as measured by thermogravimetric analysis (TGA) (see figure 2).

DMTA scans were obtained on a Polymer Laboratories Mk II instrument operating in tensile geometry. The following conditions were employed for standard (1 Hz) and variable (0.3, 3 Hz) frequencies: static force, 1 N; strain,  $32 \mu\text{m}$  peak to peak displacement; thermal scan,  $-130$  to  $300^{\circ}\text{C}$ ; heating rate,  $3^{\circ}\text{C min}^{-1}$ . Sample dimensions, typically  $12 \times 5 \times 0.06 \text{ mm}$ , were kept approximately constant throughout so as to ensure reproducibility. A reducing force mode was engaged which

adjusts the static force during sample relaxation so as to minimize creep. The results are shown as plots of log storage modulus  $\log E'$  (Pa) and mechanical damping ( $\tan \delta$ ) against temperature. The DMTA was operated under external computer control using a Compaq 386 microcomputer.

DETA measurements were also made on a Polymer Laboratories instrument. Samples, in the form of flat circular discs of 35 mm diameter, were sandwiched between two metal electrodes. An excitation frequency of 1 kHz was used with the same temperature range and heating rate as for DMTA experiments. Thermograms are shown as plots of permittivity  $\epsilon$ , and dielectric damping  $\tan \delta$  against temperature. Similarly, the DETA was under computer control. Comprehensive details of both the DMTA and DETA techniques are given in the literature [1].

IR data were recorded on a Perkin-Elmer 580B spectrophotometer operating at  $3 \text{ cm}^{-1}$  resolution under a dry air purge. Spectra of free standing films were taken in transmission using samples of less than  $20 \mu\text{m}$  in thickness. Reflectance data were recorded from a thin ( $\approx 5 \mu\text{m}$ ) homogeneous film cast onto an aluminium coated glass slide. By coupling a resistive heater to the reverse side of the slide, spectra could be taken at elevated temperatures up to  $250^{\circ}\text{C}$ .

### 3. Results and discussion

#### 3.1. Dynamic mechanical thermal analysis (DMTA)

A typical thermal spectrum of an as-cast emeraldine base film is shown in figure 3. The  $\tan \delta$  spectrum is dominated by an extremely broad relaxation feature incorporating two transitions, a peak at  $180^{\circ}\text{C}$  and a shoulder at approximately  $100^{\circ}\text{C}$ . From TGA analysis (reported in section 2) we can associate these transitions with loss of NMP solvent molecules. The  $100^{\circ}\text{C}$  transition coincides with a decrease in storage modulus from  $10^9$  to  $10^7 \text{ Pa}$  and can be assigned to a film softening or glass ( $T_g$ ) transition. Such a glass-rubber transition can be thought of, using molecular relaxation theory, as cooperative thermal motion of individual chain segments along the polymer backbone. It is at temperatures around  $T_g$  that films can be stretch aligned with preferential orientation of chains [6].

The residual 25% NMP is known to act as a 'plasticizer', with the  $T_g$  transition shifting to higher temperatures with decreasing weight fraction of solvent [7]. However, the main constraint for a plasticizer is permanence. In this respect NMP is very poor as it is thermally removed during the  $T_g$  transition. The width of the relaxation feature reflects the plasticization criterion [8]; since it is extremely broad in this case, polymer and solvent do not form a single solid phase. NMP remains essentially in the liquid state and is thus more volatile than the polyaniline component. In fact, it is this solvent volatility which is responsible for the glass transition. The 'spaces' produced by removal of NMP molecules

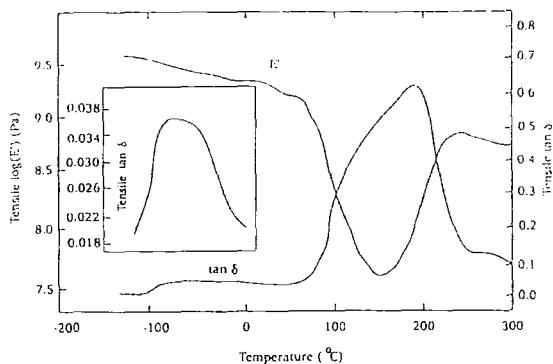


Figure 3. DMTA thermogram (1 Hz) of an as-cast film. The inset is an expansion of the  $\tan \delta$  curve.

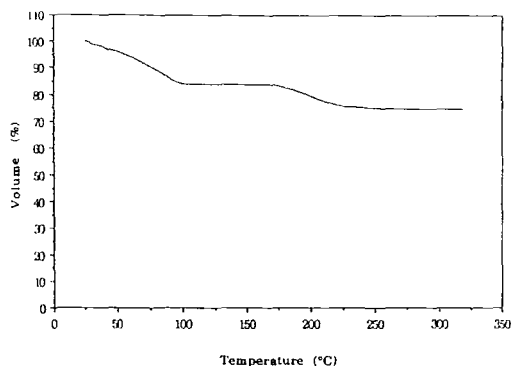


Figure 4. Dilatometric collapse in volume with temperature of an as-cast film. Data were recorded on a Stanton–Redcroft 790 series thermomechanical analysis instrument under nitrogen purge using a heating rate of  $20^\circ\text{C min}^{-1}$ .

act as a free volume around the chains, giving them rotational freedom.

However, this free volume exists for only a finite time. As the temperature rises beyond  $T_g$  the storage modulus increases to  $10^9$  Pa and the sample hardens. This process is characterized by the peak in  $\tan \delta$  at  $180^\circ\text{C}$ . Hardening occurs because sample compaction reduces the free volume to such an extent that chains become extensively entangled (i.e. physical crosslinking). The collapse in sample dimensions has been observed using thermodilatometric analysis and is shown in figure 4.

It seems clear that hardening involves a high degree of chain entanglements, but several pieces of evidence indicate that a chemical crosslinking process (involving bonding between chains) also occurs. Firstly, both chemical and physical crosslinks are indistinguishable on a short timescale [9], but if only the former are present the material should soften with time. However, an isothermal scan at  $180^\circ\text{C}$  for 1 h (figure 5) showed no such storage modulus decrease. Secondly, a similar rise in modulus due to hardening is exhibited during the cure of epoxy resins [10] and other synthetic polymers [1]. Furthermore, polyaniline samples heated through this hardening regime are totally intractable in NMP whereas as-cast samples are appreciably re-soluble.

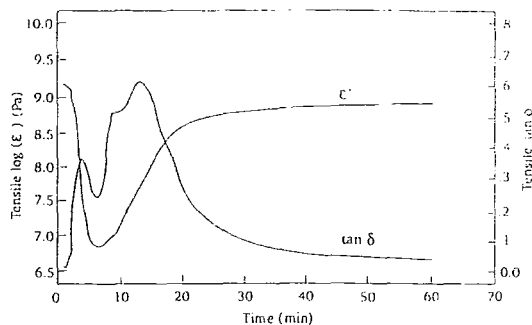


Figure 5. Isothermal DMTA scan, 1 h at  $180^\circ\text{C}$ , for an as-cast film.

The nature of the possible chemical crosslinking processes is not evident from these data—this question is addressed using IR spectroscopy. What is clear is that to avoid crosslinking, samples must be thermally processed below the  $180^\circ\text{C}$  transition temperature. The hardening reaction is highly detrimental to the physical properties of the material. For example, a crosslinked film is extremely brittle and thus mechanically weak, and cannot be stretch aligned. Added to this its conductivity when doped (1 M HCl) is approximately one hundred times smaller than the typical  $60\text{ S cm}^{-1}$  of an as-cast doped film.

Another feature of the results for as-cast films is the presence of an asymmetric relaxation at approximately  $-80^\circ\text{C}$  as shown in the inset of figure 3. This transition can be tentatively assigned to phenyl ring twisting. This type of motion is known to play a key role in the electronic properties of polyaniline [11, 12]. Using transition state theory the activation energy  $\Delta H^*$  of this peak is estimated to be  $11\text{ kcal mol}^{-1}$ , derived from peak positions at three frequencies (0.3, 1, 3 Hz). A similar ring twisting motion is observed for polyethylene terephthalate [1] where  $\Delta H^* = 17\text{ kcal mol}^{-1}$  (this relaxation also has a contribution from an ester group).

Further molecular information has been gained from the rescanning of an as-cast film. Such a sample, having been heated to  $300^\circ\text{C}$ , is crosslinked, but is also solvent free. Hence the observed transitions can only be attributed to the polymeric material with no effects due to NMP. Such a thermogram is shown in figure 6. This spectrum was then reproducible on subsequent thermal scanning.

The most obvious difference between the re-scan and the initial scan is the loss of both the  $T_g$  transition at  $100^\circ\text{C}$  and the film hardening transition at  $180^\circ\text{C}$ . This is easily explained through the absence of NMP. However, three damping peaks are observed. Firstly, the  $-80^\circ\text{C}$  transition is still present with the same magnitude in  $\tan \delta$  as measured for the as-cast film, although more symmetric in shape. Furthermore, this relaxation has also been observed in stretch aligned and doped samples. Secondly, a new damping peak is seen in  $\tan \delta$  at approximately  $85^\circ\text{C}$ . Its origin is difficult to assess using only these data but will be discussed in more detail in the following sections.

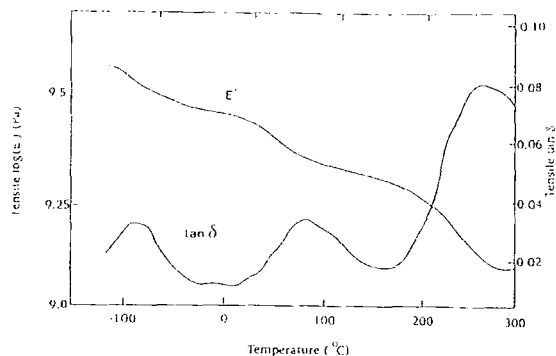


Figure 6. Re-scan (1 Hz) of DMTA data for figure 3.

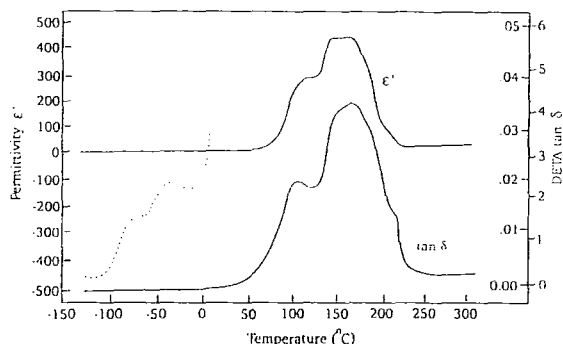


Figure 7. DETA thermogram (1 kHz) of an as-cast film. The dotted curve is an expansion of the  $\tan \delta$  plot corresponding to the inner y axis.

Lastly, a high-temperature transition is observed at approximately 265°C. This can be ascribed to the  $T_g$  transition of the crosslinked, polymeric material. The large increase in temperature over the as-cast material for this peak position is predicted from the plasticization effect of NMP. Also, the magnitude of the peak in  $\tan \delta$  must be noticed. Relative to figure 3, it has been reduced by a factor of nearly ten (with only a minor decrease in modulus). This is because polymer chains are now crosslinked and so conformational motion of the backbone is severely suppressed. Similar behaviour is exhibited by many thermosetting resins and chemically crosslinked thermoplastics [13].

Finally, it should be pointed out that all the molecular relaxations result from amorphous regions, since unoriented films have a very small crystalline content [14]. The effects of chain order are presently being studied but initial results are consistent with the assignments to unoriented chain motion.

### 3.2. Dielectric thermal analysis (DETA)

The dielectric technique is the electrical analogue of the mechanical technique previously described, but only detects molecular motions of charged or dipolar species. Therefore, it is extremely useful in identifying, or at least narrowing down the origins of, molecular motions seen in DMTA thermograms.

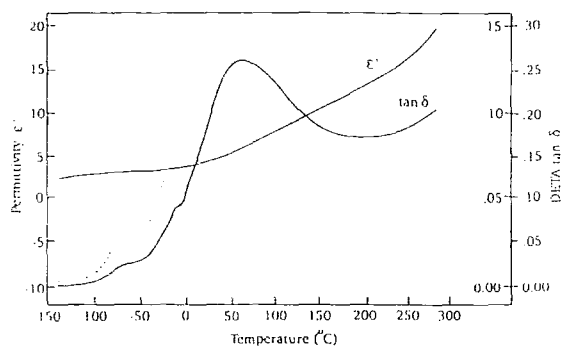


Figure 8. Re-scan (1 kHz) of DETA data for figure 7 (same notation applies).

Dielectric analysis of an as-cast polyaniline film, shown in figure 7, clearly reveals both the  $T_g$  and the crosslinking transitions ( $\tan \delta$  peaks at 100°C and 160°C respectively). The correlation of peak positions with DMTA is good despite the difference in measurement frequencies. Both transitions are very strong dielectrically—the 160°C damping peak has a magnitude of over four. This value is also similar to that observed for epoxy resins during curing and thus might imply chemical crosslinking involving dipolar species. The glass–rubber transition is prominent dielectrically since it involves rotations of the dipolar chains. The variation in  $\epsilon'$  relates to the extent of freedom attained by dipoles [15]. For polyaniline this freedom reaches a maximum during  $T_g$  and then, as expected, decreases due to the hardening process.

The low-temperature feature from the DMTA data is also seen, now possibly consisting of a double transition. This relaxation is very weak dielectrically as seen by the small intensity relative to either of the other DETA relaxations. This precludes any polar activity and compounds the original assignment to a librational ring motion.

The DETA re-scan, shown in figure 8, is dominated by the 85°C transition seen in the mechanical analogue. Therefore, this molecular motion involves polar activity. The ring relaxation can also be observed although it is rather swamped by the main 85°C relaxation. The upswing on the high-temperature side of the main transition is probably due to sample conductivity effects.

### 3.3. Infrared spectroscopy

The IR absorption spectrum of an as-cast emeraldine base film between 2000–200  $\text{cm}^{-1}$  can be seen in figure 9(a). Similar vibrational data [12, 16, 17] have been reported for this region. Key band assignments are as follows. The 1595 and 1505  $\text{cm}^{-1}$  bands are assigned to non-symmetric  $C_6$  ring stretching modes. The higher frequency vibration has a major contribution from the quinoid ring units, so that the relative intensity of these two bands gives an indication of the oxidation state of the material [12]. The 1300  $\text{cm}^{-1}$  vibration is a C–N stretch, indicative of secondary (2°) aromatic amine groups. The

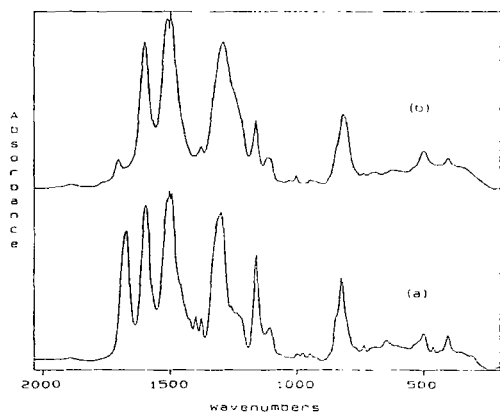


**Figure 9.** Transmission IR spectra of a polyaniline film between 2000 and 200  $\text{cm}^{-1}$ : (a) as-cast, (b) having been heated to 200°C.

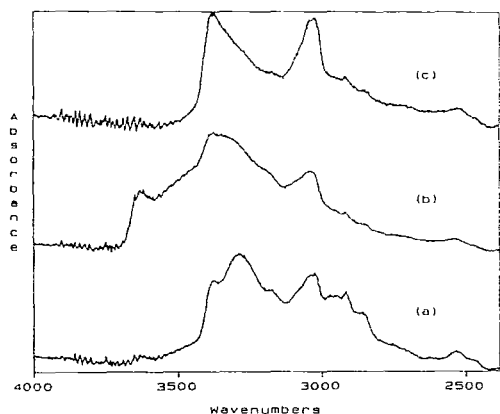


**Figure 10.** Reflectance IR spectra between 4000 and 2600  $\text{cm}^{-1}$  for (a) an as-cast film, (b) the same film having been heated to 200°C and (c) the heat treated film at 100°C.

1160  $\text{cm}^{-1}$  mode is most likely to be an in-plane C–H bending motion of the aromatic rings, while those at 825, 500 and 405  $\text{cm}^{-1}$  are out-of-plane C–H bending modes. The position of the 825  $\text{cm}^{-1}$  peak is characteristic of para-disubstituted aromatic rings [17]. Finally, the band positioned at 1675  $\text{cm}^{-1}$  is due to the carbonyl (C=O) stretching of the NMP solvent.

As well as in the fingerprint region, bands are also seen in the N–H and C–H stretching regions, shown in figure 10(a), between about 3600–2800  $\text{cm}^{-1}$ . This part of the spectrum has received less attention in the literature and so has been investigated further. The aromatic  $\nu(\text{CH})$  is easily identifiable above 3000  $\text{cm}^{-1}$  as a peak at 3040  $\text{cm}^{-1}$ . The weaker features at lower frequency are  $\text{CH}_2$  stretches of NMP. At higher wavenumbers an N–H vibration is observed at 3285  $\text{cm}^{-1}$  with a shoulder at approximately 3380  $\text{cm}^{-1}$ . For diphenylamine, which we can consider to represent the benzenoid–amine part of the polyaniline chain, a sharp peak is observed at around 3380  $\text{cm}^{-1}$  which is indicative of  $\nu(\text{NH})$  for the 2° amine [18]. This clearly

identifies the shoulder in the polyaniline spectrum.

The main N–H band, however, occurs at 3285  $\text{cm}^{-1}$ . This peak shift indicates hydrogen (H-) bonded amine groups. For example, H-bonding in the polyamide nylon 6,6 shifts  $\nu(\text{NH})$  from 3450  $\text{cm}^{-1}$  down to about 3300  $\text{cm}^{-1}$  [19]. We can further identify that this H-bonding involves NMP molecules bonding to the polar amine groups, since this band disappears in conjunction with the solvent carbonyl band when the sample is heated to 200°C (see figures 9(b) and 10(b)).

Another interesting occurrence in the N–H region is seen in the spectrum of a solvent-free film (figure 10(b)). For this sample the 3380  $\text{cm}^{-1}$  peak is extremely broad and a further band is evident at around 3600  $\text{cm}^{-1}$ . This effect is thought to be due to absorbed water vapour since these features are consistent with underlying (H-bonded) O–H stretching bands. Yet if the spectrum is taken at 100°C, as in figure 10(c), the N–H band is much sharper and the latter vibration disappears indicating that water molecules are lost at elevated temperatures. This behaviour coincides with the relaxation peak at 85°C in both the DMTA and DETA thermograms of solvent-free films. Therefore, we can assign this transition as being due to the breaking of H-bonds between absorbed water and amine groups. Furthermore, if the sample is cooled back to room temperature the spectrum returns to that of figure 10(b), so that thermal cycling involves the loss and recapture of water vapour.

Returning to the spectral region below 2000  $\text{cm}^{-1}$ , an as-cast film was heated to 200°C, cooled and the spectrum re-taken (figure 9(b)). This treatment, according to our thermal analysis results, removes the solvent and crosslinks the polymer chains. Hence, we can now evaluate this hypothesis using IR spectroscopy.

Comparing figures 9(a) and 9(b), the most striking difference is the loss of the carbonyl band at 1675  $\text{cm}^{-1}$  for the heat treated film. As previously mentioned, this is due to removal of the solvent. A small band does appear at 1705  $\text{cm}^{-1}$  which could be a quinoid–imine stretching mode or a C=O stretch due to slight sample oxidation. Examining the spectrum more closely, all the remaining absorption bands have an increased width. Such broadening indicates increased interaction of vibrational modes which we have attributed to physical chain crosslinking.

It is also noticeable, though, that significantly more broadening occurs in the region between 1300 and 1100  $\text{cm}^{-1}$ . Specifically this involves the 2° amine stretching vibration which exhibits a considerable shoulder to the low-frequency side of the mode, lowering the peak by some 10  $\text{cm}^{-1}$ . The 1160  $\text{cm}^{-1}$  vibration broadens to a lesser extent, but is also much reduced in intensity. These changes seem unlikely to be due to chain entanglement alone and could indicate chemical bonding. A possible chain bonding process, suggested by Scherr *et al* [20], is the formation of nitrogen bridges between two quinoid–imine units. No evidence is given, though, for such a reaction.

However, the possibility also exists that chain defects and impurities are responsible for chemical

crosslinking. These are present in levels of only a few per cent (elemental analysis in section 2) but the change in  $\nu(\text{CN})$  is small and therefore characteristic of a change in only a few per cent, perhaps about 5%, of the nitrogen linkages. Relatively few crosslinks are required to render a polymer structure extremely rigid. Furthermore, bands at around  $1105\text{ cm}^{-1}$  and  $645\text{ cm}^{-1}$  are observed in the as-cast spectrum of figure 9(a) which correlate with reported modes for sulphonate residues in polyaniline powder [21]. These modes shift in frequency and disappear respectively in figure 9(b), the heat treated film. Therefore, contaminant involvement in the hardening transition can be proposed. This topic is discussed further in the next section.

### 3.4. Further discussion

Much recent interest in polyaniline has involved work on 'gels' [22], formed from emeraldine base/NMP solutions. Such materials are produced by simply allowing the polymer/solvent system to stand and over a length of time a gel forms. An essential feature is the connectivity of chains as a result of crosslinks [23]. Indeed, films cast from such gels have been proposed as being physically crosslinked [24]. Gel formation is observed for the 8 wt% emeraldine base/NMP solutions used in this study, after a period of about 24 h at room temperature. This process is rapid, however, if the solution is heated. Gelation times at room temperature increase for decreasing polymer concentration down to a level of about 1 wt%, below which no reaction occurs.

However, for a second batch of emeraldine base powder it was noticed that gelation occurred at a faster rate and to a higher extent for a given concentration in NMP. An elemental analysis of the powder revealed an increase in contaminants (total S, Cl, O content 7.89 wt%), traced to inadequate purification. This information strongly suggests that crosslinking is associated with such contaminants. Increased sulphonate and chloride residues, both free ions and ring substitution defects, are likely to be responsible for the raised level in this second sample (spectroscopic data were unfortunately not conclusive). Both types of impurity are reactive, however, and will chemically bond, forming crosslinks. Heating the samples increases the reactivity of these species and the rate of gelation. Analogous chemical crosslinking reactions occur in other synthetic polymers when heated with additives such as sulphur and peroxides [1]. Therefore, polyaniline/NMP solutions and hence films appear to crosslink both physically and chemically.

All these results thus prove the need for precise control of polyaniline synthesis and processing. Only a slight variation in chemical synthesis has produced a considerable effect on the crosslinking reaction (gelation) of the polymer in NMP solution. Moreover, we have highlighted the central role of chain defects and impurities in such a crosslinking process. The quality of polyaniline is thus a crucial factor in determining the physical properties of the material. Improvements

in polyaniline synthesis are being studied by our group here in Durham and the results are soon to be published. Further thermal analysis work is also presently being undertaken.

### 4. Conclusions

Polyaniline films (emeraldine base) solution cast from NMP, have been studied using DMTA, DETA and IR spectroscopy. The analyses have identified several molecular motions occurring over the temperature range  $-130$  to  $300^\circ\text{C}$ . A librational ring motion occurs at approximately  $-80^\circ\text{C}$  and a  $T_g$  relaxation, associated with residual solvent, at  $100^\circ\text{C}$ . We have also observed a permanent hardening transition at  $180^\circ\text{C}$  which involves not only physical crosslinking, but also a degree of chemical bonding or crosslinking. Chemical crosslinking has been shown to be associated with chain defects and residual impurities in the polymeric material. Since this reaction renders films extremely brittle, the transition temperature defines an upper limit for thermal orientation processing.

Many of the wide variations in often conflicting experimental results can be explained by subtle differences in polyaniline synthesis giving rise to different amounts of contaminants. Chemical crosslinking is just one example of how these contaminants can drastically effect the physical properties of the polymer. Polyaniline thus needs to be precisely synthesized and processed so as to remove both impurities and chain defects.

### Acknowledgments

We thank SERC and BICC for funding AJM. Thanks also go to Lynn Addison and Simon Rowland at BICC and Mr G Foster at Polymer Laboratories for running DETA samples and for useful discussions on the DMTA and DETA data.

### References

- [1] McCrum N G, Read B E and Williams G 1991 *Anelastic and Dielectric Effects in Polymeric Solids* (New York: Dover)
- [2] Milton A J and Monkman A P 1992 *Synth. Met. Proc. ICSM*
- [3] Monkman A P and Adams P N 1991 *Synth. Met.* **40** 87
- [4] Adams P N and Monkman A P 1992 *Synth. Met. Proc. ICSM*
- [5] Kenwright A M, Adams P, Feast W J, Milton A J, Monkman A P and Say B J 1992 *Polymer* **33** 4292
- [6] Kromack K R *et al* 1991 *Macromolecules* **24** 4157
- [7] Wei Y, Jang G, Hseuh K F, Scherr E M, MacDiarmid A G and Epstein A J 1992 *Polymer* **33** 314-22
- [8] Ward I M (ed) 1971 *Mechanical Properties of Solid Polymers* (New York: Wiley Interscience)
- [9] Wetton R E 1986 *Developments in Polymer Characterisation* vol 5 ed J V Dawkins (London: Elsevier) pp 179-229
- [10] Wetton R E, Morton M R and Rowe A M 1986 *American Laboratory* **18** 96



- [11] Bredas J L 1992 *Proceedings of the Nobel Symposium on Conjugated Polymers and Related Materials* ed W R Salaneck (Oxford: Oxford University Press)
- [12] Epstein A J, McCall R P, Ginder J M and MacDiarmid A G 1991 *Spectroscopy of Advanced Materials* vol 19 ed R J H Clark and R E Hester (New York: Wiley) pp 355–92
- [13] Gradin P, Howgate P G, Snelden R and Brown R A *Comprehensive Polymer Science* vol 2 cd G Allen (Oxford: Pergamon) pp 533–69
- [14] Fischer J E, Tang X, Scherr E M, Cajipe V B and MacDiarmid A G 1991 *Synth. Met.* **41–43** 661
- [15] Frolich H 1958 *Theory of Dielectrics* (London: Oxford University Press)
- [16] Furukawa Y, Ueda F, Hyodo Y, Harada I, Nakajima T and Kawagoe T 1991 *Macromolecules* **21** 1297
- [17] Tang J, Jing X, Wang B and Wang T 1988 *Synth. Met.* **24** 231
- [18] Pouchert C J (ed) 1981 *The Aldrich Library of Infrared Spectra* 3rd edn (Milwaukee, WI: Aldrich Chemical Co)
- [19] Bower D I and Maddams W F (eds) 1989 *The Vibrational Spectroscopy of Polymers* (Cambridge: Cambridge University Press) p 258
- [20] Scherr E M *et al* 1991 *Synth. Met.* **41–43** 735
- [21] Ohsaka T, Ohnuki Y, Oyama N, Katagiri G and Kamisako K 1984 *J. Electroanal. Chem.* **161** 399
- [22] Tzou K and Gregory R V 1992 *Synth. Met. Proc. ICSM*
- [23] Miles M J 1988 *Developments in Crystalline Polymers-2* ed D C Basset (New York: Elsevier)
- [24] MacDiarmid A G, Min Y, Oh E J, Scherr E M, Tang X, Masters J G and Epstein A J 1992 *Synth. Met. Proc. ICSM*

### THERMAL ANALYSIS OF POLYANILINE FREE STANDING FILMS

A. J. MILTON and A. P. MONKMAN

Organic Electro-active Materials Research Group, Department of Physics, University of Durham, Durham, DH1 3LE, U.K.

#### ABSTRACT

We report on Dynamic Mechanical Thermal Analysis (DMTA) studies of free standing films of polyaniline. These films were cast from chemically synthesised emeraldine base dissolved in the solvent *N*-methyl-2-pyrrolidinone (NMP). Thermal scans show a softening 'T<sub>g</sub> process' for such films at ~100°C. This occurs as solvent molecules are being removed from the samples. The exact transition temperature is dependent on the weight fraction of the NMP solvent and increases with decreasing solvent content. Above 180°C a crosslinking of the polymer chains occurs resulting in a hardening of the films. This crosslinked material is characterised by a new transition at 265°C. A low temperature transition is also seen at -80°C. This is interpreted as a torsional motion of the aromatic rings in the polymer chains.

#### INTRODUCTION

The ability to process polyaniline into tough, air-stable, free standing films has been a fundamental factor for much of the current research into this exciting conducting polymer. Further, using stretch alignment at elevated temperatures, such films can be elongated by several hundred percent [1]. This produces an anisotropy in the physical properties of the polymer which allows increased information to be gained from measurements made both parallel and perpendicular to the stretch direction. In order to obtain highly oriented samples it is necessary to have a thorough knowledge of the thermal properties of the polymer. However, this is an area which has received little attention. Therefore, we have undertaken a detailed thermal analysis of polyaniline films.

In this communication we report on DMTA studies of free standing films. Briefly the dynamic mechanical technique, of applying a small oscillating mechanical strain on a sample and resolving the stress into real and imaginary components, detects essentially all changes in the state of molecular motion as temperature is scanned. The data is characterised in terms of the storage

ponent of the dynamic Young's modulus ( $E''$ ), the loss component ( $E'''$ ) and the loss tangent ( $\tan \delta = E''/E'$ ). For further details see [2].  
 previous study has been published [3], but it is limited in detail. Also differences in polymer  
 ssing render the information unsuitable for our samples. Our results reveal several interesting  
 al transitions and reactions which have important consequences on the processing of  
 niline at elevated temperatures.

## EXPERIMENTAL SECTION

aniline was chemically synthesised in the emeraldine base form (Figure 1) by our usual  
 step addition of the oxidant ammonium persulfate to an aqueous solution of aniline  
 chloride followed by deprotonation in ammonia solution [4]. The molecular weight of the base  
 mer was determined as approximately  $3 \times 10^4$  (350 repeat units) by gel permeation  
 chromatography using an NMP/LiCl solution and polyvinylpyridine standards [5].  
 The standing films were cast from a 10% solution of emeraldine base dissolved in NMP. Excess  
 solvent was removed at 70°C under vacuum until the samples were dry. These samples were then  
 removed from the substrate to give free standing films with a typical NMP solvent content of 25% as  
 determined by Thermogravimetric Analysis (TGA).  
 DMTA scans were obtained on a Polymer Laboratories Mk II instrument. The following  
 conditions were employed under tensile geometry: frequency, 1Hz; strain, 16  $\mu\text{m}$  peak to peak  
 displacement; thermal scan, -130°C to 300°C; heating rate, 3°C/min. Sample dimensions were kept  
 constant throughout so as to ensure reproducibility. A reducing force mode was used, which adjusts  
 the applied force (1N) during thermal transitions, so as to minimise sample creep. The results are  
 presented as plots of log storage modulus, ( $\log E'$  (Pa)) and damping ( $\tan \delta$ ) versus temperature. The  
 DMTA was operated under external computer control using a Compaq 386 micro-computer.

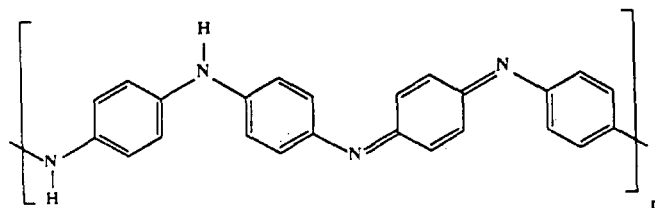


Figure 1. Emeraldine base oxidation state of polyaniline.

## RESULTS AND DISCUSSION

Figure 2 shows a typical DMTA thermal spectrum of an as cast emeraldine base film. Above room  
 temperature an extremely broad damping peak in  $\tan \delta$  is observed starting at about 50°C with a  
 shoulder at 100°C and reaching a maximum at 180°C. This feature corresponds to the onset of film  
 softening and defines the temperature region in which samples can be stretch aligned. The shoulder  
 at 100°C can be assumed to represent a transition temperature for this softening or so-called ' $T_g$   
 process'. The exact temperature of the relaxation is dependent on the amount of plasticiser (residual  
 solvent) in the film and increases for decreasing solvent content. In this case 25% as deduced by  
 TGA.

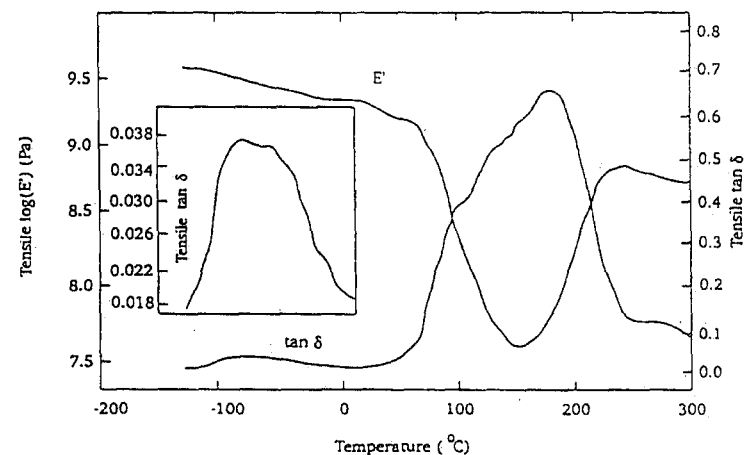


Figure 2. DMTA thermal spectrum of an as cast emeraldine base film. The inset is an expansion of the  $\tan \delta$  curve along the ordinate.

As films are exposed to temperatures in the softening regime at around 100°C, TGA weight losses  
 indicate that solvent molecules are being removed (25% weight loss recorded by ~250°C). This is  
 because the input of thermal energy is enabling the NMP molecules to escape from their hydrogen-  
 bonded positions along the polymer chains. This, in turn, creates a large free volume and allows  
 rotational freedom of the chain backbone.

However, if the temperature is raised too high above the ' $T_g$  transition' then a hardening process  
 begins to occur. Such a reaction is indicated by an increase in the storage modulus after the sharp  
 drop due to chain relaxation. This is almost certainly due to crosslinking occurring between the  
 polymer chains. It has previously been reported that emeraldine base can be thermally crosslinked

ting at 300°C under inert conditions [6]. The peak in  $\tan \delta$  at 180°C defines a transition rature for the onset of such a process. So, in order to avoid crosslinking, the temperature of should be kept well below 180°C during stretch alignment.

MTA scan of a sample that had previously been heated up to 230°C is shown in Figure 3.

room temperature there are now two distinct damping peaks in  $\tan \delta$ . The peak at 265°C represents a transition of the new crosslinked, solvent free, material. That at 85°C is probably due to amounts of loosely bound solvent, but its origin is being investigated further.

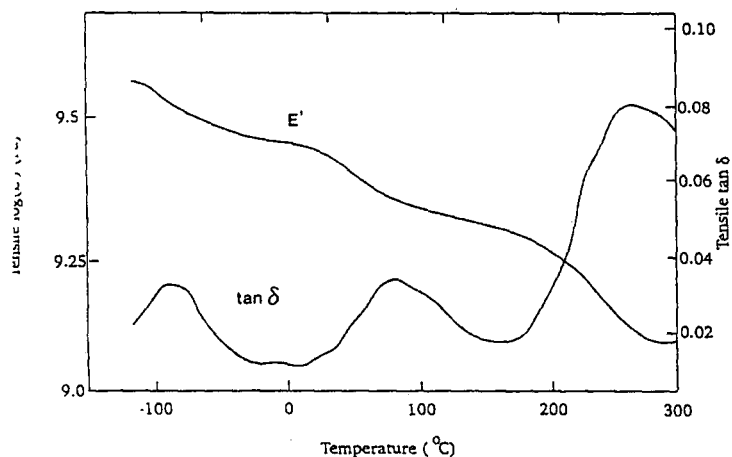


Figure 3. DMTA thermal spectrum of an emeraldine base film that had previously been heated up to 230°C. The peak in  $\tan \delta$  at 265°C represents a transition of the crosslinked material.

A further feature of our DMTA data is the presence of a low temperature relaxation at -80°C. This damping peak is seen in the thermal scans of both the as cast film (inset in Figure 2) and the heat treated, solvent free, film (Figure 3). In fact, it was also observed in both HCl doped and stretch aligned samples as well. Thus, its origin cannot be connected with the presence of NMP solvent and so, since this is a secondary transition, the relaxation is not due to movement of the chain backbone as a whole. After examining possible origins and other DMTA data, we have assigned this transition to a torsional motion of the aromatic rings in the polymer chains. This effect may be due to phenoid or quinoid ring torsion (or both). Either way, this temperature dependent motion should manifest itself in the temperature dependence of other physical properties of the polymer e.g. a change in electron delocalisation along the chains and hence a change in conductivity.

To summarise, thermal analysis by DMTA has indicated a 'T<sub>g</sub> process' for polyaniline films cast from an emeraldine base/NMP solution to be at a temperature of 100°C (for films containing 25% NMP by weight). The precise transition temperature is composition dependent. Above 180°C a crosslinking reaction is seen to occur between the polymer chains resulting in a hardened material. Further, we have also discovered the presence of a low temperature molecular relaxation, which we consider to be due to a torsional motion of aromatic rings in the chain structure.

#### ACKNOWLEDGEMENTS

We would like to thank SERC and BICC for funding (AJM). Also thanks go to Mr G. Foster at Polymer Laboratories for useful discussions on this data and Lynn Addison and Simon Rowland at BICC for helping to run the DMTA.

#### REFERENCES

- 1 A. P. Monkman and P. N. Adams, *Synth. Met.* **41-43**, (1991), 627.
- 2 R. E. Wetton in J. V. Dawkins (ed.), "Developments in Polymer Characterisation - 5", Elsevier Applied Science Publishers, (1986), pp. 179 - 229.
- 3 Y. Wei, G. W. Yang, K. F. Hsueh, E. M. Scherr, A. G. MacDiarmid and A. J. Epstein, *Polym. Mater. Sci. Eng.* **61**, (1989), 916.
- 4 A. M. Kenwright, P. Adams, W. J. Feast, A. J. Milton, A. P. Monkman and B. J. Say, *Polymer*, in press.
- 5 P. N. Adams and A. P. Monkman, these Proceedings.
- 6 E. M. Scherr, A. G. Macdiarmid, S. K. Manohar, J. G. Masters, Y. Sun, X. Tang, M. A. Druy, P. J. Glatkowski, V. B. Cajipe, J. E. Fischer, K. R. Cromack, M. E. Jozefowicz, J. M. Ginder, R. P. McCall and A. J. Epstein, *Synth. Met.* **41-43**, (1991), 735.